Magnetic targeting and exploration of novel technologies to treat cardiac diseases

Inaugural Dissertation

zur
Erlangung des Doktorgrades
philosophiae doctor (PhD) in Health Sciences

der Medizinischen Fakultät
der Universität zu Köln

vorgelegt von
Lisa Melanie Münchhalfen
aus Bergisch Gladbach, Deutschland

Köln, 2026

Betreuer*in: Prof. Dr. Kurt Paul Pfannkuche

Gutachter*in: Prof. Dr. Andreas Wodarz

Prof. Dr. David Vilchez

Datum der mündlichen Prüfung: 28.04.2026

Acknowledgments

Firstly, I like to express my gratitude towards Prof. Dr. Kurt Pfannkuche. Thank you for your supervision and offering me to explore the research field I am interested in. I really appreciate your relaxedness and your positive attitude.

To my science family, Dr. Sarkawt Hamad and Daniel Derichsweiler, Ebru Aksoy, Rezwan Firuzi, Ziwei Lu, Yajuan Jiang, thank you for your support, research input, and time for countless coffee breaks.
I also like to acknowledge the former members of research group Pfannkuche: Dr. Raja Sahito, Larissa Schmitz-Ullrich, Katharina Zahn, Annabell Storch and Dr. Julia Junghof, as well as the colleagues of the Institute for Neurophysiology, Dr. Dr. Tomo Šarić, Rebecca Dieterich, Anette Köster, Vanessa Pütz, Elke Lieske and Prof. Jürgen Hescheler.
Thanks to Prof. Gang Bao and his group for the material and knowledge transfer for many years, and for this adjuvant international collaboration.
To my former boss and collaborator, Ingo Voigt of the Max-Plank Institute for Biology of aging, I really appreciate your constant support.
My gratitude goes to the staff of the decentralized animal facility of University Hospital Cologne, especially our animal care takes Claudia, Jan, Celina, as well as Jasmin and Manuel.
Thank you to the imaging facility CECAD and Prof. Carien Niessen and Nick Poch, and the team of the uniclinic scientific workshop, Cederic, Robert and Vitaly.
Thanks to my mentors and the interdisciplinary health science (IPHS) graduate school staff.

Lastly, I want to thank my family and my friends. Thank you for keeping me grounded and listening to my whining about the PhD journey for the last years.

Abstract

The relatively new field of regenerative medicine holds unforeseen possibilities of stem cell-based replacement therapies for the future. Two main trends in application are emerging: firstly, individualized treatment with autologous *in-vitro* grown cells and tissues, and secondly, the search for a universal donor cell, a cell that is immune-compatible to all recipients, for allogenic transplantation.

Individual therapies with autologous cells are time- and cost-intensive, but issues upon transplantation, such as immunoreactivity, are minimized, one of the main issues of allogenic transplantation approaches. Specific surface markers, expressed on all cell types, mediate immune reaction and ultimately the dissociation of the cell-graft or transplant, when they are mismatched between donor and recipient. A common solution for this issue is the search and banking of cells with homologous surface markers in so-called haplobanks. Cells with homologous surface markers do not fit all, but many graft recipients. Simultaneously, genetic engineering methods allowed the modification of the cell´s surface proteins to not be detected by the immune system at all. In this work, we propose the genetic modification of a human induced pluripotent stem cell line to evade the immune system of an animal host. Xenotransplantation for basic research plays a vital role in further developing stem cell-based therapies.

At the same time, we want to make efforts to overcome the issue of engraftment upon stem cell-based transplantation. Stem cell transplantation suffers from very low engraftment rates and we propose magnetically labeling and targeting of cells as a strategy to retain transplanted cells at the injection site. Here, we introduce two methods for magnetically labeling cells.

Lastly, this work contributes to the field of organ complementation, a research field following the idea of growing full organs from patient-derived stem cells, utilizing closely related model animals, like pigs, to grow organs for transplantation on demand. This idea is still facing many unclear issues, for example, which genes need to be deactivated to grow a full organ like the heart for organ complementation. Here, we investigate an *in vivo* intra-embryonic complementation assay in mice to determine how to empty the organ developmental niches of the heart.

Zusammenfassung

Das relativ junge Gebiet der regenerativen Medizin birgt ungeahnte Möglichkeiten für stammzellbasierte Therapien der Zukunft. Zwei Hauptanwendungstrends zeichnen sich ab: Erstens die individualisierte Behandlung mit autologen, in vitro gezüchteten Zellen und Geweben und zweitens die Suche nach einer universellen Spenderzelle – einer Zelle, die für alle Empfänger geeignet ist – für die allogene Transplantation.

Individuelle Therapien mit autologen Zellen sind zwar zeit- und kostenintensiv, minimieren aber Probleme bei der Transplantation, wie beispielsweise Immunreaktionen – eines der Hauptprobleme allogener Transplantationsansätze. Spezifische Oberflächenmarker, die auf allen Zelltypen exprimiert werden, vermitteln Immunreaktionen und letztendlich die Dissoziation des Zelltransplantats, wenn die Marker von Spender und Empfänger nicht übereinstimmen. Eine gängige Lösung für dieses Problem ist die Suche und Lagerung von Zellen mit homologen Oberflächenmarkern in sogenannten Haplobanken. Zellen mit homologen Oberflächenmarkern passen zwar nicht zu allen, aber zu vielen Empfängern. Gleichzeitig ermöglichen gentechnische Methoden die Modifizierung der Zelloberflächen, sodass diese vom Immunsystem nicht mehr erkannt werden. In dieser Arbeit schlagen wir die genetische Modifikation einer menschlichen induzierten pluripotenten Stammzelllinie vor, um das Immunsystem eines tierischen Wirts zu umgehen. Xenotransplantationen spielen in der Grundlagenforschung eine entscheidende Rolle für die Weiterentwicklung stammzellbasierter Therapien.

Gleichzeitig wollen wir die Probleme des zellulären Verbleibs bei Stammzelltransplantationen lösen. Stammzelltransplantationen weisen eine sehr niedrige Anwachsrate auf. Daher schlagen wir die magnetische Markierung von Zellen vor, um transplantierte Zellen an der Injektionsstelle zu halten. Hier werden zwei Methoden der magnetischen Markierung vorgestellt.

Schließlich leistet diese Arbeit einen Beitrag zum Gebiet der Organkomplementation. Dieses Forschungsgebiet verfolgt die Idee, vollständige Organe aus patienteneigenen Stammzellen zu züchten, und nutzt dafür eng verwandte Tiermodelle wie Schweine, um Organe für die Transplantation nach Bedarf zu züchten. Dieses Konzept steht noch vor vielen offenen Fragen, beispielsweise welche Gene deaktiviert werden müssen, um ein vollständiges Organ wie das Herz im Rahmen der Organkomplementation zu züchten. Wir untersuchen hier *in vivo* ein intra-embryonales Komplementationsassay an Mäusen, um zu bestimmen, wie die Entwicklungsnischen des Herzens geleert werden können.

Table of Contents

List of Abbreviations

Abbreviation	Meaning
A	Ampere
AV	atrioventricular
BLK	Blank
BM	Bone marrow
bp	Base pair
Cas9	CRISPR associated Protein9
CCG	Cologne center for Genomics
CDS	Coding DNA Sequence
CM/CMs	Cardiomyocytes
Ctrl	Control
CRISPR	Clustered Regularly Interspaced Short Palindromic Repeats
crRNA	CRISPR RNA
d	Day/days
ddNTPs	Didesoxy nucleosid triphorsphat
Dil	1,1'-Dioctadecyl-3,3,3',3'-Tetramethylindocarbocyaninperchlorat
dNTPs	Desoxy nucleosid triphorsphat
DMEM	Dulbecco's Modified Eagle's Medium
DNA	deoxyribonucleic acid
D-PBS	Dulbecco’s phosphate buffered saline
DSB	Double Strand break
E	embryogenesis
EMT	epithelial-to-mesenchymal transition
F	Female
F1	First filial generation
F2	Second filial generation
FC	Flow cytometry
FDA	U.S. Food and Drug Administration
FHF	first heart field
gRNA	Guide RNA
GRNs	gene regulatory networks
h	Hour/hours
Hand1	Heart and neural crest derivatives expressed transcript 1
Hand2	Heart and neural crest derivatives expressed transcript 2
hESCs	Human embryonic stem cells
HF	head fold
hiPSC	Human iPSC
ICE	Inference of CRISPR Edits
iPSC	Induces pluripotent stem cells
LANUV NRW	Landesamt für Natur, Umwelt und Verbraucherschutz Nordrhein Westfalen
LV	Left ventricle
M	Male
mESCs	Murine embryonic stem cells
MEF	Murine embryonic fibroblasts
Mesp1	Mesoderm posterior 1

MF	Magnetic field
min	Minute/minutes
miPSC	Murine iPSC
ML	Midline
MMEJ	microhomology-mediated end joining
mMSC	Murine MSC
MSC	Mesenchymal stem cells
NGS	Next generation sequencing
NK	Natural killer cells
OFT	outflow tract
PAM	Protospacer adjacent Motif
PCR	Polymerase Chain reaction
Pdx1	pancreatic and duodenal homeobox 1
Pen/Strep	Penicillin-Streptomycin solution
PEO	proepicardial organ
PLA	primitive left atrium
PRA	primitive right atrium
PT	pulmonary trunk
R26mTmG	Rosa26, membrane-localized tdTomato, membrane-localized EGFP
RNP	Ribonucleoprotein complex
RPM	Rotations per minute
RV	Right ventricle
SA	sino-atrial
sec	Seconds
SHF	second heart field
SPIONs	Super paramagnetic iron oxide nanoparticles
SSA	single-strand annealing
STR	Short tandem repeats
T	Tesla
tg	Transgene/transgenic
tracrRNA	Transactivation RNA
wt	wildtype

List of Figures

List of Tables

1. Introduction

1.1. Regenerative medicine

The research field of regenerative medicine focuses on the restoration, replacement, or regeneration of cells, tissues, and organs where the body´s ability to self-renew is limited [1-3]. A great advantage of regenerative medicine is the interdisciplinary approach, combining research efforts of bio- and medical technology, pharmacology, cell and molecular biology, as well as material science and engineering, leading to rapid progress in recent years [2-5]. Regenerative medicine therapies include various approaches, such as the usage of bio-materials, laboratory-grown cells and tissues, gene therapies, or all therapies stimulating the body's own regeneration and repair processes [2-4, 6]. All with the main goal of finding applications in the human body to overcome so far incurable health issues, diseases, conditions, and aging processes [2-4, 6].

To this date, stem cell-based therapies are the most successful approach of regenerative medicine, as the greatest benefits have been observed in patients so far [4, 6, 7].

1.2. Stem cell-based therapies

Stem cell-based therapies refer to all novel approaches where stem cells are utilized as a potential therapeutic agent [5, 7].

Different stem cell types and applications are currently in various stages of clinical trials, with some already approved for application in patients [5, 7]. The First stem cell transplantation of bone marrow stem cells was carried out in 1958. To date, this is the most established and prominent stem cell therapy and is widely applied in treating malignancies of the blood forming system [5, 7, 8].

Stem cells, used in these therapies, can be divided into two groups of origin: autologous and allogenic cells [2, 5, 7]. Autologous describes the treatment with patients own cells, where patient-derived stem cells are generated, cultured *ex vivo*, following a therapy application based on these generated cells [7]. The development of CAR-T cell therapies is a current example. Although this approach is costly and time-consuming, it minimizes the immune reaction upon transplantation, because the transplanted cells are "self" tissue [9]. Allogenic transplantation, compared to autologous transplantation, is a therapy based on donor stem cells, usually derived from a healthy individual of the same species [7]. Working with donor stem cells from cell banks provides the advantage of being less time-consuming and costly, but introduces the critical issue of immune reaction [10, 11].

1.2.1. Stem cells

The term “stem cell” was first used by German biologist Ernst Haeckel in 1868 to describe the properties of zygotes to give rise to all cells of an organism [7].

To this day, this definition is still valid, although stem cells are currently more precisely described by their ability to self-renew and to differentiate, forming tissue-specific cells [7]. Stem cells can be separated into four groups for their potency characteristics: totipotent, pluripotent, multipotent, and unipotent, ranked from the highest to lowest differentiation potential (*Figure 1*) [12].

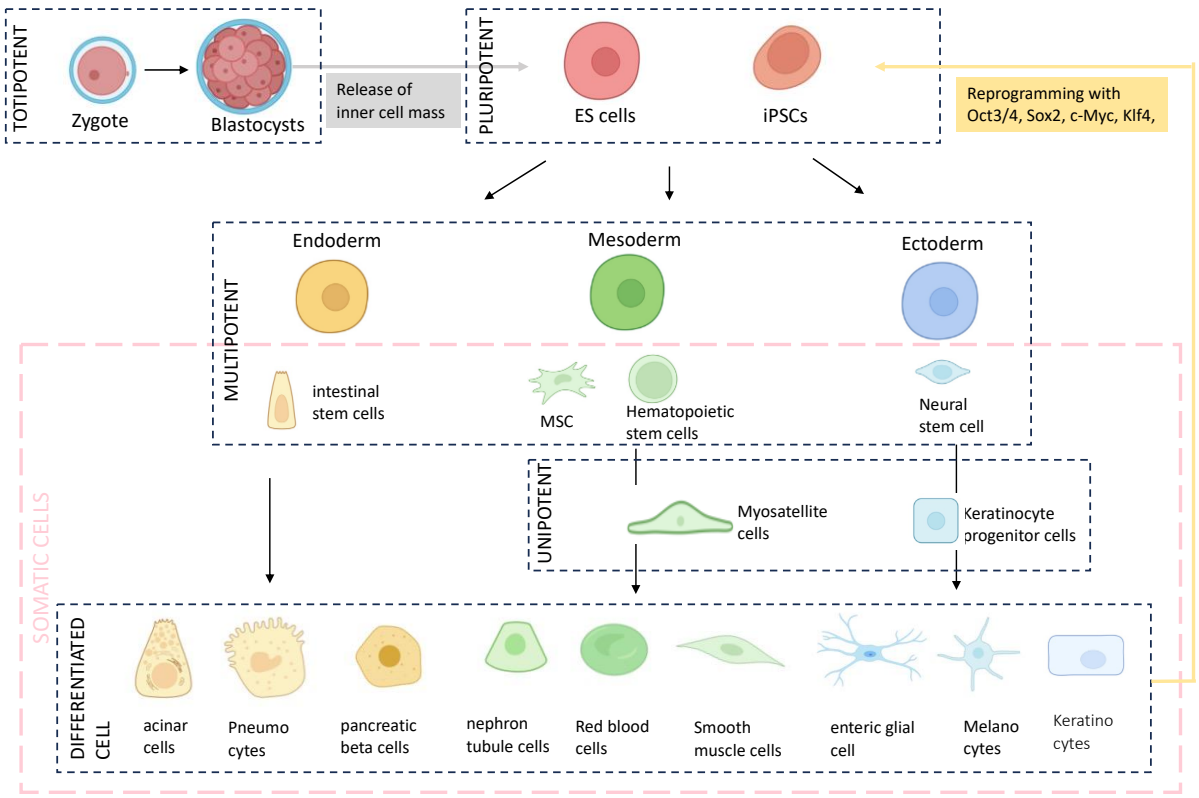

Figure 1: The four types of stem cells.

Modified after [12], created with BioRender. Four types of stem cells: totipotent, pluripotent, multipotent, and unipotent. Totipotent stem cells have the highest potential and are only found in the zygote and cells of the blastocysts. Pluripotent stem cells have a high differentiation potential, as they can still form all three germ layers (Endoderm, Mesoderm, and Ectoderm) and germ line cells. Pluripotent stem cells regularly used in experiments are embryonic stem (ES) cells, released from the inner cell mass of the blastocysts, and induced pluripotent stem cells (iPSCs), generated by reprogramming somatic stem cells with Oct3/4, Sox2, c-Myc, and Klf4. Multipotent stem cells have a more limited differentiation capability and can be found in the body. Therefore, they are also considered somatic cells. One prominent example is Mesenchymal stem cells (MSCs). Unipotent stem cells have an even higher level of specificity and can usually only be further differentiated into limited cell types. Myosatellite cells, for example, can only differentiate into smooth muscle cells. These stem cells stand in contrast to somatically differentiated cells, which that lost all potency to differentiate into other cell types.

Totipotent stem cells have the capacity to generate of all three germ layers and germ line cells, as well as extraembryonic cell types; so they can develop a complete embryo [5, 12]. Pluripotent stem cells can differentiate into cells of all three germ layers and germ line cells, but in contrast are not able to form extraembryonic tissues. At the same time, they are characterized by their

ability to self-renew. For laboratory applications, pluripotent stem cells are to be distinguished into two groups: Embryonic stem cells (ESCs) and induced pluripotent stem cells (iPSCs). ESCs are generated by releasing them from the inner cell mass of a developing blastocyst, while iPSCs are generated by reprogramming somatic differentiated cells with Oct3/4, Sox2, c-Myc, and Klf4 or combinations involving futter supportive factors [5, 13, 14]. Multipotent stem cells have even less differentiation capability, due to them being already developed to one of the three germ layers and can only further differentiate into derivatives of their germ layer. One prominent example, mesenchymal stem cells (MSCs), are only capable of differentiating into osteocytes, chondrocytes, and adipocytes [8, 12]. Unipotent stem cells form the group of the lowest level of potency, and are only able to form one derivative cell type. [12]

Since Yamanaka discovered a possibility to reprogram somatic cells into induced pluripotent stem cells in 2006 [13], iPS cells of multiple species have been studied and pathways for directed differentiation described [15], showing unprecedented research potential, with the advantage of coming with less ethical burdens than embryonic stem cells (ES) [5, 10, 13, 15].

1.2.2. Current clinical application of stem cell therapies

Approved stem cell therapies and those currently in clinical trials usually utilize cells with low proliferation and or differentiated capacity [2]. To this day, the application of stem cell-based therapies in patients is mainly based on multipotent somatic stem cells, including hematopoietic and mesenchymal stem cells (MSCs) [2, 5, 8, 11]. Bone marrow transplants of hematopoietic stem cells for treating patients with hematological cancer have been a common practice for more than 60 years [11].

MSCs combine many advantages, which is why they take over a special role in stem cell therapies. They are primary, non-specialized cells that differentiate, proliferate, and are plastic-adhesive, making them easy to handle in the laboratory [8]. But the biggest advantage is the availability in bone marrow, adipose tissue, umbilical cord, dental pulp, and other sources, making isolation procedures easier while at the same time reducing ethical burdens [11]. Another advantage is that even after allogenic transplantation, MSCs show no immunogenic properties [8, 11]. Evading immune reaction is realized by MSCs suppressing the proliferation and activation of immune cells [8]. At the same time, it is worth mentioning that the definition of MSCs is not very strict. Cells are considered MSCs when they differentiate into osteoblasts, chondrocytes, and adipocytes, and >95% of the cell population expresses the surface markers CD73, CD90, and CD105 while not expressing CD45, CD34, CD14, CD11, CD79, CD19, MHCII [8]. More than 900 clinical trials involving MSCs were conducted in the last 20 years,

including treatments for degenerative changes in joints, reconstructing bones and cartilage, endocrine and nervous system diseases, cell transplantation, and repairing damaged musculoskeletal tissue [8, 11]. Even though several studies failed, MSCs have proved their significant potential and are approved as a treatment for patients suffering from Crohn's disease in Europe and for patients in Canada suffering from graft-vs-host disease [7, 11]. Today, the biological function of MSCs as a main source to replenish the above-mentioned somatic cells of the body is under debate. Many scientists suggest referring to MSCs as medicinal singling cells instead of mesenchymal stem or stromal cells highlighting the function of these cells to regulate the activities of other cell types rather than being mainly a reservoir for tissue regeneration [16, 17].

Due to their limited tri-lineage differentiation capability, MSCs are not eligible for covering all hopes in stem cell treatments [18]. In focus are common diseases with high global prevalence and mortality, often affecting tissues and organs in the human body where stem cells with regenerative properties are absent, including the brain, liver, and heart [19].

Recently, further clinical studies were initiated using human embryonic (hESCs) or induced pluripotent (iPSCs) stem cells as potential therapy agents. For using blastocysts released ES cells, ethical issues remain, while generation of patient-derived hESCs by nuclear transfer into somatic cells remains technically challenging, making ESCs a less popular candidate, and highlighting once again the advantage of reprogrammed iPSCs [10]. Although these iPSC-focused treatments face fewer ethical issues, the induced pluripotent characteristics pose challenges regarding tumorigenesis, heterogeneity, and immune reaction [10, 20].
After iPSC transplantation in vivo, tumor formation always occurs due to the proliferation and differentiation ability of pluripotent stem cells [10].
In comparison the transplantation with differentiated cells derived from iPSCs, pose a lower risk for tumor formation. Tumor formation could only be supported by the heterogeneity of transplanted differentiated cells, remaining undifferentiated iPSCs, and the possibility of immature cells [10].
Challenges of immune reaction and cell engraftment after transplantation will be introduced separately in more detail.

1.2.3. Challenges of stem cell-based therapies: immune reactivity

Immune reaction is yet to be solved for stem cell-based transplantation [2, 21]. The major histocompatibility complex (MHC), in humans also referred to as human leukocytes antigen (HLA) both terms used concurrently, is responsible for immune reaction [9, 22] (*Figure 2*).

Immune reaction of the transplantation recipient is mainly caused by CD8+ and CD4+ T-Cells, natural killer (NK) cells, and Macrophages. Foreign MHC I and II complexes on the cell surface of the transplant are recognized by the T-Cell Receptor (TCR) of CD8+ and CD4+ T-Cells, respectively, and initiate the destruction of these foreign cells.

The signal-regulatory protein α (SIRPα) is an important immune inhibitory receptor of macrophages and NK cells, preventing or causing phagocytosis upon transplantation. The interaction of surface protein CD47 of the transplanted cell with SIRPα on recipient macrophages signals for this macrophage-mediated phagocytosis. Mis-matching of CD47 with SIRPα between different species is considered the main reason why xenografts, transplants from other species, fail in long-term studies. [23]

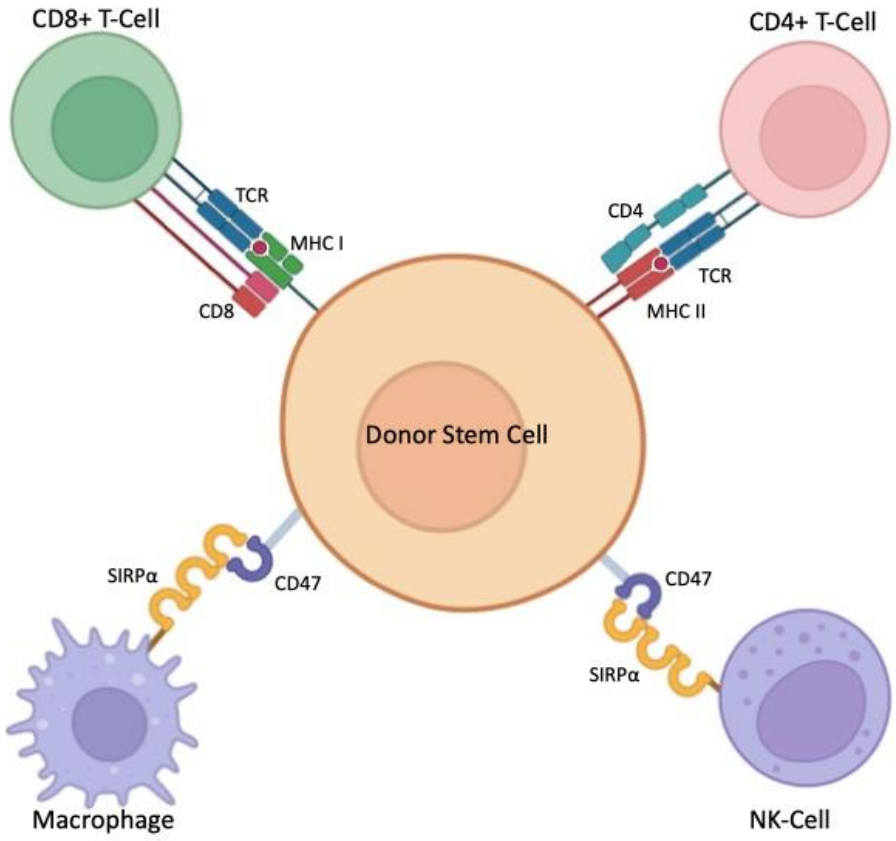

Figure 2: Reaction of immune cells to donor stem cells, simplified.

Modified after [9, 24], created with BioRender. Donor stem cells interact with T cells, Macrophages, and natural killer (NK) cells. T-Cell Receptor (TCR) on CD8+ and CD4+ T-Cells bind to MHC I and II complexes. CD47 of donor cells binds with SIRPα on Macrophages and NK cells.

To prevent an immune reaction upon allogenic transplantation, MHC-matching between graft and host is a necessity. MHC I and II show a big variance in types with heterogeneous expression for most of the world population [25]. Since Takahashi and colleagues (2014) proposed the collection of homozygous HLA donor stem cells in a so-called haplobank [26-29], many nations have adapted the idea [30].

In populations with small variance of haplotypes, like Japan or Norway, a homozygous donor could be HLA-matched with a big part of the population [28]. This way with only a few cell lines majorities of populations could receive a HLA-matched donation from a haplobank, lessening the costs and time efforts [28]. But identifying HLA matching cells for a wide proportion of population, seems to be a challenge, as MHC is one of the most polymorphic region of the human genome [10, 31] and even with HLA-matching, the long-term survivals of transplanted cells remain questionable, as studies in primates have shown, that immunological matched cells delay, but do not prevent long-term rejection of grafts [32].

Various approaches for genetically engineered immune evasive or hypoimmunogenic cells have been under investigation, with the ultimate goal to generate an universal donor cell [21, 24]. Those approaches lean more towards fully overcoming immunogenicity of stem cells upon transplantation by either cloaking cells, so they become invisible to the host immune system [33], or by removing MHC complexes from the cell surface, so T-cells can´t recognize the transplanted cells [24, 34].

Beta 2 microglobulin (ß2M/B2M) encodes for the subunit required for expression of MHC I alpha chains, and if disrupted leads to cells without MHCI complexes [21]. Deletion of class II transactivator (CIITA) impairs the expression of MHC class II [21]. The overexpression of CD47 inhibits the *in vivo* activation of NK cells, which normally recognize the “missing self” responses, leading to lysis of the target cells [21].

Pre-clinical studies of human grafts in large host animals, like pigs and monkeys, to investigate the advantages of cell-based therapies, also suffer from graft-host immune reaction [20]. To overcome these immune reactions of the host animal against the human cell graft, immunosuppression or genetically engineered animals are currently used, increasing experimental costs and making interpretation of these results challenging [20].

1.2.4. Challenges of stem cell-based therapies: Engraftment

Other challenges stem cell therapies, independent of which cell type is used, face are the delivery, adhesion, and engraftment into the target tissue [8, 35].

Low cellular retention, rapid diffusion, and limited survival rates are the reasons for low engraftment rates of cell replacement therapies, even when the cells are directly injected into the damaged tissue area [8, 36-39]. Cell adhesion proteins, like integrins, are expressed on the plasma membrane of cells, especially MSCs, and can promote quick adhesion [8].

Engraftment in the heart is especially challenging, as the heart is constantly beating, and the blood flow increases the risk for thrombosis. At the same time, it is an organ of great interest due to the low self-renewal rate of the cardiac tissue [19, 40].
Differentiating iPSCs into cardiac-specific cells can be easily realized *in vitro*, but the issue of engraftment and low cellular retention remains, even when transplanting microtissues and/or 3D spheroids with fast-adhesive cells, for example, mesenchymal stem cells (MSCs) [35, 37, 38, 40-42].

To overcome low cellular retention, reports of magnetic targeting and application of an external magnetic field show some promising results [36, 42-45].
Magnetically labelling of cells with superparamagnetic iron oxide nanoparticles (SPIONs) or magnetic iron oxide nanoparticles (MIONs) through magnetic force-mediated endocytosis is well described in the work of Zhang [46]. Iron oxide nanoparticles with diameters below 20 nm hold superparamagnetic properties and are highly biocompatible [43, 46]. Therefore, SPIONs made from iron oxide are suitable candidates for exerting magnetic forces to cells.

1.3. Heart diseases and treatments

Cardiovascular diseases (CVDs), a group of disorders of the heart and blood vessels, are the leading cause of death globally [1, 47]. CVDs are associated with the buildup of fatty deposits inside blood vessels, increasing the risk for blood clots and blockage of the systemic supply with oxygen [1, 47]. Stroke and myocardial infarction are both acute events caused by a blood flow blockage, a result of CVDs [1, 47].
Myocardial infarction irreparably damages the heart tissue by destroying cardiomyocytes and driving fibrosis of the extracellular matrix (ECM) in the heart, leading to ECM stiffening due to increased collagen type I deposition [48]. In the last decades, the risk to die of cardiac infarction has reduced due to novel treatment options, especially cather-based inventions to restore blood-flow. In turn, more patients suffer from the consequences of a survived infarction that may ultimately lead to chronic heart failure [49].

The high incidence of chronic heart failure, aggravated by societal aging, is a burden to the already overloaded health care system [1]. The main issues are the limited options for treatment and therapy, especially for damaged heart tissue [1].

Often, organ transplantation is the only treatment for patients suffering from organ failure, but the need for transplants outstrips the supply by far. The heart is one of the organs with a vast gap between availability and necessity; this leads to a great number of patients losing their lives whilst waiting on a donor organ each year [1, 50].

This becomes evident by the EuroTransplant statistics, showcasing the poor availability in the last couple of years, with only 698 donated hearts in the year 2024 [51].

Due to the imbalance of supply and demand, alternative options are being investigated.

The field of regenerative medicine has therefore found more recognition in the last years, with some breakthroughs regarding growing artificial tissue for transplantation and stem cell-based therapies [1, 37, 39], both relying on laboratory-grown materials. At the same time, more drastic approaches to organ replacement strategies are investigated, including xenotransplants and organ complementation, both possible due to new genome editing techniques [50, 52].

1.3.1. The heart function, development, and transcription factors

The physiologic functionality of the mammalian heart is closely related to its anatomy and organization into four chambers that drive the blood flow through the independent systemic and pulmonary circulation systems (*Figure 3*) [52]. In short, deoxygenated blood from the venous circulation of the body enters through the vena cava into the right atrium of the heart. The tricuspid valve opens, and the blood flows from the right atrium into the ventricle. From there, the blood passes through the pulmonary valve, into the pulmonary artery, and circulates to the lungs for oxygenation. Through the pulmonary veins, the oxygenated blood enters the left atrium. The blood is directed through the mitral valve and into the left ventricle, passing the aortic valve, and oxygenated blood is distributed into the systemic circulation through the aorta. Gas exchange occurs, and deoxygenated blood is circulated back to the heart through the vena cava. [52, 53]

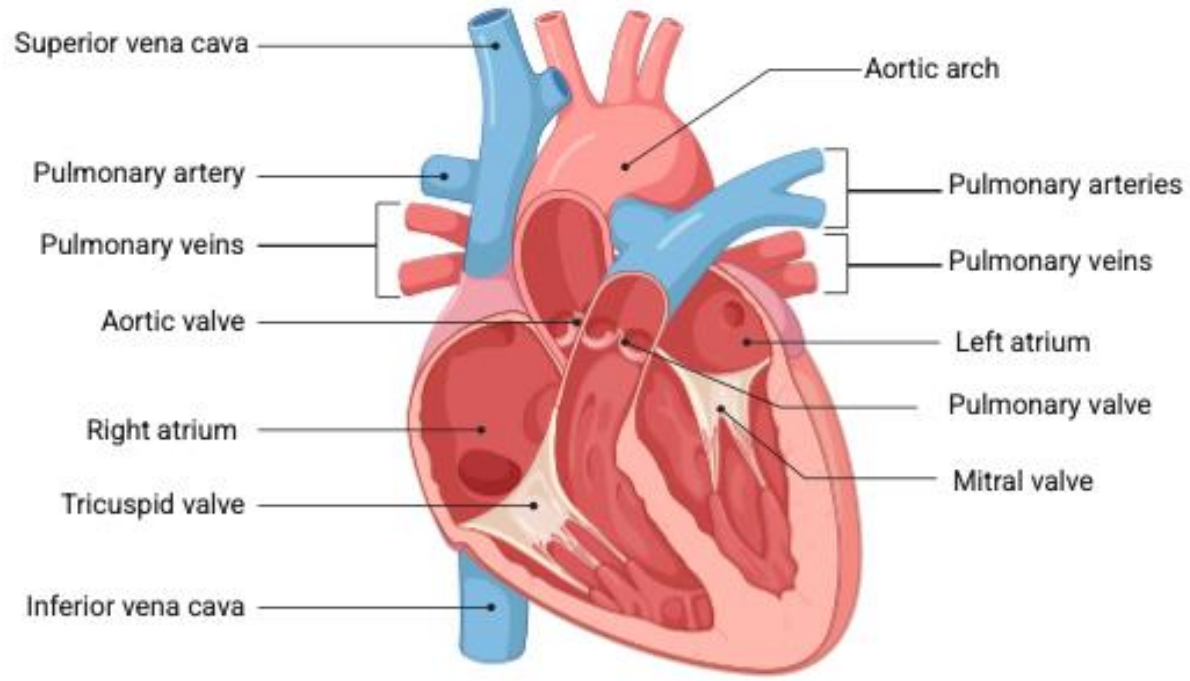

Figure 3: Anatomy of the human heart.

Modified after [52], created with Bio-render.

The function and correct structure of the heart rely on the coordinated development [52]. The function is supported by the different cell types present in the heart, like cardiomyocytes, fibroblasts, endothelial cells, pericytes, smooth muscle cells, lymphoid cells, myeloid cells, neuronal cells, and adipocytes [54]. Cardiomyocytes are the most prevalent cell type of the cardiac tissue, but the distribution of cell types varies between atrial and ventricular tissue, highlighting chamber specificity [54]. The heart is the first organ that forms in the developing vertebrate embryo, as nutrient and oxygen distribution play a vital role, once the embryo reaches a size where diffusion is no longer suitable [55, 56].

In the following paragraph about the development of the mammalian heart, the time point mentioned refers to the developmental stages of the mouse embryogenesis, which takes 21 days in total and is visualized in *Figure 4*.

The heart originates mostly from the mesoderm, the third germ layer, which separates by epithelial-to-mesenchymal transition (EMT) occurring 12 h into gastrulation [52, 56-58]. The formation of the primitive streak on day 6 of embryogenesis (E6) allows the ingression of cardiac mesoderm [52, 57] (*Figure 4a*).

The forming mesoderm spreads laterally and cranially within the embryonic plate [59] and forms two cardiac crescent structures on either side of the midline underlying the head fold

(HF) [55, 60, 61]. This structure is referred to as the first heart field (FHF), where the first myocardial cell can be detected (*Figure 4b*). The two cardiac crescents fuse and expand at the midline on E8, leading to the formation of the primitive heart tube. This tube attaches to the developing blood vessels on the cranial or arterial pole to form an outflow, the caudal end becomes attached to venous vessels, creating the heart inflow, and this way develops a circulatory system (*Figure 4c*) [55, 56, 60].

The further development of the heart after day E8 is mainly driven by the addition of cells from the second heart field (SHF). The primary heart tube serves as a scaffold for subsequent growth of the heart [55, 56]. The SHF also arises from the pharyngeal mesodermal cell population, consists of cardiac progenitor cells, and is located dorsal to the primary heart tube. The SHF has a common precursor population as the FHF cells [60].

The cells of the SHF populate the right ventricle, the outflow tract, the atria, and the inflow region. Cells of the SHF have a different molecular identity and fate depending on the contribution area [60, 62].

Other cell populations also contribute to the heart formation, such as the proepicardial organ (PEO), which grows over the myocardium of the tube to form the outer layer of the epicardium. Some of the cells of the PEO even contribute to the smooth muscle of the coronary blood vessels and therefore undergo EMT [55]. On day E9, a heartbeat is established with initial pace making at the venous pole [63].

The heart tube elongates and begins to loop characteristically to the right (*Figure 4d*). At the same time, ballooning of the future chambers takes place [63], while the SHF adds cells to the venous pole, generating the left and right atrium [55]. The junction between the bilateral atria and the ventricular loop becomes the atrioventricular (AV) canal. In the AV canal and the outflow tract (OFT), the cardiac jelly is converted to paired lumen-filling cushion structures by cellularization. These cells are derived by EMT of endocardial cells in the AV to the proximal part of the OFT [55].

In the following embryonic development days, the heart undergoes subsequently looping and separation and by day E10.5 the heart has acquired well defined chambers (*Figure 4e*), by day E14.5 the heart chambers are connected to the pulmonary trunk (PT) and the aorta (*Figure 4f*), ensuring the separate pulmonary and systemic circulation of the blood, as described the previous section [56].

The heart, as a very complex organ, consists of numerous cell types, including myocardial cells, endothelial cells, smooth-muscle cells, fibroblasts, and specialized conducting cells, which all

mostly derive from the FHF or SHF [58]. Cardiomyocytes and fibroblasts are mostly derived from the FHF and SHF [58].

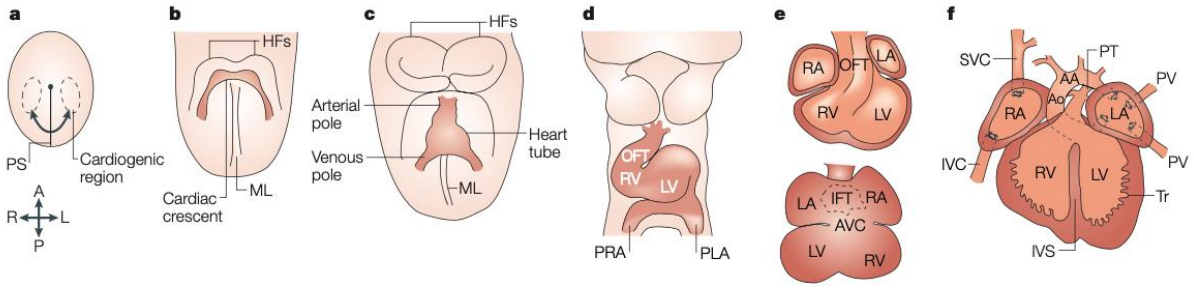

Figure 4: Morphogenesis of the mouse heart [56].

a| Formation of the primitive streak on day E6 allows the ingression of cardiac mesoderm. b| Cardiogenic region forms cardiac crescents. c| The heart tube forms through the fusion of the cardiac crescents at the midline (ML). d| The heart tube undergoes looping. The outflow tract (OFT), right and left ventricle (RV &LV), primitive right atrium (PRA), and primitive left atrium (PLA) form. e| the heart tube loops and has well-defined chambers, but is still a tube. f| E14.5 the chambers are now separated, connected to the pulmonary trunk (PT) and aorta (Ao), which ensures the separate pulmonary and systemic circulation of the blood.[56]

The correct heart formation depends on the regulation of several genes during cardio genesis (*Figure 5*). Indications for the heart arising from the progenitor cells of the FHF and SHF, were found through mutations in these regulatory genes [56].

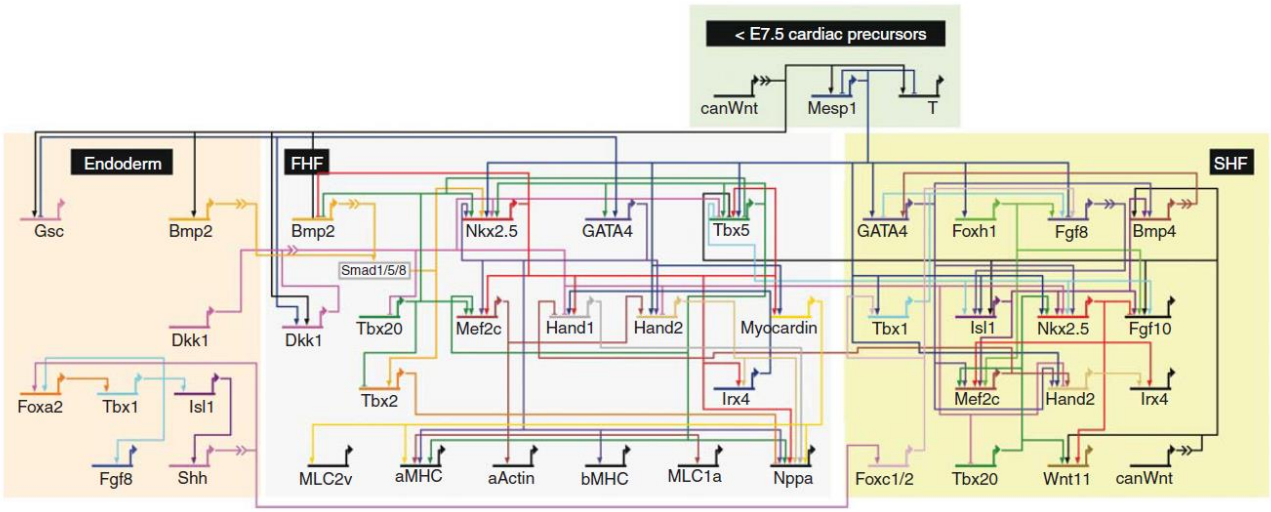

Figure 5: Early cardiac developmental gene regulatory networks (GRNs) [64].

GRNs are separated by territories of First and Second Heart Field (FHF & SHF) and Endoderm. Boolean inference modeling is used to describe relations between transcription factors, where interactions (solid), signaling inputs (broken arrows) within different territories are summarized. [64]

Mesoderm posterior 1 and 2 (Mesp1 & Mesp2) are transcription factors expressed in the mesoderm at the primitive streak, which are linked to the process of cell movement towards the anterior region, which ultimately allows the formation of cardiac progenitors [56].

First cardiac transcription factors start expressing at day E6 [52, 55, 56, 59, 61]. These include the transcription factors Nkx2-5 and Mef2c/b, which are expressed in almost all stages during cardio-genesis. Mutant phenotypes of Nkx2-5 show single atrial and ventricular compartments and a loss of ventricular tissue. Mef2c absence shows a reduced outflow tract and no right ventricle. Nkx2-5 and Mef2c are also directly linked to the activity of two additional cardiac transcription factors: Heart and neural crest derivatives expressed transcript (Hand1 & Hand2). Hand1 mutants show a left ventricle disruption, Hand2 mutants a right ventricle disruption. Mutants of both Hand1 and Hand2 transcription factors show no ventricle formation at all [56]. Tbx5 mutants show a severe defect in the atrial inflow region and right and left ventricle hypoplasia, and reduced cell population in the tissue. This indicates that Tbx5 is also linked to cardio genesis. The absence of Tbx5 upregulates Hand1 and downregulates Hand2 expression [56].

The transcription factor Isl1 is expressed in the second heart field. In its absence, the SHF does not migrate into the cardiac tube, and cells undergo apoptosis. Isl1-mediated regulation also affects Nkx2-5 and myocardial cell specification [56, 60].

SmarcD3 is also specifically expressed in the early mouse embryo heart. SmarcD3 mutants show a defect outflow tract and abnormal cardiac muscle differentiation [65].

1.3.2. Stem cell-based therapies for treating heart conditions

So far, clinical applications of stem cell-based therapies for heart diseases have mostly shown disappointing results, due to yielding no statistically significant improvement of cardiac function after cell transplantation, thus showing no therapeutic effect [7, 40]. For cardiac stem cell-based therapies, many parameters are unclear, including cell source, dosage, delivery route, timing of administration, and cell distribution after administration [7]. At the same time, the contribution of transplanted cells to the contractility of the heart remains questionable, as both electromechanical coupling and isolation between graft and host have been shown before [40, 66].

The most recent study of Jebran *et al.* (2025) for the first time shows promising results for long-term retention of transplanted heart patches in primates, where the heart patch enhances the contractility and ejection fraction of the ventricle [67].

1.3.3. Organ complementing and its research

Organ complementation is a new approach for organ replacement. The vision is to grow human organs for transplantation in animal donors such as pigs and cattle (*Figure 6*) [68]. So far, the field of organ complementation has had only a few breakthroughs.

The first organ complementation between mouse and rat was realized by Kobayashi and colleagues (2010) [69] and later Wu *et. al* (2017) [70], who were able to grow a rat pancreas from a PSC in a mouse host. The pancreas is derived from only one transcription factor: pancreatic and duodenal homeobox 1 (Pdx1). $Pdx1^{-/-}$ mice, which live 4 weeks, long enough to be fertile, were used for this experiment. The donor PSCs that occupied the empty biological niche also contributed to the development of different organs (off-targets), with the highest rate of chimerism in the heart. This observation leads to the deduction that the heart is more permissive than other organs to form chimeric tissue with transplanted cells.

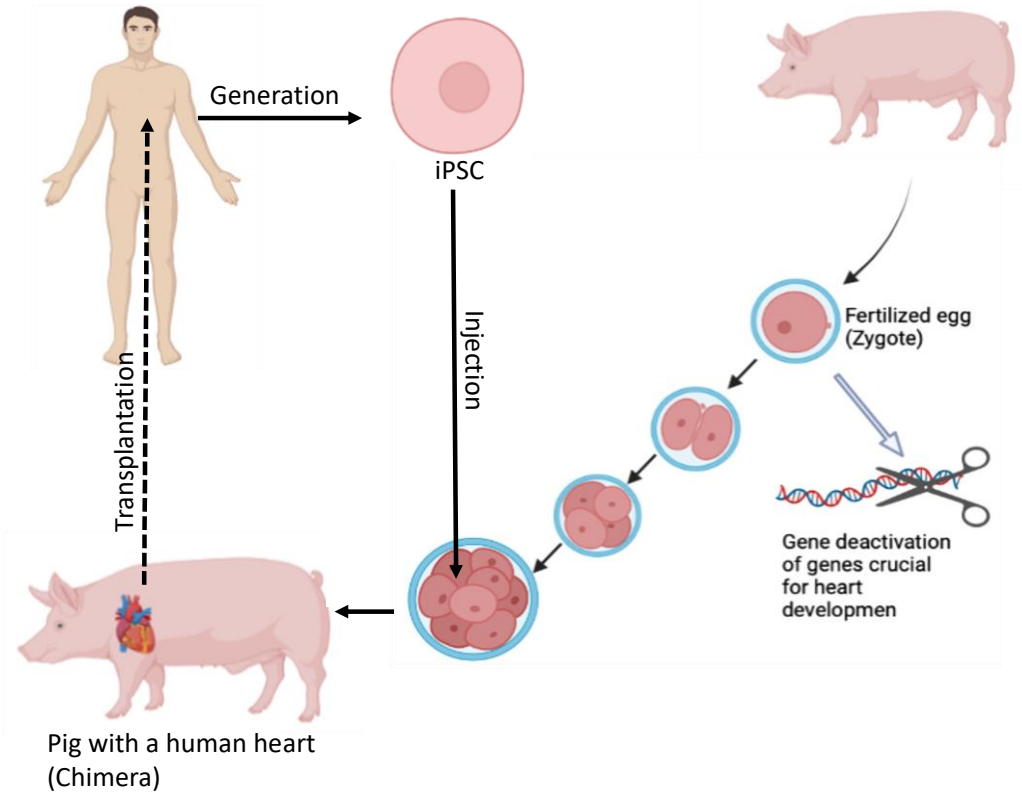

Figure 6: Concept of Organ Complementation.

Created with BioRender. The idea of organ complementation is to generate patient-derived iPSCs that are injected into genetically modified host animal blastocysts to grow human organs for transplantation purposes.

1.4. Genetic engineering using CRISPR-Cas9

CRISPR-Cas is one of the most influential molecular biotechnological inventions of the last decade. It´s a low-cost, highly efficient method for nucleic acid cleavage and can be used for genome editing in any species and cell type [71, 72].

The method is derived from the observation of the adaptive defense mechanism of prokaryotic cells. If bacteriophages, transposons, or plasmids invade prokaryotes, parts of their sequence get incorporated into the Clustered regulatory interspaced short palindromic repeats (CRISPR) array of the prokaryotic cell, yielding a new spacer sequence. That spacer sequence is transcribed into a precursor CRISPR RNA (pre-crRNA), matured into a guide RNA (gRNA), and in combination with a CRISPR associating Protein (Cas) will cleave the entered foreign sequence. The incorporation and memorization of these sequence in these CRISPR arrays of Prokaryotes are the foundation of the prokaryotic immune system [73].

Translation of this mechanism into the laboratory was optimized in the last years, and the direct introduction of a formed ribonucleoprotein complex (RNP) consisting of gRNA and Cas9, into cells, is the gold standard for CRISPR-Cas9-mediated DNA cleavage [72].
The CRISPR-Cas9 construct for DNA cleavage can be seen in *Figure 7.*

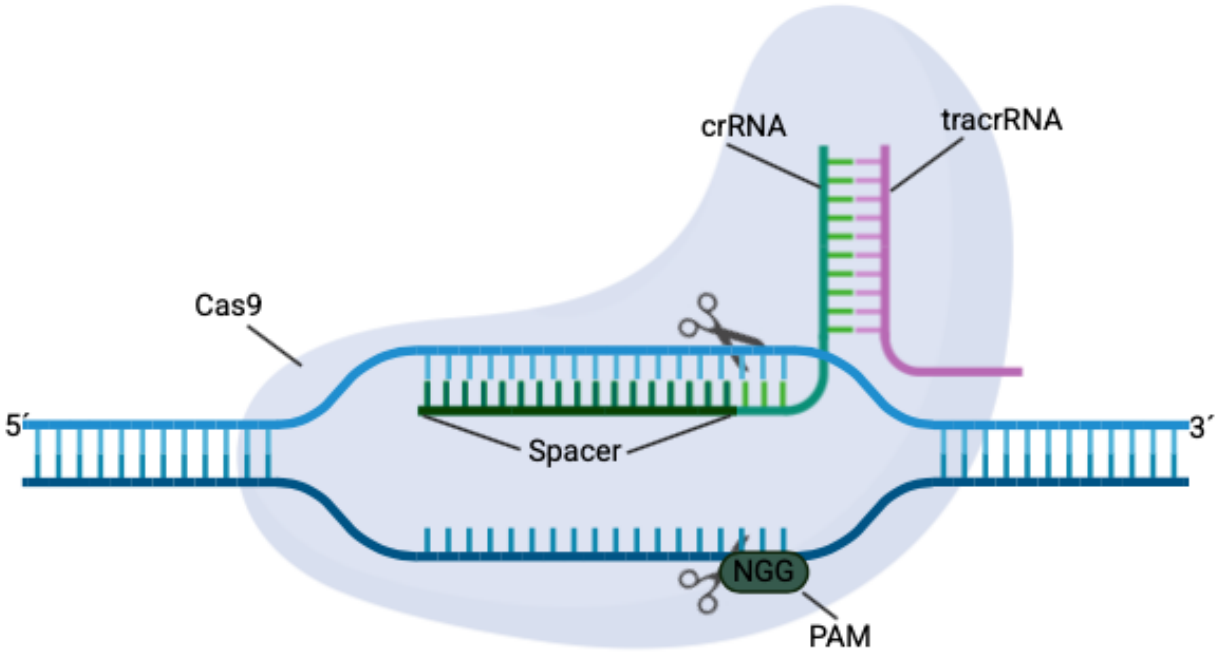

Figure 7: CRISPR/Cas9 alignment to genomic DNA.

Created with Bio-render.

CRISPR RNAs (crRNA), only limited by the PAM site and the specificity to the target gene, are bound to transactivating CRISPR RNA (tracrRNA) to form the guide RNA (gRNA) [72].
The PAM site is crucial for the binding of the Cas protein to the DNA, and consists of only three Nucleotides (nt), NGG for Cas9. The RNP complex is introduced into target cells, and the

target DNA is cleaved right before the PAM site, resulting in a double-strand break (DSB). The double-strand break is then repaired by the cell mechanisms through non-homologous end joining (NHEJ), homology-directed repair (HDR) [72, 74]. Mammalian cells have shown evidence of two more DSB repair mechanisms, microhomology-mediated end joining (MMEJ) and single-strand annealing (SSA) [74]. The efficient joining of unrelated DNA fragments by ligation, known as NHEJ, leads to random mutations, insertions, or deletions, causing frameshifts and resulting in the loss of function of that gene [72, 75]. NHEJ appears to be the dominant repair pathway in mammalian cells and is active throughout the whole cell cycle [75].

1.5. Scientific questions, aims, and strategic research plans

The overall goal of advancing regenerative medicine is to focus on three main projects, which are achieved by the following aims:

- Generation of an immune-evasive iPSC line for xenotransplantation purposes.
- Analysis of the feasibility of the magnetic targeting of cells in preparation for enhancing engraftment upon transplantation.
- Identifying key genes for emptying the cardiac niche, in preparation for cardiac organ complementation.

The first project focuses on the generation of hypoimmunogenic iPSCs for xenotransplantation purposes and aims towards modifying the surface of iPSCs in a way that immune reaction upon transplantation is evaded. For this, B2M and CIITA genes are knocked out, genes which are related to MHCI and MHCII complexes mediating the immune reaction between xenograft and T-cells of the host. At the same time CD47 surface receptor of the transplantation target animal is overexpressed, cloaking the cells from the host immune system's Macrophages and NK cells. The experimental plan (*Figure 8*) consists of a two-step modification plan.

Human iPSCs are the first nucleofector with CRISPR-RNPs to mediate the knock-out of two genes, B2M and CIITA. Single-cell clones are picked, colonies expanded, and cells verified for the genetic modification. Knock-out is confirmed with PCR, sanger sequencing and Next-Generation Sequencing (NGS). The functional absence of surface MHC complex is tested with an Interferon-γ assay, which normally induces the production of MHC proteins on the cell surface. A clone with a suitable knock-out result is picked and nucleofected with a plasmid for murine CD47. Single-cell clones are picked based on their positiveness for murine CD47 expression, verified with staining.

The second project focuses on the magnetic targeting of MSCs cells through intracellular loaded SPIONs and bio-linking Ferromagnetic particles. Here we want to show the feasibility of magnetic force-induced endocytosis, a method to load SPIONs intracellularly, is also possible in our lab, as well as introducing a novel method of magnetically targeting cells by bio-linking Ferromagnetic particles to surface receptors of cells. The ability of magnetically induced cell clumping is compared for both methods (*Figure 9*).

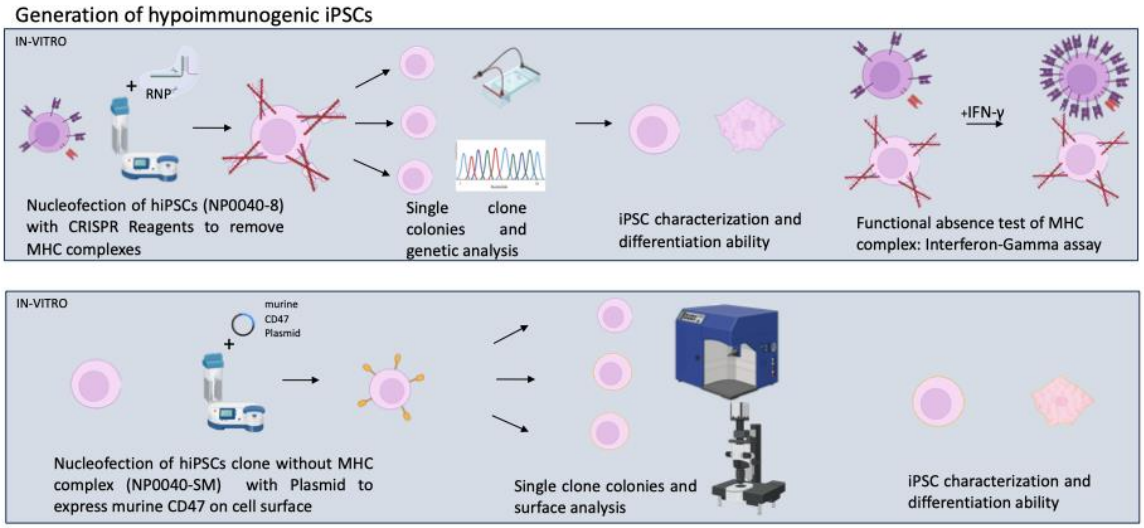

Figure 8: Experimental strategy for generation and quantity control of hypoimmunogenic iPSCs.

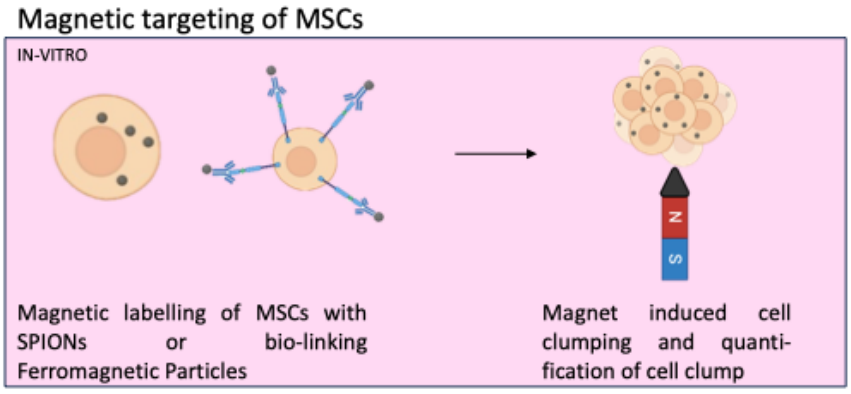

Figure 9: Experimental Plan for magnetic. targeting of cells.

The third project focuses on developing a strategy for Organ Complementation of the heart. We seek to deepen the knowledge of transcription factors that influence heart organ development and the question of whether we can identify key genetic factors for the complete depletion of the cardiac developmental niche. For this, we developed a new experimental strategy to observe the influence on organ development of lethal genes, where knock-out or knock-down models don´t exist. Various genes and their influence on cardiac organ development are observed by this new method of "*in-vivo* intra-embryonic complementation assay". Gene factors are deleted by CRISPR/Cas9 deletion.

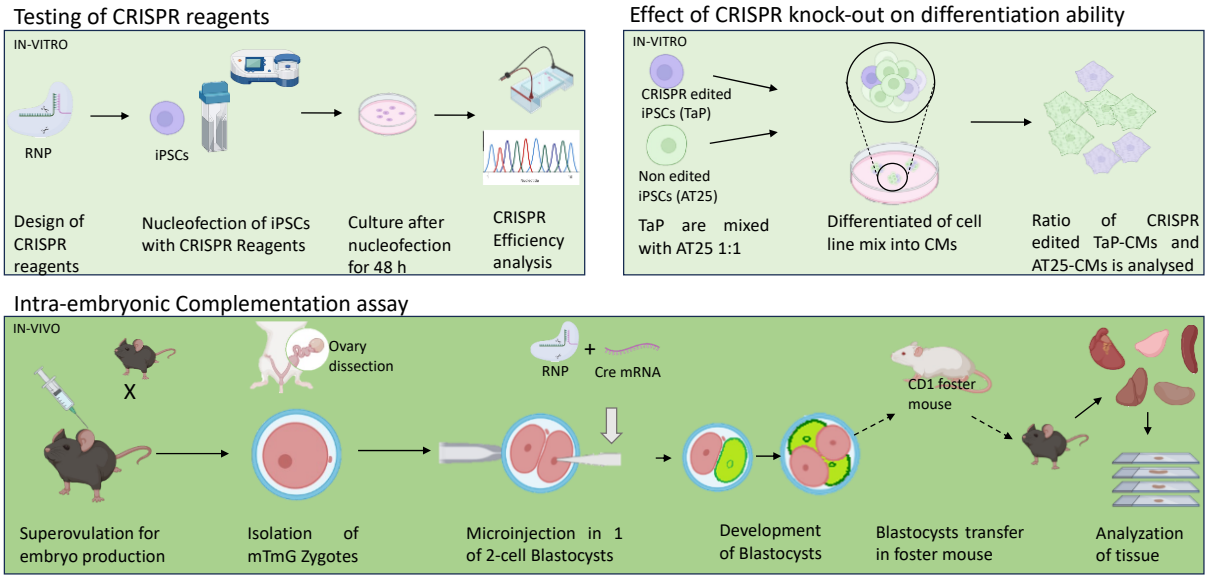

Figure 10: Experimental Plan Organ Complementation.

The experimental plan (*Figure 10*) includes in-vitro testing of designed CRISPR reagents, the influence of knock-out genes on differentiation ability, and finally the *in-vivo* intra-embryonic complementation assay.

For *in-vitro* testing of designed CRISPR reagents, murine iPSCs (cell line TaP) will be nucleofected with designed CRISPR reagents, and analyzed using Polymerase Chain Reaction (PCR), Gel electrophoresis, T7 Endonuclease I assay, and Sanger sequencing.

Nucleofected TaP cells are then mixed with AT25 cell line and differentiated to cardiomyocytes (CMs) to analyze the ratio of differentiated CMs to estimate the effect of CRISPR knock-out of genes on the differentiation ability of iPSCs to CMs.

Lastly, efficient CRISPR gRNAs are utilized in the intra-embryonic complementation assay. For this mTmG female mice are superovulated for embryo production, zygotes are isolated and develop to a 2-cell blastocyst stage. In one of the 2-cell blastocysts CRISPR-RNPs and Cre recombinase mRNA are injected and developed further, until being transferred into a pseudo-pregnant foster mouse. Due to genetic modification of mTmG mice, Cre recombinase injected cell, will induce a color switch from red to green surface fluorescence. Born offspring is analyzed for fluorescence red/green ratio. This three-step experimental plan is followed for each gene of interest.

2. Materials and Methods

2.1. Materials

Table 1: Chemicals and Reagents

Chemical/Reagent	Article no.	Supplier
0.4 % Trypan Blue Solution	15250061	Gibco
0.05% Trypsin/EDTA solution	25300-054	Gibco
1x TE Solution	11-05-01-05	IDT
1 kb DNA ladder, 200 µg	Y014.2	Carl-Roth
100 bp ladder	N0467S	New England Biolabs
2-mercaptoethanol (2-ME), 50 mM, 1000x	31350-010	Gibco
2-Methylbutan	3927.2	Carl Roth
5X Green GoTaq Reaction Buffer	M7911	Promega
50 bp DNA-Ladder	10416014	Thermo-Fischer
50x Tris-acetate-EDTA; TAE Buffer	CL86.1	Carl Roth
Agarose NEEO Ultra Qualität	232-731-8	Carl Roth
Alt-R CRISPR-Cas9 crRNA, 10nmol	Custom	IDT
Alt-R CRISPR-Cas9 tracrRNA	1072534	IDT
Alt-R S.p. Cas9 Nuclease V3	1081058	IDT
Alt-R Cas9 Electroporation Enhancer, 2 nmol	1075915	IDT
Alt-R Genome Editing Detection Kit	1075931	IDT
Amaxa mouse Embryonic Stem Cell Nucleofection kit	VPH-1001	Lonza
Ammonium acetate solution, 7.5 M	A2706-100ML	Sigma-Aldrich
B-27 Supplement Minus Insulin	A1895601	Gibco
bisBenzimid H 33342 trihydrochloride (Hoechst33342)	B2261-25MG	Sigma-Aldrich
Blasticidin HCl (10 mg/ml)	A1113903	Gibco
Bovine Serum Albumin (BSA)	A2153	Sigma-Aldrich
Carbondioxid Lab Gas		Linde
Citric acid	251275	Sigma-Aldrich
CHIR99021	C-6556	LC Laboratories
Cre recombinase mRNA	130-101-113	Stem Macs Miltenyi
Dimethyl sulfoxide (DMSO)	M6323.0100	Genaxxon bioscience
DNA/RNA Farbstoff, peqGreen	732-3196	VWR
DNEasy Blood and tissue kit	69504	Qiagen
desoxy Nukleosid-Tri-Phosphat; dNTP-Set 100mM	10297018	Invitrogen
Dulbecco´s Modified Eagle´s medium (DMEM), 1x, liquid, low glucose, with L-Glutamine, 1000 mg/L D-glucose, without sodium pyruvate	1188-5084	Gibco
Dulbecco´s Modified Eagle´s medium (DMEM), 1x, liquid, high glucose, with L-	31980-048	Gibco

Glutamine, 4500 mg/L D-glucose, without sodium pyruvate		
Dulbecco's Modified Eagle Medium (DMEM)/Nutrient Mixture F-12 (1:1) + GlutaMAX	10565018	Gibco
Dulbecco´s Phosphate buffered saline (D-PBS) without calcium and magnesium, 1x, liquid	14190-094	Gibco
Ethanol 96% (v/v)	603-002-00-5	Walter CMP GmbH & Co KG
Ethylenediaminetetraacetic Acid (EDTA)	E-4884	Sigma-Aldrich
Fast DNA ladder, 25 µg	N3238S	New England Biolabs
Fetal bovine serum (FBS)	F9665	Sigma-Aldrich
Ferrozine (3-(2-Pyridyl)-5,6-diphenyl-1,2,4-triazine-4′,4″-disulfonic acid sodium salt	82950-1G	Sigma-Aldrich
Fibroblast growth factor 2	100-18B	Peprotech
GoTag G2 Hot Start Polymerase	M7405	Promega
Heparin sodium salt	H3149	Sigma-Aldrich
Human Choriongonadotropin (hCG)		Ovogest
Human IFN- Gamma Recombinant Protein, PepoTech (IFN- γ)	300-02-100UG	Gibco
Hydrochloric acid, 37 wt. % in H2O, 99.999% trace metals basis	339253-100ML	Sigma-Aldrich
Hydroxylamine hydrochloride	431362-50G	Sigma-Aldrich
Hydroxide solution (8 M)	72068-100ML	Sigma-Aldrich
ImmersolTM 518 F	090428	Carl Zeiss
Insulin (“Humalog 100I.E.”)		Lilly
Iscove´s Modified Eagle´s Medium, high glucose, with GlutaMAX	31980022	Gibco
Iron Standard for ICP	43149-100ML-F	Sigma-Aldrich
IWP2	3533	Tocris
L-ascorbic acid phosphate magnesium n-hydrate	013-12061	Wako Chemicals Europe
L-Glutamine	A2916801	Gibco
Leukemia Inhibitor Factor from mouse	L5158	Sigma-Aldrich
Liquid Nitrogen (LN2)		Linde
M2 Medium	M7167-50ML	Sigma-Aldrich
Matrigel Matrix (hESC-qualified)	734-1440	Corning
MycoAlert Mycoplasma Detection Kit	LT07-318	Lonza
Non-essential amino acids (NEAA), 100X, liquid	11140-035	Gibco
Nuclease-free H_2O, 1 l	11-05-01-04	IDT
Opti-MEM reduced serum Medium	31985062	Gibco
Paraformaldehyde (PFA)	158127-100G	Sigma-Aldrich

PeqGreen DNA/RNA Dye	37-5010	PeqLab
Penicillin–Streptomycin Solution	15140122	Gibco
Pregnant Mare Serum Gonadotropin (PMSG)		Ovogest
Primers (Standard DNA Oligos 25 nmole Sythesis Scale)	custom	ThermoFischer
PureLink PCR Purification Kit	K310001	Invitrogen
ProLong gold anti-fade reagent	P36930	Thermo Fisher Scientific
Proteinase K, 800 units/ml	P8107S	New England Bio Labs
Puromycin-Dihydrochlorid	A1113803	Gibco
ReLeSR	100-0483	Stemcell Technologies
RNaseZap RNase decontamination solution	AM9780	Thermo Fisher Scientific
RPMI 1640 Medium	11875093	Gibco
Sodium hydroxide solution	72068-100ML	Sigma-Aldrich
Sodium selenite	S5261	Sigma-Aldrich
Tissue-Tek® FSC22 Blue Frozen Section Compound	3801481	Surgipath
Transferrin	T3705	Sigma-Aldrich
Transforming growth factor β	100-21	Peprotech
Tris-HCl, 1M pH8.0	648314	Millipore
Tris-acetat-EDTA buffer (TAE) 50x	CL86.1	Carl Roth
Triton-X 100	85111	Thermo Fisher Scientific
Trypan Blue Solution, 0.4%	15250061	Gibco
Tween20	8.22184	Sigma-Aldrich
QuickExtract DNA Extraction Solution	QE09050	Lucigen
XAV939	X3004	Sigma-Aldrich
Y27632 Rho kinase (ROCK) inhibitor	A11001-5	Adooq

Table 2: List of Laboratory Consumables

Consumable name	**Article No**	**Supplier**
6-well culture plate CELLSTAR®	657160	Greiner Bio-One
8-tube strip with flat attached caps	AB2000	Thermo Fisher Scientific
10 µl pipette tips	4042-DV	Discovery comfort
15ml sterile centrifuge tubes	188271-N	Greiner Bio-One
50ml sterile centrifuge tubes	227261	Greiner Bio-One
100 µl pipette tips	4045-DV	Discovery comfort
1000 µl pipette tips	4049-DV	Discovery comfort
Aluminum Foil 99.99% (Metallbasis)	040760.HP	Thermo Fisher Scientific
Coverslips thickness 1, round 12 mm	P231.1	Carl-Roth
EASYstrainer 40 µm	542040	Greiner Bio-One
EASY strainer 100 µm	542000	Greiner Bio-One
ibidi 8-well confocal dish	80827	ibidi
Microscope slides 76 x 76 x 1mm	0810000	Mareinfeld

Mix2Seq Sequencing kit	-	Eurofins
Needles (27 G x ¾ BD)	9816174B	Braun
Nunc cryotubes vials	375418	Thermo Fisher Scientific
Petri Dish 94 x 16 with vents	633180	Greiner Bio-One
SafeSeal reaction tubes 1.5 ml, PP, PCR Performance Tested, Low DNA-binding	72.706.700	Sarstedt
Serologic Plastic pipettes 5 ml	2081674K	Greiner Bio-One
Serologic Plastic pipettes 10 ml	2081674M	Greiner Bio-One
Serologic Plastic pipettes 25 ml	2081674P	Greiner Bio-One
Serologic Plastic pipettes 50 ml	2081674Q	Greiner Bio-One
Sterile Pasteur pipette for suction	612-1701	VWR
Square dishes 120 x 120x 17 mm	688102	Greiner Bio-One
Tissue culture dish 100 x 20 mm	833902	Sarstedt
Tissue culture dish 35 x 10 mm	353001	Falcon
Tissue culture dish 60 x 15 mm	353002	Falcon
Tissue Tek Cryomold	32663	Sakura
Syringe Omnifix, 100 I.U. 1 ml	9161708V	Braun
Sterile injection filter Sterifix 0,2 µm	4099206	Braun

Table 3: Designed crRNA for CRISPR Experiments

crRNA Name	**Sequence**	**PAM**	**Additional Information**
B2M-Deuse-crRNA	CGTGAGTAAACCTGAATCTT	TGG	Deuse et al. [34]
B2M-Lisa-crRNA	AAGTCAACTTCAATGTCGGA	TGG	Designed with ChopChop
CIITA-Deuse-crRNA	GATATTGGCATAAGCCTCCC	TGG	Deuse et al. [34]
CIITA-Lisa-crRNA	TCAACTGCGACCAGTTCAGC	AGG	Designed with ChopChop
Nkx2-5_crRNA-1	CTACCCCAGCTACGGCGGCG	CGG	Designed with ChopChop
Nkx2-5_crRNA-2	CACGCCGTAGGCGGGAGCGT	AGG	Designed with ChopChop
Nkx2-5_crRNA-3	CTGGACAAAGCCGAGACGGA	TGG	*Predesigned IDT Design ID: Mm.Cas9.NKX2-5.1.AF
Hand1_crRNA-1	CCGCTCCTGGTGGCAACGCG	AGG	Designed with ChopChop
Hand1_crRNA-2	TAGGTGGTGGCCCGCCGGCA	GGG	Designed with ChopChop
Hand1_crRNA-3	CTCCACGAACCCTTCCTGTT	TGG	*Predesigned IDT Design ID: Mm.Cas9.HAND1.1.AF
Hand2_crRNA-1	CGGGCGGCACTCCCCCATAA	TGG	Designed with ChopChop
Hand2_crRNA-2	GCGCCGCTCCTTGCGGTTGG	CGG	Designed with ChopChop
Hand2_crRNA-3	AGAACCCCTACTTCCACGGC	TGG	*Predesigned IDT Design ID: Mm.Cas9.HAND2.1.AD
Tbx5_crRNA-1	GTATCGGCCATGGTGCGCAG	GGG	Designed with ChopChop
Tbx5_crRNA-2	TATCACTCGGTACACGGCG	CGG	Designed with ChopChop

Tbx5_crRNA-3	CGAATCGCAAGACCTGTCTT	TGG	*Predesigned IDT Design ID: Mm.Cas9.TBX5.1.AB
Isl1_crRNA-1	CGATGTGGTACACCTTAGAG	CGG	Designed with ChopChop
Isl1_crRNA-2	AGACGAATTCGCCCTGCGGG	AGG	Designed with ChopChop
Isl1_crRNA-3	CCGTGCAGACCACGATGTGG	TGG	*Predesigned IDT Design ID: Mm.Cas9.ISL1.1.AC
Mesp1_crRNA-1	CAGACGCTGTTCCCATCGGA	AGG	Designed with ChopChop
Mesp1_crRNA-2	CAGACGGCCGGGCTTAAACG	GGG	Designed with ChopChop
Mesp1_crRNA-3	AGGACAACCTCCGGCGACAG	CGG	*Predesigned IDT Design ID: Mm.Cas9.MESP1.1.AB
SmarcD3_crRNA-1	ATGGCCGCGGACGAAGTTGC	CGG	Designed with ChopChop
SmarcD3_crRNA-2	GCACCGGACACCCACAACCC	AGG	*Predesigned IDT Design ID:Mm.Cas9.SMARCD3.1.AD
SmarcD3_crRNA-3	GGGTCCAATTTGAACTGGGG	AGG	*Predesigned IDT Design ID:Mm.Cas9.SMARCD3.1.AB
Pdx1_crRNA-1	CAGTGAGGAGCAGTACTACG	CGG	Designed with ChopChop
Pdx1_crRNA-2	GGACCCGTGCGCATTCCAGA	GGG	Designed with ChopChop
Pdx1_crRNA-3	GGCTCGGTTCCATTCGGGAA	AGG	*Predesigned IDT Design ID: Mm.Cas9.PDX1.1.AB

Table 4: List of PCR Primers

Primer Name	**Sequence**
B2M-h-3537-F	TGGGGCCAAATCATGTAGACTC
B2M-h-3748-F	TATTCTTCAAAATGGAGGTGGC
B2M-h-3818-F	GGAGAAATCGATGACCAAATGT
B2M-h-3987-F	TCCTGAATTGCTATGTGTCTGG
B2M-h-4145-R	TCAGTGGGGGTGAATTCAGTGT
B2M-h-4188-R	TGACAAAGTCACATGGTTCACA
B2M-h-4368-R	ATTCCCTGACAATCCCAATATG
CIITA-h-28996-F	CTGGGAGTTGTTGTAGGTGTCA
CIITA-h-29044-F	TGAGGTGACTGAGCATTGTCTT
CIITA-h-29134-F	CTTAACAGCGATGCTGACCCC
CIITA-h-29269-F	CTTGCTGTAGAGACGGCAATC
CIITA-h-29505-F	GTTGTGTGACATGGAAGGTGAT
CIITA-h-29627-R	GATATTGACAAGTGGCAGCAAA
CIITA-h-29741-R	TGGCCTCCATCTCCCCTCTCTT
CIITA-h-29768-R	ATTAGTGAAGGGGCCTATTTCC
Nkx-5250-F	CAGAGTGATACTCCCTGCCAC
Nkx-5565-F	CCAGAACCGTCGCTACAAGT
Nkx-5373-F	ACTTCGTGAACTTTGGCGTC
Nkx-5588-R	TTGCACTTGTAGCGACGGTT
Nkx-6022-R	CGCCCTTCTCCTAAAGGTGG

Nkx-6203-R	CGGTCCTAGTGTGGAATCCG
Hand1-184-F	GCCTACAGAAACCTTCAAGAGG
Hand1-385-F	ACATCATCACCATCATCACCAC
Hand1-671-R	CTCTCCTTCTTGGGTCCTGAG
Hand1-876-R	CACCATCCGTCTTTTTGAGTTC
Hand1-973-R	GTTTGCAGGCCTGTTCTTACTT
Hand2-405-F	CGAGGTAGCTCCACGCTAAG
Hand2-913-F	ACGGAAGGCGAGATGAGTC
Hand2-964-F	ACCATGAGGGCTACCCATTc
Hand2-1118-R	CTGTAGGACAGGGCCATACTGT
Hand2-1339-R	TGATCTTGGAGAGTTTGGTGTC
Hand2-1497-R	CGATCCCTTAGTACTGACCAGC
Tbx5-40113-F	GGCTCTTCCAGGAGTTCAGAC
Tbx5-40313-F	CTTGTCCCCTATGTCGCTAGAC
Tbx5-40557-R	CTTTTCTTACCTGCTGGGTGAA
Tbx5-40716-R	GATAAACGCCTCGATAAAGTGG
Tbx5-86690-F	ACTTCTCCGCTCATTTCACCT
Tbx5-86776-F	GATGTTTCAGCACCAGACCTC
Tbx5-87081-R	GGGGTTCTCATCACTACTGTCC
Isl1-4062-F	GCCCAACTTTGCTATTGCTATT
Isl1-4202-F	GTTCATTCAGGTTGTACGGGAT
Isl1-4243-F	ATAGGCTTCAGCAAGAACGACT
Isl1-4483-R	GTGGAGGAGTACCTGCCATTT
Isl1-4540-R	AGGTTGCAGGAAAGAAAGGTTA
Isl1-4566-R	ACTTTCTGCACCACTGTGTGAC
Mesp1-7-F	CACACCTAGGGCTCAGGATAAA
Mesp1-73-F	GCGAGCCGCGCTCCGAGT
Mesp1-95-F	AGTCCTGGATCCTGAGTCCC
Mesp1-337-R	GTGTGCGCATACGTAGCTTCTC
Mesp1-398-F	AGAACCTGACCAAGATCGAGAC
Mesp1-687-R	GGATGCTGTTTCTGCGTACAG
Mesp1-735-R	GTTACTAACCGGAGATGAGGGA
SmarcD3-22663-F	ACTCCGCTCGAGTAGAAGTGTG
SmarcD3-22851-R	CAAAAAGTTTGCTTTTCGTGG
SmarcD3-22935-R	ATCATCCCTCCATTCAGCC
SmarcD3-29345-F	GAAAGCCCTAGGCTCTACCAAT
SmarcD3-29366-F	TCCAGATGGGTCTGTGTGTAAC
SmarcD3-29568-R	AGTAGGAAGACAGTGGGGTCTG
SmarcD3-29608-R	GGAGGTTAGGGTCCTTAGCAGT
SmarcD3-29587-F	ACTGCTAAGGACCCTAACCTCC
SmarcD3-29775-R	GTCCTGTAGCCTGTTGGTCTTC
SmarcD3-29807-R	TCCGTTACCTGCTGGAAATACT
Pdx1-14-F	AGGAGAGCAGTGGAGAACTGTC
Pdx1-141-F	CCATGAACAGTGAGGAGCAGTA
Pdx1-598-R	CCAAGTCCAGACTAGGGAAAGA

CECAD-31-tg-R	TCAATGGGCGGGGGTCGTT
CECAD-32-wt-R	CGAGGCGGATCACAAGCAATA
CECAD-31-F	CTCTGCTGCCTCCTGGCTTCT

Table 5: List of Fluorophore-conjugated Antibodies

Antibody name	**Conjugate**	**Order number**	**Supplier**
α-Actinin (Sarcomeric) Antibody, anti-human/mouse/rat, REAfinity	PE	130-106-996	Miltenyi
Cardiac Troponin T Antibody, anti-human/mouse/rat, REAfinity	FITC	130-119-575	Miltenyi
CD31 Antibody, anti-human, REAfinity	APC	130-110-670	Miltenyi
MLC2a Antibody, anti-human/mouse/rat, REAfinity	APC	130-118-674	Miltenyi
MLC2v Antibody, anti-human/mouse/rat, REAfinity	PE	130-119-680	Miltenyi
Anti-CD29-Biotin	Biotin	130-101-943	Miltenyi
CD47 mouse-Biotin	Biotin	130-101-959	Miltenyi
CD47 Antibody, anti-mouse, REAfinity	APC	130-103-111	Miltenyi

Table 6: List of Primary Antibodies

Antibody name	**Order number**	**Supplier**
alpha-Actinin (ACTN2) Polyclonal Antibody	A7811	Sigma-Aldrich
Cardiac Troponin T antibody, rabbit	AB45932	Abcam
HLA ABC Antibody (W6/32), Mouse	NB100-64775	Novus BioTec
Oct3/4, mouse	SC-5279	Santa Cruz Technology
SSEA4, mouse, 200 µg/ml	SC-21704	Santa Cruz Technology
Tra1-81, mouse	SC-21706	Santa Cruz Technology

Table 7: List of Secondary Antibodies

Antibody name	**Order number**	**Supplier**
AlexaFl488, goat-anti-mouse-IgG	A11001	Invitrogen
AlexaFl488, Streptavidin	405235	BioLegend
AlexaFl555, goat-anti-mouse-IgM	A21426	Invitrogen
AlexaFl647, goat-anti-mouse, IgG	A21235	Invitrogen

Table 8: List of Laboratory Instruments and equipment

Instrument/Equipment	**Producer**
Aluminium digital heat block	VWR
Amaxa Nucleofector II Device	Lonza
Biosystem Kryostate CM3050S	Leica
BioTek Epoch Microplate Spectrophotometer	BioTek
Cellometer Vision	Nexcelom Bioscience
Centrifuge	
FACS Canto II	BD
FastGene Blue/Green GelPic LED Box, Gel imaging box	Nippon genetics
FastGene Ultra Cycler Gradient, Thermocycler, FG-TC01	Nippon genetics
Feinwaage	Sartorius
Fluoreszenz DIC Phasenkontrast Inverses Mikroskop	Carl Zeiss AG
Fridge	
Freezer -20 °C	Liebherr-International AG
Freezer -80°C VWR40086FV	Thermo Fisher Scientific
Hemocytometer - Neubauer	Marienfeld
Hitzesterilisator kelvitronRt	Heraeus,
Incubator, A11001	Invitrogen
Invertiertes Zell-Phasenkontrastmikroskop,	Carl Zeiss AG
Axiovert 40C	
Isotherm, Dewar vessel, Typ B	KGW Isotherm
Liquid nitrogen tank for cell storage	
Magnetfeldmessgerat, MP-200	List-Magnetik GmbH
Magnet with conic iron tip	Scientific Workshop UKK
Microscope, A21426	Invitrogen
Multi-Shaker, NB-T101MT	N-Biotek,
Mr. Frosty Gefrierbehält	Thermo Fisher Scientific
NanoDrop 1000 Spectrophotometer	PeqLab
Pipette controller	Brand
Pipette 10µl	Discovery comfort
Pipette 100µl	Discovery comfort
Pipette 1000µl	Discovery comfort
Plate Magent	Scientific Workshop UKK
Stellaris 5, Cofocal Microscope	Leica
Table top centrifuge, Mini star	VWR
ThermoMixer F1.5	Eppendorf
Tischautoklav, DX200	Systec GmbH & Co. KG
Tissue Tek Cryo Mold for freezing, Standard	Sakura
Ultraschallreinigungsgerat	Elma Schmidbauer GmbH
Vacuum desiccator, VC900	KNF
Vortex Genie 2	Scientific Industries SI
Warme und Trockenschrank, T 6120	Heraeus
Water Bath Type 1003	GFL

Table 9: List of Software

Name of Software	Version	Supplier
AxioVision	4.8	Carl Zeiss Microscopy
BioEdit	7.7	Tom Hall
BioRender	-	BioRender
BioTek Gen5 Software for Detection	2.5.0	Agilent
Cellometer Vision	V 3.0.0.9	Nexcelon Bioscience LLC
ChopChop	3.0.0.	[76]
CorelDRAW Graphics Suite	26	Corel
Endnote	20.0.1	Carivate
FACSDiva Software	V6.1.3	BD Biosciences
FlowJo	7.6	BD Biosciences
GeneiousPrime	2025.0	Dotmatics
GeneMarker	3.0.1.	Softgenetics
GraphPad Prism	10.6.1	GraphPad Software, Inc.
LasX	4.5.0.25531	Leica
Microsoft Excel	2405	Microsoft Corporation
Microsoft Word	2405	Microsoft Corporation
Microsoft PowerPoint	2024	Microsoft Corporation
NanoDrop 1000	V3.8	Thermo Fischer Scientific
Synthegos ICE tool	-	Synthego
Python based Relational Animal Tracking (PyRAT)	v5.0.0-732-g6a87d23a5d	Scionics
Primer-BLAST	Online-tool	NIH

2.2. Molecular Biology Methods

All molecular laboratory work was carried out on the bench top. Bench top and equipment were cleaned regularly with 70% Ethanol (Walter CMP GmbH & Co KG) and RNase-Zap (Thermo Fischer Scientific) to remove cross-contamination risks and RNases. CRISPR reagents were prepared in the sterile workbench in the cell culture laboratory, as CRISPR experiments were applied to cells.

2.2.1. CRISPR-Cas9-mediated gene knock-out using Ribonucleoprotein complex

CRISPR RNAs (crRNA) designs for gene knock-out were planned using online tools, like Integrated DNA Technologies (IDT) crRNA design tool, Chop-Chop (https://chopchop.cbu.uib.no/), Synthego (https://www.synthego.com/) and CRISPOR (https://crispor.gi.ucsc.edu/). The genome sequence for each gene of interest was downloaded on the National center for Biotechnology Information (NCBI) homepage (https://www.ncbi.nlm.nih.gov/) as a genbank file. Analyzation of the sequence was done in BioEdit (Tom Hall) while automatically annotate the Coding Sequence (CDS) information from GenBank feature files. Possible gRNAs were selected based on their PAM-site, location on the Coding Sequence, on-target/off-target score, GC-content, following sequence after PAM site, and secondary structure of the gRNA.

Custom designed crRNAs (IDT) were prepared following Max-Planck Institute for Biology of Aging SOP (see Appendix II.a). crRNA was dissolved in 1x TE Solution (IDT) to a stock concentration of 400 µM. Transactivation RNA (tracrRNA) (IDT) was also dissolved in 1x TE Solution to a stock concentration of 400 µM. An active gRNA with a stock concentration of 200 µM was annealed by adding crRNA and tracrRNA to in equimolar concentration, heating for 5 min at 95 °C in an aluminum block and slowly cooled down inside the aluminum block to room temperature. The slow quenching of the annealing reaction ensures correct folding of the gRNA. Annealed gRNA and dissolved crRNA and tracrRNA were aliquoted into single use volumes and stored in -80 °C for long term storage.

The ribonucleoprotein complex (RNP) was formed by adding 200 µM gRNA, 62 µM Cas9 Nuclease V3 (IDT) and 1x TE Solution together and incubate in the fridge overnight.

2.2.1.1. Nucleofection of RNP in-vitro into iPSCs

For transfection of iPSCs the Amaxa mouse Embryonic Stem Cell Nucleofection kit (Lonza) and the Amaxa Nucleofector II Device (Lonza) were used. The supplied reagents of the kit were mixed with the RNP complex and an Electroporation Enhancer (IDT). The mixture was incubated under the bench for 5 min. iPS cells were nucleofected with a final concentration of

0.5 µM Cas9, 5.5 µM gRNA and 0.9 µM EP Enhancer using the program A030 or A023 for murine iPSCs and program B016 for human iPSCs.

2.2.1.2. Microinjection of RNP and Cre Recombinase mRNA

For microinjection of CRISPR reagents into mouse zygotes, a final concentration of 0.2 µM Cas9 and 6.4 µM gRNA was prepared the day before injection following the CRISPR-Cas9 preparation protocol supplied by the Transgenic core facility of the Max Plank Institute for Biology of Aging (see Appendix II.a). On day for micro-injection, Cre Recombinase mRNA is added to a final concentration of 2 nM into the RNP mix.

2.2.2. DNA Isolation

DNA was isolated from cells or mouse tissue. For DNA Extraction the QuickExtract DNA Extration Solution (Lucigen) or DNEasy Blood and tissue kit (Qiagen) was used following the manual of the supplier. In brief, for the Lucigen QuickExtract DNA Extration Solution, the cell suspension with up to 10^4 cells was spun down in a centrifuge using 160 xg (=1000 rpm), the supernatant was aspirated and the cell pellet was re-suspended in 500 µl Solution. The extraction procedure consists of two incubation steps, first 6 min incaution at 65 °C, followed by a 2 min incubation at 98 °C. DNA Isolation with the DNEasy Blood and tissue kit from Qiagen is a silica-membrane based procedure and was used for isolating DNA from cell pellets and from mouse tissue. First the sample is lysed by adding Proteinase K and incubating the sample at 56 °C, and then the sample is loaded onto the silica-membrane column to bind the DNA. After washing the membrane, to eliminate all contaminations such as proteins and divalent cations, the DNA was eluted from the membrane using water or kit supplied elution buffer 10 mM Tris-EDTA.

DNA concentration is measured with Nanodrop (PeqLab) at 260 nm wavelength and giving the Absorbance ratio of A_{260}/A_{280} to determine DNA purity. DNA concentration is calculated using Beer-Lambert law and given in ng/µl.

2.2.3. Polymerase Chain reaction (PCR)

Polymerase Chain Reaction (PCR) was set up using the GoTag G2 Hot Start Polymerase (Promega) and the 5X Green GoTaq Reaction Buffer (Promega). Polymerase was supplemented in PCR reaction to a final concentration of 1.0 units and PCR buffer at 1X. desoxy Nukleosid-Tri-Phosphat (dNPTs) (Invitrogen) were added to a concentration of 0.8 mM and custom Primers (Thermo Fischer Scientific) to a concentration of 0.5 µM each. The mix was diluted in Nuclease-free H_20 (IDT) and 0.2 µg DNA template was added, volume of DNA

extract depending on measured concentration of DNA. PCR reaction was usually set up as a Master Mix, combining all reagents without DNA, which was pipetted individually into PCR tubes and Master Mix was added on top to a final volume of 20 µl PCR mix/ sample.
Primer were designed using online tools like Chopchop or Primer-BLAST (NCBI) and named in a way that Gene, position of Primer in the gene locus and direction can be followed up quickly and amplicon size can be calculated from primer names by subtracting forward primer number from reverse primer number. Costume Primers were ordered as DNA Oligos 25 nmole synthesis scale and dissolved in 5 mM Tris, stored at 100 µM stock solution, diluted to 10 µM working solutions. A List of Primers for PCR amplification can be found in Table 4.
Standard PCR program for GoTaq HotStart Polymerase was set up in Thermocycler (Nippon Genetics) with an initial denaturation of 95 °C for 2 min. Afterwards PCR cycle started, usually running with 35x cycles. Each cycle consisted of denaturation at 95 °C for 30 sec, Primer annealing at 54-62 °C for 30 sec, and extension at 72 °C for 1-3 min. Primer annealing temperature was dependent on the Primer composition and Extension time was dependent on the amplicon size. Last step of PCR program was final extension at 72 °C for 3 minutes.

2.2.4. Agarose Gel electrophoresis

The DNA fragments, amplified by PCR were analyzed using agarose gel electrophoresis. A 1% (w/v) Agarose gel was poured using Agarose NEEO Ultra Qualität (Carl Roth) dissolved in 1x Tris-acetate-EDTA (TAE) (Carl Roth) adding 0,05 µl peqGreen (VWR) per ml 1x TAE. The samples were run next to a Fast DNA, 50 bp or 500 bp DNA ladder, at 130 V for 30 – 60 min. For visualization, a LEDBox Gel imager (Nippon genetics) was used.

2.2.5. Genome editing detection with T7 Endonuclease I

Following the PCR the genome editing detection kit (IDT) was used for analyzing genomic cleaving. This kit was used only for analyzing PCR amplicons of a cell suspension 48 h after CRISPR experiment. Cell suspension, without picking single cell clones, were analyzed as a batch to determine whether DNA modification happened at all. This method was used to determine efficacy of gRNAs, and modifying efficacy before single cell clone picking. The genome editing detection was performed as described in the supplier protocol. In short, PCR products were denatured at 95 °C for 10 minutes and then reannealed by running two RAMP program, first from 95 °C to 85 °C with -2 °C/sec followed 85 °C to 25 °C with -0.3 °C/ sec. Afterwards the Endonuclease I was added and incubated at 37 °C for 1 hour. The samples were

visualized by running an agarose gel electrophoresis next to kit supplied positive and negative controls and visualization with Gel imager. Multiple Bands indicate DNA cleavage.

2.2.6. Sanger Sequencing

For Sanger sequencing PCR products were clean up using PureLink PCR Purification Kit (Invitrogen). Following the Kit instructions, 4 times volume of binding buffer that includes isopropanol, is mixed with 1 time volume of PCR product, added to the purification column, washed with ethanol and released from column using 10 mM Tris-HCl pH 8.5. This process of PCR product clean up removes primers, dNTPs, enzymes, and salts interfering with Sanger Sequencing.

Sanger sequencing is a method determining DNA sequence by using chain-terminating didesoxy nucleosid triphorsphat (ddNTPs) that are base-specific fluorescent labeled. In Sanger sequencing reaction ssDNA, sequencing Primer, Polymerase, dNTPS and ddNTPs are mixed. These ddNTPs are built in randomly and stop synthesis due to the missing OH-group. The DNA fragments of varying length are separated using capillary electrophoresis, and the last base of the fragment is identified by florescence markers of ddNTP. The position in DNA fragments is determined by fragment length and sequencing result is summarized in a DNA chromatogram. [77]

For Sanger sequencing Eurofins Mix2Seq is 5 µl of purified PCR product with a concentration of 5 ng/ µl was mixed with 5 µM sequencing Primer, added to a tube of the Mix2Seq kit (Eurofins), and send to Sanger Sequencing at Eurofins.

Samples were sequenced and raw data in chromatogram trace file (.ab1), Base Sequence (.fasta), and quality report (.pdf). Sanger sequencing results are analyzed by checking quality report and alignment of FASTA sequence to reference sequence using BioEdit (Tom Hall).

2.2.7. Inference of CRISPR Edits (ICE) tool

ICE tool is an open source tool (Synthego) for re-analyzation of sanger sequencing results.[78] Two chromatogram trace files, edited and non-edited sample, are quality controlled, aligned, trimmed around the CRISPR cut area and possible genotypes are being listed. A regression algorithm calculates the frequency of resulting genotypes, utilizing the weight of the regression model to determine possible genotypes and their frequencies. Output of the ICE tool is a trace file spanning the cut site in the control and edited sample, with the CRISPR-RNA being underlined in black. At the same time a discordance trace file, indel size and prevalence, referred to as indel percentage, and sequence calls and their prevalence are calculated and

shown. The Model fit (R^2) score and Pearson correlation coefficient (r) is computed. The editing efficiency is then assigned a "knock-out score", a score expressing the proportion of cells with either a frameshift or a indel of at least 21 bp. Editing efficiency can then be interpreted using the provided knock-out score and confirming the model fit using R^2. [78]

2.2.8. Next generation Sequencing

For Next Generation Sequencing (NGS) purified PCR product was handed over to Cologne Center for Genomics (CCG).

NGS is based on fragmentation of DNA, followed by attaching adapters to create a library and the amplification of the fragments. Sequencing happens during synthesis and the resulting short reads are assembled and annotated. Results were analyzed using Geneious Prime Software (Dotmatics).

2.2.9. Short Tandem Repeats (STR)

Short Tandem Repeats (STR) is a method based on analyzation of length variation in non-coding sequenced in the genome, used for identity profiling. [79] For STR analyzation pure isolated DNA was handed over to CCG. STR was run with GenePrint 24 System (Promega) and analyzed using Software GeneMarker (Softgenetics).

2.3. In-vitro experimental methods

All cell culture work was carried out in a sterile working bench environment. Before working sterile bench was cleaned with 70% ethanol and all labware and consumables entering the sterile work bench environment were disinfected as well, to prevent contamination of cell cultures.

Cell culture of different species were worked with, as well as primary cells and induced pluripotent stem cells (*Table 10*). Cells culture workflows of different cell lines was strictly separated and different cell lines were also stored separately in multiple humified incubators. Culture was observed daily under the phase contrast microscope to rule out contamination and long-term cultures were regularly checked for mycoplasma (MycoAlert, Lonza), a form of contamination that can not be observed under the microscope.

To prevent degradation of supplements over time and contamination of materials, reagents for cell culture were stored in single use aliquots and cell culture medium only prepared in batches of 50 ml (*Table 11*).

All cell lines were cultured on cell culture dishes, in different sizes (3.5 cm – 10 cm dish) and different coatings. Cell cultures were observed under microscope and regularly passaged to thin out culture and experiments were started during passage, when cells were released from plate and in single cell suspension. Released cells were stained with 0.4% Trypan blue (Gibco) and counted using Hemocytometer (Marienfield) to determine cell number per microliter (ml).
Cells were cryo-preserved and stored in liquid nitrogen for long-term storage. For this single cell suspension was mixed with freezing medium consisting of FBS with 20% DMSO and added to a cryovials and slowly cooled down in a Mr. Frosty (Thermo Fischer Scientific) in a -80 °C freezer ensuring -1 °C/minute. Cryovials were transferred to liquid nitrogen tank on the next day.

2.3.1. Cell lines and Culture medium

Table 10: Cell lines

Cell line name	Species	Cell type	Producer	Order number/ Specification
AT25 Rosa	Murine	iPSC	Tomo Šarić Group	Puromycin-N-acetyl transferase and eGFP are expressed under alpha-myosin heavy chain promotor
HSM47M	Human	iPSC	Lisa Münchhalfen	CRISPR/Cas9 mediated knock-out of B2M and CIITA + overexpression of murine CD47 through plasmid
NP0040-8	Human	iPSC	Tomo Šarić Group	https://hpscreg.eu/ name: UKKi011-A
NP0040-SM	Human	iPSC	Lisa Münchhalfen	CRISPR/Cas9 mediated knock-out of B2M and CIITA
S129 mMSCs	Murine	Bone Marrow MSCs	Daniel Derichsweiler & Raja Sahito	Sahito et al. [35]
TaP clone 4	Murine	iPSC	Kurt Pfannkuche Group	Puromycin-N-acetyl transferase expressed under alpha-myosin heavy chain promotor

Table 11: Culture Medium

Medium Name	Supplements/Ingredients
15% DMEM low Glucose	DMEM low glucose (1 g/l) (Gibco) 15% (v/v) Fetal Bovine Serum (Sigma-Aldrich) 1x non-essential amino acids (Gibco) 100 µM 2- Mercaptoethanol (Gibco)
15% DMEM	DMEM high glucose (4.5 g/l) (Gibco) 15% (v/v) Fetal Bovine Serum (Sigma-Aldrich) 1x non-essential amino acids (Gibco) 100 µM 2- Mercaptoethanol (Gibco)
20% IMDM	IMDM (Gibco) 20% (v/v) Fetal Bovine Serum (Sigma-Aldrich) 1x non-essential amino acids (Gibco) 100 µM 2- Mercaptoethanol (Gibco)
E8 ++	DMEM / F12 (1:1) + GlutaMAX (Thermo Fisher Scientific) 64 µg/ml L-ascorbic acid phosphate magnesium n-hydrate (Wako Chemicals Europe) 20 µg/ml insulin (Lilly Deutschland GmbH) 5 µg/ml transferrin (Sigma-Aldrich) 14 ng/ml sodium selenite (Sigma-Aldrich) 100 ng/ml heparin sodium salt (Sigma-Aldrich) 100 ng/ml fibroblast growth factor 2 (Peprotech) 2 ng/ml transforming growth factor β (Peprotech)
RPMI differentiation medium	RPMI 1640 (Gibco) 1 x B27 supplement (Gibco) 50 µg/ml L-ascorbic acid phosphate magnesium n-hydrate (Wako Chemicals Europe)

2.3.2. Isolation of Primary mice mesenchymal stem cells

Primary murine bone marrow mesenchymal stem cells are isolated form femur of 6 week old mice. Mice are sacrificed by cervical dislocation and fur is cleaned with 70% Ethanol supplemented with 1x Pen/Strep (Gibco) to minimize Mycoplasma contamination. First the fur, skin and muscle tissue of the limbs were removed and the bones removed from the body. The bone was opened by cutting the edge off and the bone marrow was flushed out using 15%

DMEM low Glucose medium using a needle and syringe. The bone marrow is broken up by pipetting up and down slowly and passing through a 100 µm Easy strainer (Greiner Bio-One). Cells are plated on 10 cm culture dish without coating, relying on the ability of MSCs to adhere to plastic. Cells are cultured in 15% DMEM low Glucose medium and medium is changed for the first time after 4 h to remove other primary cells.

2.3.3. Culture of murine mesenchymal stem cells

MSCs were cultured at 37 °C with 5% CO_2 in a humidified incubator in 15% DMEM low Glucose medium (see *Table 11*). MSCs were sub-cultured after reaching 80-90% confluency using 0.05% Trypsin-EDTA solution (Gibco) seeding directly on a 10 cm cell culture dish in a seeding density of 0.8 x 10^4 cells /cm^2.

2.3.4. Propagation of undifferentiated murine iPSCs

Undifferentiated murine iPS cells are cultured following Fatima 2016 [80] and stored in the humidified incubator at 37°C, with 5% CO_2.

In short, murine iPSCs are cultured on mouse embryonic fibroblasts (MEFs), seeded on a 6 cm culture dish in a density of 3.2 x10^4 cells/cm^2 prepared on the day before sub-culturing. Cells are cultured in 15% DMEM culture medium (see *Table 11*). Cells are regulatory sub-cultured on Mondays, Wednesdays and Fridays, started by observing the culture dish under the light microscope, aspirating the old medium and washing with D-PBS. Dissociation of iPSCs was done by adding 0,05% Trypsin and incubating for 5 min at 37 °C. After incubation, Trypsin reaction was quenched by adding 15% DMEM, and dissociated iPSCs are collected from plate in a 15 ml Falcon tube. Centrifuge to separate cells from Trypsin and medium. The supernatant is aspirated and the cell pellet is re-suspended in 15% DMEM, counted using a hemacytometer, and a fixed number of cells, 0.4 x10^6 cells on Monday and Wednesday and 0.2 x10^6 cells on Fridays, are plated on a new MEFs plate in 15% DMEM culture medium adding 5000 U Leukemia inhibitor factor (LIF).

2.3.5. Propagation of undifferentiated human iPSCs

Human iPSCs NP0040-8 generated by Šarić group were used in the experiments. hiPSC line is registered (https://hpscreg.eu/) under the name UKKi011-A. NP0040-8 were cultured in E8 ++ medium and coated cell culture plates using 10 µg/cm^2 Matrigel Matrix incubated for one hour at room temperature. Cells are stored in a humidified incubator at 37°C, with 5% CO_2. Culturing is described in Hamad et. al 2019 [81]. In short, the old medium on a human iPSC culture dish

is aspirated, the culture is washed with D-PBS and cells are released from the dish using ReLeSR (Stemcell). 1 min after adding ReLeSR onto the plate, it is aspirated and the plate is further incubated for 3 more minutes at room temperature. To produce a homogenous cell culture, the dish is knocked against the cell culture bench, and re-suspended in 1 ml E8++ medium. 0.05–0.20 ml of hiPSC cluster suspension is transferred into a new 3.5 cm culture dish, coated with Matrigel and add 10 µM ROCK Inhibitor (Adooq). The culture dish is placed inside a humidified incubator at 37°C, with 5% CO2, medium is changed every day and cells are passaged every 3-4 days.

2.3.6. Differentiation of murine iPS cells into cardiomyocytes

Differentiation procedure is described in Fatima 2016 [80]. Following the enzymatic dissociation of murine iPSCs form culture dish, the cells are counted, and cardiac differentiation is started by seeding 1.0 x 10^6 iPSCs in 14 ml 20% IMDM on a 10 cm bacterial dish and supplemented with 100 µM Ascorbic acid (Wako Chemicals Europe). The dish is cultured for two days at 37 °C with continuous horizontal shaking inside a humidified incubator with 5% CO_2. On Day 2 the formed embryonic bodies are collected, counted, and plated in a density of 2000 EBs in 14 ml 20% IMDM supplemented with ascorbic acid in same concentration. The dish is cultured at 37 °C with continuous horizontal shaking inside a humidified incubator with 5% CO_2 for 7 more days without medium change in between. On day 9 of cardiac differentiation, the EBs are observed under the fluorescence microscope and checked for eGFP expression and spontaneous beating. Medium is changed to fresh 20% IMDM and selection with Puromycin is started in supplementing 8 µg/ml Puromycin (Gibco). On day 11 medium is changed again and EBs are selected with Puromycin again.

On day 14 the EBs are dissociated. For dissociation 0.05% Trypsin is added to collected EBs in a 15 ml falcon tube and incubating at 37 °C while shaking for 30 - 40 min. Reaction is quenched by adding 20% IMDM and further dissociating by pipetting. Cardiomyocytes are counted and analyzed.

2.3.7. Differentiation of human iPS cells into cardiomyocytes

Differentiation protocol for hiPSCs into Cardiomyocytes follows Hamad et al 2019 [81], which is an adapted version of Lian and colleagues published protocol from 2013 [82]. Single cells of human iPSCs are seeded in a density of 0.8-1.0 x10^5 cells/ cm^2 on 2 ml of E8++ medium supplemented with 10 µM ROCK inhibitor (Adooq). Medium is changed on the following day without supplementing ROCK inhibitor and differentiation is started when culture reaches 80%

confluency. Start of differentiation (Day 0) is determined by switching from E8++ culture medium to RPMI differentiation medium (see Table 11) and by supplementing 8 µM CHIR99021 (LC Laboratories) for exactly 24 hours, before switching back to just RPMI differentiation medium for the following 48 hours. On day 3 of differentiation only half of the old medium is removed from the dish and 1 ml of fresh RPMI differentiation medium is added, supplemented with 5 µM IWP2 (Tocris) and 5 µM XAV939 (Sigma-Aldrich). On day 5 medium is changed again, without adding supplements. On day 7 of differentiation, beating cells can be observed. Medium is regularly changed every 3 days and cells are released for differentiation on day 15 of differentiation.

For releasing cardiomyocytes from the plate, the culture dish is washed with D-PBS and 0.05% Trypsin-EDTA is added and incubated for 15 min at 37 °C inside the humidified incubator, with 5% CO_2. Trypsin reaction is quenched by adding FBS in equivalent volume. Single cell suspension is transferred to a falcon tube and spun down at 120 g (=1000 RPM). Cell pellet is re-suspended in D-PBS and cells are counted in 0.4% Trypan Blue and Hemacytometer. After counting cells are characterized by staining for immunostaining and flow cytometry.

2.3.8. Magnetic targeting of mesenchymal stem cells

Mesenchymal Stem cells (MSCs) are magnetically targeted following two strategies. First, is the intracellular loading of Superparamagnetic iron oxide nano particles (SPIONs), and second is the cell surface targeting bio-linking Ferromagnetic Particles through Antibodies to the cell surface.

2.3.8.1. Intracellular loading of superparamagnetic iron oxide nanoparticles (SPIONs)

SPIONs with a particle size of 15-17 nm, were made of Fe_2O_3 nanoparticles with a PEG coating. A separate batch of SPIONs with a PEG - 1,1'-Dioctadecyl-3,3,3',3'-Tetramethylindocarbocyaninperchlorat (Dil) coating, which can be detected at a wavelength of 546 nm, were produced in Research lab of Prof. Gang Bao at Rice University, Huston, Texas, USA. Production procedure is described in Zhang (2023)[46].

For loading MSCs with SPIONs, cells were co-incubated with 60 µg/ml SPIONs supplemented in 10% DMEM low glucose Medium overnight. The incubator was either done with a plate magnet under the culture dish for magnetic forced endocytosis (+MF) or without placing a magnet under the culture dish (-MF) inside humidify incubator with 37 °C and 5% CO_2 (*Figure 11*). Intracellular loading success was confirmed by fluorescence microscopy and ferrozine based quantification of iron concentration.

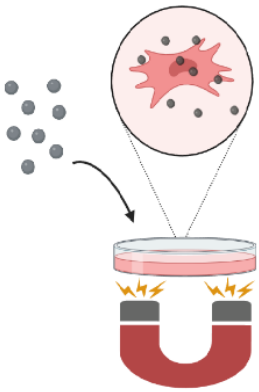

Figure 11: Concept of force mediated endocytosis of SPIONs into MSCs. Created with BioRender.

2.3.8.2. Cell surface magnetic targeting using anti-CD29

Ferromagnetic particles, with a diameter of 2 µm, were bio-linked to MSCs through the surface receptor Integrin beta-1. The expression of CD29 on the surface of mMSCs was determined with flow cytometry using anti- CD29-Biotin (Miltenyi) and secondary Streptavidin-AlexaFlour488 (BioLegend), antibody.

For magnetically targeting the mMSC cell surface, 0.25 x 10^6 mMSCs were firstly incubated 1:50 with anti-CD29 antibody conjugated with Biotin (Miltenyi) for 30 min at 4 °C, followed by incubation with 1:10 SPHERO Streptavidin Ferromagnetic Particles (Spherotech) and 1:1000 Hoechst 33342 (Thermo Fischer) for 30 min at 4 °C (*Figure 12*). With a Streptavidin-Alexa Flour 488 stain (BioLegend), the CD29 Biotin conjugated antibodies were visualized for Fluorescence microscopy.

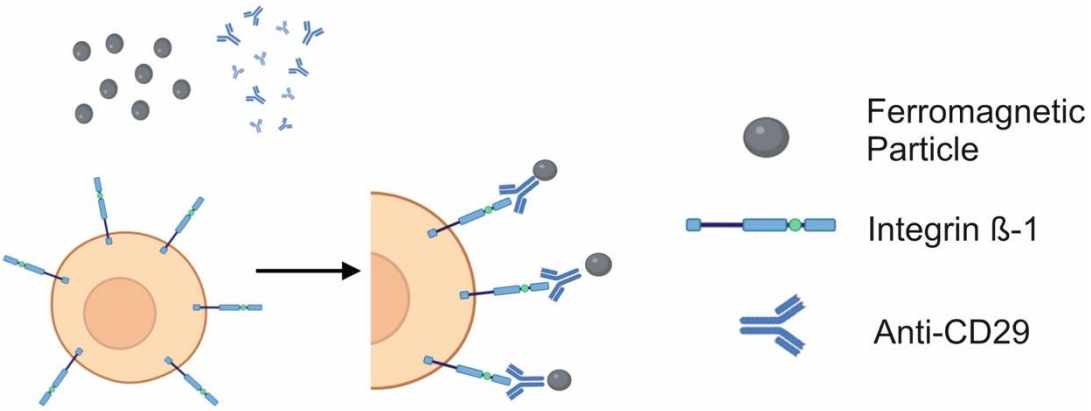

Figure 12: Concept of bio-linking Ferromagnetic Particles to surface receptor Integrin ß-1 of murine MSCs with Anti-CD29 antibody. Created with BioRender.

2.4. In-vivo experimental methods

2.4.1. Permission for animal experiments and animal housing

All animal experiments were conducted with permission by German authorities following laws for animal welfare (Genehmigung eines Versuchsvorhabens gemäß § 8 Abs. 1 Tierschutzgesetz), licensed under TV 81-02.04.2020.A200 by local authorities Landesamt für Natur, Umwelt und Verbraucherschutz Nordrhein-Westfalen (LANUV NRW).

Mice were housed in the decentralized animal house of the Medical Faculty Cologne in the Pharmacology Institute, following laws for animal welfare and animal facility guidelines. Mice were housed in individually ventilated cages (IVC), fed ad libitum, daily cared for by animal care taker of the facility, and managed though Python based Relational Animal Tracking (PyRAT) software.

2.4.2. Mouse strains

The mouse strain worked with in this project was STOCK Gt(ROSA)$^{26Sortm4(ACTB-tdTomato,-EGFP)Luo}$/J, also referred to as R26mTmG or just mTmG. Mice were kindly provided by Cologne Excellence Cluster for Aging and Aging-Associated Diseases (CECAD) animal facility. Generation of R26mTmG mice was published by Muzumdar and collegues in 2007 [83].

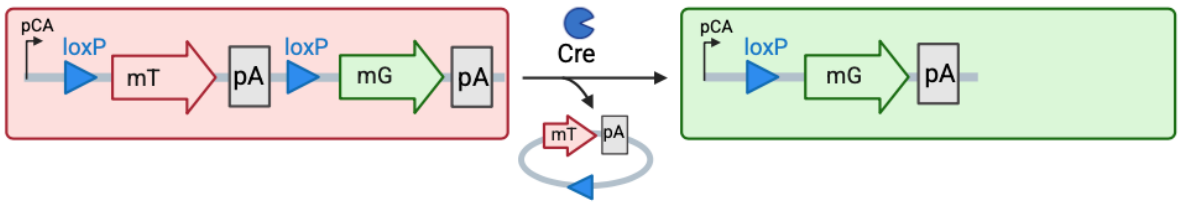

Figure 13: mTmG construct before and after Cre- recombination of R26mTmG mouse strain.

Figure modified based on Muzumdar 2007 [83], created with BioRender. A chicken b- actin core promoter with a CMV enhancer (pCA) is followed by a loxP sequence, membrane-targeted tandem dimer Tomato (mT) sequence, a polyadenylation (pA) sequences, a loxP Sequence, membrane-targeted enhanced green fluorescent protein (mG), and a polyadenylation (pA) sequence. Before Cre-Recobination all cell membranes fluorescent red. After Cre-mediated intra-chromosomal recombination, the mT+ pA sequence is excised allowing the pCA promoter expression of mG, all cells fluorescent green.

The mTmG refers to a cell membrane targeted expression of fluorescent proteins, Tomato (mT) and eGFP (mG). Both transgenes, followed by a polyadenylation sequence (pA) were inserted into the Rosa26 gen locus. The mT transgene is flanked by two loxP sites and can be conditionally removed by Cre-Recombinase. Removal of mT transgene and it´s pA sequence,

resolves in a membrane color switch from red to green, due to eGFP being expressed (*Figure 13*).

2.4.3. Mice breeding calculation and cross breeding to retain animal strain

mTmG mice were breed for strain maintenance and for experimental usage. For Intraembryonic complementation assay experiments 5-10 female mTmG mice in the age of 4 weeks are utilized. Mice were used for breeding starting from week 8 following SOP (Appendix II.c) and after approval of breeding calculation (Appendix l). With a litter size approximately 8 pubs and probability of 50% for the pubs sex being female, we calculated to set up 2 breeding's of female and male mice prior to experiment to produce 5-10 female mice. Mice breeding was set up in PyRat for permanent breeding, male and female mice are permanently in one cage, or 1. Generation breeding, where the male mice is removed once a vaginal plug is observed. Permanent breeding was set up in the beginning of this project and switched to 1. Generation breeding once the mice strain was established.

Later C57BL6/J mice were cross-breed into the C57BL6/J Rosa26 mTmG strain, to stabilize breeding results. C57BL6/J female mice were ordered from Charles River. Following Mendelian inheritance laws, homozygote male R26mTmG mice (tg) were breed with homozygote wildtype (wt) mice and first generation (F1) offspring was characterized by PCR to confirm law of uniformity, indicating heterozygote Rosa26 gen locus wt/tg. For PCR SOP for R26mTmG characterization from CECAD AG Niessen was applied (see II.d). F1 was then cross breed and second generation (F2) was also characterized by PCR to identify Individuals with homozygote mTmG transgene (tg/tg) following the Mendelian inheritance laws of segregation of genes [84].

Homozygote transgenic mTmG mice were then further breed for mice strain maintenance.

2.4.4. Superovulation of mouse females for embryo production and manipulation

Hormone injection to stimulate ovaries increasing the number of oocytes, and at the same time increasing the number of zygotes after mating, is a common practice for embryo production and manipulation. Following the Protocol provided by the Transgenic core facility of the Max Plank institute for Biology of aging (see II.e) female mice are administered two hormones before breeding with male mice.

First, 0.2 ml (5-10 units) of hormone solution PMGS (Ovogest) are injected intra-peritoneally, followed by a second injection 48 hours later of 0.2 ml (5-10 units) of hormone solution hCG (Ovogest). Important is the age of female mice of 4 weeks, so superovulation occurs before mice enter their biological cycle, which is harder to manipulate.

Male mice age is not as important and is adjusted to animal house guidelines, where mice can be used for breeding starting at week 8. Male mice are single housed 2 weeks before superovulation.

After second hormonal injection, females and male mice are mated 1:1 over night and plugged females are exported from animal house to Room 1007 Institute for Neurophysiology on the next day. Mice are painlessly killed by cervical dislocation, the ovaries, easily identified through swealing after hormonal injection, are removed from the fallopian tubes / the uterus and transferred to a tube of pre-warmed M2 medium. Isolated Ovaries are transferred to the Transgenic core facility of the Max-Planck-Institute for Biology of Ageing, where the zygotes are flushed out of the ovaries.

2.4.5. Intraembryonic Complementation assay: 2-cell embryo Microinjection Experiment

The isolated zygote is developed in an incubator overnight and 2-cell blastocysts are injected on the next day. For this the blastocysts is hold in place by a suction pipette while microinjecting RNP Complexes and Cre Recombinase mRNA into one of the cells pronucleus. Injected Blastocysts are embryo transferred into the uterus of a pseudo pregnant CD1 female mice, which was mated with a vasectomized male mouse.

For a control experiment only Cre mRNA was injected into one of the 2-cell embryo.

Injection of blastocysts was carried out by Ingo Voigt, head of the transgenic core facility (TCF) of the Max-Planck Institute AGE.

2.4.6. Mice dissection

4 week old transgenic mice of intra-embryonic complementation assay are killed by cervical dislocation and dissected following “Kückenthal” dissection guides [85].

Dissection is started by cutting open the skin on the ventral side, starting from the midline of the body, through a median incision forward to the angle of the lower jaw and then backward laterally past the clitoris or the tip of the penis. Secondly, the abdomen is opened by slightly lift the abdominal wall with forceps and cut open with scissors. Skin and abdominal wall can be fixed with needles to the side to fully open the abdominal cavity. With forceps carefully remove Liver, Spleen and Kidney to a D-PBS filled petri dish and wash away any excess blood. The abdominal cavity is separated from the thoracic cavity by muscular diaphragm. For opening the chest cavity, make an incision on each side from the sternum along the costal arch and fold back. Remove heart and Lung to the petri dish as well. Empty the heart of any excess blood

carefully by pressing on it with a forceps. Anatomical positions of organs in the mouse can be seen in *Figure 14*.

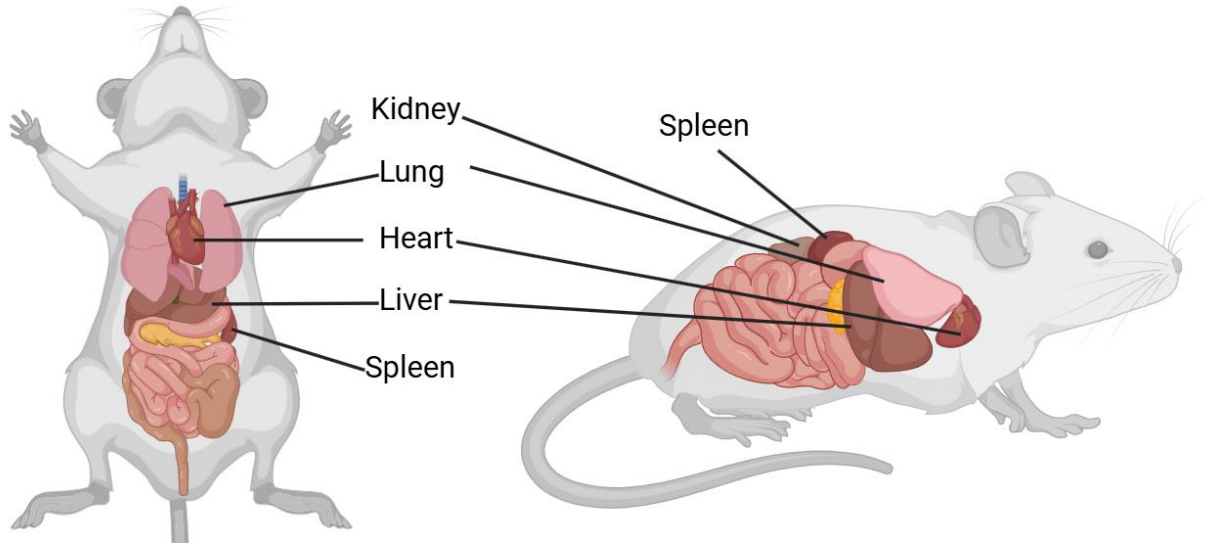

Figure 14: Position of Organs in a mouse. Ventral and side view.

Created with BioRender.

2.4.7. Cryopreservation and sectioning of Tissue

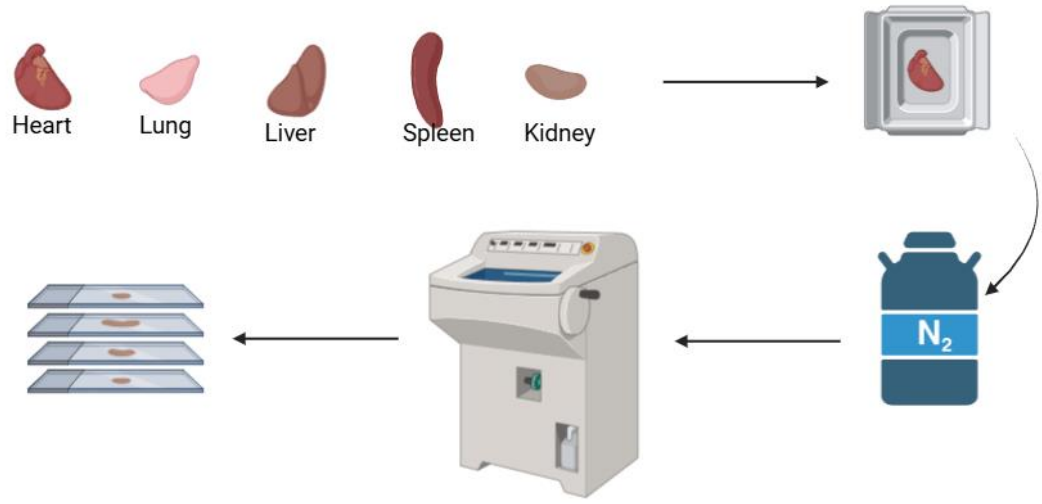

Figure 15: Procedure of cryo-preservation of tissue.

Created with BioRender.

Following dissection of mice, the removed Tissue is cryo preserved following the procedure described by Wu *et al.* (1985) [86], process can be seen in *Figure 15*. Tissue is placed in a tissue mold (Sakura) and embedded in Tissue Tek (Surgipath) ensuring complete and bubble free coverage. The mold is placed in a 2-Methylbutan (Carl Roth) filled vessel, which is cooled by liquid nitrogen (Linde). The cooled 2-Methylbutan has an estimated temperature of -150 °C,

which ensures a quick freezing procedure, but prevents tissue damage. The tissue of Rosa26 mTmG mice is not fixed in PFA prior to freezing, as fixation is denaturing the surface RFP and GFP proteins. Frozen tissue is covered with aluminum foil and place in a -80 °C freezer overnight. On the next day, tissue is moved to -20 °C for sectioning and long-term storage. Tissue samples embedded in Tissue Tek is removed from the mold and sectioned to 8 µm thickness on a cryostat. Sliced tissue is transferred to a glass slide and observed under a fluorescence microscope (Carl Zeiss AG).

2.5. Validation parameters

2.5.1. Cell characterization with Flow Cytometry (FC)

For characterization of cells, flow cytometry (FC) was used. Prior to FC analysis, cells were labeled with fluorescent antibodies targeting specific markers.

Released cells from cell culture were passed through a 40 µm easy strainer (Greiner Bio-One) and fixed in 4% PFA for 10 min at 4 °C. Cells were washed in D-PBS and if necessary, permeabilized with 0.5% Triton-X for 15 min at RT and washed again. FC receptors were blocked by incubating cells in 3% BSA for 15 min at 4 °C and finally cells were stained 1:50 with fluorophore-conjugated antibodies (see Table 5) in 0.5 mM EDTA for 30 min at 4 °C.

FC is based on detection and quantification of physical and fluorescent properties of individual cells passing through a laser beam. FACs Canto II (BD) and FACs Diva software were used for FC analyzation. Cells were measured by gating based on forward (FSC) and side scatter (SSC) to assess cell size and internal complexity respectively and exclude debris from detection. FSC against fluorescence plot was used to assess marker expression and determine stopping gate for measurement of 10,000 events. For multi-color staining, appropriate compensation control to correct spectral overlap between fluorochromes was applied. FC results were analyzed using FlowJo (BD).

2.5.2. Immunostaining for cell characterization

Immunostaining for different purposes was usually applied in a two-step staining procedure.

Dissociated Cells were either seeded on a coated round cover slip (Carl-Roth), that was placed inside a 12-well plate, on a coated ibidi 8-well confocal slide (ibidi), or cells were stained in suspension. Seeded cells were usually cultured 2-5 days to ensure confluency before starting immune staining procedure.

Staining procedure of seeded cells was started by fixing cells in 4% Para formaldehyde (PFA) for 10 minutes at 4 °C, followed by permeabilization with 0.5% Triton-X (Thermo Fischer Scientific) for 15 minutes at room temperature only when staining structures in the cytoplasm. The Primary antibody was diluted 1:200 added to the sample and incubated at 4 °C overnight. On the next day, cells were washed with D-PBS (Gibco), and secondary antibody was incubated with 1:800 for 2 hours at room temperature in the dark. At the same time Hoechst33342 (Sigma Aldrich), for staining cell nucleus, was applied.

For a quick staining procedure in suspension, cells were transferred to a 1.5 ml Eppendorf tube and were usually not fixed or permeabilized. Cell pellet was resuspended in primary antibody diluted 1:200 and stained for 30 min at 4 °C. After incubation of primary antibody (see Table 6), cells were washed in D-PBS and stained with secondary antibody (see Table 7) 1:800 for 30 min at 4 °C.

Stained cells were imaged using either florescence (Carl Zeiss AG) or confocal microscope (Stellaris 5, Leica).

2.5.3. Interferon-Gamma assay

hiPSCs were seeded on a 6-well plate in usual culture condition and colony density. 24 h after seeding, fresh medium was added containing either 20 ng/ml or 50 ng/ml of Human IFN-Gamma Recombinant Protein, PepoTech (IFN- γ) (Gibco) and was incubated for 48 h with the iPSCs. After 48 h cells were released from plate and stained for FC analyzation or immunostaining using HLA-A,B,C Antibody (Novus BioTec) (see Table 6) and secondary Antibody AlexaFlour488 (Invitrogen) (see Table 7).

2.5.4. Ferrozine based quantification of intracellular iron concentration

Ferrozine based quantification was assessed to determine iron concentration of cells, after loading them with SPIONs. Protocol was established in Prof. Gang Baos research group and SOP can be found in Appendix II.f. Cells that were co-incubated with SPIONs overnight, were washed multiple times with D-PBS to remove extracellular SPIONs and were released from plate. Then cells were counted using 0.4% Trypan Blue solution (Gibco) and hemacytometer, centrifuges at 300 g for 5 min, the liquid was removed and the cell pellet was vacuum dried overnight using vacuum desiccator (KNF).

On the next day 50 µL of HCl (37 wt. %) (Sigma-Aldrich) was added to the cell pellet and incubated for 1 h at 37 °C while shaking at 250 rpm. After incubation 70 µL of sodium hydroxide solution (8 M) (Sigma-Aldrich), 100 µL of ammonium acetate solution (4 M)

(Sigma-Aldrich), 100 µL of hydroxylamine hydrochloride solution (5%) (Sigma-Aldrich) was added, and vortex to mix well. The sample was diluted with 680 µl of distilled water, and incubated for 1 h at 37 °C while shaking with 250 rpm. The mixture was centrifuge at 21,000 g for 15 min and 40 µL of the supernatant is transferred to a 96-well plate. Iron standard (Sigma-Aldrich) was dissolved in water to a dilution series spanning from 0 – 500 µg/ml and was also treated with Ammonium acetat, hydroxylamine hydrochloride and H_2O. 60 µL of Ferrozine solution (0.1%) (Sigma-Aldrich) was added to each sample on the 96-well plate and mix carefully to form the ferrous-ferrozine complex. Absorbance was read at 562 nm using a Microplate Spectrophotometer (BioTek Epoch). Iron concentration was calculated though absorbance standard curve using Iron Standard.

2.5.5. Magnetically induced cell clumping and quantification

As a prove of concept for magnetic labelling of cells, cells were induced to clump using permanent magnet with conic iron tip.

Cells were magnetically labelled and tip magnet was placed under a cell culture dish, or Eppendorf tube containing these cells. Cell clump was observed under the microscope and quantified through DNA concentration. For this the formed clump was transferred to a new Eppendorf tube with a pipette, DNA was isolated as described before and cell number was calculated through linear equation of DNA concentration of fixed cell number.

3. Results

3.1. Generation of hypoimmunogenic hiPSC for xenotransplantation purposes

For overcoming immune reaction upon xenotransplantation, human iPSCs are modified by removing MHC class surface proteins via CRISPR /Cas9 mediated gene knock out and by overexpressing murine CD47 via transposon-mediated transgenesis.

3.1.1. Generation of MHC knock out humane iPSCs

Human iPSCs (cell line NP0040-8) were nucleofected with RNP complexes for mediating knock-out of MHC genes. B2M and CIITA were both targeted with two gRNAs in a double knock-out design, as using single gRNA in pre-test showed no editing results upon T7 Endonuclease I assay. Sequence of gRNAs can be found in Table 3 and of Primers in Table 4. An overview of the design strategy and position of Primers are summarized in *Figure 16.*

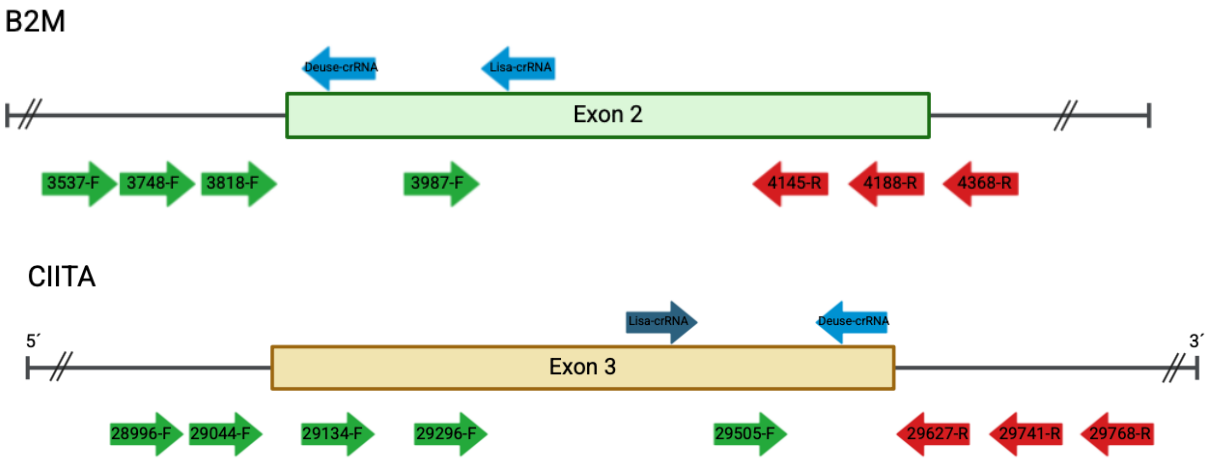

Figure 16: Genetic concept map displaying CRISPR design strategy for knock-out of human B2M and CIITA.

Created with BioRender. Forward (green arrows) and reverse Primers (red arrows) named after their starting position in gen, annotated from genbank file. Exons (box) and crRNA (blue arrows) are shown on top, color coded forward crRNA (dark blue) on Watson strand and reverse crRNA (light blue) on Crick strand.

NP0040-8 cells were nucleofected with all four RNPs at the same time, and after 2 days of culture, when cells were sub-cultured, excess cells were analyzed with T7Endonuclease I assay, to check for genetic modification. Two nucleofection batches, named NP0040-SM and NP00SM, were compared. For NP0040-SM multiple bands for both genes B2M and CIITA could be observed on a 1% Agarose gel run for 30 min at 130 V, indicating different fragment sizes of PCRs in the un-selected cell batch (*Figure 17*). NP0040-SM culture was continued, and 12 single cell clones were analyzed by isolating DNA, PCR and Sanger sequencing. First for B2M gene, promising B2M knock-out candidates ($B2M^{-/-}$) were then analyzed for modification in CIITA gen. Sanger sequencing results were aligned to reference sequence in BioEdit (Tom

Hall) and knock-out was analyzed by running pairwise alignment while allowing ends to slide (*Figure 18*).

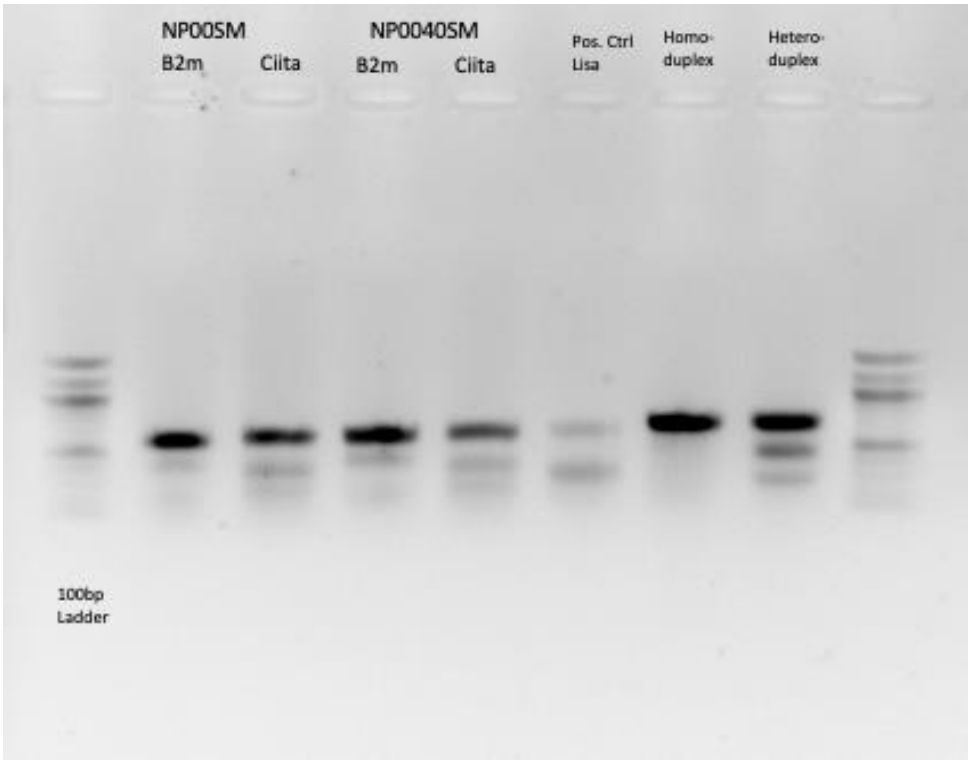

Figure 17: T7 Endonuclease I assay on two Nucleofection batches. NP0040-SM was continued in culture and single cell clones were picked.

Figure 18: Sanger Sequencing results of NP0040-SM clones 1-12 for B2M.

After sager sequencing, no clone with clearly assigned knock out areas could be found in multiple sequencing runs for each sample. For the most promising candidate NP0040-SM-Colony 9 sanger sequencing results were analyzed with ICE tool (Synthego). Due to the good

model fit R^2 and therefore a high probability of heterozygote knock-out in both genes for Colony 9, B2M with model fit 0.95 and CIITA with R^2 0.83 (see a), cells were analyzed with Next generation sequencing to confirm heterozygote knock-out (*Figure 19*). NGS confirmed a heterozygote knock out of B2M with a 18 bp and 27 bp deletion, respectively, while CIITA was confirmed with a 15 bp and 57 bp deletion. NP0040-SM (Colony 9) a $B2M^{-/-}$ $CIITA^{-/-}$ hiPSC line, was characterized and used for murine CD47 overexpression.

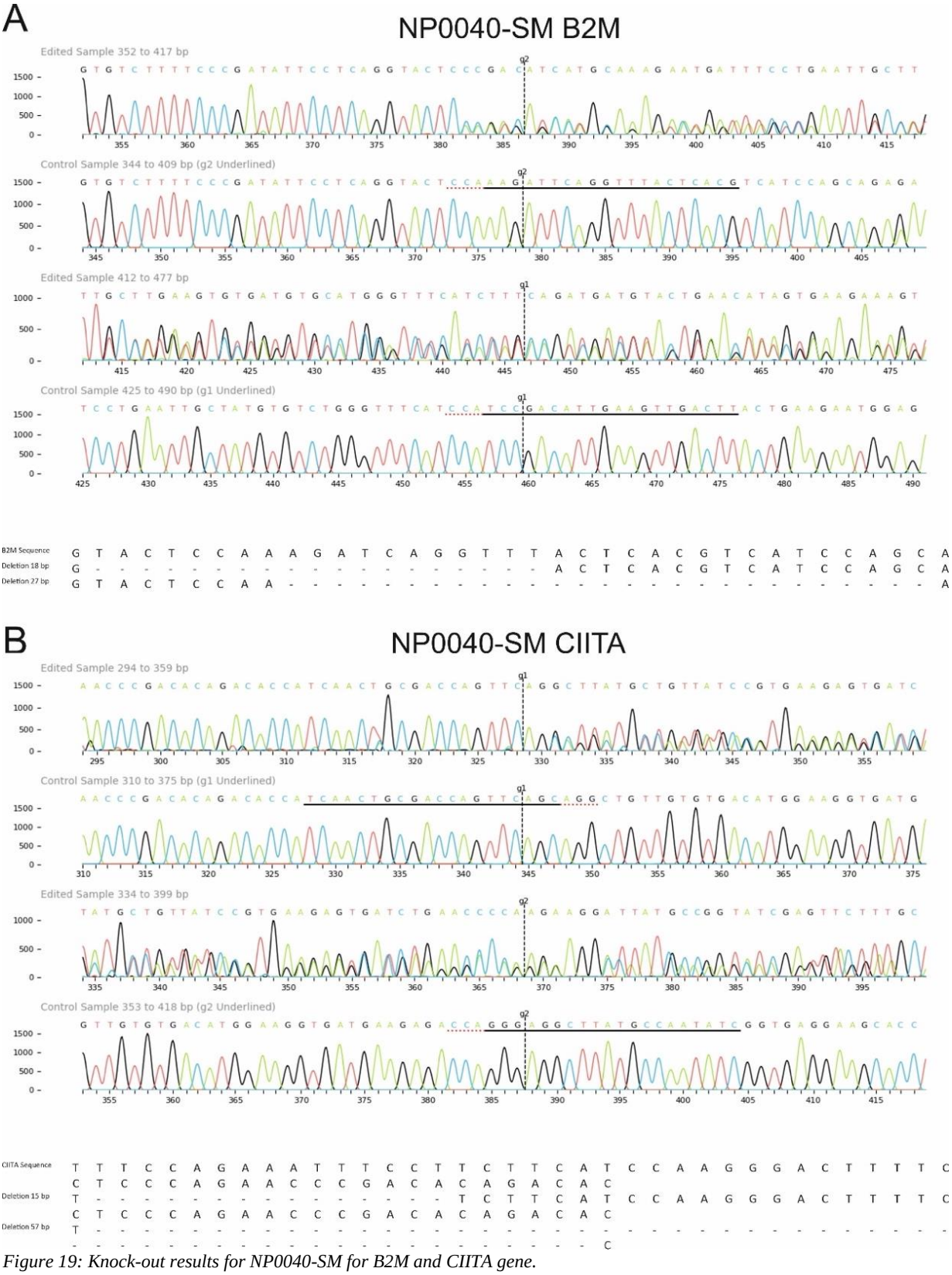

Figure 19: Knock-out results for NP0040-SM for B2M and CIITA gene.

ICE trace and NGS summary for NP0040-SM for genes B2M (A) and CIITA (B) (see Appendix a and b).

3.1.2. NP0040-SM iPSC characterization

The B2M$^{-/-}$CIITA$^{-/-}$hiPSC line NP0040-SM was compared to their origin cell line NP0040-8 for iPSC characterization. Morphology and expression of pluripotency markers was compared. No morphological and staining for Sox2, Oct3/4, Tra1-81 and SSEA4 differences could be observed between both cell lines (*Figure 20*).

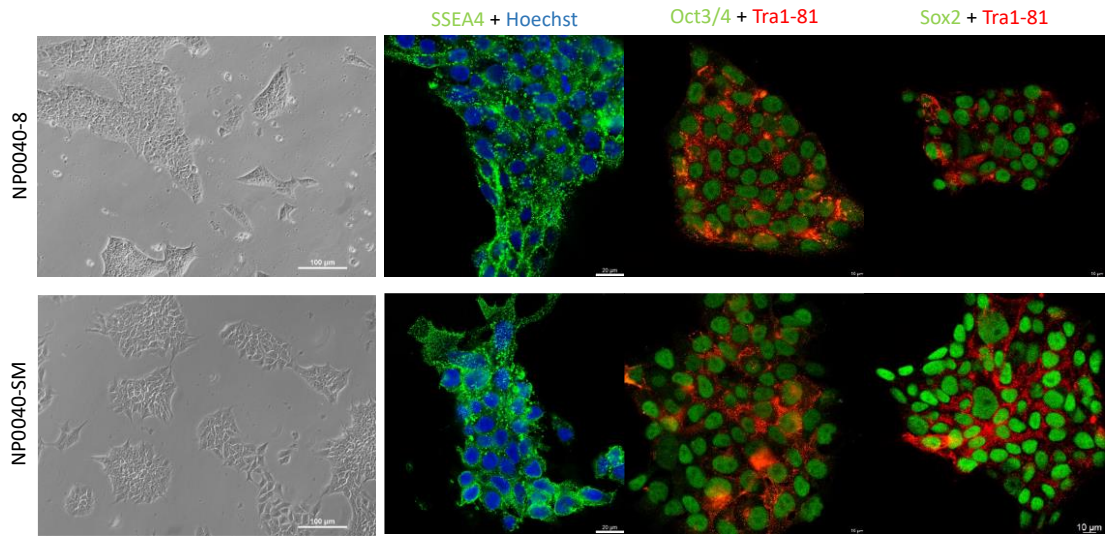

Figure 20: iPSC characterization of hiPSC knock-out cells NP0040-SM.

NP0040-SM is compared with NP0040-8. Morphology and Pluripotency immunostaining. Brightfield microscopy for morphology compared. Scale bar 100 µm. Immunostaining for SSEA4 + AlexaFL488 and Hoechst33342. Oct3/4 + AlexaFl488 and Tra1-81+AlexaFl555 and Sox2+AlexFl488 and Tra1-81+AlexaFl555. All imaged on confocal microscope (Stellaris5, Leica) with scalebar 10 µm.

Expression of SSEA4 was used for quantitative comparison of pluripotency of NP0040-8 and NP0040-SM. iPSCs were stained with SSEA4-FITC conjugated antibody and flow cytometry was used to determine percentage of fluorescent detected cells. Mean and standard deviation of was calculated. No significant difference in expression levels of SSEA4 could be observed (*Figure 21*).

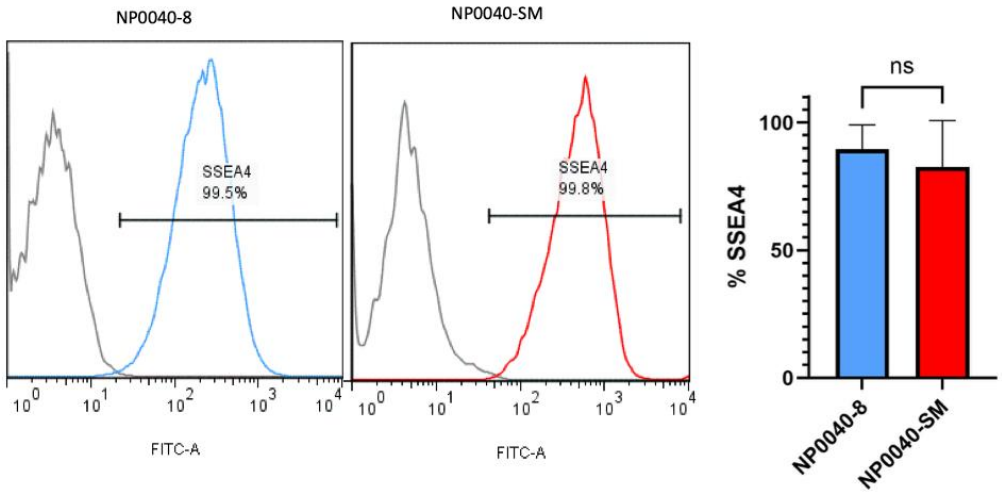

Figure 21: Flow cytometry of SSEA4-FITC conjected antibody stain on NP0040-8 (blue (n=10)) and NP0040-SM (red (n=5)) against unstained control (grey).

Statistical analyzation of SSEA4 % of positive stained cells for NP0040-8 and NP0040-SM no significant difference between all two groups. (FC Statistics raw data see Appendix c)

Lastly, STR profile of NP0040-8 and NP0040-SM was generated (*Figure 22*). In summary no significant difference were observed between these two cell lines and we concluded that knock out cell line can be consider an intact iPSC cell line.

	AMEL	D3S1358	D1S1656	D2S441	D10S1248	D13S317	PENTA E	D16S539	D18S51	D2S1338	CSF1PO	PENTA D	TH01	VWA	D21S11	D7S820	D5S818	TPOX	DYS391	D8S1179	D12S391	D19S433	FGA	D22S1045
NP0040-8	X,Y	15,16	16.3,17.3	11,14	13,17	10,11	15,16	10,12	12	23,24	10,12	13,16	6,9.3	15,17	29,30	10,11	11	8,9	11	13,15	21,22	15	21,24	11,15
NP0040-SM	X,Y	15,16	16.3,17.3	11,14	13,17	10,11	15,16	10,12	12	23,24	10,12	13,16	6,9.3	15,17	29,30	10,11	11	8,9	11	13,15	21,22	15	21,24	11,15

Figure 22: iPSC characterization of hiPSC knock-out cells. NP0040-8 is compared with NP0040-SM.

STR summary for NP0040-8 and NP0040-SM. (see Appendix d)

3.1.3. NP0040-SM Human iPSCs derived cardiomyocytes

After differentiation of iPSCs to cardiomyocytes, differentiation efficiency was analyzed by immunostaining and flow cytometry. Differentiation was repeated in 5 individual repetitions (n=5). Morphology of differentiated CMs was imaged with Phase-contrast microscopy and cells appeared to have normal CM morphology. CMs were seeded on a confocal microscopy slide with 8 wells (ibidi), cultured for a few more days and stained on day 20 of differentiation for cardiac markers cardiac Troponin T (TNNT2) and alpha-Actinin (ACTN2) (*Figure 23*).

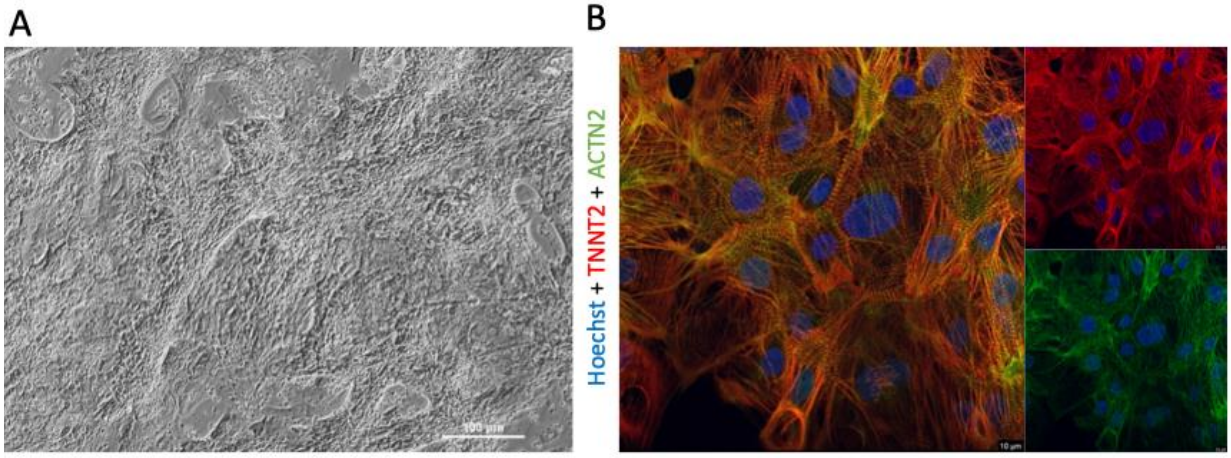

Figure 23: NP0040-SM Day 15 cardiomyocytes (CMs).

A: Brightfield image of CMs on day 15. Scale bar 100 µm. B: Stained CMs day 20 on ibidi confocal slide imaged with confocal microscope (Leica). Stained for cTNNT-AlexFl-555 ACT2-AlexFl647 and Hoechst33342.Scale bar 10 µm.

CMs were stained with 5 markers for flow-cytometry to confirm cardiac characteristics of cells (*Figure 24*). And lastly, percent of expression of all markers was calculated for all repetitions (n=5) and compared.

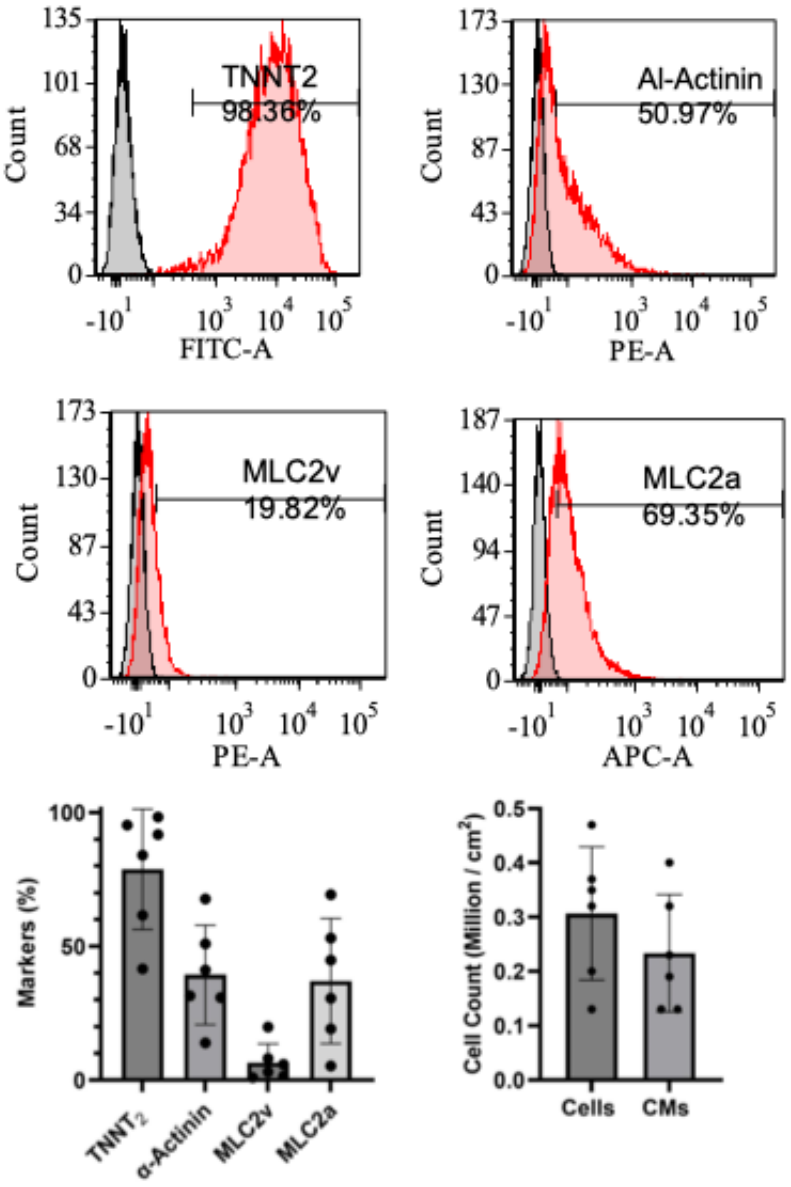

Figure 24: NP0040-SM Day 15 cardiomyocytes (CMs).

FC results of NP0040-SM CMs on day 15, stained with cTNNT-FITC, A-Actinin-PE, CD31-APC, MLC2v-PE and MLC2a-APC. Statistical analyzation of NP0040-SM CMs. FC statistics data (see Appendix e)

3.1.4. In-vitro Immune-reaction assay with Interferon-Gamma

Functional absence of MHCI complex was shown through interferon-γ stimulation and HLA staining. NP0040-8 and NP0040-SM cells were treated with 50 ng/ml interferon-γ for 48 h and stained with Anti-HLA,A,B,C + AlexaFlour488 and Hoechst33342 (*Figure 25*). NP0040-8 Control group shows that interferon-γ treatment stimulates the MHCI complexes on the cell surface. NP0040-SM shows no MHCI expression, even after interferon-γ treatment.

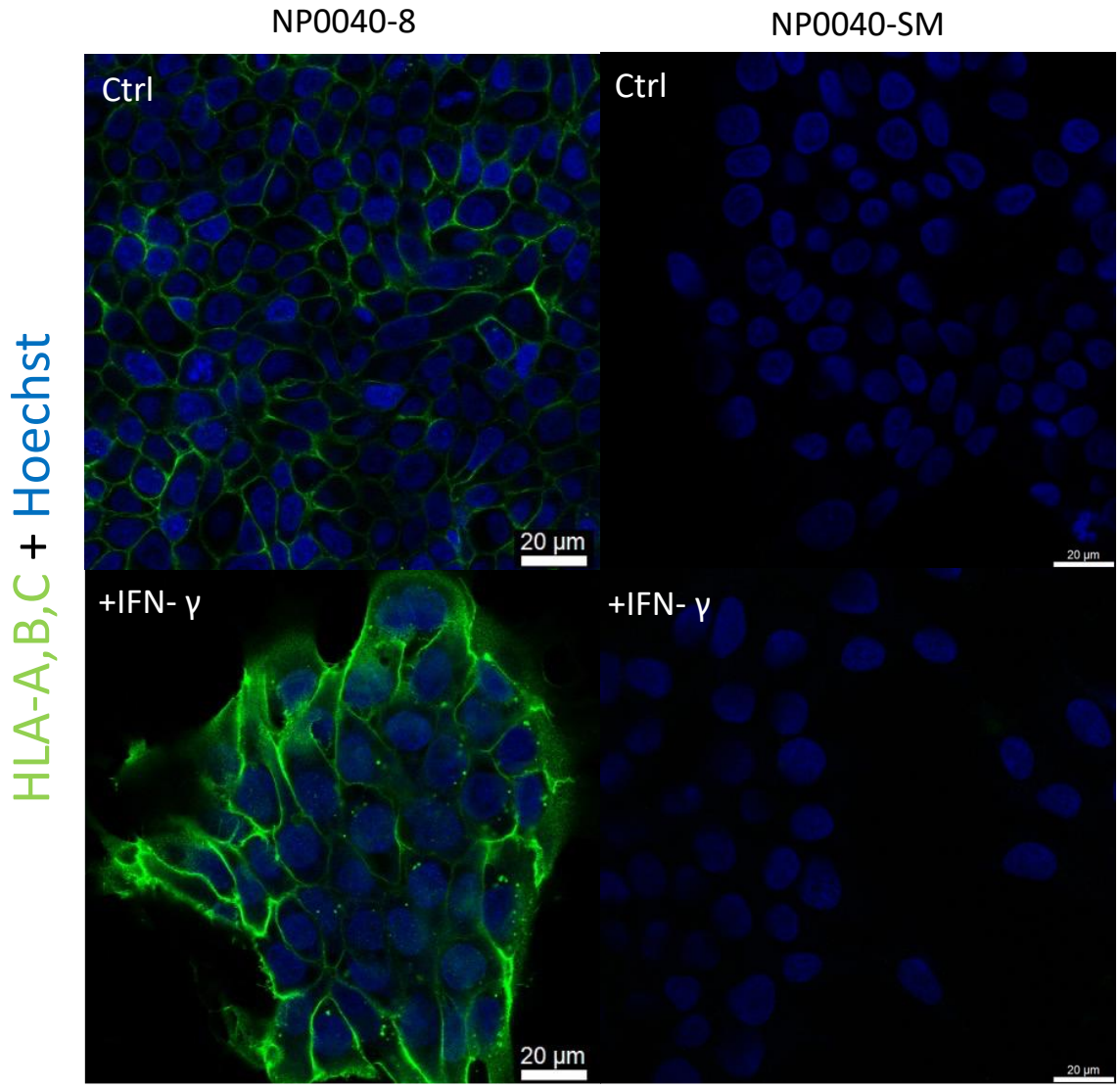

Figure 25: In-vitro testing of functional absence of MHCI on surface of NP0040-SM.

HLA staining of NP0040-8 and NP0040-SM before and after Interferon-Gamma treatment for 48 h. Cell nucleus was stained with Hoechst33342 and MHCI complexes were stained with HLA-A,B,C primary antibody and AlexaFl488. Cells were cultured on ibidi confocal slide and imaged with confocal microscope (Stellaris 5, Leica). Scale bar 20 µm.

FC analysis of interferon-γ treatment of NP0040-8 cells (n=4) also shows a significant difference ($P < 0.05$) of MHCI expression between treated and untreated hiPSCs (*Figure 26*). Mean Fluorescence Intensity is compared, highlighting the upregulation of MHCI complexes on the cell surface after Interferon-γ treatment. Both immunostaining and FC show, that in NP0040-8 the MHCI complexes expression is upregulated through interferon-γ (*Figure 25 & Figure 26*). NP0040-SM show no significant expression of MHCI even after interferon-γ treatment. Comparted to the control group absence of MHC I complexes on NP0040-SM cells was shown, even after treatment with interferon-γ, compared to NP0040-8, significance difference between groups was calculated with $p = 0.0023$ and R^2 0.8 (*Figure 26*).

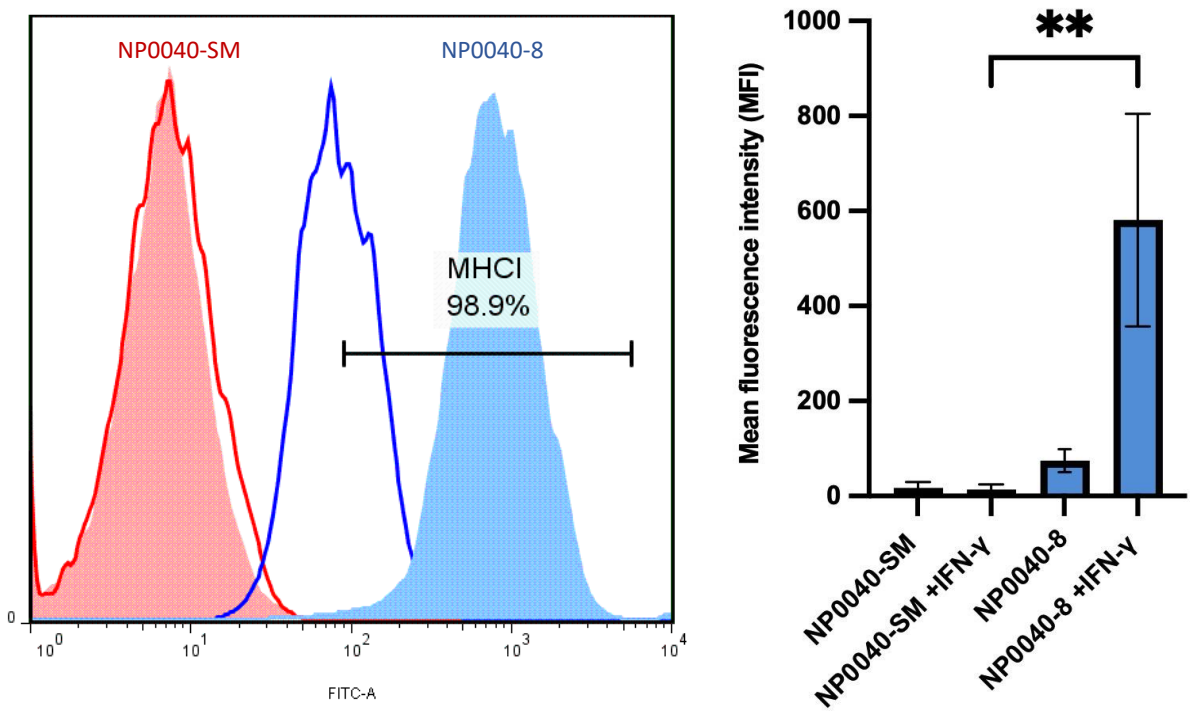

Figure 26: In-vitro testing of functional absence of MHCI on surface of NP0040-SM.

Flow cytometry data of NP0040-8 (blue) and NP0040-SM (red) before (line) and after (filled) 48 h treatment with Interferon-gamma. Cells were stained with HLA-A,B,C primary antibody and AlexaFl488 for Flow cytometry. Statistical analyzation of NP0040-8 and NP0040-SM expressing MHCI on the cell surface. Mean fluorescence intensity was normalized against the MFI of cells stained with only secondary antibody.(see Appendix f)

3.1.5. Over-expression of murine CD47 in hiPSCs

NP0040-SM were nucleofected with pgk-mCD47-T2A-BsdR_ARSpiggyBac plasmid to generate human iPSCs expressing murine CD47, plasmid map can be seen in *Figure 27*.

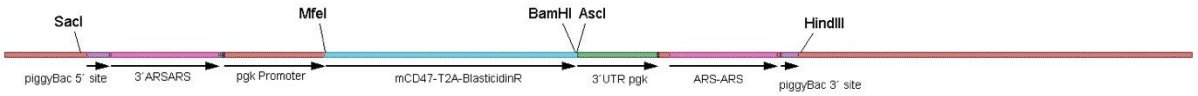

Figure 27: Plasmid map of pgk-mCD47-T2A-BsdR_ARSpiggyBac.

NP0040-SM were nucleofected with 0.5 µg plasmid, adding 5x Hyperactive piggy bac transposase using Nucleofection kit (Lonza) and Nuleofector device II (Lonza) with program B016. Cells were selected using 5 µg/ml Blasticidin (Gibco) for 5 days, and single cell clones were picked and analyzed for expression of murine Cd47 with immunostaining and confocal microscopy (*Figure 28*), as well as flow cytometry (*Figure 29*). Expression of murine CD47 on the surface of cells was compared for murine iPSCs (cell line AT25fluc Rosa), hiPSCs (NP0040-8) and transgenic hiPSCs (HSM47M). Cells with significant expression of murine CD47, were named HSM47M cell line (*Figure 30*).

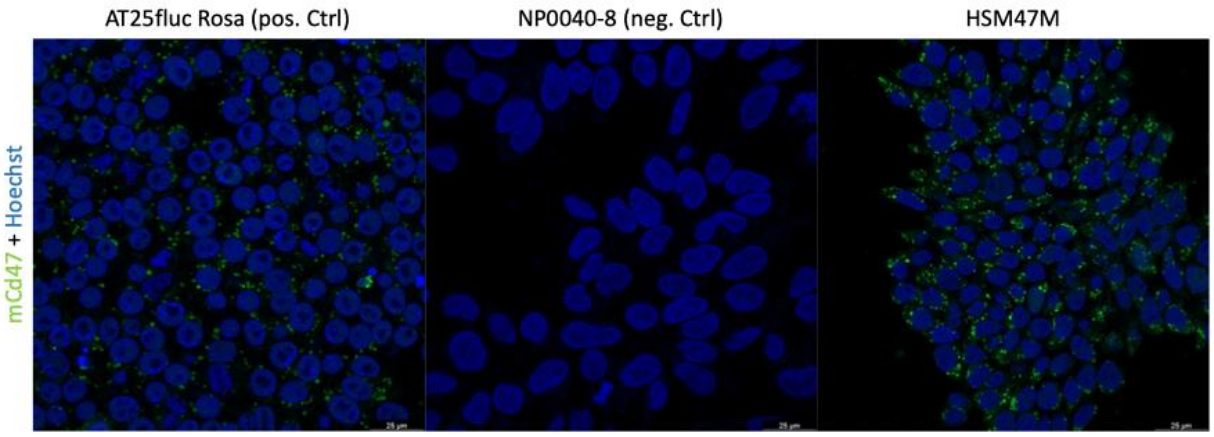

Figure 28: AT25fluc Rosa, NP0040-8 and HSM47M (B2M$^{-/-}$CIITA$^{-/-}$tg mCD47) stained for murine CD47.

Murine positive control group (AT25 fluc Rosa), human negative control group (NP0040-8) and transgenic cell line HSM47M were stained for expression of murine CD47 on the surface with Anti-mCD47-Biotin+ Streptavidin-AF488 and Hoechst 33342. Cells were imaged on confocal microscope (Stellaris 5, Leica) scale bar 25 µm.

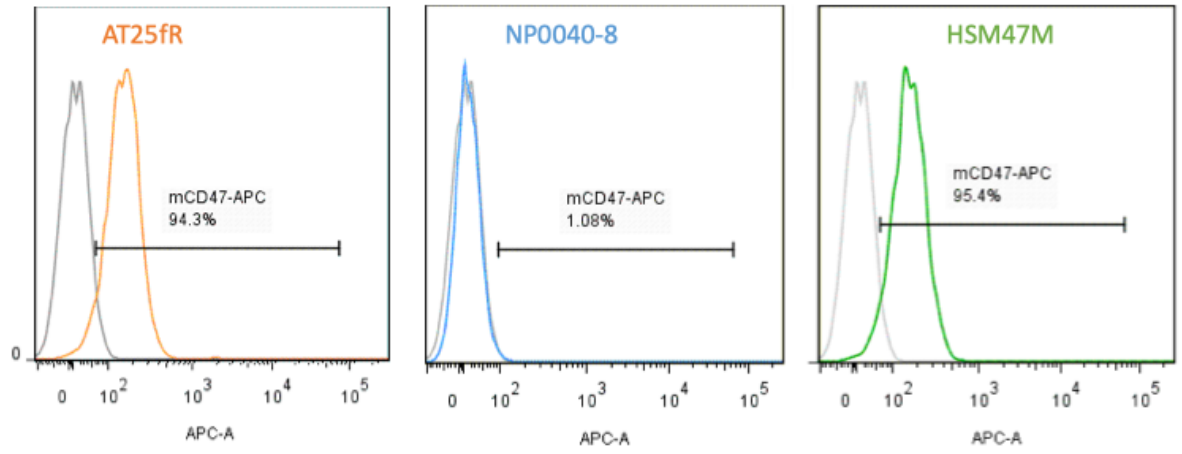

Figure 29: Presence of murine CD47 on HSM47M hiPSCs.

Flow cytometry data of murine iPSC (AT25fluc Rosa (orange)), human iPSCs (NP0040-8 (blue))) and transgenic human iPSCs (HSM47M (green)) stained with Anti-mouse CD47-APC conjugated against unstained control (grey).

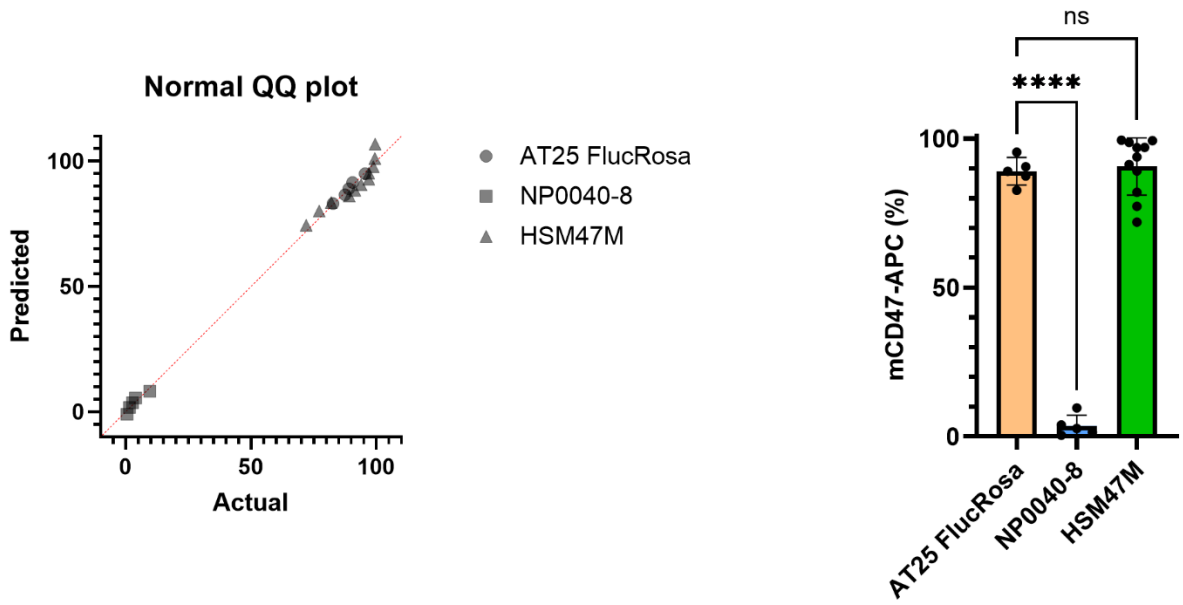

Figure 30: Statistical analyzation of expression of murine Cd47 on the surface of different iPSCs cells, after staining with Anti-CD47-APC.

Statistical analyzation of Expression level of CD47-APC on iPSC (AT25fluc Rosa (orange) n=5), human iPSCs (NP0040-8 (blue) n=5) and transgenic human iPSCs (HSM47M (green) n=11) on cell surface (see Appendix g).

3.1.6. iPSC characterization of HSM47M cell line

The B2M$^{-/-}$CIITA$^{-/-}$ tg murineCD47 iPSC cell line HSM47M was compared to their origin cell line NP0040-8 for iPSC characterization. Morphology and expression of pluripotency markers was compared. No morphological and staining for Sox2, Oct3/4, Tra1-81 and SSEA4 differences could be observed between both cell lines (*Figure 31*).

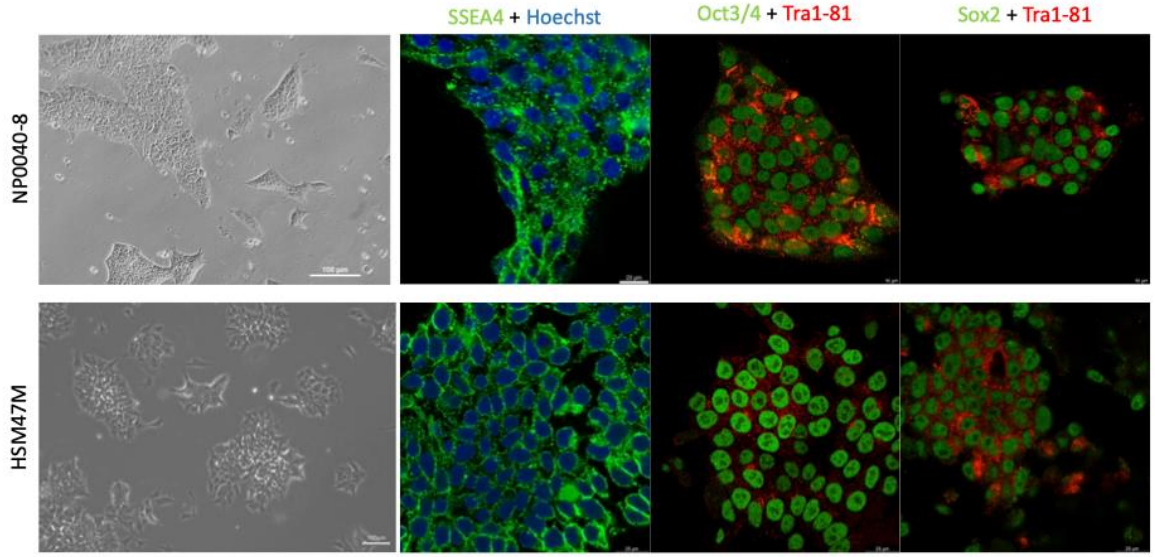

Figure 31: iPSC characterization of hypoimmunogenic hiPSC HSM47M.

HSM47M is compared with NP0040-8. Morphology and Pluripotency immunostaining. Brightfield microscopy for morphology compare. Scale bar 100 µm. Immunostaining for SSEA4 + AlexaFL488 and Hoechst33342. Oct3/4 + AlexaFl488and Tra1-

81+AlexaFl555 and Sox2+AlexFl488 and Tra1-81+AlexaFl555. All imaged on confocal microscope (Stellaris5, Leica) scalebar 25 µm.

Expression of SSEA4 was used for quantitative comparison of pluripotency of NP0040-8 and HSM47M, detecting no significant difference in expression levels of SSEA4 for all three groups, NP0040-8, NP0040-SM and HSM47M (*Figure 32*).

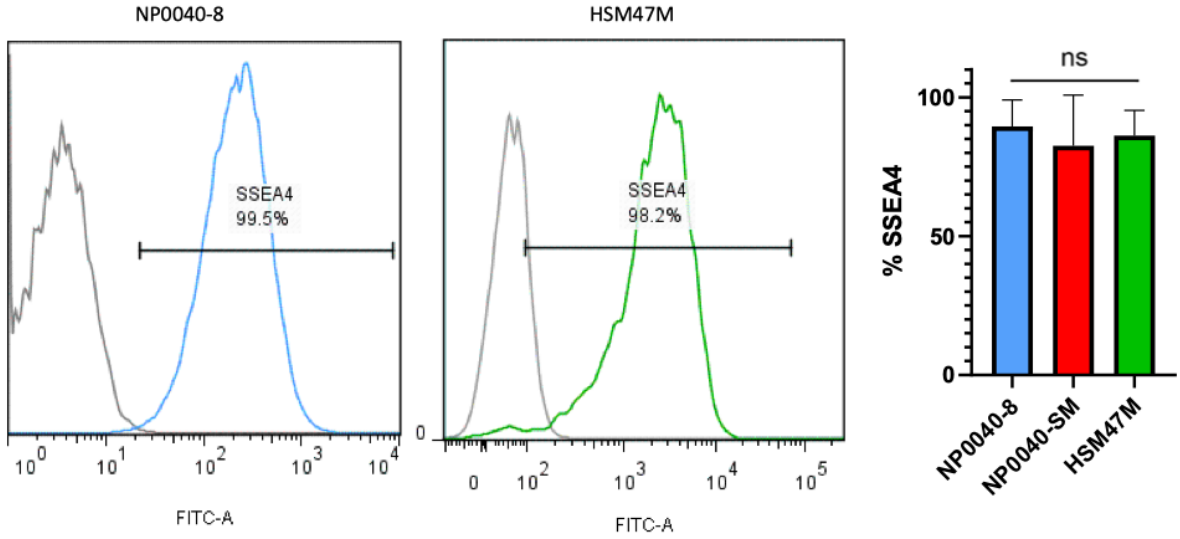

Figure 32: Flow cytometry of SSEA4-FITC conjected antibody stain on NP0040-8 (blue (n=10)) and HSM47M (green (n=3)) against unstained control (grey).

Statistical analyzation of SSEA4 % of positive stained cells for NP0040-8, NP0040-SM and HSM47M, no significant difference between all three groups. (FC Statistics raw data see Appendix c)

3.2. Magnetic targeting of mesenchymal stem cells (MSCs)

The following results of Chapter 3.2. have already been published in:

Halhouli, T.; Münchhalfen, L.; Hamad, S.; Schmitz-Ullrich, L.; Nitsche, F.; Gaedke, F.; Schauss, A.; Zhang, L.; Pham, Q.-K.; Bao, G.; et al. Cell-Based Therapies: Ferromagnetic Versus Superparamagnetic Cell Targeting. Bioengineering 2025, 12, 657. https://doi.org/10.3390/bioengineering12060657

See Appendix I for full publication.

For magnetically targeting murine MSCs two strategies are compared, magnetic force mediated intracellular loading of SPIONs and bio-linking of ferromagnetic particles to cell surface receptors through antibodies. The analyzation of the feasibility of magnetically targeting cells, is done in preparation for enhancing cellular retention upon cell transplantation.

3.2.1. Intracellular loaded SPIONs and Bio-linking Ferromagnetic particles

Force mediated endocytosis of SPIONs into mMSCs was tested and confirmed with fluorescence microscopy (*Figure 33*).

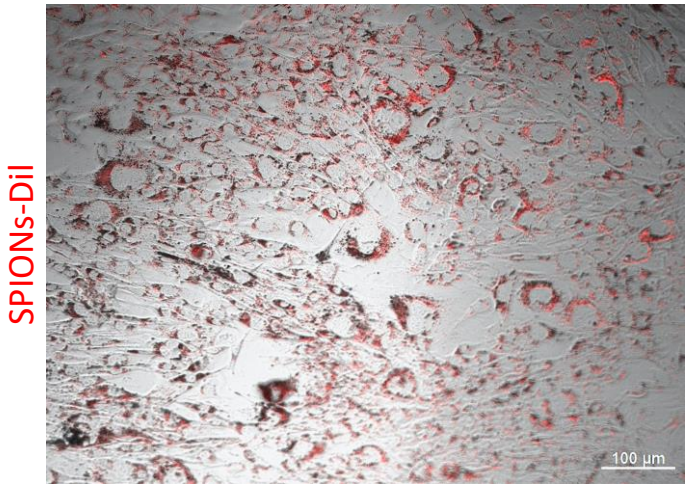

Figure 33: SPIONs loaded mMSCs with SPIONs-PEG-DiI imaged with fluorescence microscope. Scale bar 100 µm.

To confirm intracellular loading success, iron content of loaded mMSCs was measured using ferrozine assay. SPIONs are 15 nm in size and made of Fe_2O_3 with a PEG-coating. Adding Ferrozine to Fe^{2+} the ferrous-ferrozine complex forms, which can be detected at 562 nm wavelength in a micro plate reader (Epoch). For linking absorbance to the iron concentration, an iron standard was established. In order to link absorbance at 562 nm of Ferrozine to Iron

concentration in probes. Plate reader (Epoch) was measured with an empty 96-well plate to calculate a mean measurement error, which was 0,045. Linear equation was described with y = 0.0025x with a calculated model fit R2 = 0.99 (see Appendix h).

Measured iron concentration of SPIONs loaded mMSCs was normalized against unloaded control group (None, only MSCs) (n=3) and iron content in µg/0.3 x10^6 cells was calculated (see Appendix i). SPIONs loaded mMSCs using magnetic force-mediated endocytosis (+MF) contained 54.55 ± 25.90 µg iron oxide per 0.3 x10^6 cells (n = 5), compared to SPIONs loaded mMSCs without using magnetic force (-MF) (n = 5), where iron content was 4.46 ± 3.18 µg. Iron Concentration unloaded MSC group and loaded +MF group was significantly ($P < 0.05$) different (*Figure 34*).

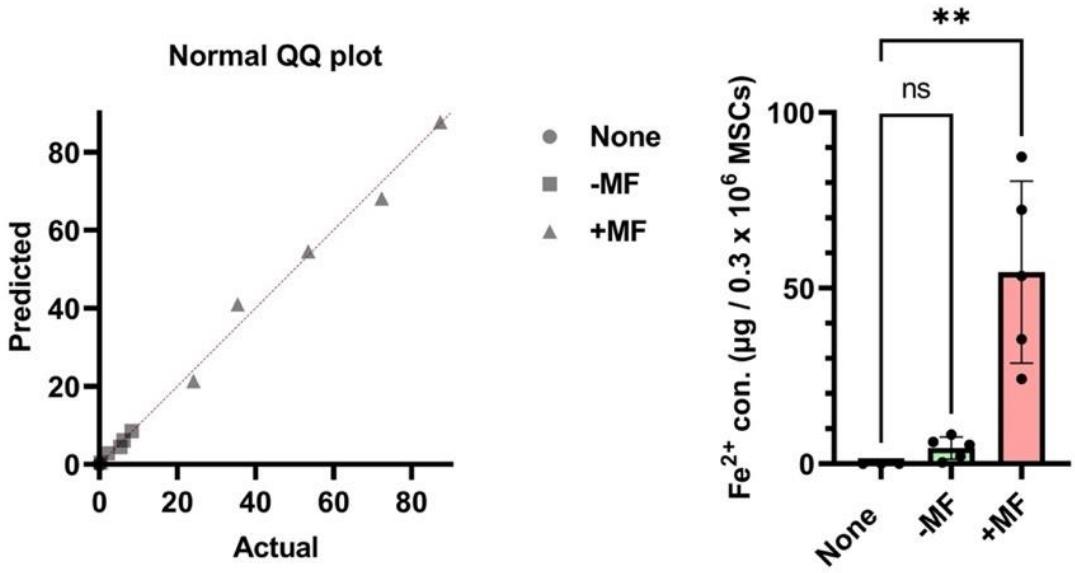

Figure 34: Quantification of Iron content of SPIONs loaded cells using Ferrozine-based quantification assay.

Data was normalized and Fe^{2+} concentration in µg/0.3 x10^6 cells was compared for unloaded cells (None), cells loaded with SPIONs using force mediated incubation (+MF) and without magnetic force (-MF). (see Appendix k)

3.2.2. Bio-linking Ferromagnetic particles

Feasibility of bio-linking ferromagnetic particles to the surface receptors of MSCs is shown in the following figures. Firstly, mMSCs surface markers were first validated with flow cytometry. Ferromagnetic particle were bio-linked via antibodies to the cell surface and imaged with fluorescence microscopy. To show successful magnetic labeling of cells, magnetic induced cell clumping was applied to the cell suspension by exposing cells to a permeant magnet with a conic iron tip with a magnetic force of 150 mT. As surface receptor Integrin-ß was stained with Anti-Cd29 (*Figure 35*).

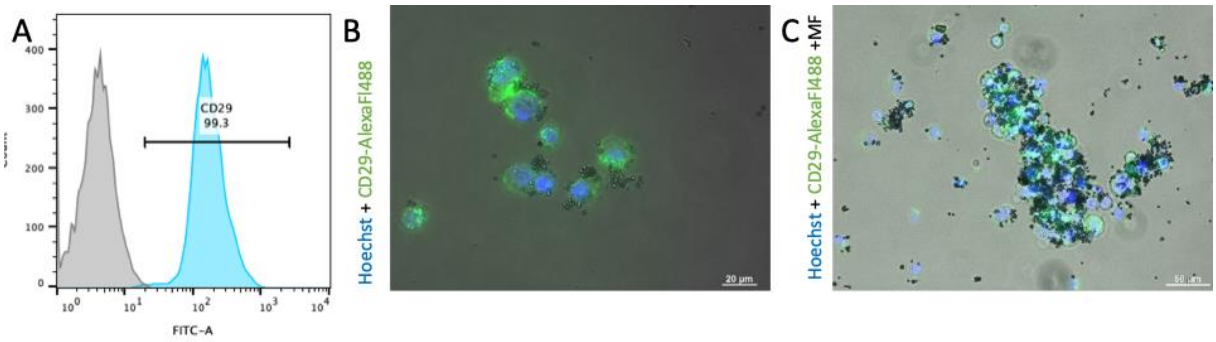

Figure 35: mMSCs magnetically targeted by bio-linking Ferromagnetic particle to cell receptor using CD29.

A: mMSCs are stained for CD29 and analyzed by FC, verifying CD29 expression on the cells surface of mMSCs.B: mMSCs are Bio-linking to Ferromagnetic particle and then stained. CD29 is stained with Anti-CD29-Biotin conjugated (Miltenyi) and AleaFl488-Streptavidin (Biolegend). Cell nucleus is stained with Hoechst33342.Scale bar 20 µm. C: Cell suspension is exposed to a permanent magnet with a conic iron tip with a magnetic force of 150 mT, cell clumps are imaged after 1 minute of magnetic exposure. Scale bar 50 µm.

3.2.3. Aggregation of magnetically targeted cells and quantification

Next, we investigated the cell clustering and/or cell aggregation through magnetic force. SPIONs and ferromagnetic particle-labelled mMSC were placed close to a magnet with conic iron tip (see exemplary for Ferromagnetic labelled cells *Figure 36*).

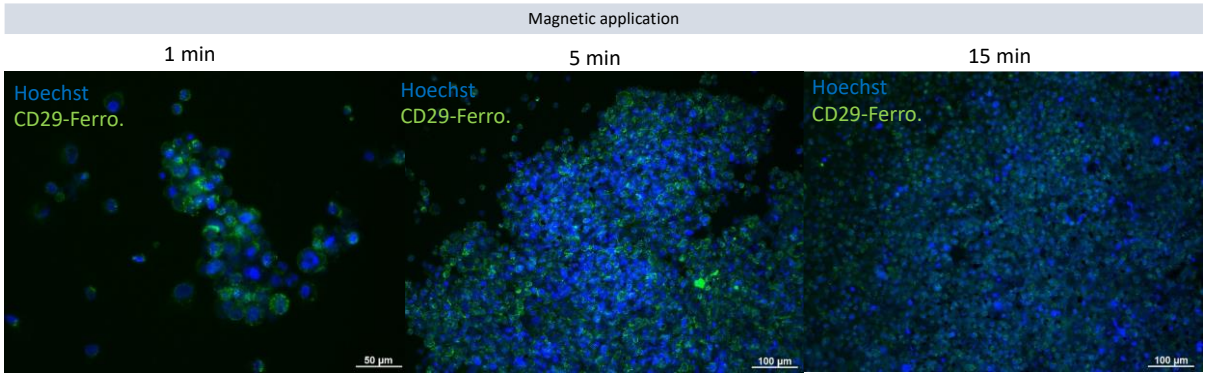

Figure 36: Aggregation of magnetically targeted mMSCs.

CD29 on surface of mMSCs is stained with Anti-CD29-Biotin and AlexaFl488-Stretavidin. Cell nucleus is stained with Hoechst33342. Permanent magnet with conic iron tip is applied for 1, 5 and 15 min and cell cluster formation is imaged with fluorescence microscopy. After 1 min magnetic application cell cluster is imaged, scale bar 50 µm. Cell cluster after 5 and 15 min magnetic application were imaged with 10X, scale bar 100 µm.

The formation of cell clusters was observed and the cell number per cluster was determined through DNA quantification. For this a linear slope connecting cell number to DNA concentration through OD measurement was carried out (see Appendix j). Application of magnetic force was performed for 1, 5 and 15 min and the effect of cell clumping observed by fluorescence microscopy. DNA was isolated from the induced cell clumps for indirect cell quantification. The percent of cells inside the cell clumps was calculated by dividing the calculated cell number after DNA OD measurement with the total cell number of the experiment and visualized in *Figure 37* (see Appendix k). Mean (n=3) and the standard deviation was

calculated. After 15 min, 100.00±28.84 % of mMSCs were found in the cell aggregate for ferromagnetic particle labelled cells and 98.12 ± 0.38% for SPIONs loaded cells.

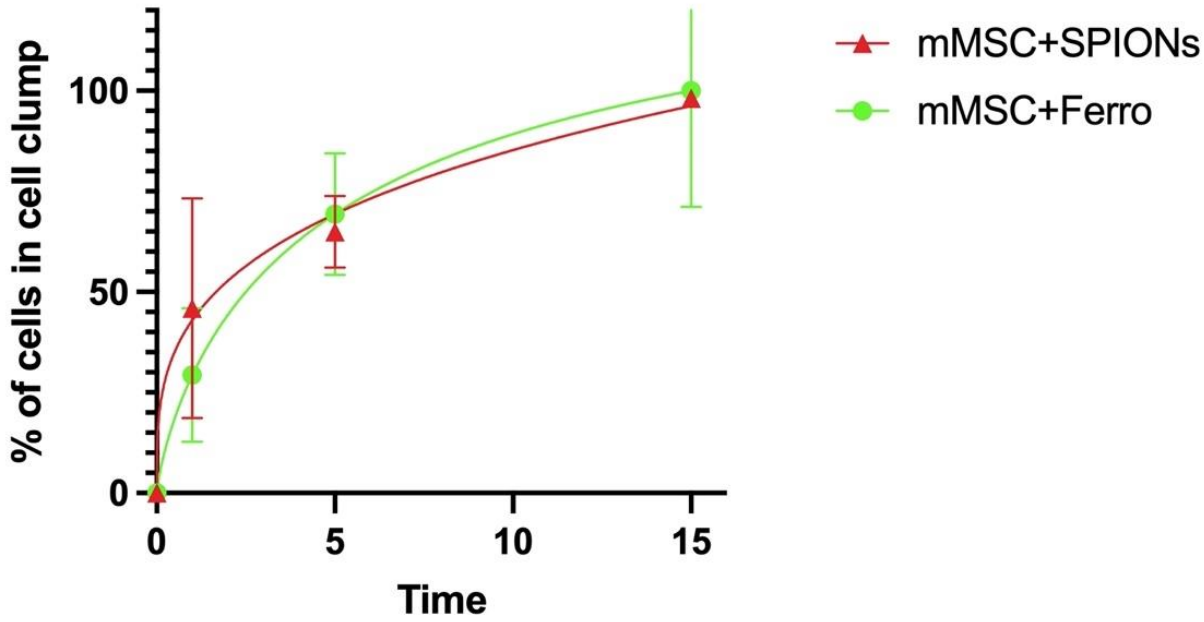

Figure 37: Quantification of magnetically induced cell clumps.

Both methods of magnetically targeting cells, intracellular loading with SPIONs (red) and Ferromagnetic particle bio-liniking (green) were compared for their characteristics to form magnetically induced cell clumps. Percent of cells in cell clumps was quantified through DNA concentration (see Appendix k)

3.3. Emptying the cardiac niche for Organ Complementation

A new approach for the cardiac replacement therapy, organ complementation, is investigated. For this the influence of cardiac related genes on cardio genesis is evaluated, firstly with an *in vitro* testing of the CRISPR/Cas9 mediated knock out strategy on murine iPSCs, followed by an *in vivo* intraembryonic complementation assay approach in mice.

3.3.1. Design strategies for CRISPR/Cas9 mediated knock out in genes for cardiac niche

The design strategy for knocking out murine cardiac genes Nkx2-5, Hand1, Hand2, Tbx5, Mesp1, and Ils1can be seen in *Figure 38.* Red and green arrows show the position of Primers (Reverse= red; Forward=green) blue arrows show the position of designed crRNAs.

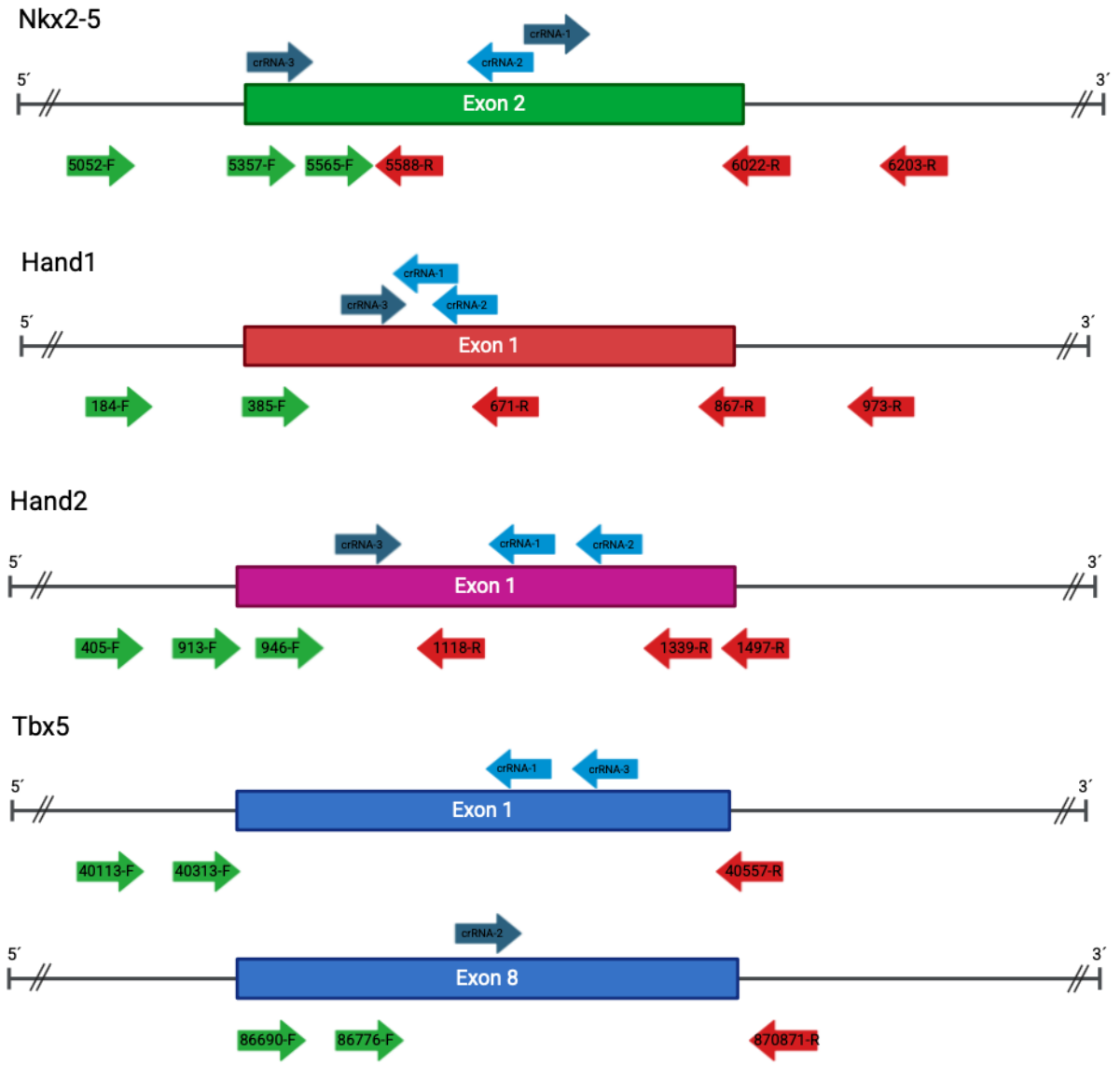

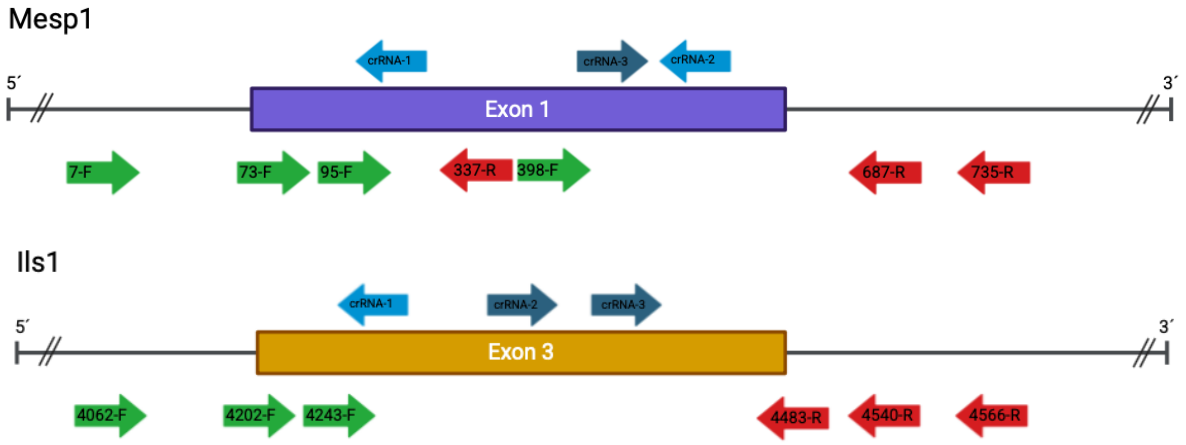

Figure 38: Location of CRISPR-RNAs in exons of genes of interest for emptying the cardiac niche. Created with BioRender.

3.3.2. In-vitro testing of CRISPR/Cas9 designs for emptying the cardiac developmental niche

All designs were tested in the same way. TaP murine iPS cells were nucleofected with RNP as described in methods *2.2.1.1*. Cells were cultured for 2 days and analyzed by isolation DNA, running PCR amplification and running T7Endonucease I assay. After T7 Endonuclease I assay, digested products were separated on a 1% agarose gel again. Run gels are shown for a Nkx2-5 (*Figure 39*), Hand1 (*Figure 40*), Hand2 (*Figure 41*), Tbx5 (*Figure 42*), Mesp1 (*Figure 43*) and Ils1 (*Figure 44*). Multiple bands after T7 Endonuclease I assay indicates heteroduplex complexes and there for successful genetic modification after CRISPR experiment. Control A is a kit provided homoduplex control and Control B a heteroduplex control.

3.3.2.1. Nkx2-5

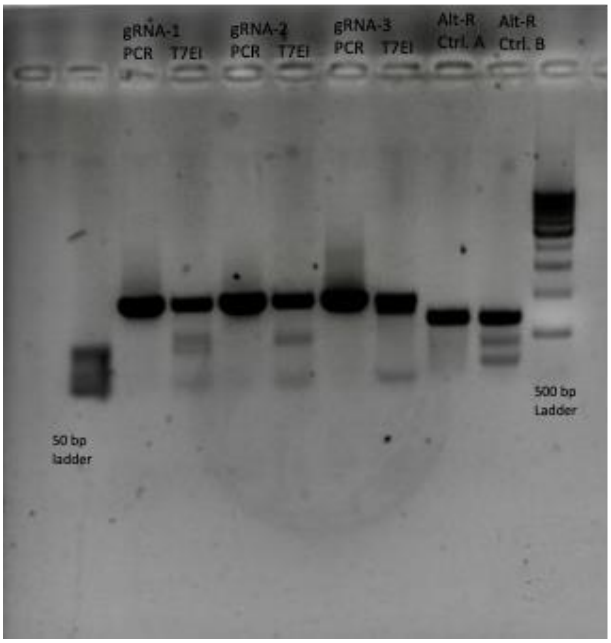

Figure 39: Agarose gel of T7Endonuclease I assay for Nkx2-5.

1% Agarose gel run 30 min at 130 V. Lane 1: PCR product of TaP-Nkx2.5-gRNA-1 PCR. Lane 2 digested PCR product using T7 Endonuclease I. Lane 3: PCR product of TaP-Nkx2.5-gRNA-2 PCR. Lane 4 digested PCR product using T7 Endonuclease I. Lane 5: PCR product of TaP-Nkx2.5-gRNA-3 PCR. Lane 6 digested PCR product using T7 Endonuclease I Lane 7 Homoduplex control, Lane 8 Heteroduplex control.

3.3.2.2. Hand1

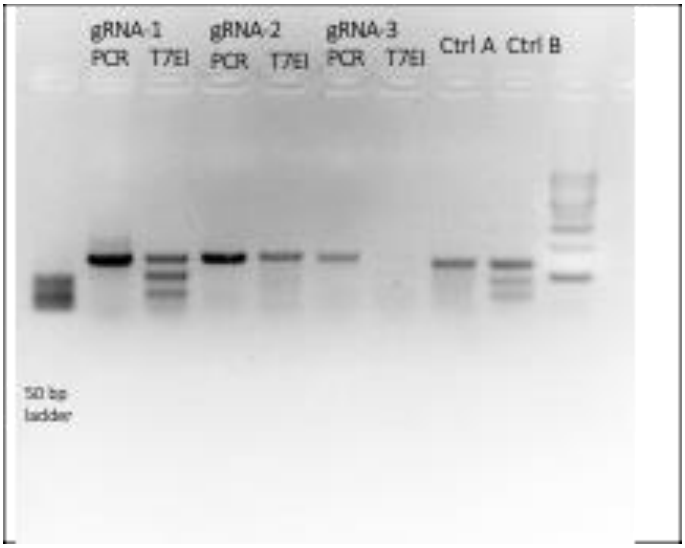

Figure 40: Agarose gel of T7Endonuclease I assay for Hand1.

1% Agarose gel run 30 min at 130 V. Lane 1 PCR product of TaP-Hand1-gRNA-1 PCR. Lane 2 digested PCR product using T7 Endonuclease I. Lane 3: PCR product of TaP-Hand1-gRNA-2 PCR. Lane 4: digested PCR product using T7 Endonuclease I. Lane 5: PCR product of TaP-Hand1-gRNA-2 PCR. Lane 6: digested PCR product using T7 Endonuclease I. Lane 7: Homoduplex control, Lane 8: Heteroduplex control

3.3.2.3. Hand2

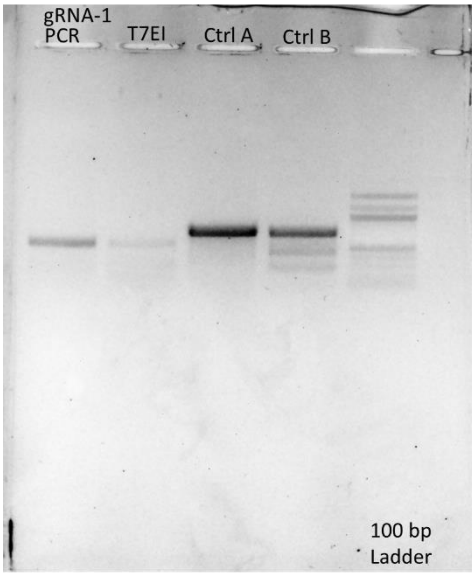

Figure 41: Agarose gel of T7Endonuclease I assay for Hand2.

1% Agarose gel run 30 min at 130 V. Lane 1 PCR product of TaP-Hand2-gRNA-1 PCR. Lane 2 digested PCR product using T7 Endonuclease I. Lane 3: Homoduplex control, Lane 4: Heteroduplex control.

3.3.2.4. Tbx5

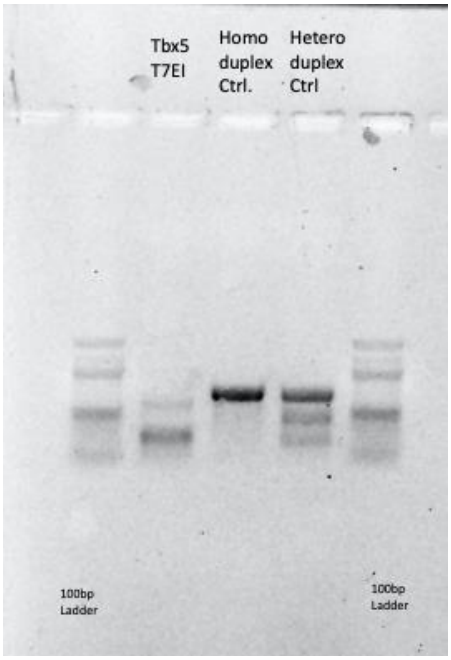

Figure 42: Agarose gel of T7Endonuclease I assay for Tbx5.

1% Agarose gel run 30 min at 130 V. Lane 1: digested PCR product using T7 Endonuclease I of TaP-Tbx5-ko cells. Lane 2 Homoduplex control, Lane 3 Heteroduplex control.

3.3.2.5. Mesp1

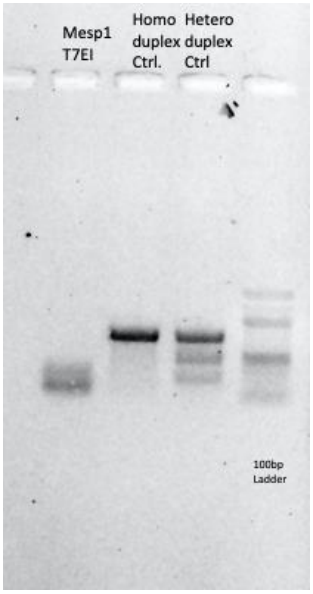

Figure 43: Agarose gel of T7Endonuclease I assay for Mesp1.

1% Agarose gel run 30 min at 130 V. Lane 1: digested PCR product using T7 Endonuclease I of TaP-Tbx5-ko cells. Lane 2 Homoduplex control, Lane 3 Heteroduplex control.

3.3.2.6. Ils1

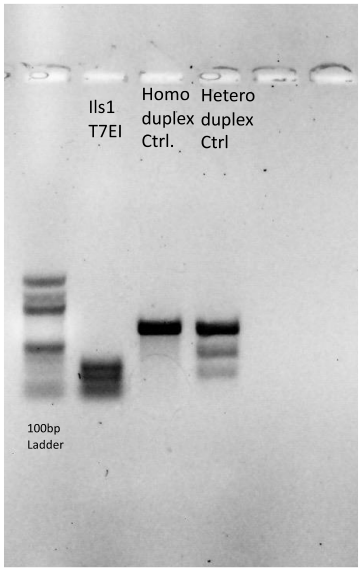

Figure 44: Agarose gel of T7Endonuclease I assay for Ils1.

1% Agarose gel run 30 min at 130 V. Lane 1: digested PCR product using T7 Endonuclease I of TaP-Isl1-ko cells. Lane 2 Homoduplex control, Lane 3 Heteroduplex control.

3.3.3. In-vitro testing of differentiation capability of knock-out iPSCs to Cardiomyocytes (CMs)

Knock-out TaP murine iPSCs were mixed 1:1 with AT25fluc murine iPSCs and differentiated into Cardiomyocytes as described in 2.3.6. On day 14 of differentiation Embryonic bodies were dissociated using 0.05% Trypsin (Gibco) and cells were counted with Nexceloms Vision 2 device determining cell count and GFP positive ratio of cells. AT25fluc cells are GFP positive when successfully differentiated to Cardiomyocytes.

Table 12: Differentiation summary of TaP-Hand1$^{-/-}$ + At25fluc

Cell type	Diff Start	Results	Conc cells in x10^6/ml	GFP positive CMs in %
AT25+ TaP-Hand1-gRNA-1	20.10.2021	Day 14	0,8	29,9
AT25+ TaP-Hand1-gRNA-2			1,74	40,3
Control AT25+ TaP			2,59	23,1
AT25+ TaP-Hand1-gRNA-1	22.10.2021	Day 14	0,91	18,0
AT25+ TaP-Hand1-gRNA-2			1,69	6,4
AT25+ TaP-Hand1-gRNA-3			0,84	6,3
Control AT25+ TaP			2,52	17,3
AT25+ TaP-Hand1-gRNA-2	25. 10.2021	Day 14	0,6	6,9
AT25+ TaP-Hand1-gRNA-3			0,6	23,1
Control AT25+ TaP			0,4	12,8

AT25+ TaP-Hand1-gRNA-1	27.10.2021	Day 14	0,8	18,7
AT25+ TaP-Hand1-gRNA-2			0,4	18,0
AT25+ TaP-Hand1-gRNA-3			0,2	10,5
Control AT25+ TaP			0,4	14,6

Table 13: Differentiation summary of TaP-Nkx2.5$^{-/-}$ + At25fluc

Cell type	**Diff Start**	**Results**	**Conc cells in x10^6/ml**	**GFP positive CMs in %**
AT25+ TaP-Nkx2.5-gRNA-1	03.10.2021	Day 14	0,67	4,3
AT25+ TaP-Nkx2.5-gRNA-2			0,8	12,2
AT25+ TaP-Nkx2.5-gRNA-3			0,8	9,0
Control AT25+ TaP			0,8	9,0
AT25+ TaP-Nkx2.5-gRNA-1	06.10.2021	Day 14	0,26	15,7
AT25+ TaP-Nkx2.5-gRNA-2			0,43	38,1
AT25+ TaP-Nkx2.5-gRNA-3			0,21	15,0
Control AT25+ TaP			0,4	20,0
AT25+ TaP-Nkx2.5-gRNA-1	18.10.2021	Day 14	0,04	15,8
AT25+ TaP-Nkx2.5-gRNA-2			0,69	28,3
AT25+ TaP-Nkx2.5-gRNA-3			0,27	14,6
Control AT25+ TaP			1,72	19,1
AT25+ TaP-Nkx2.5-gRNA-1	22.10.2021	Day 14	3,05	13,4
AT25+ TaP-Nkx2.5-gRNA-2			1,78	13,2
AT25+ TaP-Nkx2.5-gRNA-3			1,94	21,6
Control AT25+ TaP			2,52	17,3

3.3.4. Intraembryonic Complementation assay

3.3.4.1. Breeding Results

On May 25th 2021 4 mice from the CECAD animal house were imported to the animal facility in the Pharmacology. 2 Female mice (ID # 0000RS-00188 and -00189) both born on Jan 08th 2021, and 2 male mice (ID # 000RS-00187 and -00190) both born on February 06th 2021 were picked up, moved to the Pharmacology and quarantined for 7 days following SOP THNW 003 (see Appendix II.b).

On June 1st breeding of imported animals was set up, for establishing the animal line under our care. Female mice were age of 20 weeks, male mice 16 weeks.

Table 14: List of all Female mice house in the Pharmacology, summarized are the breeding results and/or if the mouse was utilized for superovulation experiment.

Animal ID	Date of Birth	ID of Mother	Breeding start	With Male ID	Breeding Result
00188	08.01.21	-	01.06.21	00187	22.06. gave birth, 3 pubs dead on 23.06
					22.07 gave birth (5M and 4F)
			20.07.21	00190	16.08 gave birth (3M and 3F)
					29.09 gave birth, 1 pub dead on next day
					31.10 gave birth (1M and 1F)
					24.11 gave birth (3M and 1F)
00189	08.01.21	-	01.06.21	00190	02.07 gave brith (4M and 1F)
00195	02.07.21	00189	28.10.21	00191	03.12 gave birth (1 M and 4F)
00201	22.07.21	00188	28.10.21	00191	03.12 gave birth (3M and 2F)
00202	22.07.21	00188	28.10.21	00192	27.11 gave birth (5M and 2F)
00203	22.07.21	00188	28.10.21	00192	02.12 gave birth (3Mand 4F)
00204	22.07.21	00188	28.10.21	00196	20.11 gace birth (1M and 2F)
					10.12 gave birth (3M and 1F)
00208	16.08.21	00188	28.10.21	00197	30.11 gave birth, 4 pubs dead on 06.12
00209	16.08.21	00188	28.10.21	00197	18.11 gave birth (5 M and 3F)
00210	16.08.21	00188			Found dead
00212	31.10.21	00188			
00218	18.11.21	00209			
00219	18.11.21	00209			
00220	18.11.21	00209			
00222	20.11.21	00204	22.03.22	00248	12.04 gave birth to 5 pubs, 3F2M
00223	20.11.21	00204	31.05.22	00257	05.07 gave birth, 5 pubs all dead on 08.07
					02.08 gave birth, 4 pubs all dead on next day
00227	24.11.21	00188	22.03.22	00252	13.04 gave birth, 3 M 3 F
					31.07 gave birth, 4 pubs all dead on 01.08
00233	27.11.21	00202			*Superovulation 03.01.2022*
00234	27.11.21	00202			*Superovulation 17.01.2022*
00238	02.12.21	00203			*Superovulation 17.01.2022*
00239	02.12.21	00203			*Superovulation 17.01.2022*
00240	02.12.21	00203			*Superovulation 17.01.2022*
00241	02.12.21	00203			*Superovulation 17.01.2022*
00243	03.12.21	00195			*Superovulation 03.01.2022*
00244	03.12.21	00195			*Superovulation 03.01.2022*
00245	03.12.21	00195			*Superovulation 03.01.2022*
00246	03.12.21	00195			*Superovulation 03.01.2022*

00250	03.12.21	00201	22.03.22	00252	no breeding results
00251	03.12.21	00201	22.03.22	00254	08.08. gave birth (2M and 4F)
00255	10.12.21	00204	31.05.22	00256	31.07 gave birth, 5 pubs all dead on 01.08
00258	12.04.22	00222			*Superovulation 16.05.2022*
00259	12.04.22	00222			*Superovulation 16.05.2022*
00260	12.04.22	00222			*Superovulation 16.05.2022*
00264	13.04.22	00227			*Superovulation 16.05.2022*
00265	13.04.22	00227			*Superovulation 16.05.2022*
00266	13.04.22	00227			*Superovulation 16.05.2022*
00269	08.08.22	00251	04.10.22	00267	no breeding results
00270	08.08.22	00251	04.10.22	00267	31.10 gave birth, (2M and 5F)
00271	08.08.22	00251	04.10.22	00268	26.10 gave birth (8F) 08.12 gave brith (2M and 2F)
00272	08.08.22	00251	04.10.22	00268	17.11 gave birth (2M and 4F)
00273	26.10.22	00271			*Superovulation 28.11.2022*
00274	26.10.22	00271			*Superovulation 28.11.2022*
00275	26.10.22	00271			*Superovulation 28.11.2022*
00276	26.10.22	00271			*Superovulation 28.11.2022*
00277	26.10.22	00271			*Superovulation 28.11.2022*
00278	26.10.22	00271			
00279	26.10.22	00271			
00280	26.10.22	00271			
00283	31.10.22	00270			
00284	31.10.22	00270			
00285	31.10.22	00270			
00286	31.10.22	00270			
00287	31.10.22	00270			
00290	17.11.22	00272	19.01.23	00282	23.04 gave birth, 2 pubs all dead on next day
00291	17.11.22	00272	19.01.23	00281	09.02 gave birth (1M and 3F) 27.03 gave birth (4M and 5F) 19.04 gave birth (1M and 2F)
00292	17.11.22	00272			
00293	17.11.22	00272			
00296	08.12.22	00271	03.03.23	00295	25.03 gave birth (3M and 2F)
00297	08.12.22	00271	03.03.23	00294	no breeding results
00303	09.02.23	00291			
00304	09.02.23	00291			
00305	09.02.23	00291	15.11.23	00307	10.12 gave birth, all pubs dead on 27.12
00309	25.03.23	00296			*Superovulation 01.05.2023*
00310		00296			*Superovulation 01.05.2023*
00315	27.03.23	00291			*Superovulation 01.05.2023*

00316	27.03.23	00291			sacrificed 28.04 due to health condition
00317	27.03.23	00291			*Superovulation 01.05.2023*
00318	27.03.23	00291			*Superovulation 01.05.2023*
00319	27.03.23	00291			*Superovulation 01.05.2023*
00321	19.04.23	00291	06.09.23	00314	no breeding results
			15.11.23	00308	no breeding results
00322	19.04.23	00291	06.09.23	00320	27.09 gave birth (2F)
00323	27.09.23	00322			Exported for MSC isolation experiment (§4.23.017)
00324	27.09.23	00322			Exported for MSC isolation experiment (§4.23.017)

After initial breeding and generation of our own line, breeding was set up when female reached fertile age of 8 weeks or utilizing youngest available female. Breeding indicating a litter size of 8 pubs with 50% female, lead to setting up a minimum of two breeding's at the same time for production of 4 week old females for experiment.

In total we had 33 breeding results over the span of 27 months (June 2021 – September 2023). Mean litter size was 5,5 pubs with a 55% quota of female offspring. Mean duration of breeding time (days from sitting female and male together in a breeding cage until pubs are born) was 33 days with an extreme outlier of 162 days.

Of these 33 breeding results we observed 9 breeding's, 27% of all breeding cases, where pubs were observed, registered in PyRat and then at some point in their infancy phase were found dead or missing presumably eaten by their parents.

Last possible breeding opportunities were set up with the youngest female mice on 15 November 2023 with mouse 305 and 321. Mouse 305 gave birth after 25 days, but litter was found dead on infancy day 17. On Jan 12th 2024, we changed the feed to special breeding food. On Feb 06th, 2024 after 84 days of unsuccessful breeding, we stopped the breeding with females 305 and 321, due to no results and the age of mice (almost 1 year old).

3.3.4.2. Cross-breeding with wildtype C57BL6/J

On June 14th 2024 two male C57BL6 mTmG mice could be imported from the CECAD Animal house again. Both males (000RS-00325 and -00326) were borne on 28.01.2024.

Wt female mice (000RS-00001 and -00002) were ordered from Jackson and imported into the animal house on 18.06.2024 both 7 weeks old. After quarantine, initial breeding was set up on 25th June 2024 (00001 x 00326 and 00002 x 00325). Offspring of these breeding's are referred to as F1 and all carry the genotype wt/tg following Mendelian´s principle of uniformity.

Table 15: Animals of the F1 generation and their genotype

Animal ID	Sex	Date of Birth	Parents	Genotype
00327	M	16.07.24	00001 x 00326	wt/tg
00328	M	16.07.24	00001 x 00326	wt/tg
00329	M	16.07.24	00001 x 00326	wt/tg
00330	M	16.07.24	00001 x 00326	wt/tg
00331	M	16.07.24	00001 x 00326	wt/tg
00332	F	16.07.24	00001 x 00326	wt/tg
00333	F	16.07.24	00001 x 00326	wt/tg
00334	M	17.07.24	00002 x 00325	wt/tg
00335	M	17.07.24	00002 x 00325	wt/tg
00336	M	17.07.24	00002 x 00325	wt/tg
00337	F	17.07.24	00002 x 00325	wt/tg
00338	F	17.07.24	00002 x 00325	wt/tg
00339	F	17.07.24	00002 x 00325	wt/tg
00340	F	17.07.24	00002 x 00325	wt/tg
00341	F	17.07.24	00002 x 00325	wt/tg
00342	M	07.09.24	00001 x 00326	wt/tg
00343	M	07.09.24	00001 x 00326	wt/tg
00344	M	07.09.24	00001 x 00326	wt/tg
00345	F	07.09.24	00001 x 00326	wt/tg
00346	F	07.09.24	00001 x 00326	wt/tg
00347	F	07.09.24	00001 x 00326	wt/tg
00348	F	07.09.24	00001 x 00326	wt/tg
00349	F	07.09.24	00001 x 00326	wt/tg
00350	F	07.09.24	00001 x 00326	wt/tg

Probability receiving a female and male homozygote Rosa26mTmG transgenic mice in F2 generation was calculated with 12.5% respectively (*Figure 45*). With a litter size of 6, rounded up from our calculated mean litter size 5.5, and the probability for tg/tg female and male mice, 3 breeding's were set up to generate at least 16 individuals for the F2 generation.

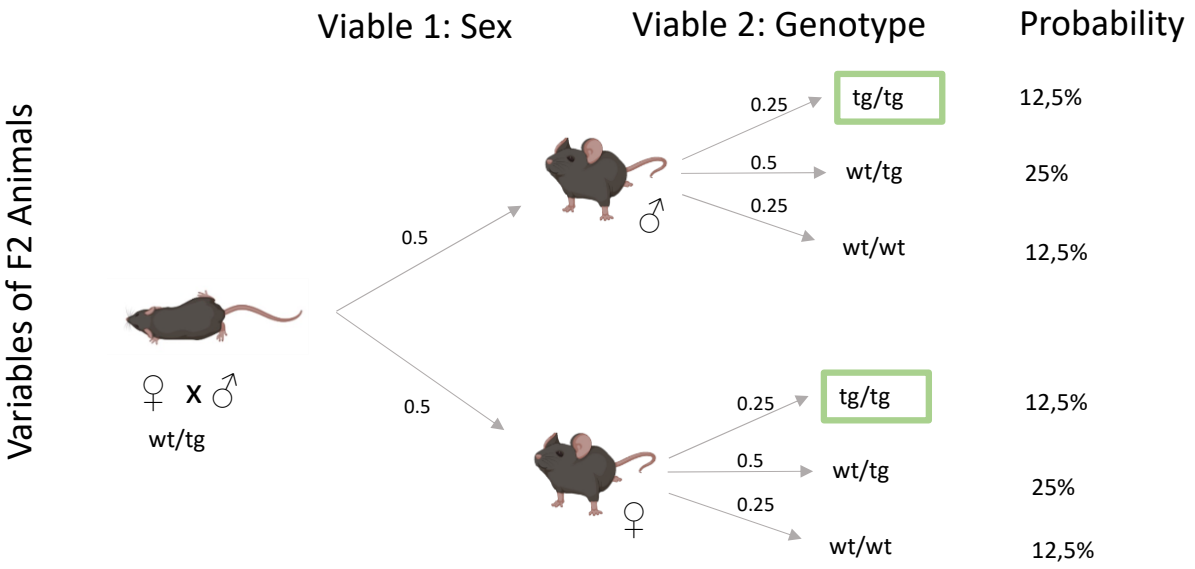

Figure 45: Calculations for breeding F1 animals to generate F2 individuals with desired genotype and sex.

When F1 generation reached age of 8 weeks 3 females were breed 1:1 with 3 male mice (338 x 328, 337 x 327, 339 x 329) avoiding brother sister mating. F2 offspring were genotyped by isolation of DNA described in 2.2.2 using tissue ear punches, taken when mice receive their Laboratory Animal ID. PCR was set up using PCR procedure describes in Appendix II.d. PCR was visualized on a 2.5% Agarose gel run for 30 min at 130 V (*Figure 46*).

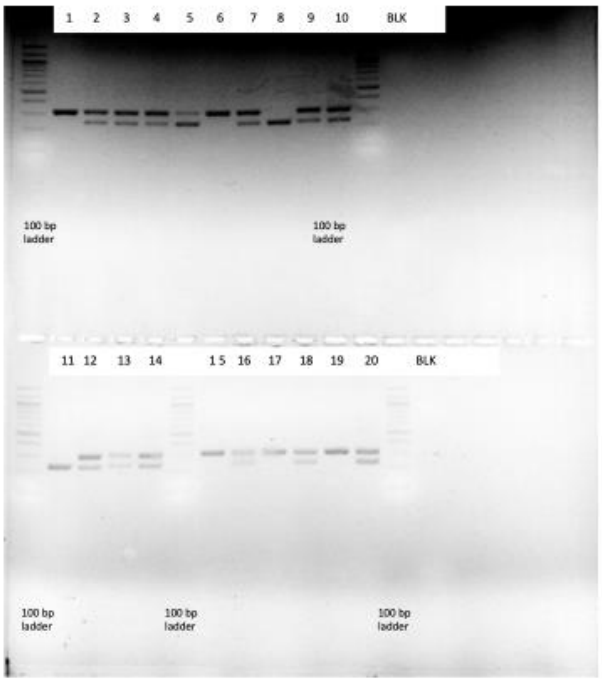

#	Mouse ID
1	00351
2	00352
3	00353
4	00354
5	00355
6	00356
7	00357
8	00358
9	00359
10	00338
11	00360
12	00361
13	00362
14	00337
15	00363
16	00364
17	00365
18	00366
19	00367
20	00339

Figure 46: Genotyping results for Rosa26 transgene mice.

PCR was run on a 2.5 % Agarose gel for 30 min at 130V. F2 offspring are loaded in the gel next to their mother of F1 generation.

Genotyping results of the F2 generation is summarized in *Table 16*.

Table 16: Animals of the F2 generation and their genotypes

Animal ID	Sex	Date of Birth	Parents	Genotype
00351	M	03.10.24	00338 x 00328	wt/wt
00352	M	03.10.24	00338 x 00328	tg/wt
00353	M	03.10.24	00338 x 00328	tg/wt
00354	M	03.10.24	00338 x 00328	tg/wt
00355	M	03.10.24	00338 x 00328	tg/wt
00356	F	03.10.24	00338 x 00328	wt/wt
00357	F	03.10.24	00338 x 00328	tg/wt
00358	F	03.10.24	00338 x 00328	tg/tg
00359	F	03.10.24	00338 x 00328	tg/wt
00360	M	05.10.24	00337 x 00327	tg/tg
00361	F	05.10.24	00337 x 00327	tg/wt
00362	F	05.10.24	00337 x 00327	tg/wt
00363	M	18.10.24	00329 x 00339	wt/wt
00364	M	18.10.24	00329 x 00339	tg/wt
00365	F	18.10.24	00329 x 00339	wt/wt
00366	F	18.10.24	00329 x 00339	tg/wt
00367	F	18.10.24	00329 x 00339	wt/wt

Mice with homozygote transgene (00358 x 00360) were cross breed starting 13th December 2024.

Table 17: Animal List of transgenic C57BL6 mTmG mice.

Animal ID	Sex	Date of Birth	Notes
00368	M	04.01.25	
00369	F	04.01.25	
00370	F	04.01.25	
00371	F	04.01.25	
00372	F	04.01.25	no breeding results
00373	F	04.01.25	no breeding results
00374	M	27.01.25	
00375	M	27.01.25	
00376	M	27.01.25	
00377	F	27.01.25	
00378	F	27.01.25	
00379	M	26.03.25	
00380	M	26.03.25	
00381	M	26.03.25	
00382	M	26.03.25	
00383	M	26.03.25	
00384	M	26.03.25	

00385	F	26.03.25	
00386	F	26.03.25	no breeding results
00387	F	26.03.25	Gave birth 06.06 (2M and 5 F)

The 5 female mice born on June 6th were used for a superovulation experiment on July 7th 2025. After last Superovulation, Injection and analyzation of the offspring mice, the animal experiments were determined due to expiration of TV 81-02.04.2020.A200 on August 31, 2025.

3.3.4.3. Pre-Testing Cre Recombinase mRNA strategy

For verification if injection of one cell of 2-cell blastocysts works in the R26 mTmG model, a small group of 2-cell blastocysts were micro-injected with just Cre-Recombinase mRNA. Blastocysts were developed for additional 72 h and imaged using fluorescence microscopy (*Figure 47*). In total 15 blastocysts were injected and checked next to 3 blastocysts (controls) that were not injected. Injected blastocysts showed a fluorescent color switch in 14 out of 15 injected blastocysts. With all 14 green and red fluorescence.

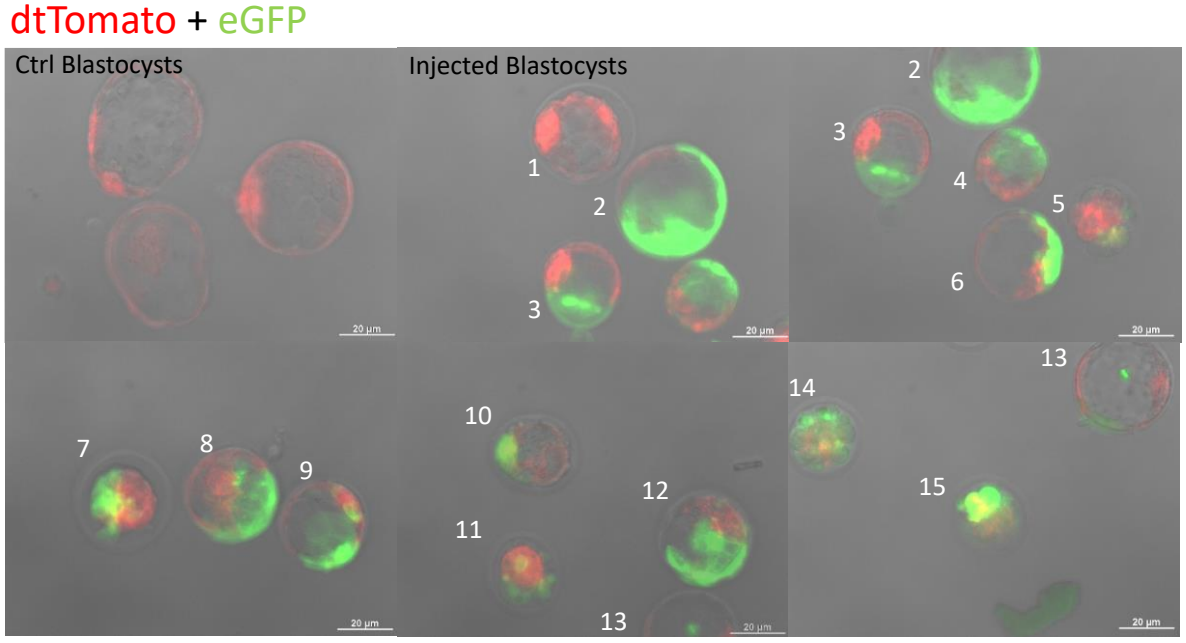

Figure 47: Microinjected 2-cell Blastocysts.

One cell was injected with Cre Recombinase mRNA. Cells were cultured for 3 days and imaged using Fluorescence microscope. 3 Control Blastocysts, without injection were compared to 15 injected Blastocysts. Scale bar 20 µm.

3.3.4.4. Nkx2-5

First animal experiment was conducted with Nkx2-5-gRNA-1. Female mTmG mice were super ovulated and one of 2-cell blastocysts were micro-injected with RNP and Cre recombinase

mRNA. Offspring mice were sacrificed and organ cryo-sections imaged with fluorescence microscopy (*Figure 48*). Out of 6 mice, 4 showed a weak eGFP signal.

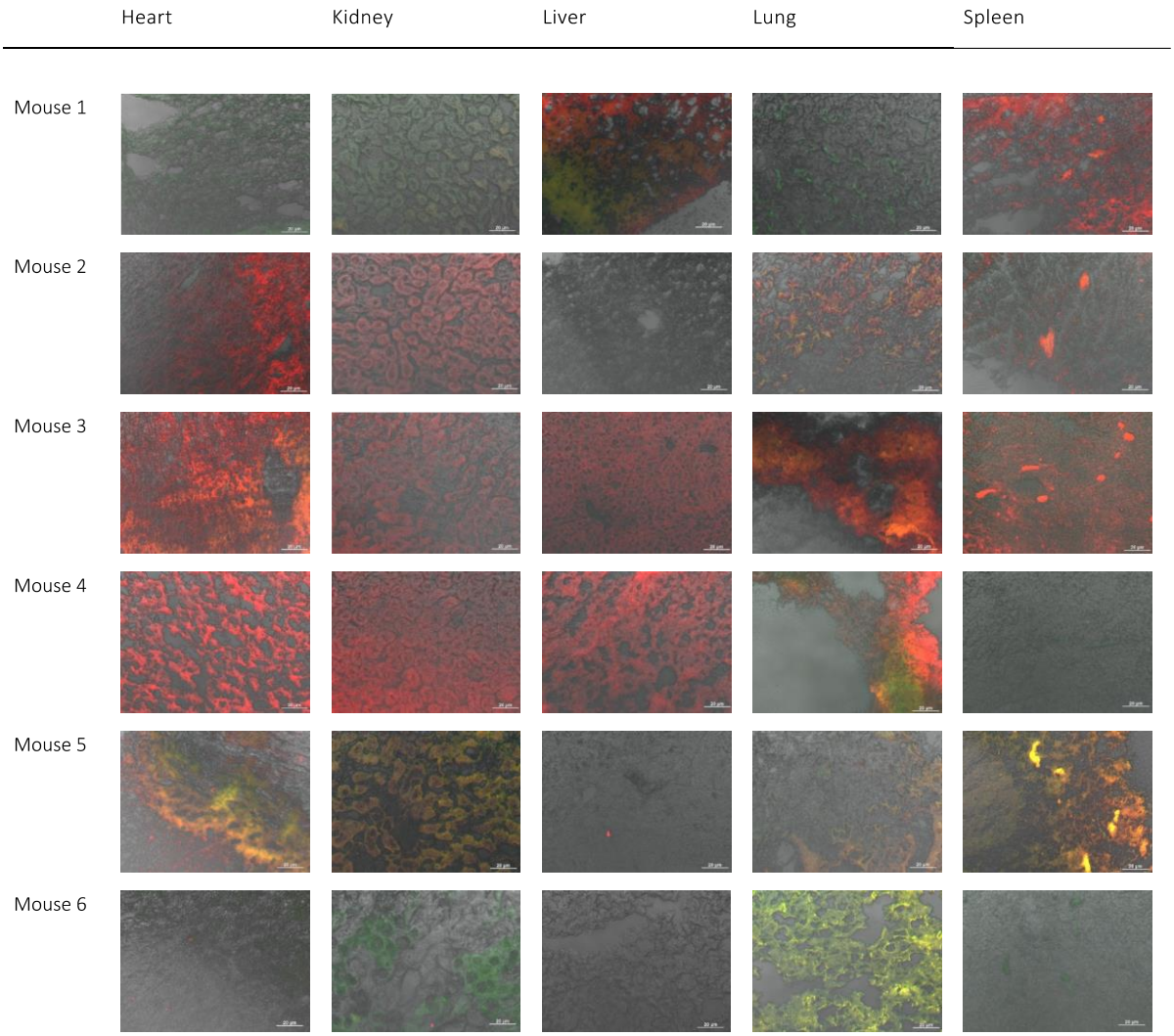

Figure 48: Intra-embryonic complementation assay mice Nkx2-5.

All mice were sectioned on cryostat and analyzed using fluorescence microscope. Floursecene is dtTomato and eGFP expressed on surface of cells due to transgenic backround of mice. Scale bar 20 µm.

3.3.4.5. Hand1

Second animal experiment was conducted with Hand1-gRNA-1. Female mTmG mice were super ovulated and one of 2-cell blastocysts were micro-injected with RNP and Cre recombinase mRNA. Offspring mice were sacrificed and organ cryo sections imaged with fluorescence micoscropy (*Figure 49*). Out of 9 mice only 3 showed eGFP and dtTomato fluorescence for all analyzed tissues(Mouse 1,2 and 6). For the heart only 2 mice showed eGFP fluorescence. Therefore, the heart of mouse 6 was cut to a deeper level and imaged to get an overview of the location of the eGFP expressing cells (*Figure 50*). Mice with both fluorescence

signals were genotyped using primers Hand1-184-F (Seq.: GCCTACAGAAACCTTCAAGAGG) and Hand1-671-R (Seq.: CTCTCCTTCTTGGGTCCTGAG) and run agarose gel (*Figure 51)*. PCR products cleaned up and used for setting up Sanger sequencing using Primer Hand1-184-F for sequencing as well. Sequencing results indicate mice 1, 2 and 6 are wildtype for Hand1 gene (*Figure 52)*.

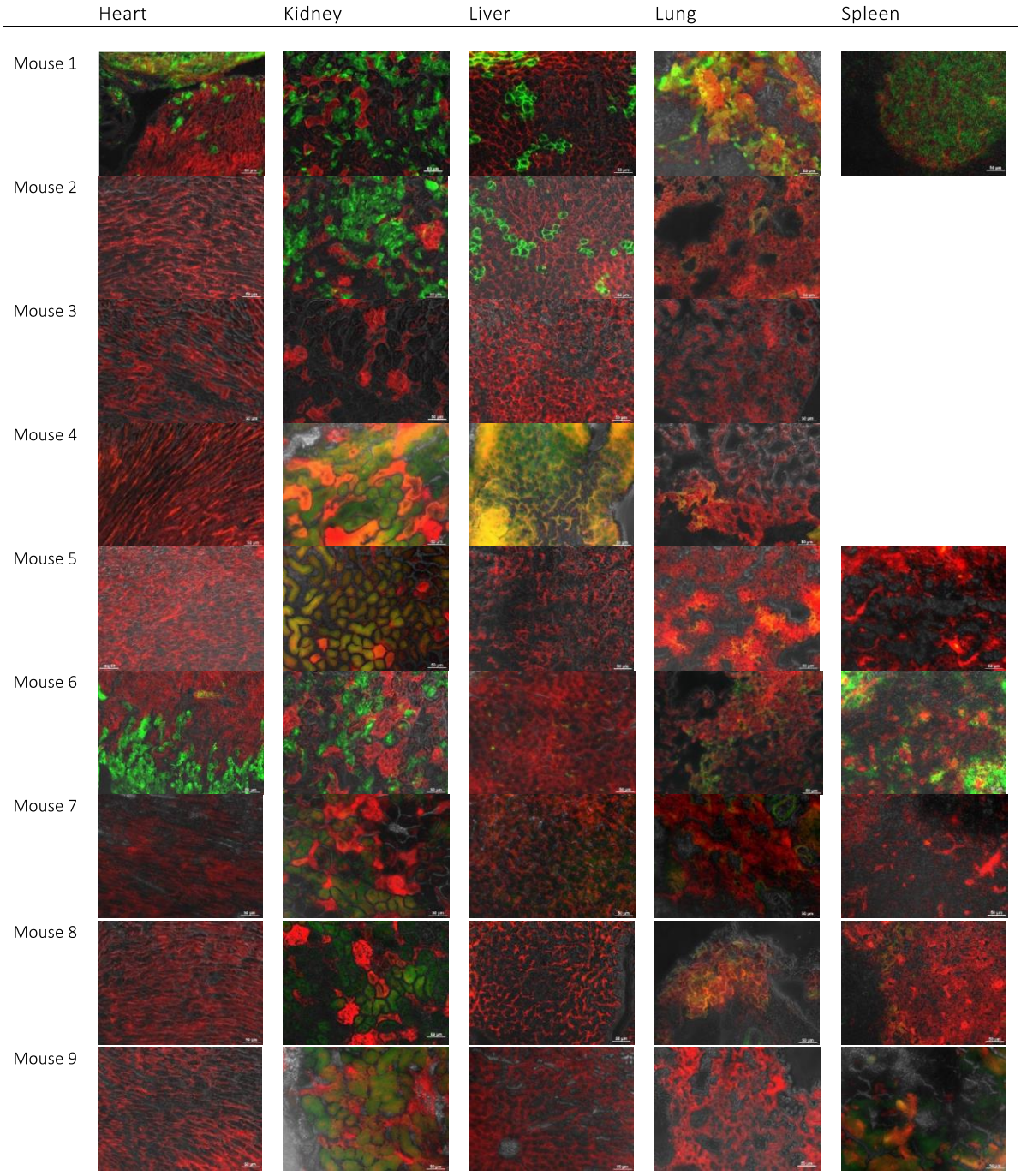

Figure 49: Intra-embryonic complementation assay mice Hand1.

All mice were sectioned on cryostat and analyzed using fluorescence microscope. Fluorescence is dtTomato and eGFP expressed on surface of cells due to transgenic background of mice. Scale bar 50 µm.

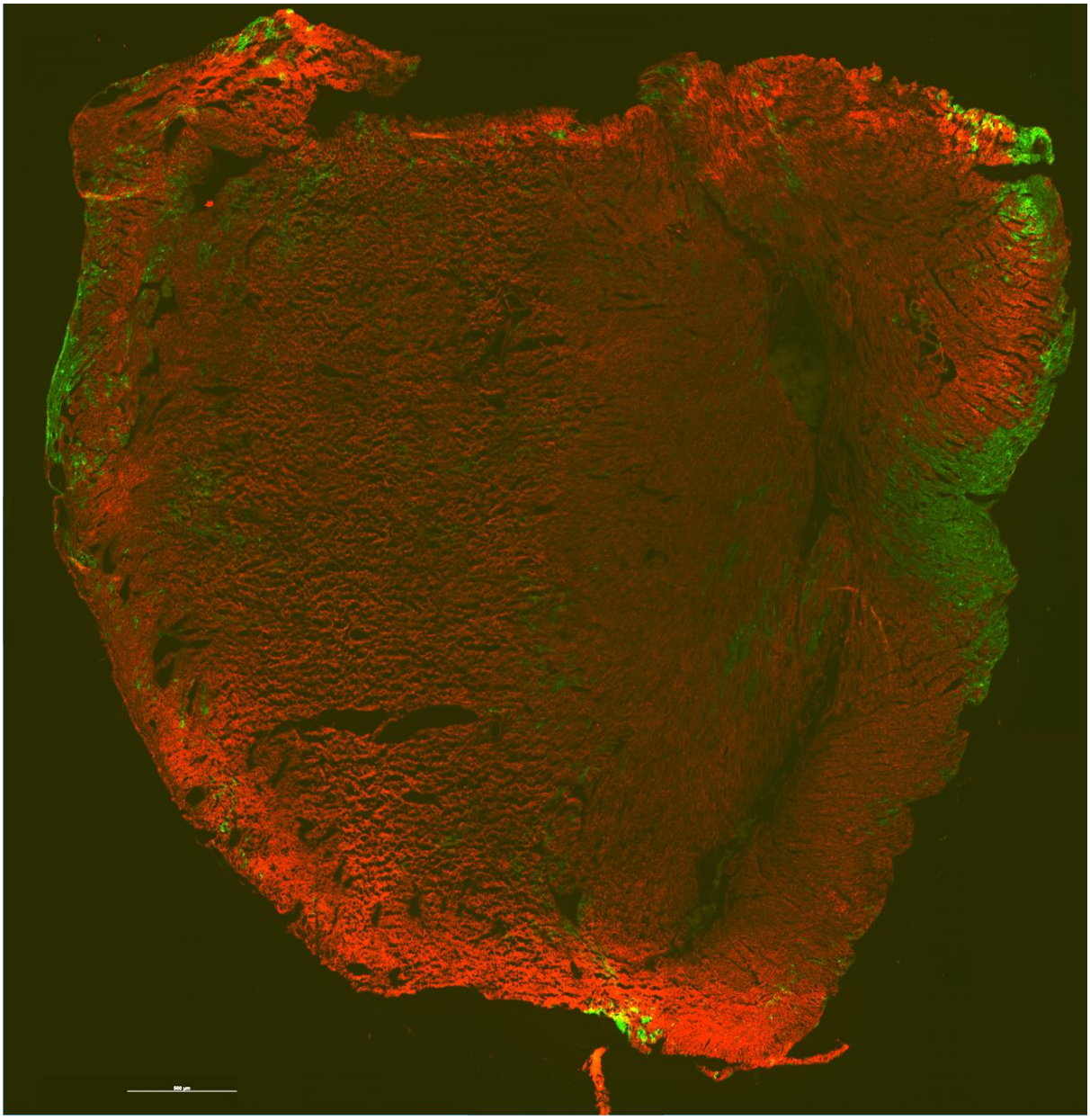

Figure 50: Microscope image of Heart slice of Intraembryonic complementation assay Hand1-mouse 6. Image is stitched out of multiple single images. Imaged with fluorescence microscope. Scale bar 500 µm.

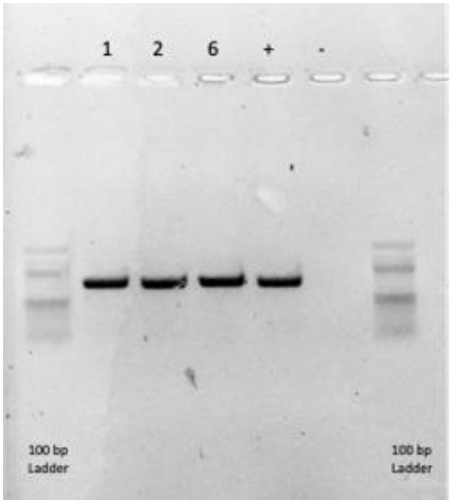

Figure 51: Genotyping of Hand1- Intraembryonic complementation assay.

Only eGFP/dtTomato fluorescent mice were analyzed: mouse 1, 2 and 6 were set up for PCR next to wt control mouse (+) and a negative Control (-) using only water as DNA template. PCR was set up with Primer Pair: Hand1-184-F to Hand1-678-R , run with usual PCR cycle and visualized on 1% Agarose gel by running for 30 min at 130V. Inverse image of LED Gel box.

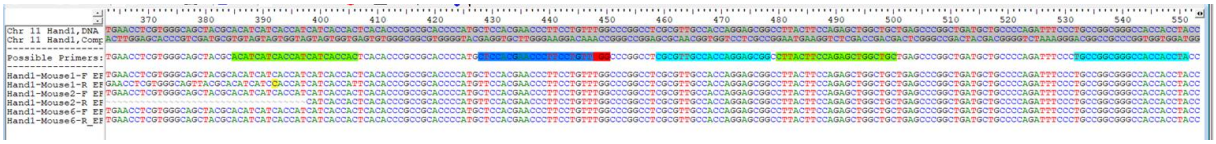

Figure 52: Sanger Sequencing of Hand1 intra-embryonic complementation assay.

3.3.4.6. Hand 2

Next animal experiment was conducted with Hand2-gRNA-1. Female mTmG mice were super ovulated and one of 2-cell blastocysts were micro-injected with RNP and Cre recombinase mRNA. Offspring mice were sacrificed and organ cryo sections imaged with fluorescence microscopy.

Tissue samples of all mice only showed red fluorescent (*Figure 53*). Mice were genotyped using Hand2-405-F (Seq.: CGAGGTAGCTCCACGCTAAG) and Hand2-1118-R (Seq.: CTGTAGGACAGGGCCATACTGT) and all mice were genotyped wildtype (*Figure 54*).

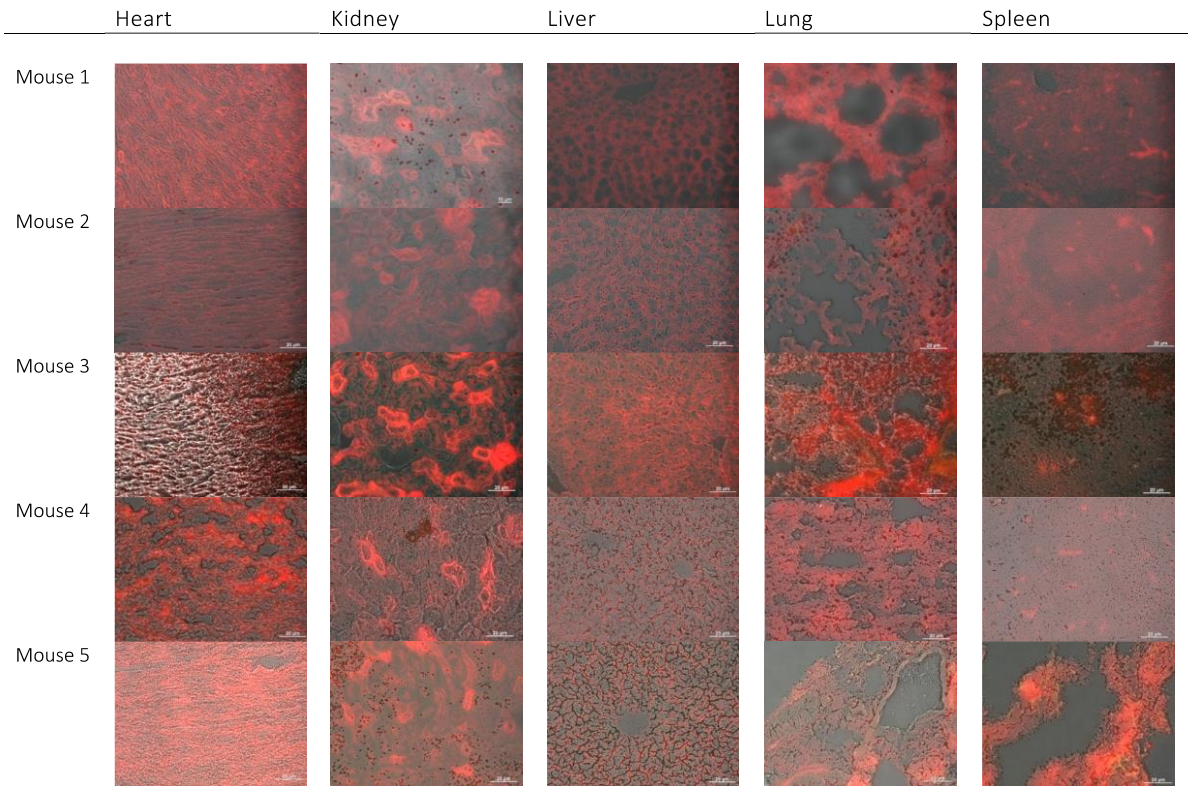

Figure 53: Intra-embryonic complementation assay mice Hand2.

All mice were sectioned on cryostat and analyzed using fluorescence microscope. Fluorescence is dtTomato and eGFP expressed on surface of cells due to transgenic background of mice. Scale bar 20 µm.

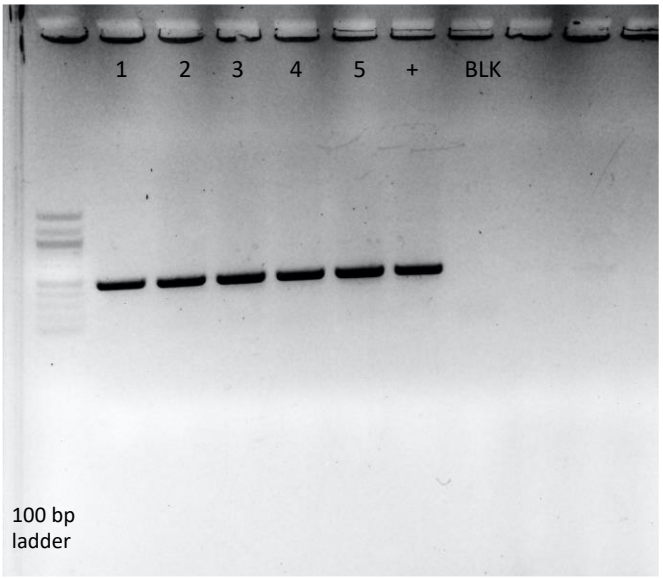

Figure 54: Genotyping PCR Hand2 on Intraembryonic complementation assay mice Hand 2.

3.3.4.7. Pdx1

As Kobayasi et al. [69] and Wu et al. [70] successfully obtained a rat PSC grown pancreas from an organ complementation experiment utilizing $Pdx1^{-/-}$ mice, we followed up our experimental strategy of *in vivo* intraembryonic complementation assay for the gene Pdx1.

Next animal experiment was conducted with Pdx1-gRNA-1. Female mTmG mice were super ovulated and one of 2-cell blastocysts were micro-injected with RNP and Cre recombinase mRNA. Offspring mice were sacrificed and organ cryo sections imaged with fluorescence microscopy (*Figure 55*).

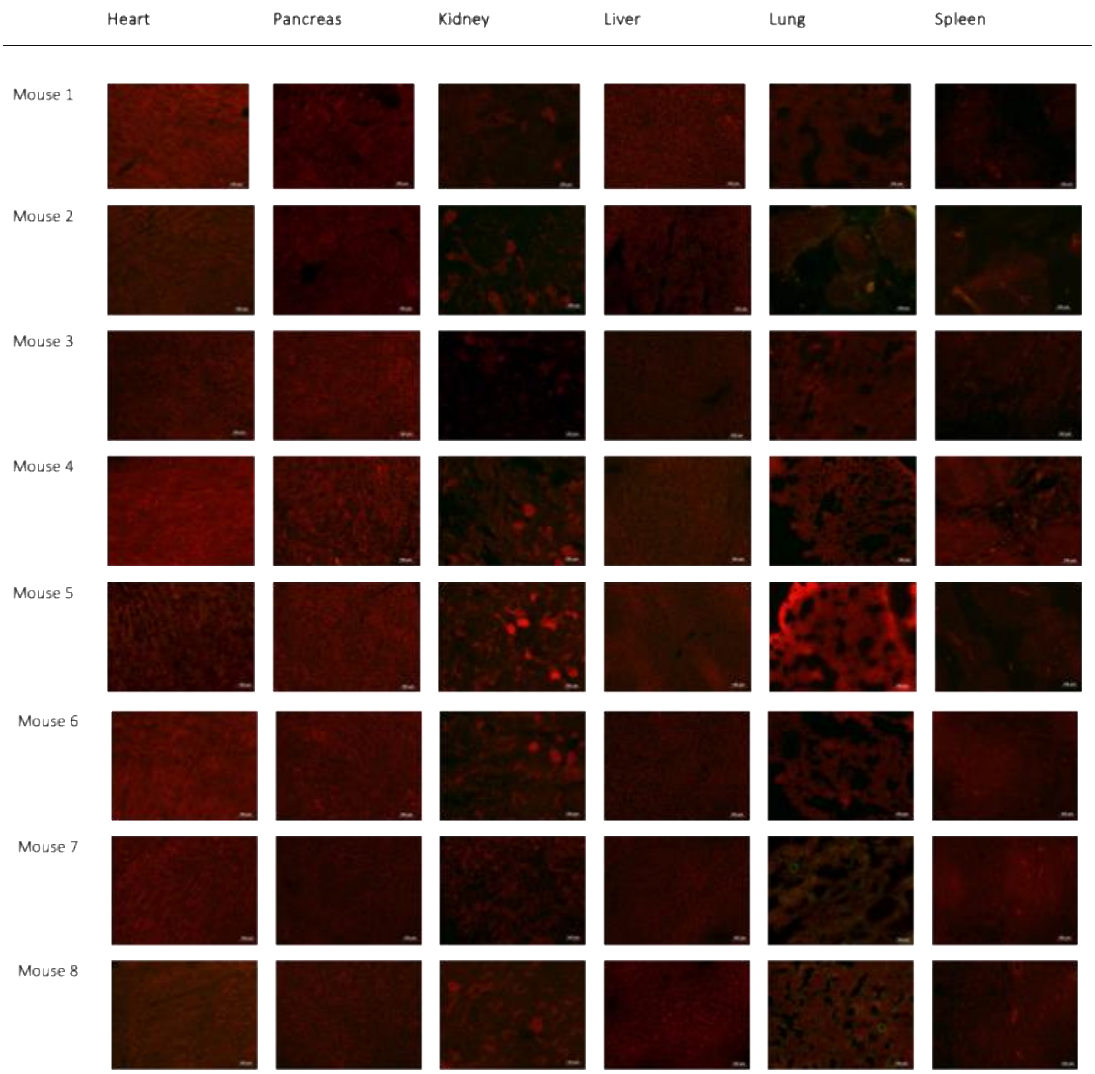

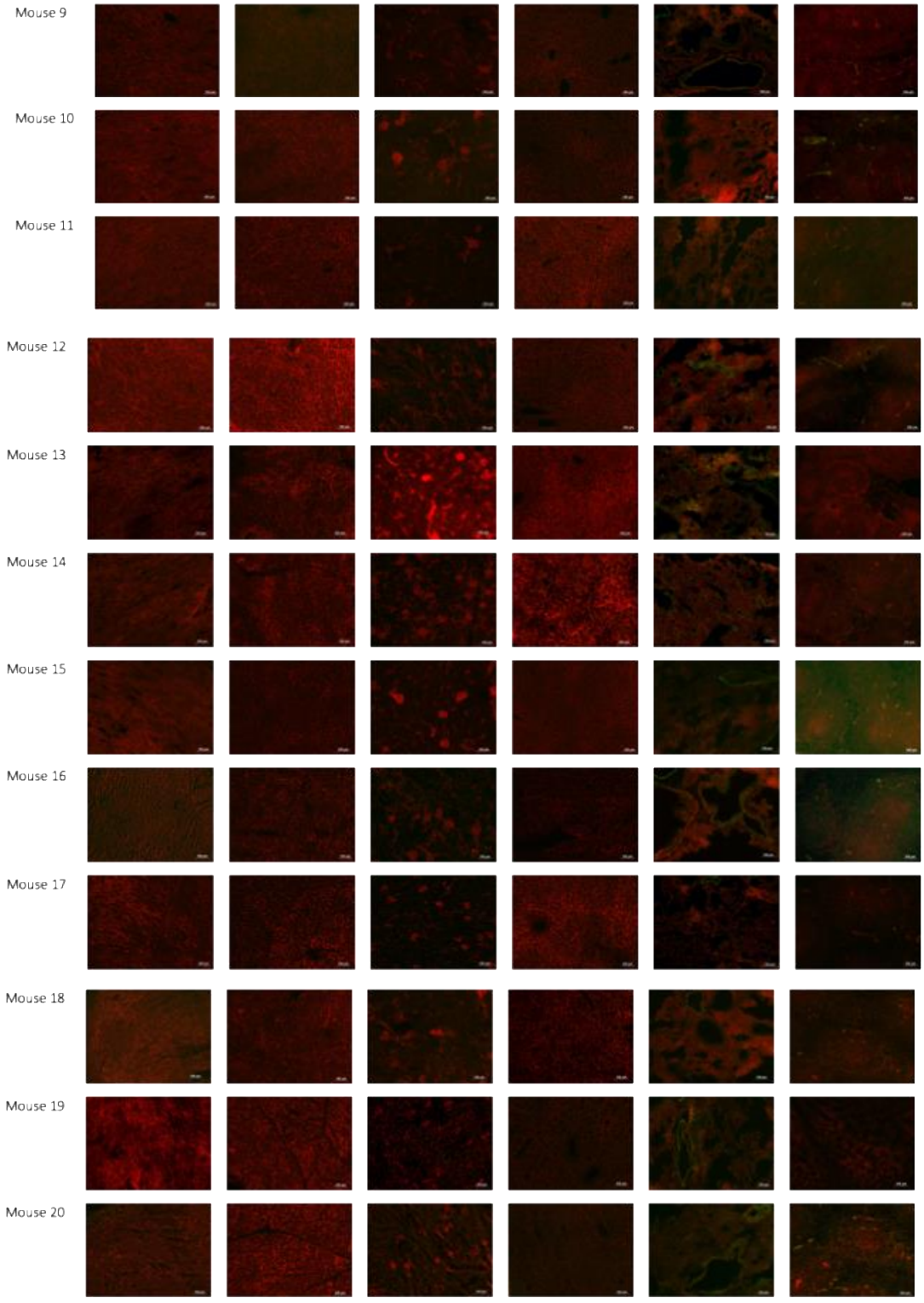

Figure 55: Intra-embryonic complementation assay mice Pdx1.

All mice were sectioned on cryostat and analyzed using fluorescence microscope. Fluorescence is dtTomato and eGFP expressed on surface of cells due to transgenic background of mice. Scale bar 100 µm.

DNA was isolated from all mice and genotyped using Primer Pair Pdx1-14-F (Seq.: AGGAGAGCAGTGGAGAACTGTC) and Pdx1-598-R (Seq.: CCAAGTCCAGACTAGGGAAAGA) and run on a 1% agarose gel to visualize genotyping results (*Figure 56*).

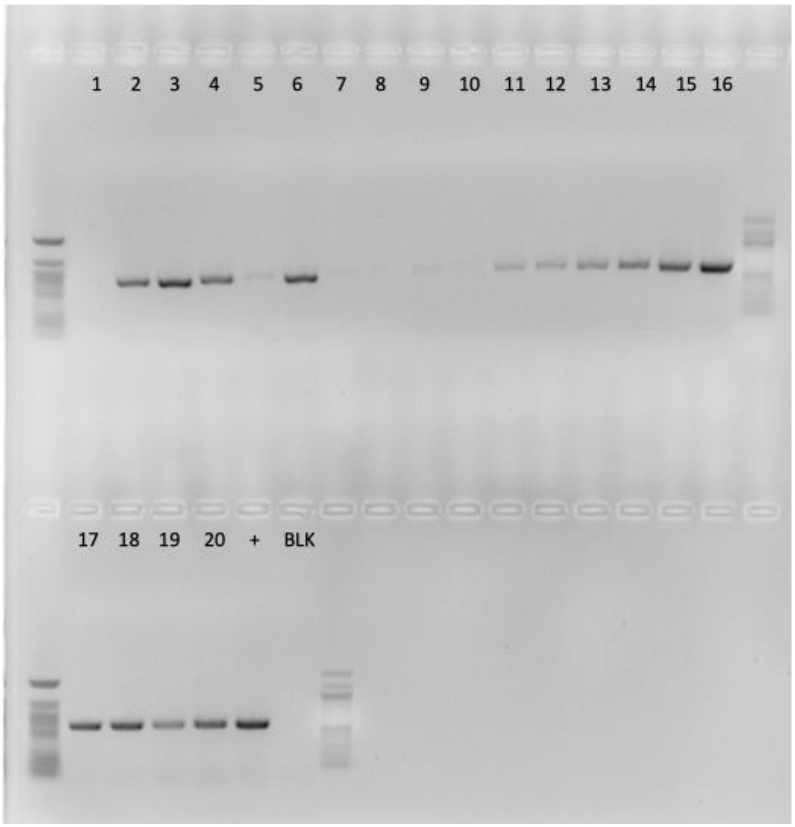

Figure 56: PCR of Pdx Mice of intraembryonic complementation assay. 1% agarose gel is poured

All mice were e set up for PCR next to wt control mouse (+) and a negative Control (-) using only water as DNA template. PCR was set up with Primer Pair: Pdx1-14-F to Pdx1-598-R , run with usual PCR cycle and visualized on 1% Agarose gel by running for 30 min at 130V. Inverse image of LED Gel box.

4. Discussion

4.1. Generation of hypoimmunogenic hiPSC for xenotransplantation purposes

Multiple published works demonstrate that the deletion of a combination of immune related surface proteins and/or over-expression of immunomodulatory proteins, can minimize the immune reaction between graft and host [24, 33, 34].
Harding *et al.* (2023) have shown by over-expressing transgenes Pdl1, Cd200, Cd47, H2-M3, Fasl, Serpinb9, Ccl21, and Mfge8 in embryonic mouse stem cells (mESCs), and transplanting them in an allogenic recipient, that these cloaked mESCs could stay hidden from the mouse immune system for several weeks [33].
Deuse and colleagues (2019) have shown promising results for murine $B2m^{-/-}$ $Ciita^{-/-}$ tgCd47 iPSCs evading surveillance by the immune system in fully immunocompetent allogeneic recipients, while at the same time showing that human $B2M^{-/-}CIITA^{-/-}$ tgCD47 iPSCs evade the immune system of humanized immunocompetent mice [34].

For studying the therapeutic effect of iPSCs or iPSC derived cells, xenotransplantation have contributed immensely to the field of regenerative medicine [87]. But xenotransplantation still relies on strong immunosuppressing medication [20, 68, 88] or on working in immune-deficient animals [89], one major issue, yet to be solved for these procedures. Immune suppression medication, like T-cell blocking antibodies, increases the experimental costs immensely, makes laboratory animals more susceptible to diseases, while leading to a higher mortality rates [20]. This is a particularly vital challenge when long-term studies on grafts are conducted. At the same time interpretation of these xenotransplantation experiments is getting more complicated. The medication might mask some physiological reactions, worth investigating, and acute rejection of the body, which may be triggered by the tissue injury alone, may be overlooked, leading to an overestimation of the therapy's effectiveness [90].

Zimmermann and his team (2025) for example recently published a studies, where the transplanted a heart patch consisting of allogenic iPSC derived CMs and fibroblasts into recipients primates relying on stringent of immune suppression medication [67]. At the same time, *in vitro* studies are often carried out with human iPSCs, to discover multiple pathways and developmental niches, as the ultimate goal of stem cell-based application is the translation into the clinical application in humans [91].

Following the conceptualization of Deuse *et al.* (2019) [34], we utilized human iPSC, deleted immune related surface proteins (MHC class I and II) and over-expressed the surface protein CD47 in the murine form for xenotransplantation purposes. This way we expect to be able to transplant human iPSC into mice as a xenograft without depending on strong immunosuppressing medication. It is important to note, that the antibody mediated rejection cannot be controlled by this strategy. However, since it typically develops with a delay, elimination of the initial T-cell and NK cell mediated rejection would be a major step ahead, improving the overall stability of the graft [92].

MHC class I and II were knocked out using a double guide RNAs approach for both targets B2M and CIITA, delivering CRISPR reagents directly as a Ribonucleoprotein complex (RNP). RNP Reagents are prepared at bench top and can be electroporated into the cell in one single nucleofection step. This way we could efficiently knock out both genes at the same time and quickly identify a double knock out candidate using T7 Endonuclease I detection kit. Verification of the knock-out candidate was done through DNA Isolation, PCR, Sanger Sequencing, ICE and finals NGS. The results indicate that we were able to generate B2M and CIITA human iPSC knockout cells (NP0040-SM). Biallelic knock out was in the end confirmed with Next generation sequencing (NGS) characterizing both targets as heterozygote knock out. B2M was knocked out with an 18 bp and 27 bp deletion spanning exon 2, while of CIITA exon 3 was knocked out with a 15 bp and 57 bp deletion. Heterogenic biallelic CRISPR-Cas9 knock-outs, have been observed before and are attributed the different cleaving properties of Cas9 on the non-complementary strand, compared to the complementary strand. On the complementary strand the Cas9 cleaves specific at the -3 bp of the PAM site, while the non-commentary strand seems to be cleaved at multiple sites leading to a 5´overhang of the complementary strand [93]. At the same time Non-homologous end-joining (NHEJ) shows a strong influence by sequence context resulting in different repair patterns after double strand breaks (DSB) [93].

Characterizing these knock out cells, showed us that the pluripotent properties of NP0040-SM were not affected, including the differentiation capability, here shown through iPSC differentiation to cardiomyocytes.
Next, we proved the functional absence of MHC I of generated knock out cells (NP0040-SM) by stimulation with Interferon-γ. Expression of MHCI complexes on the surface of NP0040-SM did not increase after Interferon-γ stimulation, compared to NP0040-8 were Interferon-γ stimulated the MHCI expression significantly.

In these knock out cells (NP0040-SM), murine CD47 was constitutively expressed from a piggyback transposon stably integrated into the genome. Expression of the transgene was confirmed with immunofluorescence utilizing antibodies specifically directed against murine CD47 protein. The overexpression of murine CD47 is necessary as human and murine CD47 proteins differ in the N-Terminal domain critical for binding to the SIRPα receptor [94]. Even though human CD47 binds to the SIRPα receptor of mice macrophages, the affinity is weaker, leading to macrophage mediated phagocytosis [95]. With the overexpression of murine CD47 on the human iPS cells, the binding to the SIRPα receptor of the murine macrophages and NK cells can be mediated, protecting them from macrophage mediated phagocytosis.

With the generation of the $B2M^{-/-}$ $CIITA^{-/-}$ tg murine CD47 hiPSCs (cell line HSM47M) we expect the cells to survive long term in a xenotransplantation experiment in mice, due to their hypoimmunogenic properties.

4.2. Magnetic targeting of mesenchymal stem cells (MSCs)

Low cellular retention is one of the issues of stem cell-based transplantation applications. Magnetic targeting is one approach to enhance cellular retention upon transplantation, linked to the potentially increased duration of cell at the injection site.
Ottersbach and colleague (2017) could show the 7 fold increase of cellular retention when injecting magnetically labeled cells to the myocardium and applying a magnet for 10 min to the injection site, while at the same time showing that longer exposure to the magnetic field did not increase the engraftment rate further [96]. The mechanism of magnetic targeting is not understood so far.
In experiments carried out in our group we could, observe that cellular engraftment could be increased when transplanting microtissues consisting of cardiomyocytes and quick attaching MSCs [35]. Similar effects were observed by Zimmermanns research group, where heart patches of a cardiomyocytes and fibroblasts co-culture generated better functionality results [97].
We speculate that both methods, the utilization of CMs + MSCs microtissues and magnetically targeting, could significantly increase the cellular engraftment after transplantation in the heart. This is why we showed in a "prove of concept", that we can magnetically target MSCs.

For this, two different approaches of magnetically targeting are utilized. First the intracellular SPIONs loading of cells using force mediated endocytosis, well described in Zhang *et al.* (2023) [46], and secondly the novel strategy of bio-linking ferromagnetic particles to the surface of cells through antibodies. We showed adhesion (see Appendix I) and cell clustering kinetics for both magnetic targeting methods, *in vitro* both strategies performed equality.

No significant difference could be measured between SPIONs intracellular targeted MSCs compared to ferromagnetic particles labelled cells, for cell clustering. At the same time SPIONs loaded spheroids showed tendencies to adhere quicker than ferromagnetic targeted spheroids (see Appendix I). Initially we hypothesized that ferromagnetic cell clustering would hold an advantage, due to the ferromagnetic properties, compared to the SPIONs that only hold superparamagnetic properties. Ferromagnetic materials stay magnetized even after the magnetic field is removed again, this way magnetized particles, and the bio-linked cells, could form long-lasting cell clumps. This minimizes the necessary exposure time to the magnet an advantage of ferromagnetic materials for utilizing them in *in vivo* experimental settings.
But it could be possible that the ferromagnetic particles, bound to the cell surface through Anti-Integrin-ß-1 antibodies, block the integrin surface proteins, necessary for cell adhesion or sterically hinder the cells from attachment.
SPIONS loaded cells surprisingly performed equally for both adhesion and cell clustering kinetics, even though this material only holds superparamagnetic properties, meaning once the magnet is removed, SPIONs do not stay magnetized. This property is directly linked to the particle size of SPIONs, particle size used in our experiments was 15 nm [46].
The TEM images of SPIONs loaded cells showed us, that SPIONs tend to stay in vesicles inside the cells (see Appendix I). SPIONs clusters, like in the observed vesicles, have shown to have an effect called remanent magnetic moment, which is comparable to ferromagnetic properties and may explain the observations [98]. An advantage of SPIONs over the ferromagnetic particles is than that the surface of SPIONs loaded cells stays unbound, free for cell attachment. Because the underlying mechanism of increased cellular retention upon magnetic targeting in experiments by Ottersbach and colleagues [96] stays unclear, we hypothesize it’s not adhesion kinetic but far more the cell clustering that retains cells at the injection site. This conclusion is supported by the data presented in this stuy, which indicates that call clustering can be achieved in as little as 10 minutes matching the kinetics described by Ottersbach although with other cells.

Cell clusters might not be as quickly washed out of the injection site compared to single cells. Of course, Ottersbach experiments have some limitations, because they only worked with cardiomyocytes. Therefore, potential supportive effects of other cells such as connective tissue cells are neglected in this study.
We assume that combining both methods, quick adhesion kinetics due to using micro-tissues composed of MSCs and Cardiomyocytes and magnetic targeting, exposure to a magnetic field after cell injection, might be the combination necessary to ensure optimal retention and engraftment for cell-based replacement therapy approaches in the heart.

4.3. Emptying the cardiac niche for Organ Complementation

We worked on a method to test gene influence *in-vivo* in an intra-embryonic complementation assay, specifically to follow up the influence of cardiac organ development genes. This method was used to prepare for organ complementation in the heart.
For the intra-embryonic complementation assay genetic modification of cardiac genes using CRISPR/Cas9 knock out strategies is utilized.
In preparation for *in vivo* experiments in mice, CRISPR gRNAs were pre-tested *in vitro* on murine iPS cell line TaP. For all genes of interest designed gRNAs showed effective modification upon T7Endonuclease I assay.
Next cardiomyocytes differentiation capability was tested for unselected batch of Hand1 and Nkx2-5 knock out cells mixed with AT25fluc iPSCs. Both cell lines, TaP and AT25fluc are subclones derived from the TiB7.4 cell line initially provided to the institute by Prof. Rudolf Jaenisch and Prof. Alexander Meissner [99]. We assumed that cell lines hold the same differentiation capability, but that genetic knock out of cardiac genes would impair the differentiation capability. The mixing of the CRISPR/Cas9 genetically modified TaP cells with unmodified At25fluc cells 1:1, should result in an increase of GFP positive cells, if the differentiation capability of knock out TaP cells is impaired, compared to a 50% GFP^+ to 50% GFP^- control for an unmodified Tap (GFP negative) + AT25fluc (GFP positive). But due to the control group not reaching the 50:50 ratio and the differentiation results not being reliable for interpretation, this experimental design was discarded. No clear connection between knout out of genes and differentiation capability could be drawn because of the control group.

The top candidate for all CRISPR RNA designs (gRNA-1) always showed the most promising result and was used for intraembryonic complementation assay. CRISPR designs that worked

in vitro were moved to *in vivo* testing in the intra-embryonic complementation assay. The experimental design includes the modification of one blastomere of a 2-cell blastocysts and of a Rosa26mTmG mouse strain, while at the same time utilizing Cre recombinase to cleave the red fluorescence out of the modified blastomere. This way the starting point for experiments is a 2-celler with one blastomere being red and genetically unmodified and one blastomere being green and genetically modified.

For this experiment we imported mTmG mice from the CECAD institute and set up breeding, list of breeding results can be found in 3.3.4.1. Breeding in the institute for pharmacology institute of the University Hospital Cologne posed some challenges, leading to shortage of female mice of 4 weeks of age that could be used for superovulation and zygote production. In the end the whole mice strain was lost. Reason for the loss of the strain was regular vibrations and noise from ongoing constructions next door of the animal house. Genetically impaired fertility of inbred transgenic mice cannot be excluded either.

The *in vivo* experiments carried out were a test Cre-recombinase injection into blastocysts and the intra-embryonic complementation assay for the genes Nkx2-5, Hand1, Hand2 and finally Pdx1.

First, we injected just Cre Recombinase mRNA in one of a 2-cell blastomere and analyzed the Blastocysts three days later for red and Green fluorescence (see *Figure 47*) to test, if we are able to inject in just one cell. Fourteen out of 15 injected blastocysts showed both fluorescence colors. These results indicated that it was possible to continue animal experiments with injection of one of 2-celll blastocyst, a method both challenging in handling and at the same time we wanted to ensure the R26 mTmG transgene was intact before continuing animal experiments.

Nkx2-5 intraembryonic complementation assay mice were cryo sectioned and afterwards fixed in 4%PFA. This was the first animal experiment and we thought fixation was possible for the samples. It appears the paraformaldehyde (PFA) fixation denatures the transgenic fluorophores on the cell surface. For Nkx2-5 it is impossible to interpretate the results, due to the denaturation of the florescence proteins. It appears some animals of the Nkx2-5 experiment have both fluorescence while others just show the red fluorescence.

For Hand1 intraembryonic complementation assay mice were cryo sectioned and not fixed in PFA afterwards, but instead immediately imaged. Mouse 1,2 and 6 showed GFP and dTomato fluorescence for multiple organs. Sanger Sequencing of these 3 animals revealed wildtype genotype for the Hand1 gene, indicating that the GFP fluorescence cannot be linked to a successful genetic modification.

For Hand2 intraembryonic complementation assay mice were cryo sectioned and not fixed afterwards but immediately imaged. All mice where only dTomate fluorescent and genotyped wildtype.

We realized that the experimental design did not allow us to interpretate the cardiac organ development as we had expected. We were not able to connect green fluorescence to the genetic knock out of genes and some intra-embryonic complementation experiments resulted in only red fluorescence. This made us question the remains of the injected blastomeres.

For the test injection of Cre Recombinase into the Blastomere we could confirm that the injected blastomere survives the injection, but it is questionable, if this knowledge can be transferred to the intra-embryonic complementation assay. In the test injection we just injected the Cre Recombinase mRNA but generated no CRISPR-Cas9 mediated knock out. Maybe this double strand break (DSB) is the reason why injected blastomers do not survive in the *in vivo* intraembryonic complementation assay. We wonder if the Cre Recombinase is for some unknown reason not working, or if the loss of GFP fluorescence is linked to the genetic modification.

It is possible that the CRISPR-Cas9 mediated double strand break (DSB) is being detected but not repaired, but instead the cell mediates for apoptosis or cell-cycle arrest [75]. Usual survival rates for microinjection into zygotes are around 50% with a CRISPR-Cas9 mediated cleavage rate around 80% [100]. These low green fluorescence results in our experiments could indicate for apoptosis or cell-cycle arrest, this way only the unmodified blastomere would contribute to the forming embryo, leading to all cells expressing dTomato and being red fluorescent.

Trying to investigate this experimental design further, we wanted to test the effect of a non-cardiac related gene, where viable chimera organ complementation experiments have been published before [69, 70]. We decided on pancreatic and duodenal homeobox1 (Pdx1) the gene for pancreas formation. Organ complementation of the pancreas was realized by Kobayashi *et al.* (2010) [69] and Wu *et al.* (2017) [70] respectfully, showing organ complementation for the pancreas in possible, when using rat Es cells in $Pdx1^{-/-}$ mice blastocysts.

Transferring this to our intra-embryonic complementation assay, we assumed that genetic modification of Pdx1 while adding Cre recombinase mRNA in one blastomere, the offspring would be viable and show the desired result of only red fluorescent pancreas, while all other organs would be formed out of red and green fluorescent cells.

Pdx1 intra-embryonic complementation assay also did not work and only produced red fluorescent offspring. This Pdx1 experimental run, did not clarify for us if the experimental

design works, if the CRISPR injected blastomere has the potential to survives in general, if trying to knock out lethal genes was the challenge, injected even though organ complementation for this gene has already been published [69, 70].

The same experimental design was worked with before, published by Wang *et al.* (2017) [101]. Modification of just one blastomere of a 2-cell embryo was also worked with before by Wu and colleagues (2019) [102], showing that modification of just one cell of two cell embryo is possible. Comparing their experimental strategy with ours, only the concentration of CRISPR/Cas9 reagents differed, Wu and colleagues (2019) [102], used a 5x times lower concentration of CRISPR/Cas9 compared to us. Other studies indicate that higher Cas9 and gRNA concentrations, similar to the concentration we worked with, is effectively increasing the mutation efficiency [103]. Still the experimental design poses a lot of issues. For one it the GFP fluorescence only serves as a marker for the injected cell, but works independently to the knock-out of the targeted gene. This effect we could observed in our intra-embryonic complementation Hand1 mice, where the experiment resulted in mice of green and red fluorescence but were genotyped wildtype. The results of the Hand 1 mice indicate that maybe the mice showing both fluorescent colors (30% in this experiment) are the once where the DNA cleavage through CRISPR is not working and the injected blastomere survives, at least this correlates with the general CRISPR efficiency of 70-80%. This ratio is not transferable to our other animal experimental results, where only red fluorescence was observed. Wang *et al.* (2017) [101] also observed the independence of green fluorescence and genetic modification with CRISPR-Cas9, as the green fluorescent cells in their mice, showed mosaic genotypes for their targeted gene, including wildtype genotype.
To come to a generalized conclusion is impossible, as we could only test 4 gen modifications during the period of our application for animal experiments.
As most of our in-vivo experiments resulted in only red fluorescence animals, the assumption of the impairment of the mTmG transgene or technical issues with the quality of our Cre recombinase RNA, despite following suppliers' preparation protocol and storage suggestions, is imminent. But we were able to produce red and green blastocyst and mice.

To really follow up and understand the mechanistic of genetically engineering of one of the 2-cell blastomere further research will be needed.

5. Conclusions and outlook

In this work, advancements in stem cell-based replacement therapies were investigated. Three primary objectives were addressed: the generation of a hypoimmunogenic human iPSCs line for xenotransplantation purposes, the evaluation of magnetic targeting of cells to enhance engraftment upon transplantation and the identification of key genes required for emptying the cardiac niche, in preparation for cardiac organ complementation.

As presented in the results (see 3.1) we were able to generate genetically modified hiPSC for xenotransplantation purposes. If these cells actually evade immune reaction *in-vivo*, needs to be tested in the future and is currently in planning. Same goes for safety concerns of MHC deleted cells of causing tumor formation, because they remain undetected by the immune system [21].

The cell line generated here (HSM47M) will be used in mice experiments, as it expresses the murine CD47 on the surface. If these cells evade the immune rejection by the host, the future perspectives of this model could be to move to an animal model closer in physiology to humans, like pigs. For this porcine CD47 could be overexpressed in the to the human knock-out iPSC cells (NP0040-SM) generating a new model for xenotransplantation. These hypoimmunogenic cells could be of interest for cardiac replacement therapies, as pre-clinical cardiac transplantations experiments are still carried out under strong immunosuppression medication.

The results (see 3.2) show the feasibility of magnetically targeting cells *in-vitro*. If magnetically targeting of micro-tissues can synergistically increase cardiomyocyte engraftment in the myocardium, will have to be investigated further.

Unfortunately, this work was unable to elucidate which cardiac-related genes must be depleted to fully empty the cardiac niche, an essential step for organ complementation of the heart.

6. References

1. Terzic, A. and A. Behfar, *Regenerative heart failure therapy headed for optimization.* European Society of Cardiology, 2014. **35**.
2. Mao, A.S. and D.J. Mooneya, *Regenerative medicine: Current therapies and future directions.* PNAS, 2015. **112**: p. 14452–14459.
3. Greenwood, H.L., et al., *Regenerative medicine: new opportunities for developing countries.* International Journal of Biotechnology, 2006.
4. Mason, C. and P. Dunnill, *A Brief Definition of Regenerative Medicine.* Regenerative Medicine, 2007. **3**(1): p. 1-5.
5. Aly, R.M., *Current state of stem cell-based therapies: an overview.* Stem cell investigation, 2020. **7**.
6. McKinley, K.L., M.T. Longaker, and S. Naik, *Emerging frontiers in regenerative medicine: Bridging knowledge gaps could enable regenerative therapy.* Science, 2023. **380**(6647): p. 796–798.
7. Hoang, D.M., et al., *Stem cell-based therapy for human diseases.* Signal Transduction and Targeted Therapy, 2022. **7**.
8. Musiał-Wysocka, A., M. Kot, and M. Majka, *The Pros and Cons of Mesenchymal Stem Cell-Based Therapies.* Cell Transplantation, 2019.
9. Cerneckis, J., H. Cai, and Y. Shi, *Induced pluripotent stem cells (iPSCs): molecular mechanisms of induction and applications.* Signal Transduction and Targeted Therapy, 2024. **9:112**.
10. Yamanaka, S., *Pluripotent Stem Cell-Based Cell Therapy—Promise and Challenges.* Cell stem Cell, 2020. **27**.
11. Kimbrel, E.A. and R. Lanza, *Next-generation stem cells — ushering in a new era of cell-based therapies.* Nature Reviews Drug Discovery, 2020. **19**: p. 463-479.
12. Ivkošić, I.E., et al., *Unlocking the Potential of Mesenchymal Stem Cells in Gynecology: Where Are We Now?* Personalized Medicine, 2023. **13**.
13. Takahashi, K., et al., *Induction of Pluripotent Stem Cells from Adult Human Fibroblasts by Defined Factors.* Cell, 2007. **131**.
14. Takahashi, K. and S. Yamanaka, *Induction of Pluripotent Stem Cells from Mouse Embryonic and Adult Fibroblast Cultures by Defined Factors.* Cell, 2006. **126**: p. 663–676.
15. Williams, L.A., B.N. Davis-Dusenbery, and K.C. Eggan, *SnapShot: Directed Differentiation of Pluripotent Stem Cells.* Cell, 2012. **149**.
16. Caplan, A.I., *Mesenchymal Stem Cells: Time to change the Name!* Stem cells translational Medicine, 2017. **6**.
17. Pham, P.V., *MSCs, but not mesenchymal stem cells.* Biomedical Research and Therapy, 2024. **11**(9).
18. Wilson, A., A. Webster, and P. Genever, *Nomenclature and heterogeneity: consequences for the use of mesenchymal stem cells in regenerative medicine.* Regenerative Medicine, 2019. **14**.
19. Parsons, X.H., *Current State of Regenerative Medicine: Moving Stem Cell Research from Animals into Humans for Clinical Trials.* JSM Regenerative Medicine and Bioengineering, 2013. **1**(1).
20. Harding, J., R.M. Roberts, and O. Mirochnitchenko, *Large animal models for stem cell therapy.* Stem cell research& therapy, 2013. **4:23**.
21. Simpson, A., A.W. Hewitt, and K.A. Fairfax, *Universal cell donor lines: A review of the current research.* Stem Cell Reports 2023. **18**.

22. Muntjewerff, E.M., et al., *Reverse Signaling by MHC-I Molecules in Immune and Non-Immune Cell Types.* Frontiers in Immunology, 2020. **11:605958.**
23. Ide, K., et al., *Role for CD47-SIRPα signaling in xenograft rejection by macrophages.* PNAS, 2007. **104**(12).
24. Deuse, T. and S. Schrepfer, *Progress and challenges in developing allogeneic cell therapies.* Cell Stem cell, 2025. **32**.
25. Tsai, Y.-Y., et al., *Heterozygote advantage at HLA class I and II loci and reduced risk of colorectal cancer.* Frontiers in Immunology, 2023. **14**.
26. Taylor, C.J., et al., *Generating an iPSC Bank for HLA-Matched Tissue Transplantation Based on Known Donor and Recipient HLA Types.* Cell Stem cell, 2012. **11**.
27. Álvarez-Palomo, B., et al., *Evaluation of the Spanish population coverage of a prospective HLA haplobank of induced pluripotent stem cells.* Stem cell research& therapy, 2021. **12:233**.
28. Yoshida, S., et al., *A clinical-grade HLA haplobank of human induced pluripotent stem cells matching approximately 40% of the Japanese population.* Cell Press, 2023. **Med 4**.
29. Taylor, C.J., et al., *Banking on human embryonic stem cells: estimating the number of donor cell lines needed for HLA matching.* Lancet, 2005. **366**.
30. Escribá, R., et al., *Current Landscape of iPSC Haplobanks.* Stem Cell Reviews and Reports, 2024. **20**.
31. Robinson, J., et al., *IPD-IMGT/HLA Database.* Nucleic Acid Researcg, 2020. **48**.
32. Badin, R.A., et al., *MHC matching fails to prevent long-term rejection of iPSC-derived neurons in non-human primates.* Nature Communications, 2019. **10:4357**.
33. Harding, J., et al., *Immune-privileged tissues formed from immunologically cloaked mouse embryonic stem cells survive long term in allogeneic hosts.* nature biomedical engineering, 2023. **8**.
34. Deuse , T., et al., *Hypoimmunogenic derivatives of induced pluripotent stem cells evade immune rejection in fully immunocompetent allogeneic recipients.* Nature Biotechnology, 2019. **Mar; 37**.
35. Sahito, R.G.A., et al., *In Vitro Grown Micro-Tissues for Cardiac Cell Replacement Therapy in Vivo.* Cell Physiol Biochem, 2019. **52**(6).
36. Cheng, K., et al., *Magnetic Enhancement of Cell Retention, Engraftment, and Functional Benefit After Intracoronary Delivery of Cardiac- Derived Stem Cells in a Rat Model of Ischemia/Reperfusion.* Cell Transplant, 2012. **21**.
37. Günter, J., et al., *Microtissues in Cardiovascular Medicine: Regenerative Potential Based on a 3D Microenvironment.* Stem cell international, 2016.
38. Bauer, M., et al., *Adult Cardiac Progenitor Cell Aggregates Exhibit Survival Benefit Both In Vitro and In Vivo.* PLOS ONE, 2012. **7**.
39. Emmert, M.Y., R.W. Hitchcock, and S.P. Hoerstrup, *Cell therapy, 3D culture systems and tissue engineering for cardiac regeneration.* Advanced Drug Delivery Reviews, 2013.
40. Yanamandala, M., et al., *Overcoming the Roadblocks to Cardiac Cell Therapy Using Tissue Engineering.* J Am Coll Cardiol, 2017. **70**.
41. Kobayashi, T., et al., *A Novel Cell Delivery System Using Magnetically Labeled Mesenchymal Stem Cells and an External Magnetic Device for Clinical Cartilage Repair.* The Journal of Arthroscopic and Related Surgery,, 2008. **24**(1).
42. Huang, Z., et al., *Magnetic targeting enhances retrograde cell retention in a rat model of myocardial infarction.* Stem Cell Research & Therapy, 2013. **4**.
43. Cores, J., T.G. Caranasos, and K. Cheng, *Magnetically Targeted Stem Cell Delivery for Regenerative Medicine.* Journal of Functional Biomaterials, 2015. **6**.

44. Oshima, S., et al., *Enhancement of muscle repair using human mesenchymal stem cells with a magnetic targeting system in a subchronic muscle injury model.* J Orthop Sci, 2014. **19**.
45. Silva, L.H.A., et al., *Magnetic targeting as a strategy to enhance therapeutic effects of mesenchymal stromal cells.* Stem cell research& therapy, 2017. **8:58**.
46. Zhang, L., et al., *Force-Mediated Endocytosis of Iron Oxide Nanoparticles for Magnetic Targeting of Stem Cells.* Applied Materials & Interfaces, 2023. **15**(44).
47. (WHO), W.H.O., *Cardiovascular diseases*. 2021, WHO.
48. Frangogiannis, N.G., *The extracellular matrix in myocardial injury, repair, and remodeling.* The Journal of Clinical Investigation, 2017. **127**: p. 1600-1612.
49. Laforgia, P.L., et al., *The reduction of mortality in acute myocardial infarction: from bed rest to future directions.* International Journal of Preventive Medicine, 2022.
50. Lewis, A., et al., *Organ donation in the US and Europe: The supply vs demand imbalance.* Transplantation Reviews, 2020.
51. Eurotransplant, *Deceased donors used in All ET, by year, by organ 1042P_AllET*. 2020.
52. Harvey, R.P., *Patterning the vertebrate heart.* nature reviews genetics, 2002. **3**: p. 544-556.
53. Flanigan, M. and S.M. Gaskell, *Structure and function of the heart.* Home Healthcare Nurse, 2004. **22**(1).
54. Litviňuková, M., et al., *Cells of the adult human heart.* nature, 2020. **588**.
55. Vincent, S.D. and M.E. Buckingham, *How to make a heart: the Origin and Regulation of Carduac Progenitor Cells.* Current Topics in Developmental Biology 2010. **90**.
56. Buckingham, M., S. Meilhac, and S. Zaffran, *Building the mammalian heart from two sources of myocardial cells.* nature reviews genetics, 2005. **6**: p. 826-835.
57. Nahaboo, W., et al., *Visualizing Mouse Embryo Gastrulation Epithelial-Mesenxhymal Transition Trough Single Cell Labeling Followed by Ex Vivo Whole Embryo Live Imaging*, in *The Epithelial-to Mesenchymal Transition*, K.T. Campbell, Eric, Editor. 2020: Humana, New York, NY.
58. Epstein, J.A., *Cardiac Development and Implications for Heart Disease.* The New England Journal of Medicine 2010. **363**: p. 1638-1657.
59. Moorman, A., et al., *Development of the heart: (1) Formation of the Cardiac Chambers and Arterial Trunks.* heart, 2003. **89**(7): p. 806-814.
60. Mohun, T.J., N.A. Brown, and R.H. Anderson, *Development of the Heart and great Vessels*, in *Kaufman´s Atlas of Mouse Development Supplement with Coronal Sections*, R.B. Bladock, Jonathan; Davidson, Duncan R.; Morriss-Kay, Gillian, Editor. 2016, Sara Tenney: London, England. p. 95-109.
61. Gittenberg-De Groot, A., et al., *Basics of cardiac development dor the understanding of congenital heart malformations.* Pediatric Research, 2005. **57**(2).
62. Meilhac, S.M., et al., *The Clonal Origin of Myocardial Cells in Different Regions of the Embryonic Mouse Heart.* Cell Press, 2004. **6**: p. 685–698.
63. Savolainen, S.M., J.F. Foley, and S.A. Elmore, *Histology Atlas of the Developing Mouse Heart with Emphasis on E11.5 to E18.5.* Toxicologic Pathology, 2009. **37**(4).
64. Waardenberg, A.J., et al., *Genetic Networks Governing Heart Development.* Cold Spring Harb Perspect Med, 2014. **4**(11).
65. Lickert, H., et al., *Baf60c is essential for function of BAF chromatin remodelling complexes in heart development.* Nature, 2004. **432**: p. 107-111.
66. Aitova, A., et al., *Novel molecular vehicle-based approach for cardiac cell transplantation leads to rapid eöectromechanical graft-host coupling.* International Journal of Molecular Science, 2023. **24**.

67. Jebran, A.-F., et al., *Engineered heart muscle allografts for heart repair in primates and humans.* Nature, 2025. **639**.
68. Nagashima, H. and H. Matsunari, *Growing human organs in pigs. A dream or reality?* Theriogenology, 2016. **86**(1): p. 422-426.
69. Kobayashi, T., et al., *Generation of Rat Pancreas in mouse by interspecific blastocysts injection of pluriptent stem cells.* cell, 2010. **142**(5).
70. Wu, J., et al., *Interspecies Chimerism with Mammalian Pluripotent Stem Cells.* Cell, 2017. **168**.
71. Pallares Masmitja, M., N. Knödlseder, and M. Güell, *CRISPR-gRNA Design*, in *CRISPR Gene Editing*, Y. Lou, Editor. 2019, Humana Press: New York, USA. p. 3-12.
72. Technologies, I.D., *The CRISPR Basic handbook* 2025.
73. Hille, F. and E. Charpentier, *CRISPR-Cas: biology, mechanisms and relevance*, in *Philosophical Transactions B The Royal Society Phublishing*. 2016.
74. Lin, L. and Y. Luo, *Tracking CRISPR's Footprints*, in *CRISPR Gene Editing*, Y. Lou, Editor. 2019, Humana Press: New york, USA.
75. Deriano, L. and D.B. Roth, *Modernizing the Nonhomologous End-Joining Repertoire: Alternative and Classical NHEJ Share the Stage.* Annual Review of genetics, 2013. **47**: p. 433-455.
76. Labun, K., et al., *CHOPCHOP v3: expanding the CRISPR web toolbox beyond genome editing.* Nucleic Acids Research, 2019. **47**.
77. Reinard, T., *Molekularbiologische Methoden 2.0*. 2021, Stuttgart, Deutschland: utb.
78. Conant, D., et al., *Inference of CRISPR Edits from Sanger Trace Data.* The CRISPR Journal, 2022. **5**(1).
79. Butler, J.M., M.D. Coble, and P.M. Vallone, *STRs vs. SNPs: thoughts on the future of forensic DNA testing.* Forensic Sci Med Pathol, 2007. **3**.
80. Fatima, A., et al., *Murine transgenic iPS cell line for monitoring and selection of cardiomyocytes.* Stem cell research, 2016. **17**: p. 266-272.
81. Hamad, S., et al., *Generation of human induced pluripotent stem cell-derived cardiomyocytes in 2D monolayer and scalable 3D suspension bioreactor cultures with reduced batch-to-batch variations.* Theranostics, 2019. **9 (24)**.
82. Lian, X., et al., *Directed cardiomyocyte differentiation from human pluripotent stem cells by modulating Wnt/beta-catenin signaling under fully defined conditions.* Nature Protocols, 2013. **8**(1).
83. Muzumdar, M.D., et al., *A Global Double-Fluorescent Cre Reporter Mouse.* genesis, 2007. **45**.
84. Strome, S., et al., *Clarifying Mendelian vs. non-Mendelian inheritance.* Genetics, 2024. **227**.
85. Storch, V. and U. Welsch, *"Kückenthal" Zoologisches Praktikum*. 27 ed. 2014: Springer.
86. Wu, J.-s., G. Hogan, and J. Morris, *Modified Methods for Preparation of Cryostat sections of skeletal Muscle.* Muscle & Nerve, 1985. **8**(8).
87. Jiang, L.-L., H. Li, and L. Liu, *Xenogeneic stem cell transplantation: Research progress and clinical prospects.* World Journal of Clinical Cases, 2021.
88. Chong, J.J.H., et al., *Human Embryonic Stem Cell-Derived Cardiomyocytes Regenerate Non-Human Primate Hearts.* Nature, 2014. **510**.
89. Hayama, T., et al., *Generation of Mouse Functional Oocytes in Rat by Xeno-Ectopic Transplantation of Primordial Germ Cells.* Biology of Reproduction, 2014. **91**.
90. Wood, K.J. and R. Goto, *Mechanisms of Rejection: Current Perspectives.* Transplantation, 2012. **93**(1).

91. Aboul-Soud, M.A., A. Alzahrani, and A. Mahmoud, *Induced Pluripotent Stem cells (iPSCs)- Roles in regeneratuve Therapies, Disease Modelling and Drug Screening.* Cells, 2021. **10**.
92. Kohei, N., et al., *Natural Killer cells play a crictival role in mediating inflammaation and graft failure during antibody- mediated rejection of kidney allografts.* Kidney Int., 2016. **89**.
93. Chen, W., et al., *Massively parallel profiling and predictive modeling of the outcomes of CRISPR/Cas9-mediated double-strand break repair.* Nucleic Acids Research, 2019. **47**(15).
94. Subramanian, S., et al., *Species- and cell type-specific interactions between CD47 and human SIRPa.* Blood, 2006. **107**.
95. Kwong, L.S., M.H. Brown, and D. Hatherley, *Signal-regulatory protein a from the NOD mouse binds human Cd47 with an exceptionally high affinity - implications for engraftment of humane cells.* Immunology, 2014. **143**.
96. Ottersbach, A., et al., *Improved heart repair upon myocardial infarction: Combination of magnetic nanoparticles and tailored magnets strongly increases engraftment of myocytes.* Biomaterials, 2017. **155**.
97. Tiburcy, M., et al., *Defined Engineered Human Myocyrdium with advanced maturation for Applications in heart failure Modelung and repair.* Circulation, 2017. **135**(19).
98. Bender, P., et al., *Influence pf clustering on the magnetic properties and hypothermia perfomance of iron oxide nanaoparticles.* Nanotechnology, 2018. **29**.
99. Meissner, A., M. Wernig, and R. Jaenisch, *Direct reprogramming of genetically unmodified fibroblasts into pluripotent stem cells.* Nature Biotechnology, 2007. **25**.
100. Schlapp, G., et al., *Zygote cryobanking applied to CRISPR/Cas9 microinjection in mice.* PLOS ONE, 2024. **19**.
101. Wang, L., et al., *CRISPR-Cas9-mediated genome editing in one blastomere of two-cell embryos reveals a novel Tet3 function in regulating neocortical development.* Cell Research, 2017. **27**.
102. Wu, Y., et al., *Generating viable mice with heritable embryonically lethal mutations using the CRISPR-Cas9 system in two-cell embryos.* Nature Communications, 2019.
103. Tanihara, F., et al., *Effect of concentration of CRISPR/Cas9 components on genetic mosaicism in cytoplasmic microinjected porcine embryos.* Journal of Reproduction and Development, 2019. **65**.

Appendix

I. Publication

bioengineering

MDPI

Article

Cell-Based Therapies: Ferromagnetic Versus Superparamagnetic Cell Targeting

Tasneem Halhouli [1,2,†], Lisa Münchhalfen [1,2,†], Sarkawt Hamad [1,2,3,*,†], Larissa Schmitz-Ullrich [1,2], Frank Nitsche [4], Felix Gaedke [5], Astrid Schauss [5], Linlin Zhang [6], Quoc-Khanh Pham [6], Gang Bao [6] and Kurt Paul Pfannkuche [1,2,7,8,*]

1 Center for Physiology and Pathophysiology, Institute for Neurophysiology, University of Cologne, Medical Faculty and University Hospital of Cologne, 50931 Cologne, Germany
2 Marga-and-Walter-Boll Laboratory for Cardiac Tissue Engineering, University of Cologne, 50931 Cologne, Germany
3 Biology Department, Faculty of Science, Soran University, Soran 44008, Kurdistan Region, Iraq
4 Institute for Zoology, General Ecology, University of Cologne, 50674 Cologne, Germany
5 Excellence Cluster on Cellular Stress Responses in Aging-Associated Diseases (CECAD), Imaging Facility, 50931 Cologne, Germany
6 Department of Bioengineering, Rice University, Houston, TX 77030, USA
7 Department of Pediatric Cardiology, University Hospital of Cologne, 50937 Cologne, Germany
8 Center for Molecular Medicine Cologne (CMMC), University of Cologne, 50931 Cologne, Germany
* Correspondence: shamad@uni-koeln.de (S.H.); kurt.pfannkuche@uni-koeln.de (K.P.P.); Tel.: +49-221-478-6968 (S.H.); +49-221-478-6960 (K.P.P.)
† These authors contributed equally to this work.

Abstract: Stem-cell-based therapies rely on the transplantation of stem cells or stem-cell-derived organotypic cells into injured tissues in order to improve or restore tissue function that has been impaired by various diseases. The potential of induced pluripotent stem cells has created many applications in the field of cell therapy, for example. Some applications, for example, those in cardiac cell therapy, suffer from low or very low efficiencies of cell engraftment. Therefore, magnetic cell targeting can be discussed as a method for capturing superparamagnetic nanoparticle-labelled cells in the tissue. Here, we employ superparamagnetic iron oxide nanoparticles (SPIONs) for the intracellular magnetic loading of mesenchymal stem cells (MSCs). In addition, we test a novel strategy of labelling MSCs with ferromagnetic particles. The adhesion assays demonstrate a faster adhesion kinetic of SPIONs-loaded MSC spheroids when a magnetic field was applied, resulting in >50% spheroid adhesion after 30 min. Clustering of cells inside the magnetic field is a second potential mechanism of magnetic cell retention and >80% of cells were found to be aggregated in clusters when placed in a magnetic field for 10 min. SPIONs-loaded and ferromagnetic-particle-loaded cells performed equally in the cell clustering assay. In conclusion, the clustering of SPION-labelled cells explains the observation that magnetic targeting reaches maximal efficiency in vivo after only 10 min of magnetic field application. This has significant implications for magnetic-targeting-assisted stem cell and cell replacement therapies.

Keywords: superparamagnetic iron oxide nanoparticles (SPIONs); ferromagnetic particles; murine MSCs

check for updates

Academic Editor: Xiaoming He

Received: 2 May 2025
Revised: 6 June 2025
Accepted: 8 June 2025
Published: 16 June 2025

Citation: Halhouli, T.; Münchhalfen, L.; Hamad, S.; Schmitz-Ullrich, L.; Nitsche, F.; Gaedke, F.; Schauss, A.; Zhang, L.; Pham, Q.-K.; Bao, G.; et al. Cell-Based Therapies: Ferromagnetic Versus Superparamagnetic Cell Targeting. *Bioengineering* **2025**, *12*, 657. https://doi.org/10.3390/bioengineering12060657

1. Introduction

Cell replacement therapies often face the issue of low cellular retention. Even though in vivo studies confirm that cell transplantation can replace and improve the function of

damaged tissue, rapid diffusion and limited survival rates after cell injection are the reason for low engraftment rates [1–4].

To overcome low cellular retention, mainly in the field of cardiac cell therapy, reports of magnetic targeting and application of an external magnetic field show promising results; however, the overall efficiency remains often low, and the underlying mechanism of enhanced cell engraftment remains unclear [1,5–9]. The efficiency of cell engraftment depends on the type of cell included in a study; while intramyocardial transplantation of cardiomyocytes usually results in poor cell engraftment rates, magnetically assisted transplantation of cardiac myofibroblasts engineered to express connexin 43 resulted in very high (30% of injected cells) engraftment rates [10]. Other studies indicate that cell therapies with microtissues (i.e., assemblies of organotypic cells to a functional tissue in mm scale) and/or 3D spheroids (i.e., microtissues characterized by a regular spherical shape) can enhance engraftments. But these approaches still struggle with the same problem of low retention, even when adding fast-adhesive cells, e.g., mesenchymal stem/stromal cells (MSCs) [2,3,6,11,12].

Magnetically labelling cells with superparamagnetic iron oxide nanoparticles (SPIONs) or magnetic iron oxide nanoparticles (MIONs) through magnetic-force-mediated endocytosis is described well in the work of Zhang [13]. Iron oxide nanoparticles with diameters below 20 nm hold superparamagnetic properties and are highly biocompatible [5,13]. Therefore, SPIONs made from iron oxide are suitable candidates for exerting magnetic forces on cells. Potential applications that have been tested in vivo include the targeting of endothelial cells to the site of large artery injury [14], the targeting of mesenchymal stem cells to improve sphincter structure in a model of urinary incontinence [15], the targeting of endodermal progenitors to the liver [16], and the targeting of cells to the brain after experimental disruption of the blood–brain barrier [17]. Targeting of embryonic and pluripotent stem-cell-derived cardiomyocytes to the heart showed a 7-fold increase in cell retention 2 weeks after transplantation [18]. Taken together, these and other studies suggest an increased engraftment of magnetically loaded cells when an external magnet is applied.

In this study, we show the feasibility of magnetically targeting murine mesenchymal stem cells through SPIONs loading and a second method of ferromagnetic particle labelling. We propose two potential mechanisms of action by which magnetic targeting could enhance cell retention. Firstly, it is postulated that the attachment of magnetically labelled cells to an extracellular matrix can be improved by applying magnetic force. A faster and/or closer contact of the cells to the matrix and an increased dwell time will contribute to this effect. Secondly, magnetic forces could result in a forced aggregation of cells, thereby reducing wash out or cell death mediated by lack of cell–cell interactions. Based on the assumption that forced aggregation could improve persistence of cells, we hypothesize that ferromagnetic labelling of cells could outcompete SPIONs, because ferromagnetic particles become permanently magnetised during exposure to a strong magnetic field. This could result in a fast and stable aggregation of cells even when the external field is removed. This hypothesis is based on the fact that ferromagnetic particles, unlike superparamagnetic particles, generate magnetic forces that stabilize the cluster in the absence of an external magnetic field.

2. Methods

2.1. Mesenchymal Stem Cell Culture

Murine mesenchymal stem cells (mMSCs) were isolated from the bone marrow of 6–8-week-old male mice (129S2), as described previously [11]. In short, the mouse was sacrificed by cervical dislocation, the femur bones were isolated, and the bone marrow was flushed with DMEM using a syringe with an injection cannula. The flushed cell

suspension was filtered and plated on 10 cm culture dishes inside DMEM high glucose (4.5 g/L) (Gibco by Thermo Fisher, Karlsruhe, Germany #21885108), supplemented with 15% (*v*/*v*) foetal bovine serum (FBS, Sigma-Aldrich, Darmstadt, Germany #F9665) and Primocin antimicrobial agent for primary cell culture (InvivoGen, Tolouse, France, #ant-pm-05), and incubated at 37 °C with 5% CO_2 in a humidified incubator. Non-adherent cells were removed after 12 h culturing. When the cell culture reached 80–90% confluence of attached cells, the cells were sub-cultured using 0.05% trypsin–EDTA solution (Gibco, #25300054). The mMSC culture medium was DMEM low glucose (1 g/L) (Gibco, #11885084) supplemented with 15% (*v*/*v*) FBS, 1x non-essential amino acids (Gibco, #11140050), 100 µM 2-mercaptoethanol (Gibco, #31350010), and 6 ng/mL fibroblast growth factor 2 (Peprotech by Thermo Fisher, Karlsruhe, Germany # 100-18B); mMSCs were incubated in a humidified incubator at 37 °C, with 5% CO_2.

2.2. Synthesis of Magnetic Nanoparticles

Phospholipid–PEG-coated magnetic iron oxide nanoparticles were synthesized in two steps. First, magnetite nanocrystals were synthesized by the thermal decomposition of Tris(acetonylacetonato)-iron(III) (Fe(acac)3) according to previous publications [13,19]. The nanocrystals were dispersed in either toluene (10 and 15 nm) or chloroform (19 and 25 nm). Next, water-dispersible magnetic nanoparticles were obtained by coating these hydrophobic nanocrystals with amphiphilic DSPE-mPEG copolymers using a dual-solvent exchange method. For example, to coat 15 nm nanocrystals, 5 mg of nanocrystals, 14 mg of DSPE-mPEG, and 1.12 mg of LysoPC were mixed in 2 mL of chloroform, and 20 mL of DMSO was added dropwise to the mixture with gentle shaking. After toluene and chloroform were removed by evaporation under a vacuum, 40 mL of distilled water was slowly added to the mixture and DMSO was removed by solvent exchange with Vivaspin centrifugal filter tubes (MW = 100 kDa). To remove empty micelles formed by DSPE-mPEG and LysoPC, the solution was centrifuged twice (80,000× *g*, 4 °C and 1 h) and the supernatant was discarded. After centrifugation, coated nanoparticles were dispersed in distilled water. For 10, 19, and 25 nm nanocrystals, the weights of nanocrystals were changed to 3.7, 6.3, and 8.3 mg, respectively, to keep the total surface area of the nanocrystals constant during coating. The coating procedure and characterization has been described in detail before [20].

To characterize the magnetic properties of the nanocrystals, the nanocrystals dispersed in toluene were precipitated with ethanol and the pellets were dried by an argon beam. Magnetisation of the collected powder was measured at room temperature with a superconducting quantum interference device (SQUID). The hydrodynamic diameter of the magnetic nanoparticles was measured by dynamic light scattering (DynaPro Nanostar, Wyatt Technology, Santa Barbara, CA, USA). The mass-weighted diameter and polydispersity index were reported.

2.3. Intracellular Loading of Superparamagnetic Iron Oxide Nanoparticles (SPIONs)

SPIONs with a particle size of 15 nm were made using Fe_3O_4 nanoparticles with a PEG coating. Separate batches of SPIONs with PEG and 1,1′-Dioctadecyl-3,3,3′,3′-Tetramethylindocarbocyaninperchlorat (Dil) coating, which can be detected at a wavelength of 546 nm, were produced in the laboratory of Gang Bao (Department of Bioengineering, Rice University, Houston, TX 77030, USA), as described in [13].

For loading MSCs with SPIONs, cells were co-incubated overnight with 60 µg/mL SPIONs-supplemented medium. The incubator was equipped with a plate magnet under the culture dish for magnetic-force-mediated endocytosis (+MF) or without placing a magnet under the culture dish (−MF). The cultures were maintained overnight inside a

humidified incubator at 37 °C and 5% CO_2. Intracellular loading success was confirmed by flow cytometry, fluorescence microscopy, and transmission electron microscopy (TEM).

2.4. Quantification of Iron Content of Cells Through a Ferrozine-Based Assay

Quantification of intracellular iron oxide was measured by a ferrozine-based assay following Zhang (2023) [13]. Briefly, SPION-loaded cells were detached from the culture plate, evacuated overnight, and iron was released from the cells by adding 12 M hydrochloric acid (Sigma-Aldrich, Taufkirchen, Germany, 339253-100ML), 8 M sodium hydroxide solution (Sigma-Aldrich, 72068-100ML), 4 M ammonium acetate (Sigma-Aldrich, #A2706-100ML), 5% (*w*/*w*) hydroxylamine hydrochloride (Sigma-Aldrich, #431362-50G), and H_2O. Ferrozine of 0.1% (*w*/*w*) concentration (Sigma-Aldrich, #82950-1G) was added to form a ferrous–ferrozine complex, and the formation of the complex was determined at 562 nm absorbance. The unknown sample iron concentration was calculated through the slope of an iron standard curve. The iron standard (Sigma-Aldrich, #43149-100ML-F) was prepared in a dilution series from 0 to 500 µg/mL in water and treated similarly with ammonium acetate, hydroxylamine hydrochloride, and H_2O, and each standard concentration was determined at 562 nm absorbance after adding 0.1% (*w*/*w*) ferrozine.

2.5. SPIONS Cytotoxicity Assay

Following ISO-Norm 10993-5, the cytotoxicity of SPIONs in vitro was evaluated by observing morphology, proliferation, and viability for three days. mMSCs were seeded and loaded with PEG-coated SPIONs and stained at three different time points (24, 48, and 72 h) with Hoechst33342 (Thermo Fisher, #62249), propidium iodide (Invitrogen by Thermo Fisher, #P3566), and fluorescein diacetate (Invitrogen, #F1303) to determine the alive–dead ratio and morphology of the mMSCs.

2.6. Cell Surface Magnetic Targeting Using Anti-CD29

Ferromagnetic particles with diameters of 2 µm were bio-linked to MSCs through the surface receptor Integrin beta-1. The expression of CD29 on the surface of the mMSCs was determined with flow cytometry using anti-CD29–Biotin (Miltenyi Biotec, Bergisch Gladbach, Germany #130-101-943) and a secondary Streptavidin–Alexa Flour 488 (BioLegend, San Diego, CA, USA #405235) antibody.

For magnetically targeting the mMSC cell surface, 0.25 × 10^6 mMSCs were firstly incubated 1:50 with anti-CD29 antibody conjugated with Biotin (Miltenyi, #130-101-943) for 30 min at 4 °C, followed by incubation with 1:10 SPHERO Streptavidin Ferromagnetic Particles (Spherotech, Lake Forest, IL, USA #SPH-SVM-80-5) and 1:1000 Hoechst 33342 (Thermo Fischer, #H3570) for 30 min at 4 °C. With a Streptavidin–Alexa Flour 488 stain (BioLegend, #405235), the CD29–Biotin-conjugated antibodies were visualized for fluorescence microscopy.

2.7. Generation of 3D Cellular Spheroids by Hanging Drop Technique

Hanging drop mMSC spheroids were formed with a density of 800 cells per 20 µL drop in mMSC culture medium. Cell suspension drops were placed on the inner surface of a culture dish lid and incubated for two days. For SPION-loaded mMSC spheroids, cells were loaded with SPIONs using magnetic-force-mediated endocytosis prior to spheroid formation.

Ferromagnetic-labelled spheroids were formed by co-incubating 60 µg/mL ferromagnetic particles with mMSCs on a shaker incubator for 5 min before drop formation.

2.8. Adhesion Test of Magnetically Labelled Spheroids on Collagen

Cell culture plates were coated with 50 µg/mL collagen type I rat tail (Sigma-Aldrich, #08-115) and SPIONs and ferromagnetic particle mMSC spheroids were tested for their adhesion time for a period of 2 h against an unlabelled control group. Coated plates were placed on top of a magnet. The adhesion of spheroids was checked at the following time points: 0, 15, 20, 30, 35, 45, 60, 75, 90, 105, and 120 min. At each time point, one plate was transferred from the incubator to the microscope and the number of spheroids was counted before and after removing the medium from the plate. To count the attached spheroids, 1 mL medium was added to the plate slowly and under the microscope and only the non-moving spheroids were counted as attached spheroids.

2.9. Magnetically Labelled Single Cells Aggregation and Clumping

For the aggregation of magnetically targeted single cells, a Nd permanent magnet with a conic iron tip (the magnetic field close to the conic tip is measured with a Gauss meter determined as 150 mT) was applied in the proximity of a single cell suspension. This work was carried out in an Eppendorf tube. The tip magnet was applied for 1, 5, or 15 min at room temperature. The formed clusters were removed gently with a micropipette and placed onto a glass slide for fluorescence microscopy or in a microtube for DNA extraction.

2.10. Quantification of Magnetically Induced Cell Clumps

After the aggregation of single cells with a tip magnet, cell clumps were quantified through nucleic acid concentration. For DNA extraction, the DNEasy DNA extraction kit (Qiagen, Hilden, Germany #69506) was used, following the manufacturer's protocol. DNA concentration was measured with absorbance at 260 nm with a nanodrop spectrophotometer (peqLab, Erlangen, Germany #ND1000). A standard curve of nucleic acid concentration of fixed cell numbers was performed before, measuring the DNA concentration of formed cell clumps.

2.11. Scanning Electron Microscopy (SEM)

Cell cultures were fixed with cacodylate-buffered glutaraldehyde (3%) at 4 °C for 120 min followed by post-fixation with 1% osmium tetroxide for 10 min. For dehydration, an ethanol series comprising 30%, 50%, 60%, 80%, 90%, 96%, and pure ethanol was applied. Samples were washed twice with the corresponding ethanol concentration and finally remained for 10 min in each solution. After this procedure, a 50:50 hexamethyldisilazane (HMDS)–ethanol solution was applied for 30 min followed by 100% HMDS for 30 min as a substitute for critical point drying. Afterwards, the samples were allowed to dry. SEM samples were sputter-coated with a 120° A layer of gold before examination by SEM (FEI Quanta 250 FEG, FEI Deutschland GmbH, Frankfurt, Germany).

2.12. Transmission Electron Microscopy (TEM)

Cells were grown on small discs of aclar foil (Science Services, Munich, Germany, #E50425-10) and fixed for 1 h in 2% Glutaraldehyde (Sigma-Aldrich, Taufkirchen, Germany, # G5882-100ML) with 2.5% Sucrose (Carl Roth, Karlsruhe, Germany, # 4621.1) and 3 mM CaCL2 (Sigma-Aldrich, Taufkirchen, Germany, # C7902-500G) in 0.1M HEPES buffer (Sigma-Aldrich, Taufkirchen, Germany # C7902-500G), pH 7,4. Samples were washed three times with 0.1M HEPES buffer and incubated with 1% Osmiumtetroxid (Science Services, Munich, Germany, # E19190) and 1% Potassium hexacyanoferrat (Sigma-Aldrich, Taufkirchen, Germany, # P8131) for 1 h at 4 °C. After 3 × 5 min wash with 0.1 M Cacodylate buffer (Applichem, Darmstadt, Germany, # A2140,0100), samples were dehydrated at 4 °C using ascending ethanol series (50%, 70%, 90%, 3 × 100%) for 7 min each. Infiltration was

performed with a mixture of 50% Epon/ethanol for 1 h, 70% Epon/ethanol for 2 h, and with pure Epon (Science Services, Munich, Germany, # E14120) overnight at 4 °C. Samples were embedded into TAAB capsules (Agar Scientific, Rotherham, UK #G3744) and cured for 48 h at 60 °C.

Ultrathin sections of 70 nm were cut using an ultramicrotome UC6 (Leica Microsystems, Wetzlar, Germany) and a diamond knife (Diatome, Biel, Switzerland). Sections were stained with 1.5% uranyl acetate (Agar Scientific, # R1260A) for 15 min at 37 °C and with 3% Reynolds lead citrate solution made from lead (II) nitrate (Carl Roth, # HN32.1) and trisodium citrate dehydrate (Carl Roth, Karlsruhe, Germany, #4088.3) for 4 min. Images were acquired using a JEM-2100 Plus Transmission Electron Microscope (JEOL, Akishima, Japan) operating at 80 kV, equipped with a OneView 4K camera (Gatan, Pleasanton, CA, USA).

3. Results

The feasibility of two methods for magnetically targeting MSCs is shown in Figures 1 and 2. Firstly, the magnetic-force-mediated endocytosis of SPIONs into mMSCs was tested (Figure 1A) and confirmed with fluorescence microscopy (Figure 1B) and TEM, showing the intracellular locations of SPIONs inside the vesicles and solitarily in the cytoplasm (Figure 1C). Flow cytometry analysis revealed that, after 24 h of loading with a magnetic field (+MF) underneath, 90.64% of mMSCs had Dil-labelled SPIONs intracellularly. In contrast, after 24 h of loading without a magnetic field (−MF), 85.69% of mMSCs had Dil-labeled SPIONs inside the cells. Dil-labelled SPIONs were detected by fluorescence (Figure 1D). In flow cytometric measurements, the mean fluorescence intensity (MFI) of SPIONs-loaded cells shows that loading with a magnetic field (+MF) leads to double fluorescence intensity compared to cells loaded without a magnetic field (−MF) (n = 3), indicating a higher uptake of SPIONs per cell (Figure 1E).

To confirm this, the iron content of loaded mMSCs was measured using a ferrozine assay due to the availability of Fe^{+2} in the composition of the SPIONs. The measured iron concentration was normalized against an unloaded control group (none, only MSCs) (n = 3) and the iron content in µg/0.3 × 10^6 cells was calculated. SPION-loaded mMSCs using magnetic-force-mediated endocytosis (+MF) contained 54.55 ± 25.90 µg iron oxide per 0.3 × 10^6 cells (n = 5), compared to SPIONs-loaded mMSCs without using magnetic force (−MF) (n = 5), where the iron content was 4.46 ± 3.18 µg (Figure 1F). The iron concentrations of the unloaded MSC group and the loaded +MF group were significantly ($p < 0.05$) different.

The cytotoxic effect of SPIONs on mMSCs was tested for three days after the intracellular loading process (Figure 1G). To determine the live–dead ratio, mMSCs were stained with PI and FDA and the mortality of SPION-loaded MSCs was compared with the mortality of a control group; no difference could be observed.

Secondly, bio-linking ferromagnetic particles to the surface receptors of mMSCs using antibodies for magnetic targeting was shown (Figure 2A). Fluorescence microscopy (Figure 2B) demonstrated the successful bio-linking of ferromagnetic particles with antibodies. Flow cytometry with antibodies against CD29 verified the existence of an integrin- ß1 surface receptor on the cell membrane of the mMSC (Figure 2C). Scanning electron microscopy confirmed the location of ferromagnetic particles on the cell membrane (Figure 2C).

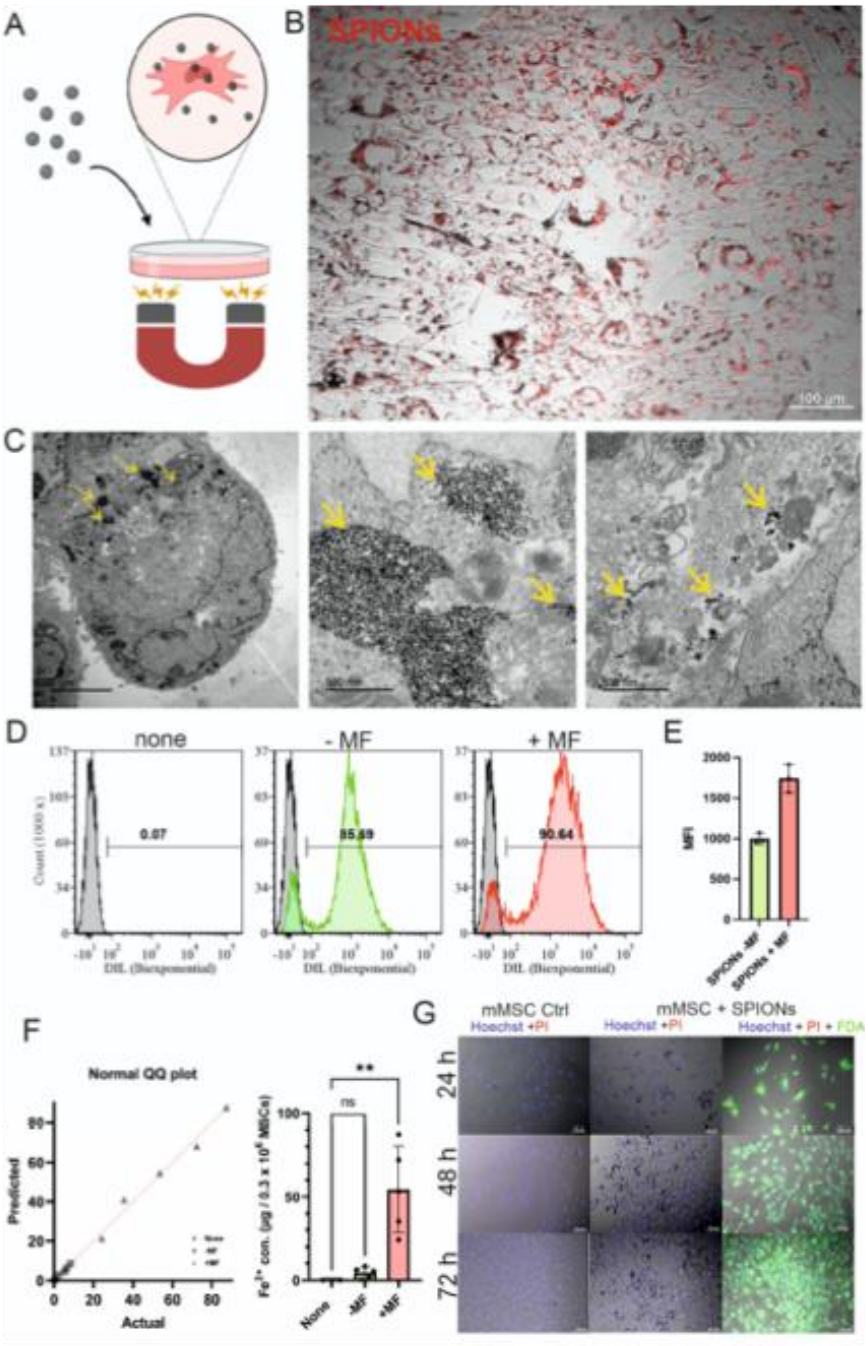

Figure 1. Concept of intracellular SPIONs loading. (**A**) The dish with plated mMSCs is placed on top of a magnet overnight. Medium is supplemented with 60 µg/mL SPIONs. (**B**) Fluorescence

microscopic image of mMSCs loaded with Dil-labelled SPIONs; 10×. (**C**) TEM images of SPIONs-loaded mMSCs at 2000× and 25,000× magnification. SPIONs (arrows) were observed in cells in vesicles or inside the cytoplasm. (**D**) Flow cytometry of Dil-labelled SPIONs loaded intracellularly into mMSCs with (+MF) and without (−MF) magnet. (**E**) Mean fluorescence intensity (MFI) of SPIONs-loaded cells with (+MF) and without (−MF) a magnetic field. (**F**) Iron content of loaded mMSCs. Medium was supplemented with 120 µg SPIONs. Cells were loaded with SPIONs either without plate magnet (−MF) or with plate magnet (+MF) underneath the cell culture dish. Iron concentration was quantified through ferrozine assay and absorbance was measured at 562 nm. ** $p < 0.05$. (**G**) Cytotoxicity of SPIONs loaded intracellularly into mMSCs. Unloaded mMSC control in comparison with mMSCs loaded with SPIONs. Cell morphology was observed for 3 days and stained with Hoechst33342 and PI. SPIONs-loaded mMSCs were also stained with FDA. Scale bar: 100 µm.

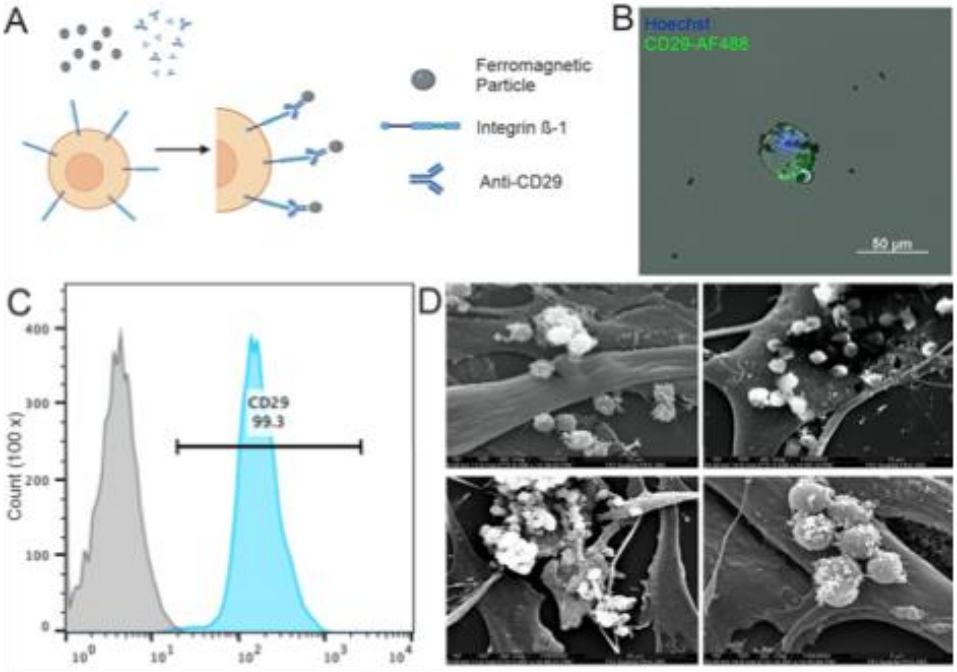

Figure 2. Ferromagnetic loading of mesenchymal stromal cells. (**A**) Concept of bio-linking ferromagnetic particles to the surface through anti-CD29 antibody. (**B**) Fluorescence microscopy of mMSC bio-linked to ferromagnetic particles. Cell nucleus is stained with Hoechst33342, Integrin ß-1 is stained with anti-CD29–Biotin–Streptavidin–Alexa Fluor 488; 20X. (**C**) Flow cytometry of unstained mMSCs control (grey) and mMSC stained with anti-CD29–Biotin–Streptavidin–Alexa Fluor 488. (**D**) SEM images of mMSCs bio-linked with ferromagnetic particles.

To compare the adhesion speed of mMSC spheroids on a collagen-I-coated plastic dish, mMSCs were loaded with SPIONs. Alternatively, ferromagnetic particles were bio-linked to CD29 cell surface receptors. Cell spheroids were generated by the hanging drop method. Spheroids were examined by transmission light and fluorescence microscopy showing control (no particles; colourless), SPION-labelled (Dil-labelled; red), and ferromagnetic-particle-labelled (CD29-linked Ferro; green) mMSC spheroids (Figure 3A). Next, the attachment of the mMSC spheroids was quantified at eleven time points during a total observation time of 120 min (n = 8). Statistical analysis showed that the first 45 min is the critical time

window for mMSC spheroids adhesion. SPIONs significantly ($p < 0.05$) reduced the mMSC spheroids' adhesion time in comparison with the control and Ferro (Figure 3B).

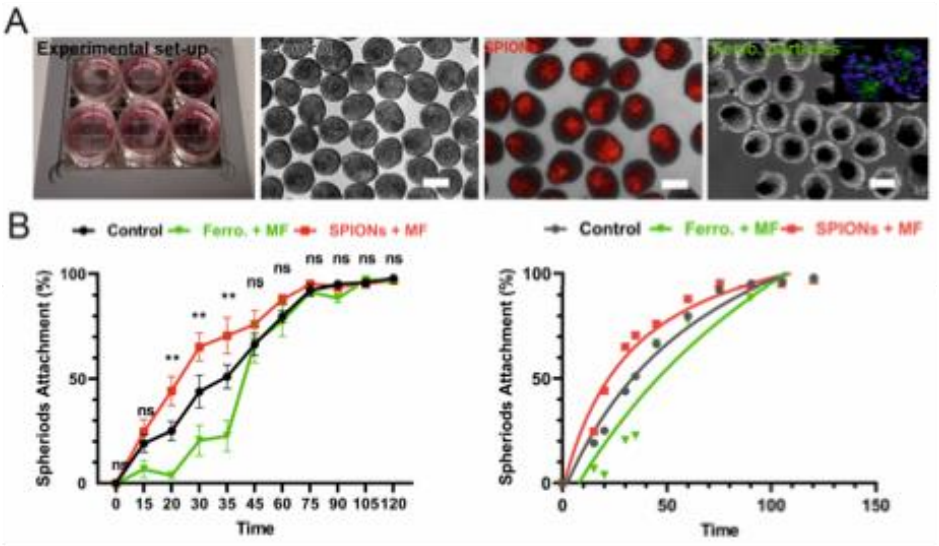

Figure 3. Adhesion experiment of magnetically targeted cellular spheroids on collagen-coated plates. (**A**) Experimental setups and morphologies of different spheroids. SPIONs (Dil-labelled, red colour)-loaded and ferromagnetic particle (Anti-CD29-AlexaFlour 488; green) co-incubated spheroids were visualised by fluorescence microscopy. Scale bars: 100 µm. (**B**) Attachment ratio was quantified at different time points. Left panel: experimental data. Right panel: mathematical curve fitting. Data are represented as mean ± SD. ** $p < 0.05$.

Next, we investigated the cell clustering and/or cell aggregation through magnetic force. SPION-labelled mMSCs (group 1) or ferromagnetic-particle-labelled mMSCs (group 2) were placed close to a magnet with a conic iron tip. The formation of cell clusters was observed and the cell number per cluster was determined through DNA quantification. The application of magnetic force was performed for 1, 5, and 15 min and the effect of cell clumping was observed by fluorescence microscopy (Figure 4A). DNA was isolated from the induced cell clumps for indirect cell quantification (Figure 4B). The percentage of cells within the cell clumps was calculated by dividing the calculated cell number after DNA OD measurement by the total cell number of the experiment. After 15 min, 100.00 ± 28.84% of mMSCs were found in the cell aggregate for ferromagnetic-particle-labelled cells and 98.12 ± 0.38% for SPIONs-loaded cells. Cell aggregates of SPION-labelled mMSCs macroscopically followed a permanent magnet (Video S1). When placed in the magnetic field of the permanent magnet (1 h), the aggregates formed a stable agglomerate (Video S2).

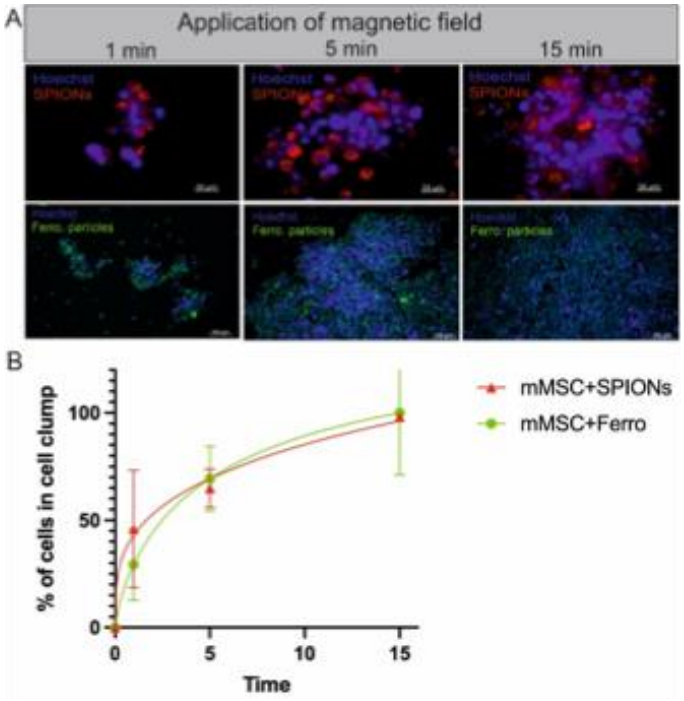

Figure 4. Magnetically induced cell clumping. (**A**) A magnet with a conic iron tip is placed under the dish harbouring the magnetically labelled cells, either labelled with SPIONs or with ferromagnetic particles, for 1, 5, and 15 min, and transferred to a slide for microscopy. Cells were stained with Hoechst33342. Cell clumps were imaged by fluorescence microscopy. (**B**) Quantification of cell count in magnetically induced clumps based on DNA content.

4. Discussion

Magnetic targeting has the potential to increase cell retention in different settings of cell replacement therapy. This is especially useful in applications where cell engraftment is critical, for example, in cardiac cell replacement therapy. In a previous study, Ottersbach and colleagues demonstrated the potential of magnetically targeting murine pluripotent stem-cell-derived cardiomyocytes (PSC-CMs) and murine embryonic cardiomyocytes (eCMs) to the myocardium [18]. Placing a magnet close to the injection site for 10 min was found to be sufficient for increasing cell retention by about 7-fold in the two weeks following the injection. Longer exposure to the magnet did not result in further improvement.

These data demonstrate the potential of magnetic targeting to increase cell engraftment in the heart. Although promising, the absolute cell retention remained low: when 200,000 PSC-CMs were transplanted, magnetic targeting increased the absolute number of engrafted CMs from 653 ± 34 to 4453 ± 724 cells 2 weeks after transplantation.

In a previous study, we showed that monocultures of murine PSC-CMs hardly engraft when transplanted into an acutely injured murine myocardium [11]. Real-time PCR-based quantification of engrafted PSC-CMs revealed a cell persistence of only 0.8% one day after transplantation. Interestingly, the engraftment rate remained the same when clumps of PSC-CMs were transplanted instead of single cell suspensions. In contrast, the generation of clumps from mouse bone marrow stromal cells and PSC-CMs resulted in a substantial increase in cell retention that outcompetes the previously discussed effect of magnetic

targeting. It can be speculated that both methods, i.e., the formation of clusters of PSC-CMs with mMSC and the application of magnetic cell targeting, may act synergistically to enhance cell engraftment. Therefore, we use spherical clusters of mMSCs in this study to analyse the effect of magnetic forces on mMSC adhesion in vitro, and to pave the way for improved experimental designs for future pre-clinical experiments in vivo.

SPIONs were used to magnetically label mMSCs. For the adhesion experiments, clusters of mMSCs were prepared. The results show significantly faster cell adhesion when clusters are exposed to a magnetic field. More than 50% of the cell spheres attached within 30 min. We also employed a novel technology and labelled mMSCs with ferromagnetic particles that were hooked up to the cell membrane by antibodies against CD29 but could not demonstrate faster adhesion of the loaded mMSC clusters when exposed to a magnetic field.

These data suggest that faster attachment of cells to the extracellular matrix contributes to the enhancement effects of magnetic targeting when SPIONs are employed to load cells. On the other hand, it is possible that the effect is also due to forced cell aggregation. By using cell-surface-bound ferromagnetic particles, we aimed to generate a system were the short application of a strong magnetic field results in the permanent magnetisation of the particles resulting in the formation of forces between the labelled cells, even in the absence of the external magnet. The basic idea of this approach is to generate ferromagnetically labelled cells that can be rapidly magnetised by an external field and can result in the mechanically stable formation of aggregates.

We could show that there is a trend towards the faster attachment of SPION-loaded MSC spheroids. MSC clusters loaded on the surface with ferromagnetic particles attach more slowly; the presence of ferromagnetic cells on the cell membrane could be a possible explanation for this. To assess the aggregation of cells, SPION-labelled and ferromagnetic-particle-labelled cells were used, and cell aggregation was measured. In both experiments, aggregation was efficient and cell numbers in aggregates did not point to a more pronounced effect when ferromagnetic particles were used. Taking into account the fact that SPIONs from ferric oxide did not show toxic effects on the cells, loading with SPIONs seems favourable as compared to loading with ferromagnetic particles; this is because the ferromagnetic particles in this study contained chromium dioxide, and large extracellular particles may cause unforeseen effects in the myocardium. Moreover, uses of iron-oxide-based SPIONs have already advanced to clinical uses, showing minimal toxicity (for a review, see [21]).

With respect to the potential mechanism of magnetic targeting, we found that the adhesion of mMSCs to the matrix takes places in less than an hour, with more than 50% of the cells being attached after 30 min in the presence of a magnetic force. In contrast, the aggregation of cells in suspension appears faster, reaching 80% saturation within only 10 min. This finding points to the conclusion that the effects of increased cardiomyocyte engraftment observed by Ottersbach and colleagues is due to forced cell aggregation, because the application of the magnetic field for 10 min was sufficient for reaching the maximal effect.

In conclusion, magnetic targeting is a potential method for ensuring controlled cell aggregation, thus reducing the washout of transplanted cells. This has significant implications for more effective stem cell and cell replacement therapies. In future in vivo studies, we will investigate whether magnetic targeting acts synergistically with microtissue transplantation and improves cell retention after intramyocardial cell transplantation.

Supplementary Materials: The following supporting information can be downloaded at: https://www.mdpi.com/article/10.3390/bioengineering12060657/s1, Video S1: Movement of SPION la-

belled MSC spheroids along magnetic field gradients. Video S2: Formation of macroscopic assemblies of MSC spheroids following 1 h incubation in the magnetic field.

Author Contributions: Conceptualization, S.H., G.B. and K.P.P.; methodology, T.H., L.M., S.H., L.S.-U., F.N., F.G., A.S., L.Z. and Q.-K.P.; formal analysis, S.H.; investigation, T.H., L.M., L.S.-U., F.N., F.G., L.Z. and Q.-K.P.; writing—original draft preparation, L.M. and S.H.; writing—review and editing, G.B. and K.P.P.; supervision, G.B.; project administration, K.P.P.; funding acquisition, G.B. and K.P.P. All authors have read and agreed to the published version of the manuscript.

Funding: This work was supported by the German Research Foundation (405831333 to K.P.P.), the Marga and Walter Boll-Foundation (to K.P.P.), and the Cancer Prevention and Research Institute of Texas (RP220518 to G.B.). Funding for instruments: JEOL JEM2100 Plus: DFG-INST 216/793-1 FUGG.

Institutional Review Board Statement: Not applicable.

Informed Consent Statement: Not applicable.

Data Availability Statement: Data is available on request.

Acknowledgments: We thankfully acknowledge support provided by Daniel Derichsweiler and Raja Sahito with MSC preparation. Magnetic tools were assembled by the Scientific Workshop of the Medical Faculty, University of Cologne.

Conflicts of Interest: The authors declare no conflict of interest.

References

1. Cheng, K.; Malliaras, K.; Li, T.-S.; Sun, B.; Houde, C.; Galang, G.; Smith, J.; Matsushita, N.; Marbán, E. Magnetic Enhancement of Cell Retention, Engraftment, and Functional Benefit After Intracoronary Delivery of Cardiac- Derived Stem Cells in a Rat Model of Ischemia/Reperfusion. *Cell Transpl.* **2012**, *21*, 1121–1135. [CrossRef] [PubMed]
2. Günter, J.; Wolint, P.; Bopp, A.; Steiger, J.; Cambria, E.; Hoerstrup, S.P.; Emmert, M.Y. Microtissues in Cardiovascular Medicine: Regenerative Potential Based on a 3D Microenvironment. *Stem Cell Int.* **2016**, *2016*, 9098523. [CrossRef]
3. Bauer, M.; Kang, L.; Qiu, Y.; Wu, J.; Peng, M.; Chen, H.H.; Camci-Unal, G.; Bayomy, A.F.; Sosnovik, D.E.; Khademhosseini, A.; et al. Adult Cardiac Progenitor Cell Aggregates Exhibit Survival Benefit Both In Vitro and In Vivo. *PLoS ONE* **2012**, *7*, e50491. [CrossRef]
4. Emmert, M.Y.; Hitchcock, R.W.; Hoerstrup, S.P. Cell therapy, 3D culture systems and tissue engineering for cardiac regeneration. *Adv. Drug Deliv. Rev.* **2014**, *9–70*, 254–269. [CrossRef]
5. Cores, J.; Caranasos, T.G.; Cheng, K. Magnetically Targeted Stem Cell Delivery for Regenerative Medicine. *J. Funct. Biomater.* **2015**, *6*, 526. [CrossRef]
6. Huang, Z.; Shen, Y.; Sun, A.; Huang, G.; Zhu, H.; Huang, B.; Xu, J.; Song, Y.; Pei, N.; Ma, J.; et al. Magnetic targeting enhances retrograde cell retention in a rat model of myocardial infarction. *Stem Cell Res. Ther.* **2013**, *4*, 149. [CrossRef]
7. Oshima, S.; Kamei, N.; Nakasa, T.; Yasunaga, Y.; Ochi, M. Enhancement of muscle repair using human mesenchymal stem cells with a magnetic targeting system in a subchronic muscle injury model. *J. Orthop. Sci.* **2014**, *19*, 478–488. [CrossRef] [PubMed]
8. Silva, L.H.A.; Cruz, F.F.; Morales, M.M.; Weiss, D.J.; Rocco, P.R.M. Magnetic targeting as a strategy to enhance therapeutic effects of mesenchymal stromal cells. *Stem Cell Res. Ther.* **2017**, *8*, 58. [CrossRef] [PubMed]
9. Chen, Y.; Hou, S. Application of magnetic nanoparticles in cell therapy. *Stem Cell Res. Ther.* **2022**, *13*, 135. [CrossRef]
10. Schiffer, M.; Wagner, K.; Carls, E.; Nicke, J.; Hesse, M.; Fratila, R.M.; Hildebrand, S.; Eberbeck, D.; Mohr, T.; Mohammadi, M.M.; et al. Nanoparticle-assisted targeting of heart lesions with cardiac myofibroblasts: Combined gene and cell therapy. *Theranostics* **2025**, *15*, 4287–4307. [CrossRef]
11. Sahito, R.G.A.; Sheng, X.; Maass, M.; Mikhael, N.; Hamad, S.; Heras-Bautista, C.O.; Derichsweiler, D.; Spitkovsky, D.; Suhr, F.; Khalil, M.; et al. In Vitro Grown Micro-Tissues for Cardiac Cell Replacement Therapy in Vivo. *Cell Physiol. Biochem.* **2019**, *52*, 1309–1324. [CrossRef] [PubMed]
12. Kobayashi, T.; Ochi, M.; Yanada, S.; Ishikawa, M.; Adachi, N.; Deie, M.; Arihiro, K. A Novel Cell Delivery System Using Magnetically Labeled Mesenchymal Stem Cells and an External Magnetic Device for Clinical Cartilage Repair. *J. Arthrosc. Relat. Surg.* **2008**, *24*, 69–76. [CrossRef] [PubMed]
13. Zhang, L.; Hajebrahimi, S.; Tong, S.; Gao, X.; Cheng, H.; Zhang, Q.; Hinojosa, D.T.; Jiang, K.; Hong, L.; Huard, J.; et al. Force-Mediated Endocytosis of Iron Oxide Nanoparticles for Magnetic Targeting of Stem Cells. *Appl. Mater. Interfaces* **2023**, *15*, 50574–50585. [CrossRef] [PubMed]

14. Li, Z.; Zhang, Y.; Ma, M.; Wang, W.; Hui, H.; Tian, J.; Chen, Y. Targeted mitigation of neointimal hyperplasia via magnetic field-directed localization of superparamagnetic iron oxide nanoparticle-labeled endothelial progenitor cells following carotid balloon catheter injury in rats. *Biomed. Pharmacother.* **2024**, *177*, 117022. [CrossRef]
15. Wang, Y.; Zhou, S.; Yang, R.; Rahman, M.; Sequeira, R.C.; Cao, N.; Zhang, Y.; Zhao, W.; Fu, Q. Magnetic targeting of superparamagnetic iron oxide nanoparticle labeled myogenic-induced adipose-derived stem cells in a rat model of stress urinary incontinence. *Nanomedicine* **2020**, *30*, 102281. [CrossRef]
16. Fagg, W.S.; Liu, N.; Yang, M.J.; Cheng, K.; Chung, E.; Kim, J.S.; Wu, G.; Fair, J. Magnetic Targeting of Stem Cell Derivatives Enhances Hepatic Engraftment into Structurally Normal Liver. *Cell Transpl.* **2017**, *26*, 1868–1877. [CrossRef]
17. Shen, W.B.; Anastasiadis, P.; Nguyen, B.; Yarnell, D.; Yarowsky, P.J.; Frenkel, V.; Fishman, P.S. Magnetic Enhancement of Stem Cell-Targeted Delivery into the Brain Following MR-Guided Focused Ultrasound for Opening the Blood-Brain Barrier. *Cell Transpl.* **2017**, *26*, 1235–1246. [CrossRef]
18. Ottersbach, A.; Mykhaylyk, O.; Heidsieck, A.; Eberbeck, D.; Rieck, S.; Zimmermann, K.; Breitbach, M.; Engelbrecht, B.; Brugmann, T.; Hesse, M.; et al. Improved heart repair upon myocardial infarction: Combination of magnetic nanoparticles and tailored magnets strongly increases engraftment of myocytes. *Biomaterials* **2018**, *155*, 176–190. [CrossRef]
19. Zhang, L.L.; Tong, S.; Zhang, Q.B.; Bao, G. Lipid-Encapsulated Fe3O4 Nanoparticles for Multimodal Magnetic Resonance/Fluorescence Imaging. *Acs Appl. Nano Mater.* **2020**, *3*, 6785–6797. [CrossRef]
20. Tong, S.; Hou, S.J.; Ren, B.B.; Zheng, Z.L.; Bao, G. Self-Assembly of Phospholipid-PEG Coating on Nanoparticles through Dual Solvent Exchange. *Nano Lett.* **2011**, *11*, 3720–3726. [CrossRef]
21. Tong, S.; Zhu, H.B.; Bao, G. Magnetic iron oxide nanoparticles for disease detection and therapy. *Mater. Today* **2019**, *31*, 86–99. [CrossRef] [PubMed]

II. Standard operation Procedures (SOPs) from collaboration Laboratories

a. Preparation of CRISPR-Cas9 Reagents for Microinjection: Max-Planck Institute for Biology of Aging Transgenic Core Facility

MAX PLANCK INSTITUTE FOR BIOLOGY OF AGEING
TRANSGENIC CORE FACILITY
Joseph-Stelzmann-Str. 9b, 50931, Cologne, Germany

Laila M.R. Singh, PhD.
Postdoctoral Fellow
Email: laila.singh@age.mpg.de

Preparation of CRISPR-Cas9 Reagents for Microinjection

Overview

The following protocols can be used to prepare CRISPR-Cas9 reagents in advance to ensure that microinjection samples are prepared in a timely and reproducible manner on the day of microinjection.

Materials

Laminar Flow Hood that can be UV sterilized
Pipettors designated for RNA/DNA use only (they should NEVER have been used for genotyping)
- P2, P10, P20, P100 & P1000

Filter Tips
Eppendorf Tubes (that have been capped in the laminar flow hood)
- 1.5 mL Safe-Lock, Nuclease-free, Protein LoBind Tubes (Cat. No. 022431081)
- 0.5 mL Safe-Lock, Nuclease-free, DNA LoBind Tubes (Cat. No. 022431005)

Tubes racks for 1.5 mL and 0.5 mL microfuge tubes
Labeller and Liquid Nitrogen-Proof Labels
- Labeller: Brady BMP21-LAB
- Labels: Brady 19.1 mm Black on White Polypropylene (Cat. No. M21-750-7425)

70% Ethanol in a spray bottle
Kimtech Precision Wipes (Cat. No. 75512) for wiping the hood without generating any dust
Heating block (eg. Grant 2BH2) with removable aluminum blocks which fit 0.5 mL microfuge tubes
Dry ice or Liquid Nitrogen for flash freezing of aliquoted reagents
-80°C Freezer

Reagents

IDTE pH 7.5 (Nuclease-free buffer, 100 mM Tris, 0.1 mM EDTA pH 7.5) stored frozen as aliquots at -20°C
Alt-R® S.p. Cas9 Nuclease V3, 500 µg (approx. 61 µM concentration) from IDT (Cat. No. 1081059)
Alt-R® CRISPR-Cas9 tracrRNA, 100 nmol (dried) from IDT (Cat. No. 1072534)
Alt-R® CRISPR-Cas9 crRNA, 10 nmol (dried) from IDT (these are custom order for each project)
Ultramer® or Megamer® ssDNA repair oligos from IDT (recommended) or another supplier like GenScript

NOTES

Before starting the reagent preparation procedure make sure that you have:

- ***access to a laminar flow hood where the UV light has been run for 60 minutes to inactivate RNAses***
- ***enough tubes for aliquoting ALL of the reagents that you will prepare, ideally cap these tubes ahead of time in the laminar flow hood, BEFORE you start to prepare your reagents label your tubes with liquid nitrogen resistant labels (Brady polypropylene labels) and by writing in blue ink on colour coded 'Tough Spots' for easy identification of the different reagents in the -80°C freezer, see below for some example labels:***
- ***dry ice (preferred) or liquid nitrogen available for flash freezing of the reagents that you have aliquoted***

CRISPR-CAS9 REAGENT PREPARATION AND ALIQUOTING

It is recommended that CRISPR and Cas9 reagents be prepared and aliquoted in the sizes shown below and that they are stored frozen until use.

300 µL IDTE pH 7.5
Nuclease free
100 mM Tris, 0.1 mM EDTA
Lot: 314711 LM 11/01/2019

0.6 µL 62 µM Cas9
Alt-R S.p. V3 IDT#: 1081059
MW= 162,200 g/mol
Lot #: 407267 LM14/01/2019

3 µL 400 µM tracrRNA
in IDTE, Alt-R IDT#: 1073191
MW= 22,182 g/mol
Lot #: 410130 LS 17/01/2019

0.43 µL of 200 µM annealed
gRNA Fgf21-D3 in
IDTE pH 7.5
LS 23/01/2019

2 µL Fgf21- D3/D6
Short ssDNA repair
500 nM in IDTE pH 7.5
LS 25-Jan-2019

10 µL Floxed Fgf21 long ssDNA
Repair template
83.76 nM in IDTE pH 7.5
LS 15/01/2019 1 of 5

Reagent Aliquots to be Prepared, Flash-Frozen on Dry Ice and Stored at -80°C
Frozen reagents should be quickly thawed in your hand or at room temperature for a few seconds, vortex mixed and then spun down in a microfuge before being placed on ice and before they are opened to ensure that the reagents do not get contaminated or lost when the tube is opened.

ALL reagents should be at 4°C before they are measured to ensure that accurate volume measurements are made because water has a very high thermal expansion coefficient (ie. the same amount of water at 20°C has a much larger volume than it does at 4°C). This is a particularly important factor to consider when aliquoting small volumes of reagents.

For dried reagents check that the cap is screwed on securely and spin the tubes at 2000 rcf in a centrifuge for 2 minutes to ensure that the dried reagent is at the bottom of the tube before you open it (since the pellet of dried reagent can become dislodged during shipping and could be stuck to the lid of the tube).

IDTE

- For each new Lot No. of IDTE, open the new bottle in the laminar flow hood and remove an aliquot for Ingo to use for microinjection to test for potential toxicity to the oocytes.
- If the microinjected oocytes develop normally to the blastocyst stage then the IDTE should be aliquoted in the laminar hood into sterile capped nuclease-free 1.5 mL Eppendorf tubes as:
  - 100 µL, 300 µL, 1 mL aliquots to be stored in the freezer at -20°C or -80°C to prevent fungal or bacterial growth in the buffer aliquots over time

Cas9

- Cas9 should be aliquoted in the laminar flow hood into sterile capped nuclease-free 1.5 mL Protein LoBind Eppendorf tubes to avoid repeated freeze-thawing of the enzyme which will reduce its activity over time. The protein storage buffer contains stabilizers which is why the Cas9 should NOT BE DILUTED and then frozen. Freeze small aliquots of Cas9 at its original concentration of 62 µM as follows:
  - 0.6 µL single use aliquots to be stored frozen at -80°C
- On the day that the Cas9 will be used it can be diluted 1:10 in IDTE to prepare a working stock solution of 6.2 µM.

tracrRNA

Overview

tracrRNA should be dissolved to a concentration of 400 µM in IDTE and frozen as single use aliquots to avoid repeated freeze-thawing which will cause degradation of the RNA

- flash freeze tracrRNAs as 3 µL and 6 µL single use aliquots to be stored frozen at -80°C

Preparation Protocol

- Spin the tube of dried tracrRNA at 2000 rcf in a centrifuge for 2 minutes, open the tube in the laminar flow hood and add the appropriate amount of IDTE to prepare a 400 µM stock solution, vortex the sample, microfuge the contents to the bottom of the tube and place the tube in a pre-heated heating block at 55°C for 5 minutes
- Briefly vortex mix the tube five times, microfuge to bring all liquid to the bottom of the tube and place on ice to cool for 10 minutes
- Once the sample has cooled, briefly vortex mix it one more time, microfuge to bring the contents to the bottom of the tube and place it on ice to cool
- The dissolved tracrRNA should be aliquoted in the laminar flow hood into sterile capped nuclease-free 0.5 mL DNA LoBind Eppendorf tubes
- Unused aliquots of tracrRNA should be flash frozen on dry ice (preferable) or in liquid nitrogen and stored frozen at -80°C
- On the day that the tracrRNA will be used to prepare annealed gRNAs it should be quickly thawed in your hand or at room temperature for a few seconds, vortex mixed and then spun down in a microfuge before being placed on ice to cool thoroughly (10 minutes) before being used

crRNAs

Overview

crRNAs should be dissolved to a concentration of 400 µM in IDTE and an aliquot should be annealed with the tracrRNA to prepare functional gRNAs, the gRNAs and unused crRNAs should be frozen as single use aliquots to avoid repeated freeze-thawing which will cause degradation of the RNA

- flash freeze annealed gRNAs as 0.43 and 0.86 µL single use aliquots to be stored frozen at -80°C
- flash freeze dissolved crRNAs as 3 µL and 6 µL single use aliquots to be stored frozen at -80°C

Preparation Protocol

- Spin the tube of dried crRNA at 2000 rcf in a centrifuge for 2 minutes, open the tube in the laminar flow hood and add the appropriate amount of IDTE to prepare a 400 µM stock solution, vortex the sample, microfuge the contents to the bottom of the tube and place the tube in a pre-heated heating block at 55°C for 5 minutes
- Briefly vortex mix the tube five times, microfuge to bring all liquid to the bottom of the tube and place on ice to cool for 10 minutes
- Once the sample has cooled, briefly vortex mix it one more time, microfuge to bring the contents to the bottom of the tube and place it on ice to cool
- In the laminar flow hood an aliquot of the dissolved crRNA should be pipetted into a sterile capped nuclease-free 0.5 mL DNA LoBind Eppendorf tubes to be annealed with tracrRNA, the remaining crRNA should be frozen as aliquots for future use
- Unused aliquots of crRNA should be flash frozen on dry ice (preferable) or in liquid nitrogen and stored frozen at -80°C
- On the day that the crRNA will be used to prepare annealed gRNAs it should be quickly thawed in your hand or at room temperature for a few seconds, vortex mixed and then spun down in a microfuge before being placed on ice to cool thoroughly (10 minutes) before being used

annealed gRNAs

Overview

gRNAs are prepared by annealing the crRNA and the tracrRNA to form an active guide RNA (gRNA) with a final stock concentration of 200 µM in IDTE. ThegRNA will guide the Cas9 nuclease to the genomic locus of interest and cleave both DNA strands at the 20 bp target sequence.

- flash freeze 6 µL of 200 µM annealed gRNAs as 5X 0.43 µL and 4X 0.86 µL single use aliquots to be stored frozen at -80°C

Preparation Protocol

- In the laminar flow hood, mix equal volumes of 400 µM stock solutions of crRNA and tracrRNA in sterile capped nuclease-free 0.5 mL DNA LoBind Eppendorf tubes, vortex mix the sample, microfuge the contents to the bottom of the tube and place the tube in a pre-heated removable aluminum heating block containing distilled water (to ensure good thermal contact) at 95°C for 5 minutes
- Place the 95°C heating block containing the annealing gRNA samples on top of a room temperature aluminum heating block on the bench top and allow the samples to cool to room temperature (~ 1 hr)
- Vortex mix the sample, microfuge the contents to the bottom of the tube and place the tube on ice for 10 minutes to cool
- In the laminar flow hood aliquot the annealed gRNAs into sterile capped nuclease-free 0.5 mL DNA LoBind Eppendorf tubes
- Unused aliquots of annealed gRNAs should be flash frozen on dry ice (preferable) or in liquid nitrogen and stored frozen at -80°C
- On the day that the annealed gRNAs will be used to prepare microinjection samples they should be quickly thawed in your hand or at room temperature for a few seconds, vortex mixed and then spun down in a microfuge before being placed on ice to cool thoroughly (10 minutes) before being used

ssDNA Repair Templates

Overview

ssDNA repair templates are EXTREMELY fragile and must be handled with the utmost of care. DO NOT VORTEX MIX or pipette the samples up and down repeatedly to mix them! ONLY mix the samples GENTLY by flicking the tube! The price for a single stranded DNA repair template is proportional to its length. A 3 µg quantity of a 3 kb ssDNA repair template costs approximately 3000 Euro and this is only enough DNA to prepare 3 or 4 microinjection samples. So these reagents are VERY PRECIOUS and should be handled accordingly! Since it is best to avoid freeze-thawing the ssDNA repair templates it is best to dissolve them the day before they will be needed and to store them at 4°C overnight. Unused ssDNA repair templates should be flash frozen and stored as single use aliquots because DNA bases may be prone to damage when stored in solution

- flash freeze unused ssDNA repair templates as single use aliquots to be stored frozen at -80°C

Preparation Protocol

- spin the tube of dried ssDNA repair template at 2000 rcf in a centrifuge for 2 minutes, open the tube in the laminar flow hood and add the appropriate amount of IDTE buffer to dissolve the DNA
  - for repair templates < 800 bases in length prepare 10 µM or 1 µM stock solutions (depending on the amount of DNA that you have) and use these concentrated stock solutions to prepare more diluted stock solutions of 83.76 nM or 500 nM (depending on the length of the repair template)
    - prepare 2 µL aliquots of 500 nM stock solutions
      OR
      prepare 10 µL aliquots of 83.76 nM stock solutions
  - for longer repair templates (>800 bases in length) prepare 83.76 nM stock solutions
    - prepare 10 µL aliquots of 83.76 nM stock solutions

NOTE
Be particularly careful when handling long ssDNA repair templates because they are very fragile

- gently flick the sample 5X to mix, microfuge the contents to the bottom of the tube and place the tube in a pre-heated heating block at 55°C for 5 minutes
- gently mix the sample by flicking the tube 5X, microfuge to bring all liquid to the bottom of the tube and place on ice to cool for 10 minutes
- once the sample has cooled, gently mix the sample one more time by flicking the tube 5X and microfuge the tube to bring the contents to the bottom of the tube and place it on ice to cool or store it at 4°C overnight (the sample is stable at 4°C for a couple of days and can be prepared in advance)
- following the preparation of the microinjection samples, unused repair template should be frozen as 2 µL or 10 µL aliquots (depending on their concentration) and they should be flash frozen and stored at -80°C

CRISPR-CAS9 MICROINJECTION SAMPLE PREPARATION PROTOCOL

Reagents
300 µL of IDTE pH 7.5 (can be put in the fridge the day before to thaw)
0.6 µL aliquot of Cas9
0.43 µL aliquot of 200 µM annealed gRNA(s)
ssDNA repair template dissolved to an appropriate concentration in IDTE (is required)

Day 1 (the day BEFORE the microinjection experiment)
- Run the UV for 30 minutes in the laminar flow hood to destroy RNases and DNases
- Quickly thaw the Cas9 and annealed gRNA(s) in your hand or at room temperature for a few seconds, vortex mix them, spin them down in a microfuge and then place them on ice, along with your aliquot of IDTE
- In the laminar flow hood dilute the 0.6 µL aliquot of Cas9 with 5.4 µL of 4°C IDTE to a final concentration of 6.2 µM, vortex mix, spin down in a microfuge and return the tube to the ice bucket
- Carefully add the appropriate amount of IDTE to the annealed gRNA samples, followed by the appropriate amount of Cas9 using the table on the following page
- Vortex mix the sample, spin it down in a microfuge and store it overnight at 4°C to allow EACH gRNA ample time to form stable complexes with Cas9

Day 2 (the day of the microinjection experiment)
- Run the UV for at least 30 minutes in the laminar flow hood to destroy RNases and DNases
- Pre-cool the centrifuge to 6°C (not 4°C, to make sure that the sample isn't accidentally freeze if the centrifuge overcools the sample)

When using SINGLE gRNAs
- In the laminar flow hood carefully dilute the sample to the appropriate volume with IDTE, vortex mix, spin down and then CAREFULLY add the ssDNA repair template (if you are using one)
- GENTLY MIX THE SAMPLE by flicking it 5X before placing it in a centrifuge that has been pre-chilled to 6°C

When using a PAIR of gRNAs
- In the laminar flow hood carefully add the 7.5 µL of Cas9 + gRNA-U1 to the other tube containing 7.5 µL of Cas9 + gRNA-D1 and dilute the sample to the appropriate volume with IDTE, vortex mix, spin down and then CAREFULLY add the ssDNA repair template (if you are using one)
- GENTLY MIX THE SAMPLE by flicking it 5X before placing it in a centrifuge that has been pre-chilled to 6°C

NOTE
ALWAYS add the ssDNA repair template to the sample(s) as close as possible to the time of microinjection because the ssDNA causes components in the sample to aggregate which can clog the microinjection needle

- Centrifuge the sample at maximum speed in the pre-chilled centrifuge for 15 minutes
- BEFORE removing the samples from the centrifuge mark which side of the tube is facing out (where any potential pellet may be) and CAREFULLY remove the tubes from the centrifuge and place them on ice
- In the laminar flow hood CAREFULLY open the tube and tip it so that the side of the tube where the pellet might be is facing up, CAREFULLY and SLOWLY pipette 15 µL of sample from the side opposite the pellet near the top of the tube
- CAREFULLY and SLOWLY pipette the 15 µL microinjection sample into a 1.5 mL Protein LoBind tube
- Keep the microinjection sample on ice until it is microinjected

b. SOP THNW 003 Tiertransport und Einschleusen von Tieren in die Tierhaltung

SOP
THNW 003
Tiertransport und
Einschleusen von Tieren in
die Tierhaltung

Thema	Diese SOP dient dazu Abläufe für die Durchführung von Importen und Exporten von Mäusen und Ratten zu definieren sowie das Einschleusen von Tieren in die Tierhaltung zu erläutern.
Inhalt	**1. Einführung** **2. Allgemeines** **3. Vorgehen und Maßnahmen beim Tiertransfer sowie Tierimport und – export** **3.1. Tiertransfer internal (von Tierhaltungen zu Tierhaltungen innerhalb des Tierhaltungsnetzwerks)** **3.2. Tiertransfer nach extern (von Tierhaltungen des Tierhaltungsnetzwerks in eine andere externe Tierhaltung)** **3.2.1 Tierexport in Nicht-EU-Länder** **3.3. Tierimport von extern (von einer externen Tierhaltung in eine Tierhaltung des Tierhaltungsnetzwerks)** **3.3.1 Tierimport aus Nicht-EU-Länder** **3.4. Export to Laboratory (von Tierhaltungen des Tierhaltungsnetzwerks in ein Labor)** **3.5. Export and Back (Ausschleusen und Wiedereinschleusen von Tieren zu Versuchszwecken)** **4. Hygienegrundlagen für Tiertransporte** **4.1. Tiertransfer internal** **4.2. Tierimport von extern** **5. Praktischer Ablauf eines Tiertransport** **5.1. Voraussetzungen zum Transport** **5.2. Durchführung des Transportes** **6. Transportboxen und Beschriftung**
Geltungsbereich	Tierhaltungsnetzwerk

Erstellung	Ersteller*in	Prüfer*in	Freigabe und letzte Prüfung	Seite
24.06.2021	Schenk/Stark	Guschlbauer/Täubner	29.07.2024	1 von 14

c. SOP THNW 022 Breeding Mouse/Rat

Tierhaltungs-Netzwerk
der Medizinischen Fakultät Köln

SOP
THNW 022
Maus/Ratte Zucht

Thema	Planung und Durchführung von Maus- und Rattenzuchten
Inhalt	**1. Einführung** **2. Vorgehen vor Beginn einer Verpaarung** **3. Fütterung** **4. Vorgehen bei Trächtigkeit** **5. Vorgehen beim Absetzen der Jungtiere** **6. Vergesellschaften der Absatztiere** **7. Ausnahmen für die Einzelhaltung** **8. Auszug aus der Richtlinie 2010/63/EU – Platzbedarf Maus und Ratte**
Geltungsbereich	Tierhaltungsnetzwerk

1. <u>Einführung</u>

Diese SOP dient dazu das tierschutzkonforme Verhalten vor Beginn und während einer Züchtung von Mäusen und Ratten zu gewährleisten. Es gilt sowohl für belastete als auch für nicht-belastete Maus- und Rattenzuchten sowie für transgene Linien und Wildtyplinien. Vorab müssen alle Personen die Züchtungen von Tieren vornehmen die entsprechende Fortbildung der Tierschutzbeauftragten dazu absolvieren (Züchten und Töten von Versuchstieren, Prozeßbeschreibung) und das entsprechende Zertifikat vorweisen können. Eine Exceltabelle mit exakter Zuchtplanung muss in PyRAT zu der Linieninformation begefügt werden.

Die Mauszucht erfolgt in einer 1:1 Verpaarung (ein Männchen, ein Weibchen). Eine Verpaarung mit 1:2 (1 Männchen, 2 Weibchen) ist zusätzlich erlaubt, wenn die Verpaarung im IVC-Käfig mit der Mindestgröße von 500cm^2 (Typ 2 lang) stattfindet. Tragende Weibchen bei einer 1:2 Verpaarung müssen sofort separiert werden. Der Zuchtkäfig muss grundsätzlich ein Häuschen sowie Nestbaumaterial erhalten.

Die Verpaarung bei der Ratte erfolgt 1:1 in einem Rattenkäfig mit mindestens 1800 cm^2. Es soll stets eine handvoll Holzwolle oder geeignetes Nistmaterial zum Bauen eines Nestes im Käfig vorhanden sein.

1. Einführung

Diese Standardarbeitsanweisung (SOP) definiert die Abläufe zum Transfer von Versuchstieren zwischen den Tierhaltungen des Tierhaltungsnetzwerkes der Medizinischen Fakultät der Universität Köln und von externen Tierhaltungen in die Tierhaltungen der Medizinischen Fakultät sowie nach außerhalb. Sie beinhaltet das Ausschleusen, den Transport und das Einschleusen der Tiere in die verschiedenen Versuchstierhaltungen. Die Verantwortung für die Durchführung des Transfers liegt bei den ausführenden Arbeitsgruppen, wobei die Überwachung der Einhaltung dieser Arbeitsanweisung und die Freigabe nach hygienischer Prüfung eines Transfers durch die Leitung bzw. die Tierärztinnen des Tierhaltungsnetzwerkes erfolgt.

2. Allgemeines

Der geplante Transfer ist im Vorfeld mit einem Auftrag über PyRAT anzumelden. Entsprechend der verschiedenen Auftragsklassen in PyRAT bzw. Transferarten gelten folgende Stichtage bis zu denen die jeweiligen Aufträge ans das Team des Tierhaltungsnetzwerks übermittelt werden müssen. Folgende Stichtage gelten:

- Tiertransfer internal (von Tierhaltungen zu Tierhaltungen innerhalb des Tierhaltungsnetzwerks) – Auftragsklasse „Export to…“:
  mindestens 24 Stunden vorher

- Tiertransfer nach extern (von Tierhaltungen des Tierhaltungsnetzwerks in eine andere externe Tierhaltung) – Auftragsklasse „Export external“:
  mindestens 7 Tage vorher

- Tierimport von extern (von einer externen Tierhaltung in eine Tierhaltung des Tierhaltungsnetzwerks) – Auftragsklasse „Import von…“:
  mindestens 7 Tage vorher

- Export to Laboratory (von Tierhaltungen des Tierhaltungsnetzwerks in ein Labor) – Auftragsklasse „Export Laboratory“:
  mindestens 24 Stunden vorher

- Export and Back (Ausschleusen und Wiedereinschleusen von Tieren zu Versuchszwecken) – Auftragsklasse „Export and Back“:
  mindestens 24 Stunden vorher

Weitere Vorgaben und Maßnahmen für die genannten Auftragsklassen/Transferarten werden im Folgenden unter Punkt 3 im Detail erläutert.

3. Vorgehen und Maßnahmen beim Tiertransfer sowie Tierimport und – export

Jeder Tiertransfer sowie jeder Tierimport oder -export wird durch die Tierärztinnen des Tierhaltungsnetzwerkes geprüft und genehmigt. Tiere von nicht genehmigten Importen oder Transfers dürfen aus hygienischen Gründen **nicht** in die Tierhaltungen eingebracht werden.

Um den hohen Hygienestatus der Tierhaltungen aufrecht zu erhalten und Kontaminationen unter den einzelnen Tierhaltungen zu vermeiden, ist es unerlässlich, die Mäuse und Ratten wie im Weiteren beschrieben zu transportieren. Im Folgenden werden die verschiedenen Arten des Tiertransfers sowie der Tierimporte bzw. –exporte entsprechend den Auftragsklassen in PyRAT erläutert.

3.1. Tiertransfer internal (von Tierhaltungen zu Tierhaltungen innerhalb des Tierhaltungsnetzwerks)

Nach der hygienischen Prüfung der angemeldeten PyRAT Aufträge durch die Tierärztinnen des Tierhaltungsnetzwerks dürfen Tiertransfers innerhalb den Tierhaltungen des Tierhaltungsnetzwerks durchgeführt werden. Ohne genehmigten PyRAT Auftrag darf **kein** Tier in eine Haltung eingebracht werden. Bei Ankunft der Tiere in einer Tierhaltung des Tierhaltungsnetzwerks wird nach Überprüfung der

PyRAT Aufträge durch den/die Tierpfleger*in die Plastiktüte vor dem Betreten der Tierhaltung desinfiziert (siehe Hygieneplan der Tierhaltung). Dabei muss ebenfalls die Einwirkzeit laut Hygieneplan eingehalten werden. Erst dann dürfen die Tiere in der Haltung unter der Umsetzstation ausgepackt und in vorbereitete Käfige umgesetzt werden.

Das Auspacken in der Haltung kann von den Tierpfleger*innen vorgenommen werden oder von den zuständigen Nutzer*innen. Die Tiere müssen umgehend in PyRAT eingepflegt werden, sodass die Käfigkarten entsprechend ausgedruckt werden können. Zudem sollte drauf geachtet werden, dass die Tiere auch vorher schon zusammengesessen haben, damit Aggressionen und Stress unter den Tieren vermieden werden können.

Sollte der/die Nutzer*in seine/ihre Tiere selbst zum Transfer einpacken, muss stets vorab kontrolliert werden, ob der/die Nutzer*in entsprechend der Karenzzeiten (siehe dazu SOP THNW 015 Ein- und Ausschleusen von Personen und Materialien) in die Empfängerhaltung gehen darf oder ob eine bestimmte Wartezeit eingehalten werden muss. Sollte letzteres der Fall sein, müssen die Tiere in der Empfängerhaltung von einer anderen Person ausgepackt werden.

3.2. Tiertransfer nach extern (von Tierhaltungen des Tierhaltungsnetzwerks in eine andere externe Tierhaltung)

Ein Export außerhalb der Haltungen des Tierhaltungsnetzwerks muss eng mit den verantwortlichen Tierärztinnen und Tierpfleger*innen besprochen werden. Die Absprachen müssen durch die Wissenschaftler*innen initiiert werden, bevor ein Transporttermin festgelegt wird. Die Tierpfleger*innen sind außerdem darüber zu informieren, welche Tiere versendet werden. Dafür muss die Wissenschaftler*innen den verantwortlichen Tierpfleger*innen eine Packliste aushändigen, damit geprüft werden kann, ob ausreichend Boxen für den Tierexport vorhanden sind. Weibliche und männliche Tiere können dabei in einer Box – getrennt durch eine Wand – transportiert werden. Auf einen korrekten Aufbau der Transportbox ist dabei zwingend zu achten.

Die Wissenschaftler*innen muss die Lieferadresse des Empfängers den

Tierpfleger*innen übermitteln, damit die Boxen außen ordnungsgemäß beschriftet werden können. Den Tieren ist bei Abholung auch das Ohrlochschema des Tierhaltungsnetzwerks beizufügen. Der Transport von belasteten Linie benötigt eine vorherige Genehmigung von der Genehmigungsbehörde

Wenn das Datum der Tierabholung durch einen anerkannten Transporteur bekannt ist, ist durch die Wissenschaftler*innen mitzuteilen, für wann der Export geplant ist. Eine Abholung von Tieren zum Export in externe Einrichtung ist nur möglich von Montag bis Donnerstag von 08:00 – 13:00 Uhr sowie Freitag von 08:00 – 11:00. In PyRAT ist der Arbeitsauftrag „Export external" zu stellen. Den Stichtag zur Übermittlung des Auftrags ist unter Punkt 2 beschrieben.

3.2.1 Tierexport in Nicht-EU-Länder

Erfolgt der Export von Tieren in Nicht-EU-Länder muss zusätzlich zu den unter Punkt 3.2. genannten Vorgaben folgendes beachtet werden: Die Begutachtung der Tiere vor dem Verpacken muss durch eine/n Vertreter*in der Veterinärbehörde am Tag des Transportes durchgeführt werden. Die Koordination dieses Ablaufes und die Kommunikation übernimmt die für den Export verantwortliche Tierärztin. Diese informiert die verantwortliche Barriereleitung der entsprechenden Tierhaltung und den/die zuständige Tierpfleger*in.

3.3. Tierimport von extern (von einer externen Tierhaltung in eine Tierhaltung des Tierhaltungsnetzwerks)

Ein Import aus einer externen Haltung ist nur mit vorheriger Prüfung und Freigabe durch die Tierhausleitung oder den Tierärztinnen gestattet. Voraussetzungen für die Importfreigabe können dem Punkt 4.2 entnommen werden und sind strikt einzuhalten. Anderenfalls kann keine Importfreigabe erteilt werden. Die Absprachen bzgl. eines geplanten Importes von Tieren aus einer externen Haltung sind frühzeitig – spätestens aber 7 Tage vor möglichem Transporttermin – durch die Wissenschaftler*innen zu tätigen. Das aktuelle Gesundheitszeugnis und eine Haltungsbeschreibung der Versenderhaltung („facility description") sind notwendige Unterlagen, die die

Wissenschaftler*innen zum Zwecke der Prüfung an die verantwortlichen Tierärztinnen per Email (office-thnw@uk-koeln.de) weiterleiten müssen. Dabei ist auch das geplante Transportdatum mitzuteilen. Nach Begutachtung der Unterlagen durch die Tierärztinnen erfolgt bei Vollständigkeit und Korrektheit der Unterlagen die Importfreigabe. Die Wissenschaftler*innen stellen nun ein PyRAT-Auftrag, um die Tierpfleger*innen über den geplanten Import zu informieren. Die Tierärztinnen geben dann ebenso in PyRAT die Importfreigabe.

Bei Ankunft der Tiere müssen vor dem Einschleusen die Transportbox und der Filter auf Beschädigungen untersucht werden. Sind Box und Filter beschädigt, darf die Transportbox mit den Tieren **nicht** in die Haltung eingebracht werden. Es ist umgehend die Tierhausleitung zu informieren und das weitere Vorgehen zu besprechen.

Ist die Transportbox und der Filter unversehrt, wird die Transportbox außen von allen Seiten mit Oberflächendesinfektionsmittel eingesprüht. Dabei ist jedoch zu beachten, dass der Filter nicht befeuchtet wird, da Feuchtigkeit den Filter undicht macht und kein Desinfektionsmittel unmittelbar an die Tiere gelangen darf. Nach Einsprühen der äußeren Oberfläche muss die Einwirkzeit laut Hygieneplan eingehalten werden. Erst dann darf die Transportbox in die Haltung gebracht werden.

Die Transportbox ist unter der Werkbank zu öffnen und die Tiere sind in einen vorbereitenden Käfig umzusetzen. Der Allgemeinzustand der Tiere ist dabei zu kontrollieren, um Auffälligkeiten ausschließen zu können. Bei Auffälligkeiten oder Unsicherheiten ist eine Tierärztin zu kontaktieren.

Weiterhin ist zu beachten, dass nur Tiere aus der gleichen Box oder Boxhälfte in einen Käfig kommen dürfen. Die Tiere müssen umgehend in PyRAT eingetragen werden und die Käfigkarten sind unverzüglich auszudrucken.

Für die Tierhaltung ZMMK ist es möglich zu definierten Zeitpunkten, die vom Büro des Tierhaltungsnetzwerks rechtzeitig bekannt gegeben werden, Wildtyp Mäuse zu bestellen, die nach erneuter Hygienetestung in die Tierhaltung importiert werden können. Für die Tierbestellung ist wie bekannt ein PyRAT-Auftrag zu stellen.

Generell gilt, dass in die Tierhaltungen ZMMK, Pathologie und Weyertal nur Tiere mit einem SOPF-Status importiert werden können. Das entsprechende Zeugnis ist beim Senden des PyRAT-Auftrages an die Bestellung anzuhängen (unter Download).

3.3.1 Tierimport aus Nicht-EU-Länder

Bei Importen von Tieren aus Nicht-EU-Ländern ist zusätzlich zu den Vorgaben dieser SOP zu beachten, dass es eine Importgenehmigung der Stadt Köln vor dem Beginn des Importes beantragt werden muss. Dies erfolgt über das Veterinäramt der Stadt Köln. Es muss hierfür eine Vorlaufzeit von ca. 2 Wochen eingehalten werden. Die Wissenschaftler*in, die Tiere aus Nicht-EU-Ländern importieren möchte, muss das Formular zur Beantragung der Importgenehmigung (SOP THNW 003 Anlage 001 Antrag auf Importgenehmigung aus dem Nicht EU Ausland) vollständig und richtig ausfüllen und an die, für den Import verantwortliche, Tierärztin schicken. Die Tierärztin leitet das Dokument an das Veterinäramt weiter und organisiert die Weiterleitung der Importgenehmigung an das entsprechende Transportunternehmen, das für den Import der Tiere nach Deutschland verantwortlich ist.

3.4. Export to Laboratory (von Tierhaltungen des Tierhaltungsnetzwerks in ein Labor)

Tiere dürfen nur an Nutzer*innen zum Zwecke der Präparation im Labor herausgegeben werden. Die Tiere kommen dann nicht mehr in die Tierhaltung zurück und werden auch in PyRAT als exportierte Tiere (und damit nicht mehr lebende) Tiere verzeichnet. Sollen die Tiere von den Tierpfleger*innen der Haltung eingepackt und herausgegeben werden, muss in PyRAT der Auftrag „Export to Laboratory" gestellt werden.

3.5. Export and Back (Ausschleusen und Wiedereinschleusen von Tieren zu Versuchszwecken)

Diese Transferart darf nur mit vorheriger und rechtzeitiger Absprache mit der Tierhausleitung bzw. mit den Tierärztinnen genutzt werden. Sie beinhaltet das

Ausschleusen und das spätere erneute Einschleusen von Tieren in eine Tierhaltung des Tierhaltungsnetzwerks für Versuchszwecke (z.B. chirurgischer Eingriff in einem anderen Raum, Nutzung des MRTs etc.). Grundsätzlich gilt, dass diese Option nur für Tierhaltungen des Hygienelevels 2 und 3 möglich ist und dass es vor Nutzung dieser Option ein schlüssiges und gutes Hygienekonzept der Arbeitsgruppe ausgearbeitet werden muss (siehe SOP42 Imaging von Mäusen und Ratten in externen Bereichen der Medizinischen Fakultät und anerkannten Institutionen). Dieses Konzept muss die Abläufe des Ein- und Ausschleusen genau und verständlich beschreiben sowie alle einzelnen Maßnahmen zur Reinigung und Desinfektion innerhalb der Versuche bzw. der Tiertransfers. Erst nach der Freigabe der Vorgänge durch die Tierhausleitung oder der Tierärztinnen darf mit der Umsetzung begonnen werden. Verstoßen Wissenschaftler*innen gegen besprochene Richtlinien, behält sich die Tierhausleitung vor, diese Tiertransfers wieder zu untersagen. Alle Räume, in denen sich Tiere – auch temporär – befinden, müssen auf der §11-Genehmigung gemeldet sein.

2. Vorgehen vor Beginn einer Verpaarung

Nachdem die Mitarbeiter*in einen Arbeitsauftrag zur Verpaarung eines Zuchtpaares von den Nutzer*in bekommen haben (Verpaarung: 1 Wurf, Verpaarung: 2 Würfe oder Verpaarung: Dauerhaft), muss vor dem Zusammensetzen von Männchen und Weibchen sichergestellt sein, dass der/die betreffend/e Nutzer*in ausreichend Käfigkontigente zur Verfügung hat, damit die Jungtiere nach der Säugungsphase abgesetzt werden können. Dabei ist zu beachten, dass ein absetzen der Jungtiere erst nach 6 Wochen erfolgt (ca. 21 Tage Trächtigkeit, ca. 21 Tage Säugung). Bei einer 1:2 Verpaarung bei der Maus muss ebenfalls sichergestellt werden, dass die Käfigkontigente ausreichen, um das sichtbar tragende Weibchen unmittelbar vom anderen verbleibenden Weibchen und vom Männchen zu separieren.

Wenn sich abzeichnet, dass keine ausreichende Platzkapazität vorhanden ist, ist noch einmal Rücksprache mit der verantwortlichen Person der Arbeitsgruppe zu halten. Sollte eine ausreichende Kapazität an Käfigen für die Jungtiere vorhanden sein, kann mit der Verpaarung begonnen werden. Sollte die Platzkapazität nicht gegeben sein, darf keine Zucht angesetzt werden.

Ausgenommen von der unter Punkt 2 beschriebenen Vorgehensweise sind Zuchten bei denen die Nutzer*in die Jungtiere schon vor dem Absatz abholen und verwenden. Dies muss explizit im Tierversuchsantrag genehmigt worden sein. Hier kann auch ohne Prüfung der Käfigkontigente mit der Zucht begonnen werden. Mit der Zucht darf nur begonnen werden, wenn die Tiere gesund sind und die Zuchtreife (Maus ab der 8 Lebenswochen und Ratte ab der 14 Lebenswoche) das Alter und das Gewicht betreffend erreicht ist. Der Beginn der Verpaarung wird durch einen Vermerk auf der Käfigkarte/PyRAT dokumentiert. Unmittelbar nach Zuchtbeginn muss eine Zuchtkäfigkarte angebracht werden.

3. Fütterung

Die Zuchttiere sind generell mit Zuchtfutter zu versorgen. Sollte dies seitens der Arbeitsgruppen nicht gewünscht sein, ist dies zu begründen.

Extrudiertes Futter steht bei Bedarf (vermehrte Jungtiersterblichkeit, Kannibalismus etc.) zur Verfügung, dies wird direkt in den Käfig gefüttert und ist als Zusatz zum Zuchtfutter in der Futterraufe gedacht.

4. Vorgehen bei Trächtigkeit

Nachdem eine Verpaarung begonnen wurde, muss das Weibchen auf das Vorliegen einer Trächtigkeit untersucht werden. Gegebenfalls wird ein Plug-Check durchgeführt. Wird kein Plug-Check durchgeführt, erfolgt die Beurteilung der Trächtigkeit optisch mindestens einmal wöchentlich beim Umsetzen der Tiere. Wenn die Mitarbeiter*in eine Trächtigkeit bei einem Weibchen erkennen, wird dieses – wenn eine 1:2 Verpaarung vorliegt – von dem anderen Weibchen und dem Männchen getrennt. Der Käfig mit dem tragenden separierten Weibchen wird mit einer rosafarbenen Büroklammer markiert. Bei Trennung der tragenden Weibchen ist das Ausdrucken einer weiteren Käfigkarte notwendig. Zwei Würfe in einem Käfig sind nicht zulässig. Bei einer 1:1 Verpaarung bei der Ratte wird bei Vorliegen einer Trächtigkeit das Männchen aus dem Käfig entfernt.

Tragende Tiere werden jeden Tag kontrolliert (Sichtkontrolle ohne Eröffnen der Käfige), um zu erkennen, ob sich ein Tier in Geburt befindet. Bei Vorliegen eines Wurfes wird die Anzahl und der Tag der Geburt auf der Käfigkarte notiert. Danach erfolgt das Eintragen des Wurfes (Anzahl, Datum) in PyRAT und die Markierung des Käfigs mit einer gelben Büroklammer als Zeichen, dass sich das Weibchen in der Säugungsphase befindet.

5. Vorgehen beim Absetzen der Jungtiere

Bei **Mäusen** werden die Jungtiere nach einer Saugperiode von 19 bis 21 Tagen von der Mutter abgesetzt. Stellen die Mitarbeiter*in fest, dass die Jungtiere noch zu klein für das Absetzen sind (unter 10 g), kann die Zeit bis zum Absatz von der Mutter nach Absprache mit der verantwortlichen Person der Arbeitsgruppe um maximal 1 Woche verlängert werden.

Bei **Ratten** werden die Jungtiere nach einer Saugperiode von 19 bis 21 Tagen von der Mutter abgesetzt. Stellen die MitarbeiterInnen fest, dass die Jungtiere noch zu klein für

das Absetzen sind (unter 35 g), kann die Zeit bis zum Absatz von der Mutter nach Absprache mit der verantwortlichen Person der Arbeitsgruppe um maximal 1 Woche verlängert werden.

Das Absetzen der Tiere in andere Käfige erfolgt nach Geschlecht, wobei bei der Maus maximal 5 Jungtiere in einen Käfig gesetzt werden dürfen. Dabei ist darauf zu achten, dass die Gruppengröße in den jeweiligen Käfigen ungefähr gleich groß ist. Eine Tieranzahl über 5 in einem Käfig ist nicht zulässig. Eventuell sind versuchsbedingte Ausnahmen möglich. Diese sind vorab mit der Tierhausleitung abzusprechen. Die Raufen werden mit Haltungsfutter befüllt. Einige Pellets Zuchtfutter können bei Bedarf auf dem Käfigboden angeboten werden. Bei der Ratte können beim Absetzen bis zu 4 Jungtiere in einen Käfig gesetzt werden. Vor dem Absatz erfolgt die sofortige Markierung der Tiere mittels Ohrlochung. Auf der (alten Käfigkarte) Karte des Zuchtkäfigs, aus dem die Tiere entnommen/abgesetzt wurden, muss anschließend der Verbleib (der Tiere) dokumentiert bzw. neue Käfigkarten müssen über PyRAT ausgedruckt werden.

6. Vergesellschaften von Absatztieren

Sobald die Tiere abgesetzt und markiert sind, ist zu prüfen, ob einzelne Tiere im Käfig verbleiben. Diese einzelnen Tiere sollen dann unmittelbar vergesellschaftet werden (3R Prinzip – Reduce – Replace – Refine). Ausnahmen gelten nur für versuchsbedingte Einzelhaltung.

Bei dem Vergesellschaften ist darauf zu achten, dass die Tiere aus den verschiedenen Würfen eindeutig identifizierbar sind. Das bedeutet, dass Tiere mit der gleichen Lochnummer nicht miteinander vergesellschaftet werden dürfen. Nach der Vergesellschaftung ist eine neue Käfigkarte zu drucken.

Bei der Vergesellschaftung von Mäusen muss benutztes Material (z.B. Nistmaterial, Nagehölzer etc.) des einzelnen Tieres mit in den neuen Käfig mit den neuen Tieren überführt werden. Dadurch kann die Akzeptanz bei der Vergesellschaftung erhöht werden.

Einzelne weibliche Mäuse können mit weiblichen Mäusen der gleichen Linie vergesellschaftet werden. Dabei spielt das Alter der Mäuse eine untergeordnete Rolle.

Einzelne weibliche Mäuse können auch über das Absatzalter hinaus vergesellschaftet werden.

Einzelne männliche Mäuse können bis zu einem Alter von 4 Wochen mit männlichen Mäusen der gleichen Linie vergesellschaftet werden. Mit zunehmenden Alter und Eintritt der Geschlechtsreife kann es zu tödlichen Revierkämpfen kommen und deswegen ist eine Vergesellschaftung dann nicht mehr möglich.

Einzelne weibliche und männliche Ratten können unabhängig von Alter und Geschlecht mit gleichgeschlechtlichen Tieren vergesellschaftet werden. Bei männlichen Ratten, die aus einer Verpaarung kommen, ist darauf zu achten, dass diese Ratten vor der Vergesellschaftung eine Woche alleine sitzen. Dadurch sollen die männlichen Ratten den Geruch des Weibchens verlieren. Die Vergesellschaftung der Ratten muss in einem sauberen Käfig mit neuem Material (Deckel, Gitter, Futter, Wasser, Enrichment,…) erfolgen. Die Ratten sollen nach dem Zusammensetzen ca. 1h beobachtet werden. Wenn in dieser Zeit Kämpfe auftreten, müssen die Tiere wieder getrennt werden.

7. Ausnahmen für Einzelhaltung

Grundsätzlich ist bei allen Tieren die Gruppenhaltung obligatorisch. Eine Einzelhaltung von Tieren wird aber unter bestimmten Voraussetzungen notwendig. Diese sind z.B.:

- separierte aggressive männliche Tiere nach andauernden Rangkämpfen
- männliche Tiere, die versuchsbedingt vorher separiert wurden und nicht vergesellschaftet werden können
- Zuchtböcke die nicht wieder vergesellschaftet werden können
- Wurfbedingte Einzelhaltung (z.B. Wurf mit nur einem männlichen Nachkommen)
- Einzelhaltung nach Abgang anderer Tiere im Käfig (z.B. Tier verstorben; nur noch ein Tier im Käfig vorhanden)

Jede Einzelhaltung wird kritisch evaluiert. Ausnahmen sind generell versuchsbedingte und genehmigte Einzelhaltungen für beide Geschlechter.

8. Auszug aus der Richtlinie 2010/63/EU – Platzbedarf Maus und Ratte

Tabelle 1.1.

Mäuse

	Körpergewicht (g)	Mindestgröße der Unterbringung (cm^2)	Bodenfläche je Tier (cm^2)	Mindesthöhe der Unterbringung (cm)	Datum gemäß Artikel 33 Absatz 2
Vorratshaltung und während der Verfahren	bis zu 20	330	60	12	1. Januar 2017
	> 20 bis 25	330	70	12	
	> 25 bis 30	330	80	12	
	> 30	330	100	12	
Fortpflanzung		330 Für ein monogames Paar (Fremd-/Inzucht) oder ein Trio (Inzucht). Für jedes zusätzliche weibliche Tier plus Wurf sind 180 cm^2 hinzuzufügen.		12	
Vorratshaltung bei den Züchtern (*) Größe der Unterbringung 950 cm^2	unter 20	950	40	12	
Größe der Unterbringung 1 500 cm^2	unter 20	1 500	30	12	

Tabelle 1.2.

Ratten

	Körpergewicht (g)	Mindestgröße der Unterbringung (cm^2)	Bodenfläche je Tier (cm^2)	Mindesthöhe der Unterbringung (cm)	Datum gemäß Artikel 33 Absatz 2
Vorratshaltung und während der Verfahren (*)	bis zu 200	800	200	18	1. Januar 2017
	> 200 bis 300	800	250	18	
	> 300 bis 400	800	350	18	
	> 400 bis 600	800	450	18	
	> 600	1 500	600	18	

	Körpergewicht (g)	Mindestgröße der Unterbringung (cm^2)	Bodenfläche je Tier (cm^2)	Mindesthöhe der Unterbringung (cm)	Datum gemäß Artikel 33 Absatz 2
Fortpflanzung		800 Muttertier und Wurf. Für jedes zusätzliche ausgewachsene Tier, das auf Dauer in den Haltungsbereich eingestellt wird, werden 400 cm^2 hinzugefügt.		18	
Vorratshaltung bei den Züchtern (**) Größe der Unterbringung 1 500 cm^2	bis zu 50	1 500	100	18	
	> 50 bis 100	1 500	125	18	
	> 100 bis 150	1 500	150	18	
	> 150 bis 200	1 500	175	18	
Vorratshaltung bei den Züchtern (**) Größe der Unterbringung 2 500 cm^2	bis zu 100	2 500	100	18	
	> 100 bis 150	2 500	125	18	
	> 150 bis 200	2 500	150	18	

d. Characterization of R26mTmG mice : CECAD AG Niessen

PCR protocol: mTmG

PCR Mastermix:

Name	Amount [µl]
Red-Taq DNA Polymerase 2X MasterMix, 1,5 mM $MgCl_2$ (Order No.: 733-2130)	12,5µl
10µM primermix	1µl
template DNA	1µl
ddH_2O	10,5µl
Total	25µl

Primermix:

Stock No.: 31	mTmG tg rp	5' TCAATGGGCGGGGGTCGTT 3'
Stock No.: 32	mTmG wt rp	5' CGAGGCGGATCACAAGCAATA 3'
Stock No.: 33	mTmG wt fb	5' CTCTGCTGCCTCCTGGCTTCT 3'

Use 10µl of each primer stock and fill up to 100µl with ddH_2O for a 10µM primermix dilution.

Cyclerprogram:

Already programed in every cycler folder "Julia" called mTmG. Do **NOT** use "Geno" folder.

94° C	30 sec	
94° C	30 sec	30x
60° C	30 sec	
72° C	30 sec	
72° C	3 min	
10° C	∞	

Gel image:

2,5% agarose gel; 1:20.000 EtBr

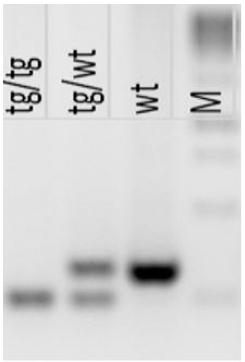

e. Superovulation of mouse females for embryo production : Max-Planck Institute for Biology of Aging Transgenic Core Facility

MAX-PLANCK-INSTITUT FÜR BIOLOGIE DES ALTERNS

Superovulation of mouse females for embryo production / manipulation

Stand 22.11.2021

Introdution:

Intraperitoneal injection of hormones to stimulate the ovaries:

Female mice are administered 0.2 ml of hormone solution intra-peritoneally twice at an interval of 46-48 hours (5-10 units of PMS - Pregnant Mare Serum, or 5-10 units of hCG - human chorionic gonadotropin).

This process increases the number of oocytes maturing for ovulation and thereby increases the number of fertilized zygotes or blastocysts obtained after mating has taken place. The injection leads to only minor stresses in the animals.

After the animals have been painlessly killed by cervical dislocation, the embryos are removed from the fallopian tubes or the uterus and are then available for manipulations (microinjection of DNA into zygotes, injection of embryonic stem cells into blastocysts).

Material:

- Needles (27Gx ¾, BD or similar)
- Syringe (1ml, Braun)
- PMSG (Ovogeest, diluted ready to use, provided by MPIage in Eppendorf tubes (P)
- hCG (Ovogeest, diluted ready to use, provided by MPIage in Eppendorf tubes (H)

- female mice (3-5 weeks old, 11-14g)
- single housed males for breeding of superovulated females

- empty mouse cage
- M2 Media, instruments and Eppendorf tubes for isolation the oviducts

Procedure:

As example for microinjection on Friday:

Monday between 12:00 - 13:00: Thaw the appropriate amount of PMSG (1-2 tubes). Immediately after thawing fill syringe with PMSG and inject **(i.p.) 200 µl** each female. (see Fig. 1).

Put injected females in an empty cage. After finishing the cage with superovulation put the females back into the original cage.

Wednesday between 12:00 - 13:00: Repeat exactly the same procedure with hCG. After finishing the superovulation females has to breed 1:1 with single housed males.

Take care about the Documentation in Pyrat or special paperwork and numder of licence on the cage cards.

Thursday morning (between 08:00 – 09:00) isolated oviducts and transfer immediately to the MPI age.

MPI age will isolate zygotes and culture over night for the microinjection of 2 cell stages.

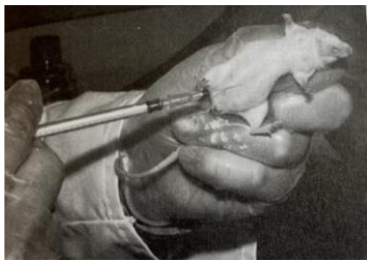

Fig. 1: from Schenkel: “Transgene Tiere“ 2. Auflage

Overview:

Day -3 (e.g. Monday)	Day -1 (e.g. Wednesday)	Day 0 (e.g. Thursday)
Superovulate females by injecting 0.2 ml PMS at 12.00 - 13:00	Superovulate females by injecting 0.2 ml hCG at 12.00 - 13:00 Setup breedings 1:1	Isolate oviduct in M2 media and transfer to MPI asap.

f. Ferrozine-based quantification of intracellular iron oxide nanaoparticles: RG Prof. Gang Bao Rice University, Huston Texas, USA

Ferrozine-based quantification of intracellular iron oxide nanoparticles

Materials

Iron Standard for ICP (Sigma-Aldrich, 43149-100ML-F)

Hydrochloric acid, 37 wt. % in H2O, 99.999% trace metals basis (Sigma-Aldrich, 339253-100ML)

Sodium hydroxide solution (Sigma-Aldrich, 72068-100ML)

Ammonium acetate solution, 7.5 M (Sigma-Aldrich, A2706-100ML)

Hydroxylamine hydrochloride (Sigma-Aldrich, 431362-50G)

Ferrozine (3-(2-Pyridyl)-5,6-diphenyl-1,2,4-triazine-4′,4″-disulfonic acid sodium salt), (Sigma-Aldrich 82950-1G)

384-well plates (Corning 3763)

Reagent Preparation

- Dilute the sodium hydroxide solution to 8 M with distilled water
- Dilute the ammonium acetate solution to 4 M with distilled water
- Prepare 5% hydroxylamine hydrochloride solution by dissolving 5 g of hydroxylamine hydrochloride in 100 mL of water
- Prepare 0.1% ferrozine solution by dissolving 0.1 g ferrozine in 100 mL of water

Protocol

1. Seed cells in TC-treated Multiple Well Plates, and let cells attach overnight.
2. Dilute magnetic iron oxide nanoparticles (MIONs) in culture medium, and added to the wells for loading. Cells without MION loading should be included as the background for subtraction.
3. After loading, remove the medium containing MIONs, and wash the cells three times with PBS to remove extracellular MIONs.
4. Detach the cells and count the cell number.
5. Centrifuge the cell suspension at 300 g for 5 min.
6. Remove the medium without disturbing the cell pellet.
7. Vacuum dry the cell pellet overnight.
8. Add 50 µL of HCl (37 wt. %) to the cell pellet, seal the tube with parafilm, and shake at 250 rpm at 37°C for 1 h.
9. Add 70 µL of sodium hydroxide solution (8 M), and vortex to mix well.
10. Add 100 µL of ammonium acetate solution (4 M), and vortex to mix well.
11. Add 100 µL of hydroxylamine hydrochloride solution (5%), and vortex to mix well.
12. Add 680 µL of distilled water, vortex to mix well
13. Seal the tube with parafilm, and shake at 250 rpm at 37°C for 1 h.
14. Centrifuge at 21,000 g for 15 min.
15. Transfer 40 µL of the supernatant from **Step 14** to 384-well plate, add 60 µL of ferrozine solution (0.1%), and mix by gently pipetting. Duplicate for each sample.
16. Read absorbance at 562 nm using a microplate reader.
17. Calculate the iron content using the standard curve generated with iron standard.

Standard Curve

1. Dilute the iron standard with distilled water to 20, 10, 5, 2.5, 1.25, and 0.625 µg/mL. Distilled water will be used as 0 µg/mL.
2. Transfer 50 µL of the standard solutions to new centrifuge tubes.
3. Add 70 µL of distilled water.
4. Follow the **Steps 10-12** in the protocol.
5. Transfer 40 µL of the standard solutions to 384-well plate, add 60 µL of ferrozine solution (0.1%), and mix by gently pipetting. Duplicate for each standard.
6. Read absorbance at 562 nm using a microplate reader.
7. Plot the mean absorbance (y-axis) against the iron concentration (x-axis).

III. Raw Data

a. B2M ICE results for NP0040-SM Colony 9 for B2M and CIITA

The contributions show the inferred sequences present in your edited population and their relative proportions (in contrast to the Indel plot (Indel Distribution tab) that does not specify sequence contributions). Cut sites are represented by black vertical dotted lines, and the wild-type sequence is marked by a "+" symbol on the far left.

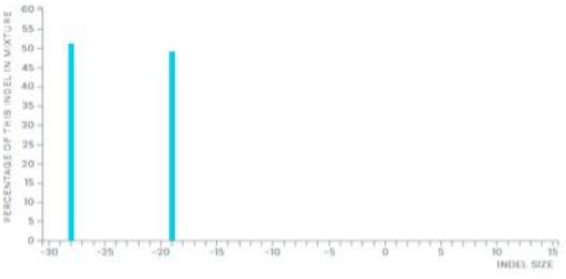

The Indel plot displays the inferred distribution of indels in the entire edited population of genomes. Hovering over each bar of the Indel plot shows the size of the insertion or deletion (+ or - 1 or more nucleotides), along with the percentage of genomes that contain it. Note: Each indel size represented in the Indel plot may not necessarily occur in the same sequence. The percentages of different indel sizes in the cell population are not the same as ICE/KO-Score scores.

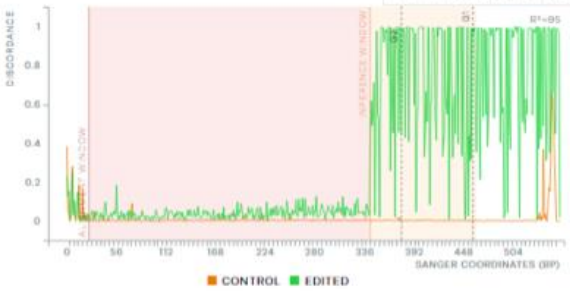

The discordance plot details the level of alignment per base between the wild type (control) and the edited sample in the inference window (the region around the cute site), i.e. it shows the average amount of signal that disagrees with the reference sequence derived from the control trace file. On the plot, the green line and orange line should be close together before the cut site, with a typical CRISPR edit resulting in a jump in the discordance near the cutsite and continuing to remain far apart after the cut site (representing a high level of sequence discordance).

CIITA

The contributions show the inferred sequences present in your edited population and their relative proportions (in contrast to the Indel plot (Indel Distribution tab) that does not specify sequence contributions). Cut sites are represented by black vertical dotted lines, and the wild-type sequence is marked by a "+" symbol on the far left.

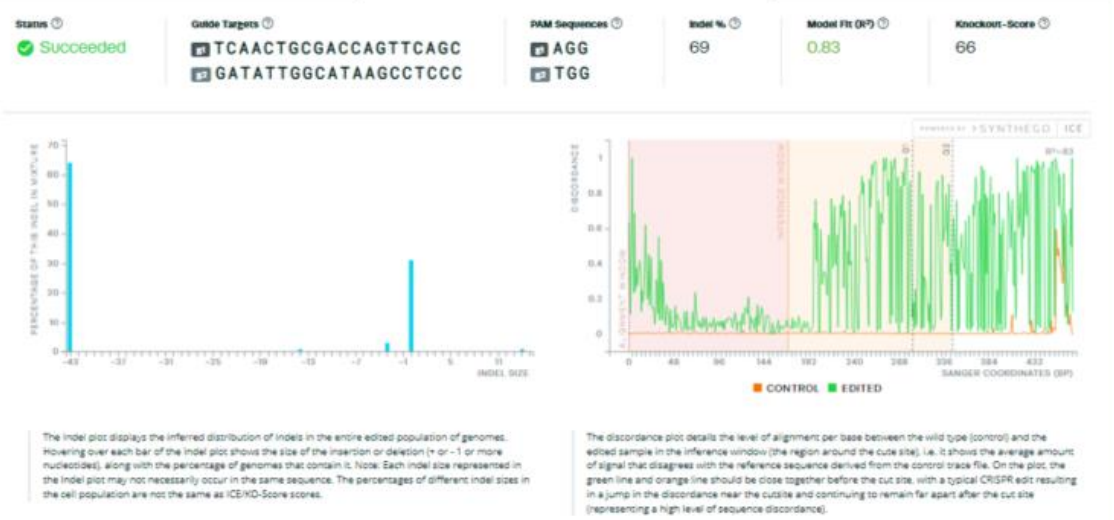

b. Next Generation Sequencing

B2M

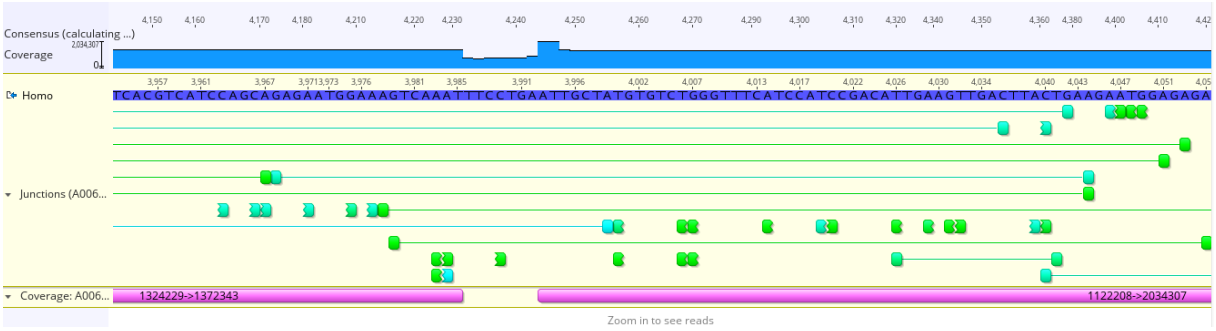

CIITA

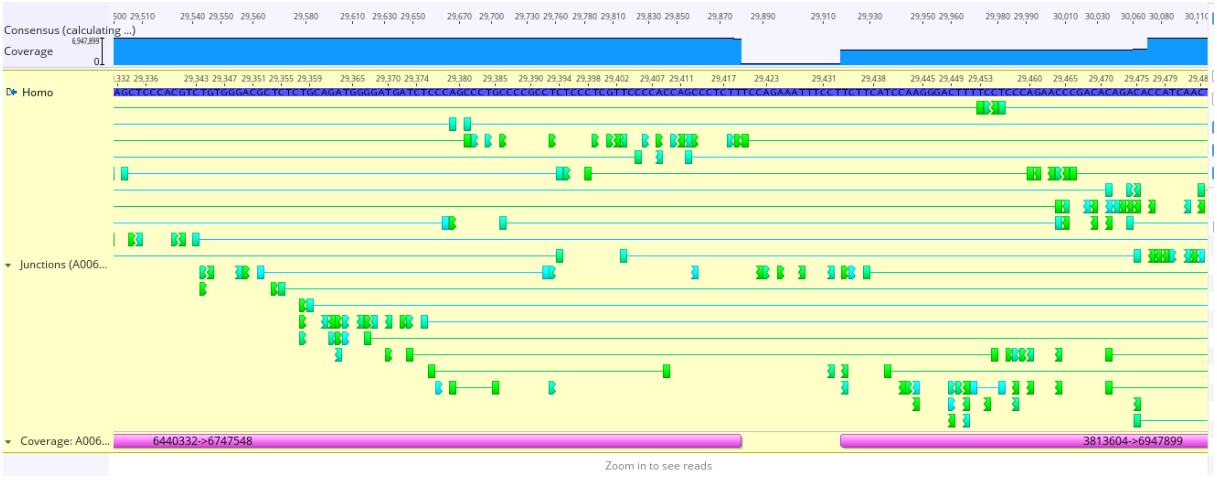

c. SSEA4-staining raw data

iPSCs stained with Anti- SSEA4-FITC											
	n=										
Group	1	2	3	4	5	6	7	8	9	10	Mean % of expression
NP0040-8	96,8	85,7	90,4	98,5	74,1	99,5	99,6	91,3	83,3	76,1	89,53
NP0040-SM	96,2	99,8	94,6	62,9	57,3	84,5					82,55
HSM47M	82	80	96,6								86,20

d. STR Data

NP0040-8

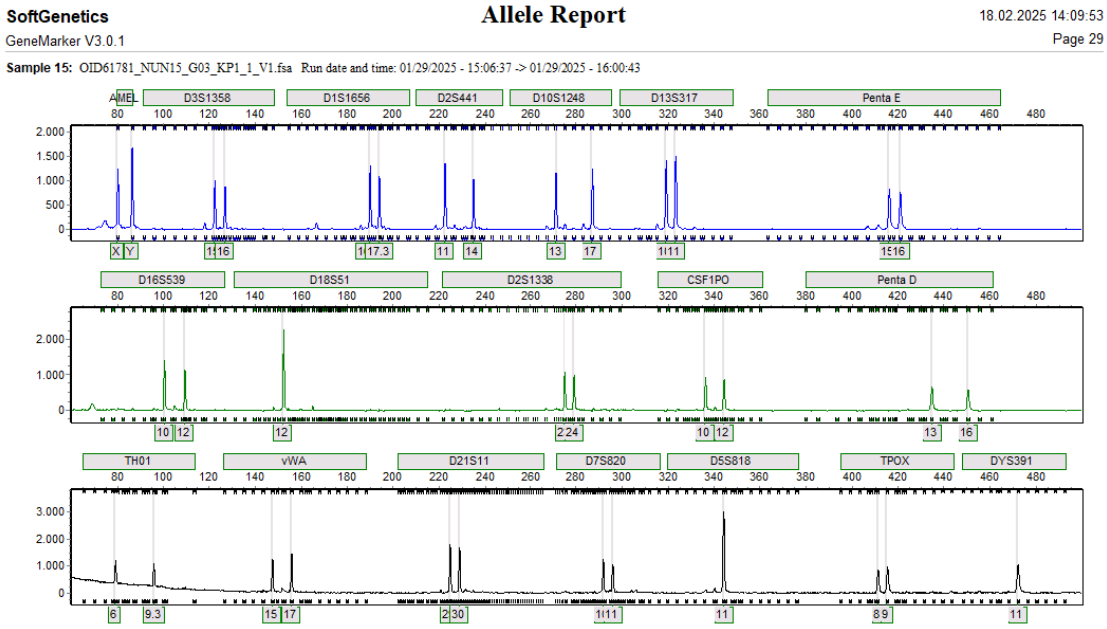

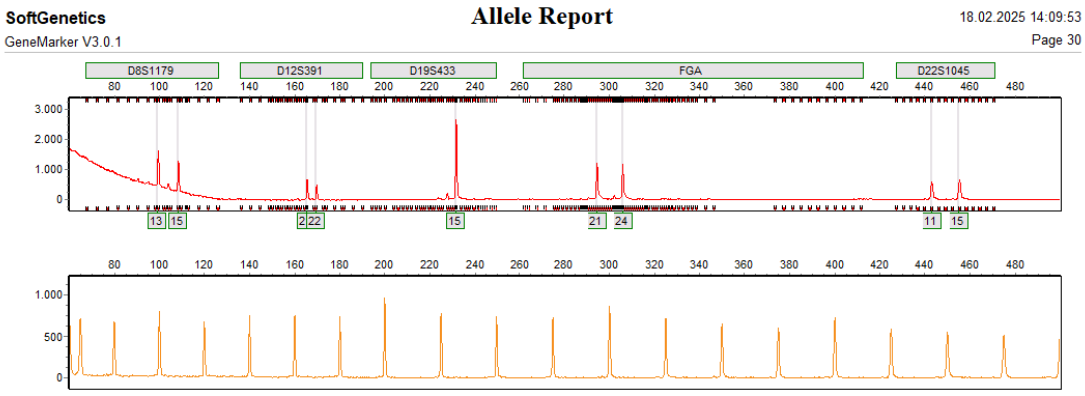

NP0040-SM

SoftGenetics **Allele Report** 18.02.2025 14:58:21

GeneMarker V3.0.1 Page 1

Project Comments:

Sample 1: OID61781_NUN39_G09_KP1_1_V2.fsa Run date and time: 01/29/2025 - 15:06:37 -> 01/29/2025 - 16:00:43

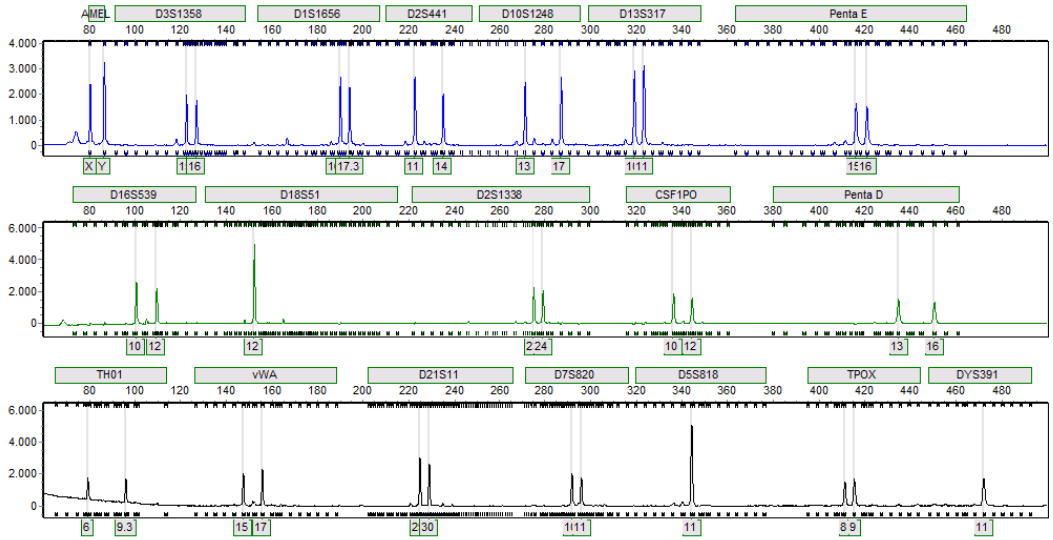

SoftGenetics **Allele Report** 18.02.2025 14:58:22

GeneMarker V3.0.1 Page 2

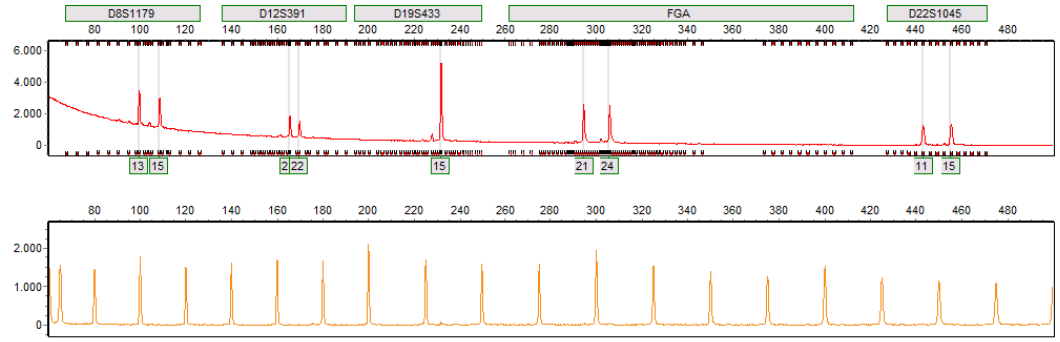

e. NP0040-SM Cardiomyocytes FC data

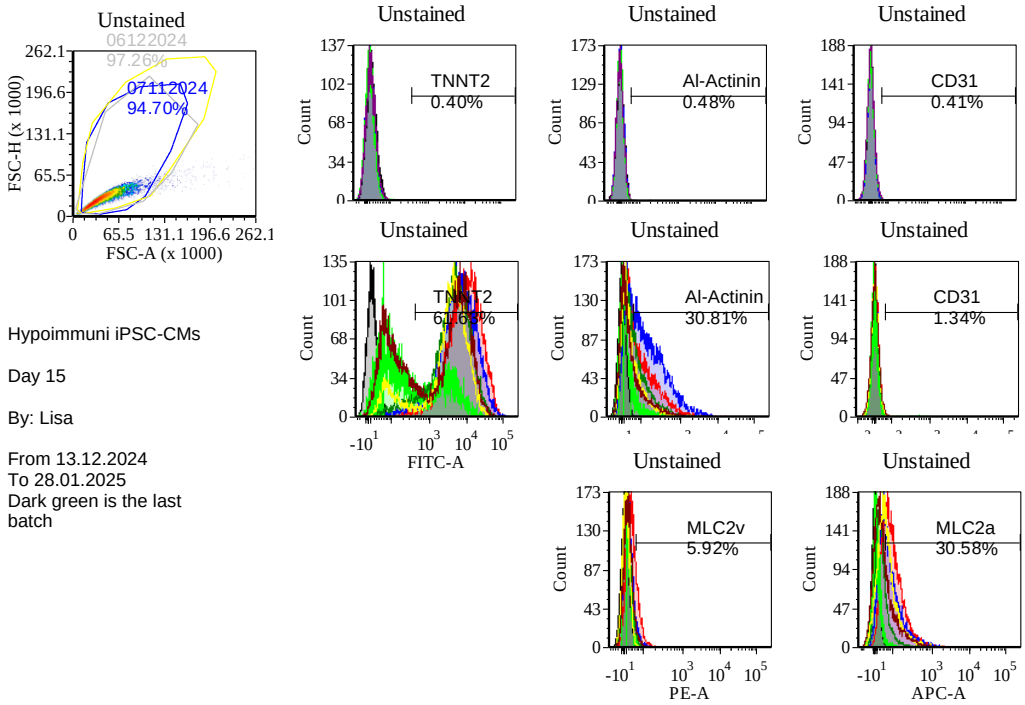

Hypoimmuni iPSC-CMs

Day 15

By: Lisa

From 13.12.2024
To 28.01.2025
Dark green is the last batch

					Cell count	CM count calculated wit
	TNNT2 [%]	a-Actinin [%]	MLC2v [%]	MLC2a [%]	[x10^6]	[x10^6]
1	98,36	50,97	19,82	69,35	1,26	1,24
2	95,27	67,75	8,06	53,04	1,9	1,81
3	41,55	13,93	1,44	5,26	3,0	1,25
4	91,7	41,16	03,06	19,12	3,3	3,03
5	84,05	31,48	1,00	44,86	4,5	3,78
6	61,63	30,81	5,92	30,58	3,5	2,16

f. Mean Fluorescence Intensity of IFN-Gamma

Assay 1	HLA-A,B,C + AlexaF488	only AlexaF488	unstained Ctrl	MFI error corrected againgst only sekundary antibody stain AlexaFl488
NP0040-8 Ctrl	106	31,1	2,37	74,9
NP0040-8 +IFN-γ 50 ng/ml	434	24,7	2,35	409,3
NP0040-8 Ctrl	39,5	27,2	2,09	12,3
NP0040-8 +IFN-γ 50 ng/ml	52,8	22,9	2,2	29,9
Assay 2				
NP0040-8 –IFN-γ	49	6,96	2,1	42,04
NP0040-8 +IFN-γ 50 ng/ml	425	18	2,05	407
NP0040-8 -IFN-γ	8,42	2,99	1,95	5,43
NP0040-8 +IFN-γ 50 ng/ml	7,62	2,86	1,81	4,76
Assay 3				
NP0040-8 –IFN-γ	110	10,6	2,3	99,4
NP0040-8 +IFN-γ 50 ng/ml	639	9,52	2,24	629,48
NP0040-8 -IFN-γ	40,6	6,52	1,96	34,08
NP0040-8 +IFN-γ 50 ng/ml	24,6	13,2	1,98	11,4
Assay 4				
NP0040-8 –IFN-γ	94,9	13,1	2,36	81,8
NP0040-8 +IFN-γ 50 ng/ml	895	16,8	2,32	878,2
NP0040-8 -IFN-γ	21,6	5,19	1,9	16,41
NP0040-8 +IFN-γ 50 ng/ml	14,1	5,69	1,86	8,41

g. Expression of murine CD47 on cell surface

iPSCs stained with Anti- mCD47-APC												
	n=											
Group	1	2	3	4	5	6	7	8	9	10	11	Mean % of expression
AT25 flucRosa	87,5	83	90,6	89	95,5							89,08
NP0040-8	9,6	3,9	1,5	2,7	0,5							3,65
HSM47M	72	77	82	89	91,4	99	99,5	99,4	93,9	97	97,1	82,38

h. Iron standard curve

Iron Standard in µg/ml	Measurement 1 Absorbance	Measurement 2 Absorbance	Mean Absorbance	Mean Absorbance Error corrected
500	1,141	1,153	1,147	1,102
250	0,58	0,569	0,5745	0,530
100	0,236	0,237	0,2365	0,192
50	0,135	0,139	0,137	0,092
20	0,085	0,085	0,085	0,040
10	0,063	0,064	0,0635	0,019
2,5	0,045	0,046	0,0455	0,001
1,25	0,042	0,042	0,042	0,000
0	0,038	0,039	0,0385	0,000

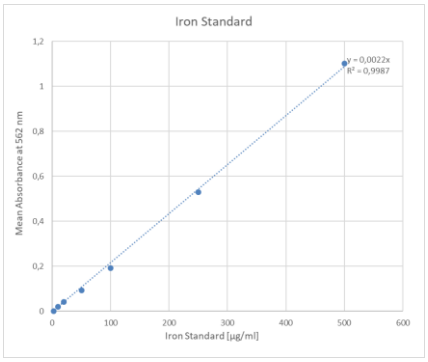

i. Iron Content of cells measurements and calculations

Sample	Loading Methode	Total Iron Content in Medium in µg	Cell count [x10⁶]	Measured at 562 nm Measurement 1 Absorbance	Measurement 2 Absorbance	Mean Absorbance	Mean Absorbance Error Corrected	Iron Content of Cells	Normalization	Iron content of cells in µg / 0,30 cells
60 µg/ml	with out Magnet; 24 h incubator	120	0,3	0,058	0,057	0,0575	0,0125	5,00	6,20	6,20
60 µg/ml	without Magnet; 24 h incubator	120	0,35	0,043	0,043	0,043	-0,002	-0,80	0,40	0,34
60 µg/ml	without Magnet; 24 h incubator	120	0,31	0,048	0,047	0,0475	0,0025	1,00	2,20	2,13
60 µg/ml	without Magnet; 24 h incubator	120	0,29	0,055	0,055	0,055	0,01	4,00	5,20	5,38
60 µg/ml	without Magnet; 24 h incubator	120	0,32	0,064	0,064	0,064	0,019	7,60	8,80	8,25
60 µg/ml + MF	with plate Magnet; 24 h incubator	120	0,39	0,27	0,284	0,277	0,232	92,80	94,00	72,31
60 µg/ml + MF	with plate Magnet; 24 h incubator	120	0,47	0,14	0,133	0,1365	0,0915	36,60	37,80	24,13
60 µg/ml + MF	with plate Magnet; 24 h incubator	120	0,33	0,141	0,138	0,1395	0,0945	37,80	39,00	35,45
60 µg/ml + MF	with plate Magnet; 24 h incubator	120	0,25	0,221	0,227	0,224	0,179	71,60	72,80	87,36
60 µg/ml + MF	with plate Magnet; 24 h incubator	120	0,35	0,2	0,196	0,198	0,153	61,20	62,40	53,49
no	only MSCs	0	0,3	0,042	0,042	0,042	-0,003	-1,20	0,00	0,00
no	only MSCs	0	0,3	0,042	0,042	0,042	-0,003	-1,20	0,00	0,00
no	only MSCs	0	0,3	0,043	0,043	0,043	-0,002	-0,80	0,40	0,40
no	only MSCs	0	0,3	0,043	0,041	0,042	-0,003	-1,20	0,00	0,00

j. DNA quantification standard curve

Cellcount	Mean DNA Conc	DNA conc. Measurment 1	DNA conc. Measurment 2	DNA conc. Measurment 3
0	0			
0,05	3,35	3,5	3,2	
0,1	3,9	3,8	4	
0,2	9,05	9,9	8,2	
0,3	12,6	13	12,2	
0,4	17,6	17,1	19,9	15,8
0,5	18,45	18,5	18,4	

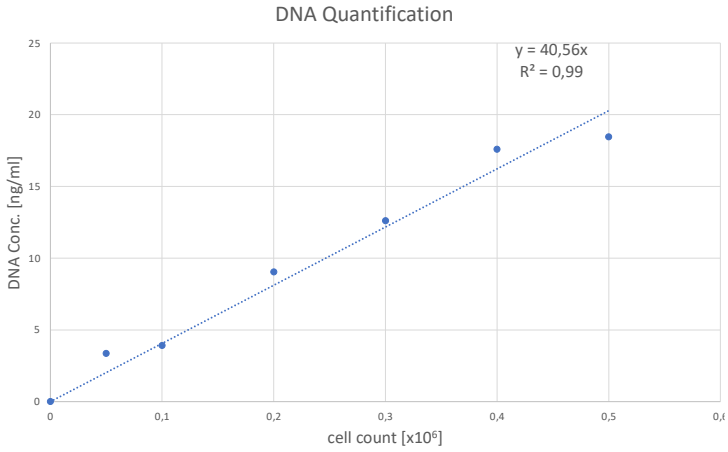

k. DNA quantification of cell clumps

time +MF	Magnetic lable	Mean OD DNA conc	Calculated cell number	% of cells in cell clump
1 min	Ferro	1,77	0,04	17,42
		4,73	0,12	46,67
		2,60	0,06	25,64
	SPIONs	6,90	0,17	47,25
		10,60	0,26	72,58
		1,90	0,05	18,01
5 min	Ferro	7,87	0,19	77,57
		8,13	0,20	80,20
		5,10	0,13	50,29
	SPIONs	10,97	0,27	75,09
		8,93	0,22	61,17
		6,17	0,15	58,47
15 min	Ferro	13,30	0,33	131,14
		9,20	0,23	90,72
		7,73	0,19	76,25
	SPIONs	14,37	0,35	98,38
		14,27	0,35	97,69
		10,37	0,26	98,29

Ferro	Mean	SD	SPIONs	Mean	SD
1 min	29,33	16,65	1 min	45,95	27,30
5 min	69,33	15,14	5 min	64,91	8,92
15 min	100,00	28,84	15 min	98,12	0,37

l. Breeding calculator

Instructions on how to use the Excel-table for breeding planning

The needs-based breeding planning must be done for each line, each strain, each allele combination. The planning is carried out using the Excel tables contained here (see tabs Breeding planning according to Cat. A, Cat. B and Cat. C). The requirements determined in each case are to be documented and made available to the animal facility management in the respective current version. This can be done digitally within the framework of the animal database(s) used with the IT solutions provided. The documented breeding plan shall be updated regularly and its most recent version shall be filed immediately.

For each individual line / strain / allele combination, planning must be carried out individually according to the tables.
If the parameters are the same, several lines / strains / allele combinations can be combined in one table, whereby the respective requirements of the lines / strains / allele combinations concerned must be documented in a comprehensible manner.

The expected litter size (6) and the number of litters per female (5) are predefined, but can be adjusted if necessary.

In the breeding plan cat B and C only the respective applicable mating steps (cat B) or purposes (cat C) are to be filled in or completed if necessary.

Breeding plan calculator for maintenance breeding

General information is to be entered in the empty white fields.
For the calculation, the red fields are to be filled in!
For reproductive performance adjustments, modify the yellow fields.
Grey fields are filled in automatically.

Allele combination		
Usual mating scheme (MxF)		
Purpose		
Target genotype		
Animals needed per genotype	per year :	20 F
Quota for target genotype		
Offsprings (Animals needed per genotype X (1/rate for the desired genotype)	per year:	60
Estimated number of required litters (Offsprings / litter size)	per year:	10
Expected litter size	**6**	
Number of possible litters per female	**5**	
Breeding animals (Number of required litters / number of possible litters per female = number of breeding pairs x 2 = breeding animals)	per year:	4
Estimated total number of animals for maintenance breeding	8	

Note: Breeding animals would be used upto 6-months

IV. Eigenständigkeitserklärung

Hiermit versichere ich an Eides statt, dass ich die vorliegende Dissertationsschrift selbstständig und ohne die Benutzung anderer als der angegebenen Hilfsmittel angefertigt habe. Alle Stellen - einschließlich Tabellen, Karten und Abbildungen -, die wörtlich oder sinngemäß aus veröffentlichten und nicht veröffentlichten anderen Werken im Wortlaut oder dem Sinn nach entnommen sind, sind in jedem Einzelfall als Entlehnung kenntlich gemacht. Ich versichere an Eides statt, dass diese Dissertationsschrift noch keiner anderen Fakultät oder Universität zur Prüfung vorgelegen hat; dass sie - abgesehen von unten angegebenen Teilpublikationen - noch nicht veröffentlicht worden ist sowie, dass ich eine solche Veröffentlichung vor Abschluss der Promotion nicht ohne Genehmigung der / des Vorsitzenden des IPHS- Promotionsausschusses vornehmen werde. Die Bestimmungen dieser Ordnung sind mir bekannt. Die von mir vorgelegte Dissertation ist von Prof. Dr. Kurt Paul Pfannkuche betreut worden.

Darüber hinaus erkläre ich hiermit, dass ich die Ordnung zur Sicherung guter wissenschaftlicher Praxis und zum Umgang mit wissenschaftlichem Fehlverhalten der Universität zu Köln gelesen und sie bei der Durchführung der Dissertation beachtet habe und verpflichte mich hiermit, die dort genannten Vorgaben bei allen wissenschaftlichen Tätigkeiten zu beachten und umzusetzen.

Übersicht der Publikationen:

Halhouli, T.; Münchhalfen, L.; Hamad, S.; Schmitz-Ullrich, L.; Nitsche, F.; Gaedke, F.; Schauss, A.; Zhang, L.; Pham, Q.-K.; Bao, G.; et al. Cell-Based Therapies: Ferromagnetic Versus Superparamagnetic Cell Targeting. Bioengineering 2025, 12, 657. https://doi.org/10.3390/bioengineering12060657

Ich versichere, dass ich alle Angaben wahrheitsgemäß nach bestem Wissen und Gewissen gemacht habe und verpflichte mich, jedmögliche, die obigen Angaben betreffenden Veränderungen, dem IPHS-Promotionsausschuss unverzüglich mitzuteilen.

04.05.2026 _____

Datum Unterschrift